

GAS PRODUCTION FROM HYDRATE RESERVOIRS

A THESIS SUBMITTED TO  
THE GRADUATE SCHOOL OF NATURAL AND APPLIED SCIENCES  
OF  
MIDDLE EAST TECHNICAL UNIVERSITY

BY

DORUK ALP

IN PARTIAL FULFILLMENT OF THE REQUIREMENTS  
FOR  
THE DEGREE OF MASTER OF SCIENCE  
IN  
PETROLEUM AND NATURAL GAS ENGINEERING

JUNE 2005

Approval of the Graduate School of Natural and Applied Sciences

---

Prof. Dr. Canan ÖZGEN  
Director

I certify that this thesis satisfies all the requirements as a thesis for the degree of Master of Science.

---

Prof. Dr. Birol DEMİRAL  
Head of Department

This is to certify that we have read this thesis and that in our opinion it is fully adequate, in scope and quality, as a thesis for the degree of Master of Science.

---

Dr. George MORIDIS  
Co-Supervisor

---

Prof. Dr. Mahmut PARLAKTUNA  
Supervisor

Examining Committee Members

Prof. Dr. Ender OKANDAN (METU, PETE) \_\_\_\_\_

Prof. Dr. Mahmut PARLAKTUNA (METU, PETE) \_\_\_\_\_

Dr. George MORIDIS (LBNL, ESD) \_\_\_\_\_

Prof. Dr. Birol DEMİRAL (METU, PETE) \_\_\_\_\_

Prof. Dr. Fevzi GÜMRAH (METU, PETE) \_\_\_\_\_

Prof. Dr. Nurkan KARAHANOĞLU (METU, GEOE) \_\_\_\_\_

**I hereby declare that all information in this document has been obtained and presented in accordance with academic rules and ethical conduct. I also declare that, as required by these rules and conduct, I have fully cited and referenced all material and results that are not original to this work.**

Name, Last name: Doruk ALP

Signature :

# ABSTRACT

## GAS PRODUCTION FROM HYDRATE RESERVOIRS

Alp, Doruk

M.S., Department of Petroleum and Natural Gas Engineering

Supervisor: Prof. Dr. Mahmut Parlaktuna

Co-Supervisor: Dr. George Moridis

June 2005, 149 pages

In this study; gas production by depressurization method from a hydrate reservoir containing free gas zone below the hydrate zone is numerically modeled through 3 dimensional, 3 phase, non-isothermal reservoir simulation.

The endothermic nature of hydrate decomposition requires modeling to be non-isothermal; hence energy balance equations must be employed in the simulation process. TOUGH-Fx, the successor of the well known multipurpose reservoir simulator TOUGH2 (Pruess [24]) and its very first module TOUGH-Fx/Hydrate, both developed by Moridis et.al [23] at LBNL, are utilized to model production from a theoretical hydrate reservoir, which is first studied by Holder [11] and then by Moridis [22], for comparison purposes.

The study involves 2 different reservoir models, one with 30% gas in the hydrate zone (case 1) and other one with 30% water in the hydrate zone (case 2). These models are further investigated for the effect of well-bore heating.

The prominent results of the modeling study are:

- In case 1, second dissociation front develops at the top of hydrate zone and most substantial methane release from the hydrate occurs there.
- In case 2 (hydrate-water in the hydrate zone), because a second dissociation front at the top of hydrate zone could not fully develop due to high capillary pressure acting on liquid phase, a structure similar to ice lens formation is observed.

- Initial cumulative replenishment (first 5 years) and the replenishment rate (first 3.5 years) are higher for case 2 because, production pressure drop is felt all over the reservoir due to low compressibility of water and more hydrate is decomposed.

Compared to previous works of Holder [11] and Moridis [22], amount of released gas contribution within the first 3 years of production is significantly low which is primarily attributed to the specified high capillary pressure function.

Keywords: Hydrate, Natural gas, Production, Numerical modeling, TOUGH

# ÖZ

## HİDRAT REZERVUARLARINDAN GAZ ÜRETİMİ

Alp, Doruk

Yüksek lisans, Petrol ve Doğalgaz Mühendisliği Bölümü

Tez Yöneticisi: Prof. Dr. Mahmut Parlaktuna

Ortak Tez Yöneticisi: Dr. George Moridis

Haziran 2005, 149 sayfa

Bu çalışmada, hidrat bölgesi altında serbest gaz bölgesi olan bir hidrat rezervuarından basınç düşürme yöntemiyle gaz üretimi; 3 boyutlu, 3 fazlı, eş-sıcaklıkta olmayan rezervuar için sayısal olarak modellenmiştir.

Hidrat çözülümünün ısı alan bir faz değişimi olması, çalışmada sıcaklık değişimlerinin modellenmesini gerektirir, bu yüzden modelleme sırasında enerji denklemleri de kullanılmalıdır. Önce Holder [11] tarafından çalışılan, daha sonra karşılaştırma amacıyla Moridis [22] tarafından tekrar çalışılan, kuramsal bir hidrat rezervuarından üretimi modellemek için; çok amaçlı rezervuar modeli TOUGH2'nin (Pruess [24]) halefi TOUGH-Fx ve onun ilk modülü TOUGH-Fx/Hydrate (Moridis [23]), kullanılmıştır.

Çalışma 2 farklı rezervuar modeli içerir, hidrat bölgesinde %30 gaz (model 1), ve %30 su (model 2). Bu modeller, ayrıca kuyu içi ısıtmasının etkilerini gözlemlemek için de incelenmiştir.

Modelleme çalışmasının belirgin sonuçları şunlardır:

- Model 1'de (hidrat bölgesinde hidrat-gaz), hidrat bölgesinin üst kısmında ikinci bir çözünme yüzeyi gelişmiş ve hidrattan en belirgin metan salınımı buradan gerçekleşmiştir.
- Model 2'de (hidrat bölgesinde hidrat-su), sıvı fazına etkiyen yüksek kılcal basınç fonksiyonu yüzünden ikinci çözünme yüzeyi tam olarak gelişmemiş ve ardışık buz katmanlarına benzer bir yapı olduğu gözlenmiştir.

- Üretilen serbest gazın hidrattan çözünen gaz ile toplam yenileme miktarı (ilk 5 yıl için) ve yenileme oranı (ilk 3.5 yıl için) Model 2'de daha yüksektir. Bu sonuç üretim kaynaklı basınç düşümünün düşük sıkıştırılabilirlikli suyun varlığı ile tüm rezervuarda kısa sürede hissedilmesinden kaynaklanmaktadır.

Holder [11] ve Moridis [22]'in önceki çalışmalarına kıyasla bu çalışmada ilk 3 yıl için elde edilen gaz salınım miktarı oldukça düşüktür, bunun temel nedeninin tanımlanmış olan yüksek kılcal basınç fonksiyonu olduğu düşünülmektedir.

Anahtar Kelimeler: Hidrat, Doğalgaz, Üretim, Nümerik Modelleme, TOUGH

## **ACKNOWLEDGEMENT**

The author wishes to express his deep gratitude to his supervisor Prof. Dr. Mahmut Parlaktuna for his patience and understanding; his guidance, advice, criticism and encouragement throughout the study, but most importantly for introducing the world of hydrates to him.

The author wishes to express his deep gratitude to his Co-supervisor Dr. George J. Moridis from Berkeley National Laboratories for providing the code, sharing his knowledge and experience both on hydrates and numerical simulation, the insight and new vision he brought, his patience, encouraging manners, serious effort and support from overseas.

For his serious effort to understand, sharing his experience on how to approach the problem, his inspiration and encouragement that reinstated self-confidence, the author especially thanks to Dr. Hakan Alkan from GRS, Germany.

His surgeon, Prof.Dr. Sinan Adiyaman from Ankara University is greatly acknowledged for literally saving the author's hand and making it possible for him to continue the study.

The author deeply appreciates his colleague Berna Haşçakır for her invaluable help with preparation of the cross-section graphs and even more invaluable companionship.

Above all, the author is deeply grateful to his parents; Zerrin and Mustafa Alp for providing by all means the conditions for him to study and especially his mother Zerrin Alp for her unconditional support and care, patience and understanding, fostering and always being there to listen.

## TABLE OF CONTENTS

ABSTRACT .....	IV
ÖZ .....	VI
ACKNOWLEDGEMENT.....	VIII
TABLE OF CONTENTS.....	IX
LIST OF TABLES.....	XI
LIST OF FIGURES.....	XII
CHAPTER	
1 INTRODUCTION.....	1
2 HYDRATES.....	3
2.1 Hydrates of Hydrocarbons (Natural Gas Hydrates) .....	4
2.2 Properties of Hydrates.....	8
2.2.1 Heat Capacity (Specific Heat).....	9
2.2.2 Heat of Dissociation.....	9
3 HYDRATE RESERVOIRS .....	11
3.1 Origin of Gas in Hydrate Reservoirs.....	13
3.2 Occurrence of Hydrate in Reservoirs .....	14
3.3 Classification of Hydrate Reservoirs .....	15
4 GAS PRODUCTION FROM HYDRATE RESERVOIRS.....	17
4.1 Production Schemes .....	18
4.1.1 Thermal Stimulation.....	19
4.1.2 Depressurization .....	20
4.1.3 Inhibitor Injection.....	20
4.2 Previous Experiences.....	21
5 PRODUCTION MODELING.....	22
5.1 Review of Previous Modeling Studies.....	24
6 STATEMENT OF THE PROBLEM .....	28
7 SOLUTION OF THE PROBLEM.....	29
7.1 Case Study.....	29
7.1.1 Case 1: The Holder problem with 30% gas in the hydrate zone .....	29
7.1.2 Case 2: The Holder problem with 30% water in the hydrate zone .....	30
7.2 Reservoir Properties.....	30
7.3 Grid Structure .....	31
7.3.1 Production Data: .....	33
7.4 Simplifying Assumptions .....	35

7.5 Governing Equations .....	35
7.6 Numerical Solution of Equations .....	38
7.7 Thermodynamic Properties .....	39
7.8 Hydrate properties .....	40
7.9 Phase Behavior .....	41
7.10 Problem Initialization .....	41
7.10.1 Method of Initialization .....	42
7.11 Rock Properties:.....	46
7.11.1 Relative Permeability:.....	47
7.11.2 Capillary Pressures:.....	48
8 RESULTS AND DISCUSSION .....	52
8.1 Hydrate Saturation Distributions.....	52
8.2 Effect of Well-bore Heating .....	54
8.3 Replenishment of Produced Methane.....	55
8.4 Comparison with Previous Work .....	123
9 CONCLUSION .....	125
10 RECOMMENDATIONS.....	127
REFERENCES.....	129
APPENDIX	
A HYDRATE FORMATION CONDITIONS .....	131
A.1 Phase Diagrams for Hydrates of Pure Hydrocarbons.....	131
A.2 Phase Diagrams for Hydrates of Gas Mixtures .....	132
A.3 The Hysteresis of Hydrate Formation .....	133
A.4 Effect of Inhibitors on Hydrate Formation .....	133
B DETERMINATION OF HYDRATE FORMATION CONDITIONS .....	136
B.1 Distribution Coefficient ( $K_i$ value) Method .....	136
B.2 Gas Gravity Method (Katz) .....	138
B.3 Pressure - Temperature Phase Diagram for Methane Hydrate.....	140
B.4 Determination of Hydrate Number $N_H$ .....	141
B.5 Hydrate Composition.....	142
B.6 System Composition .....	142
C MESSOYAKHA FIELD .....	143

## LIST OF TABLES

Table 7.1: Reservoir rock properties (Moridis [21]).....	31
Table 7.2: Layer data .....	33
Table 7.3: Production data .....	34
Table 7.4: Heat source data.....	34
Table 7.5: Hydrate properties .....	40
Table 7.6: Lower section layer data .....	43
Table 7.7: Upper section layer data .....	44
Table 7.8: Parameters for relative permeability function .....	47
Table 7.9: Capillary pressure function parameters of Case 1.....	49
Table 7.10: Capillary pressure function parameters of Case 2, lower section .....	50
Table 7.11: Capillary pressure function parameters of Case 2, upper section.....	51
Table B. 1: Parameters of $K_{vsi}$ equation (Sloan [1]) .....	137
Table C. 1: Reservoir properties of Messoyakha Field.....	144
Table C. 2: Gas composition of Messoyakha Field .....	144

## LIST OF FIGURES

Figure 2.1: Methane hydrate crystal unit.....	3
Figure 2.2: The 5 crystal units of natural gas hydrates (Sloan [1]).....	5
Figure 2.3: 3D view of some crystal units (Sloan [1]) .....	5
Figure 2.4: Structure I (Sloan [1]).....	6
Figure 2.5: Structure II (Sloan [1]).....	7
Figure 2.6: The three hydrate structures and associated crystal units (Sloan [3]) .....	8
Figure 3.1: Hydrate deposit locations (Sloan [1]).....	11
Figure 3.2: Hydrate window (Depth-Temperature diagram) for permafrost (Sloan [1]) .....	12
Figure 3.3: Hydrate window (Depth-Temperature diagram) for deep ocean (Sloan [1]) .....	13
Figure 3.4: Hydrate existence in reservoir (modified from Sloan [1]) .....	15
Figure 3.5: Hydrate reservoir Class 1 (Sawyer [5]).....	16
Figure 3.6: Hydrate reservoir Class 3 (Ji et al [8]) .....	16
Figure 4.1: Production scheme effects on equilibrium (modified from Sawyer [5]) .....	18
Figure 4.2: Production schemes (Khairkhah [9]) .....	18
Figure 4.3: Steam injection scheme (Sawyer [5]) .....	19
Figure 4.4: Production of deep water hydrates (Rose [10]).....	20
Figure 7.1: Schematic of theoretical reservoir (not to scale) .....	30
Figure 7.2: Grid structure of whole reservoir.....	32
Figure 7.3: Grid structure near well-bore .....	32
Figure 7.4: Initial vertical temperature distribution for Case 1. ....	45
Figure 7.5: Initial vertical temperature distribution for Case 2. ....	45
Figure 7.6: Initial Pressure-Temperature diagrams of Case 1 and Case 2. ....	46
Figure 7.7: Relative permeability function - Stone .....	48
Figure 7.8: Capillary pressure function of Case 1.....	49
Figure 7.9: Capillary pressure function of Case 2, lower section.....	50
Figure 7.10: Capillary pressure function of Case 2, upper section.....	51
Figure 8.1: Hydrate saturation distribution for whole reservoir, Case 1a.....	57
Figure 8.2: Temperature distribution for whole reservoir, Case 1a .....	61
Figure 8.3: Hydrate saturation distribution near well-bore, Case 1a .....	65
Figure 8.4: Temperature distribution near well-bore, Case 1a .....	70
Figure 8.5: Hydrate saturation distribution for whole reservoir, Case 1b.....	75
Figure 8.6: Temperature distribution for whole reservoir, Case 1b .....	77
Figure 8.7: Hydrate saturation distribution near well-bore, Case 1b .....	79
Figure 8.8: Temperature distribution near well-bore, Case 1b .....	82

Figure 8.9: Hydrate saturation distribution for whole reservoir, Case 2a.....	85
Figure 8.10: Temperature distribution for whole reservoir, Case 2a .....	90
Figure 8.11: Hydrate saturation distribution near well-bore, Case 2a .....	95
Figure 8.12: Temperature distribution near well-bore, Case 2a .....	100
Figure 8.13: Hydrate saturation distribution near well-bore, Case 2b .....	105
Figure 8.14: Temperature distribution near well-bore, Case 2b .....	109
Figure 8.15: Cumulative methane release rate.....	113
Figure 8.16: Replenishment rate of methane production, 10 years.....	113
Figure 8.17: Replenishment rate of methane production, 20 years.....	114
Figure 8.18: Cumulative methane release from hydrates.....	114
Figure 8.19: Cumulative replenishment of methane production, 20 years .....	115
Figure 8.20: Cumulative replenishment of methane production, 10 years .....	115
Figure 8.21: Cumulative water production, 1 .....	116
Figure 8.22: Cumulative water production, 2 .....	116
Figure 8.23: Pressure profile for case 1a, 3 years.....	117
Figure 8.24: Pressure profile for case 1a, 30 years.....	118
Figure 8.25: Pressure profile for case 2a, 2 years.....	119
Figure 8.26: Pressure profile for case 2a, 4.5 years.....	120
Figure 8.27: Pressure profile for case 2a, 8 years.....	121
Figure 8.28: Pressure profile for case 2a, 20 years.....	122
Figure 8.29: Contribution of released methane, Holder [11].....	123
Figure 8.30: Contribution of released methane, Moridis [22].....	124
Figure A. 1: P - T diagram for hydrates of pure hydrocarbons (Sloan [1]).....	131
Figure A. 2: P - T diagram for hydrates of hydrocarbon mixtures (Sloan [1]) .....	132
Figure A. 3: Hydrate formation hysteresis (modified from Sloan [1]).....	133
Figure A. 4: Effect of inhibitors on hydrate formation (modified from Sawyer [5]) .....	134
Figure B. 1: Hydrate formation conditions from gas gravity (Sloan [1]).....	139
Figure B. 2: P-T diagram for methane hydrate (modified from Sloan [1]).....	140
Figure B. 3: Temperature-Concentration diagram for pure methane (Sloan [1]).....	141
Figure C. 1: Location of Messoyakha Field (Sloan [1]).....	143
Figure C. 3: Production history of Messoyakha Field (modified from Sloan [1]).....	146
Figure C. 4: Reservoir pressure change for Messoyakha Field (Sloan [1]).....	147
Figure C. 5: Dissociating front pressure change for Messoyakha Field (Sloan [1]).....	147

# CHAPTER 1

## INTRODUCTION

Natural gas hydrates are solid substances which resemble ice. They are **clathrate** compounds of water and hydrocarbon molecules in contact. Hydrates form through a physical process (a phase change) under proper temperature and pressure conditions.

Hydrates are obviously neither a new source of energy nor recently discovered. On the contrary; natural gas hydrates, because they cause complications and clogging problems when they form in production or transport lines, have always been considered a nuisance in petroleum and especially natural gas business since their early recognition with the beginning of industry. However, hydrate reservoirs; the subsurface occurrences of hydrocarbon hydrates have turned out to be a late discovered rich source of natural gas. This can be emphasized by the fact that; 1 m<sup>3</sup> of hydrate at certain temperature and pressure contains approximately 170 m<sup>3</sup> of methane at STP, where 1 m<sup>3</sup> of methane at the very same temperature and pressure can only make 30-50 m<sup>3</sup> methane at STP (depending on the values of initial temperature and pressure).

Based on different studies of last 20 - 30 years, estimates on amount of hydrocarbon gas trapped in form of hydrate in reservoirs range between 10<sup>15</sup> to 10<sup>18</sup> m<sup>3</sup>, where this enclosed natural gas is mainly composed of methane (more than 95%). This amount roughly doubles the known recoverable fossil fuel reserves in the Earth (Sloan [1]).

The reason of recently growing interest in natural gas hydrates and attributed importance of gas production from hydrate reservoirs indeed lies in the promising but not fully explored potential of hydrate deposits as a huge and clean source for energy.

Since they are solid materials, hydrates have to be first decomposed into water and gas in the reservoir, in order to produce natural gas within. The energy required to dissolve a hydrate in the reservoir is only 10% of what the produced gas can give off. Hence with proper methods and techniques hydrates are an economical source of natural gas.

Although current knowledge of hydrates, proposed production methods shaped with today's technology and sometimes the economic constraints preclude most of the hydrate reserves

from being exploited feasibly, their apparent huge potential clearly deserves evaluation and improvement of methods, technology and knowledge.

In order to gain a better insight, acquire experience and sort out the associated difficulties, furthermore prepare foundations for future development and improvement of methods and technology, simulation modeling of gas production by depressurization from a theoretical hydrate reservoir using equilibrium model of dissociation is studied in this thesis.

In the studied 2 different reservoir models, one with 30% gas in the hydrate zone and other one with 30% water in the hydrate zone, the effect of well-bore heating is as well observed with different case studies.

## CHAPTER 2

### HYDRATES

Hydrates are solid, crystalline, ice like substances that form under appropriate pressure and temperature conditions slightly higher than freezing point of water. They are inclusion (*clathrate*) compounds of water and other (usually gaseous) molecules where water molecules build a cage of polygonal geometry (the *lattice*) surrounding a single molecule of other species. (Figure 2.1: Methane hydrate crystal unit)

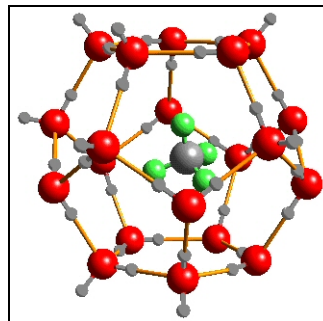


**Figure 2.1: Methane hydrate crystal unit**

Each lattice is a “crystal unit” indeed. Two or more different type of crystal unit combine in a certain pattern to form a “structure” and hydrate is build up of these repeating “structures”. In this sense, if one were to consider a single crystal unit as the “mer”, then hydrate would be the “polymer”.

The entrapped molecule is called the *guest* where the lattice of water molecules is the *host*. Any crystal unit in any structure can contain a single guest molecule at most and for sure the size of guest molecule must be small enough to occupy certain lattice. It is not required that all the crystal units in a hydrate volume be occupied by guest molecules, nonetheless a hydrate build up of completely empty lattices is unstable and thus can not exist (Holder [2]).

The type of bond between water molecules is hydrogen bond (a polar bond) and trapped molecule is encaged with Van der Waals bonds (a non-polar bond). Hence guest molecule is physically rather than chemically bonded and held inside the lattice formed by water molecules. Also the chemical bonds between the elements of water molecules or the

elements of gas molecules are not disturbed during formation of hydrate. This should be one of the reasons why hydrate formation (**hydration**) is attributed to be a phase change instead of reaction.

Hydrates are first discovered in 1810 by Sir Humphrey Davy when he identified chlorine hydrate in a laboratory study. In 1888 Villard discovered the existence of hydrocarbon hydrates. When Hammerschmidt found the occurrence of hydrates in pipelines blocking gas transmission it was 1934, then hydrates are involved in the context of oil industry. Yet, it took 35 years until naturally occurring gas hydrate deposits identified/recognized as a source of natural gas for production in 1969 by former Soviet scientists (Sloan [1]).

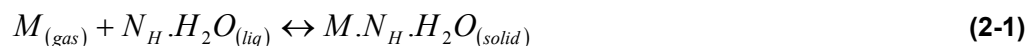
Some gases known to form hydrates are Cl<sub>2</sub>, Br<sub>2</sub>, SO<sub>2</sub>, CS<sub>2</sub>, CO<sub>2</sub>, H<sub>2</sub>S, Ar, Kr, CH<sub>4</sub>, C<sub>2</sub>H<sub>6</sub>, and C<sub>3</sub>H<sub>8</sub>.

## 2.1 Hydrates of Hydrocarbons (Natural Gas Hydrates)

At adequately low temperatures and high pressures water molecules attach and encage hydrocarbon molecules (which are in gas phase at STP) to build natural gas hydrates.

Most of the hydrate forms at the interface of fluid phase of hydrocarbon (usually gas) and aqueous phase of water. Verma has discovered that hydrates can form from the mixtures of liquid hydrocarbons and water too (Sloan [1]). Hydrates can also form from the gas dissolved in water and in the co-existence of ice and gaseous hydrocarbons.

Phase change from hydrocarbons and water to hydrate is represented with Equation (2-1):



Where;

M represents the guest species which could be either a pure component or a mixture.

N<sub>H</sub> is the hydrate number (hydration number)

Hydration number N<sub>H</sub> is the number of moles of water needed to form (one mole of) hydrate confining a single mole of gas (pure or mixture).

Five distinct crystal units (lattice) are known to result from the hydration of hydrocarbon molecules in the nature. These units are represented in numerical forms (5<sup>12</sup>, 5<sup>12</sup>6<sup>2</sup>, 5<sup>12</sup>6<sup>4</sup>, 5<sup>12</sup>6<sup>8</sup>, 4<sup>3</sup>5<sup>6</sup>6<sup>3</sup>) associated with their geometry (Figure 2.2: The 5 crystal units of natural gas hydrates and Figure 2.3: 3D view of some crystal units).

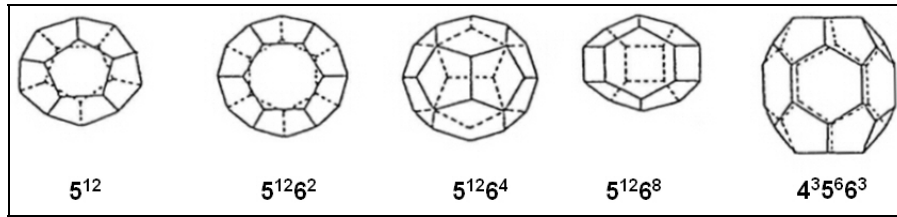


**Figure 2.2: The 5 crystal units of natural gas hydrates (Sloan [1])**

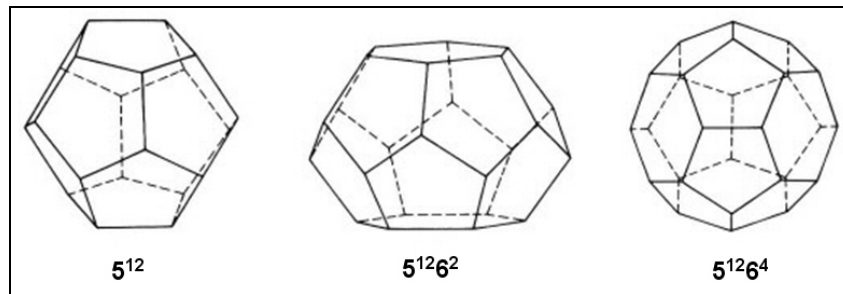


**Figure 2.3: 3D view of some crystal units (Sloan [1])**

As shown above, the general numerical representation of crystal units is:

$$n^m \tag{2-2}$$

Where;

n is edge number of certain face geometry

m is the number of faces with “n” edges

The hydration process of natural gases ensues in three distinguished combinations of crystal units; the crystal structures. And hydrate is actually built up by repetitive addition of these structures.

**Structure I (SI):**

It is a combination of 1<sup>st</sup> and 2<sup>nd</sup> type crystal units; which has 6 large and 2 small cavities per unit cell that is build up of 46 hydrogen bonded H<sub>2</sub>O molecules (Figure 2.4: Structure I). Here unit cell (a.k.a. unit cube or cubic cell) is defined as a cube of predetermined dimensions containing known number of crystal units and molecules. The ideal unit cell formula for Structure I is:

$$6X.2Y.46H_2O \tag{2-3}$$

Where;

X represents the guest molecule to fill in large cavities.

Y represents the guest molecule to fill in small cavities.

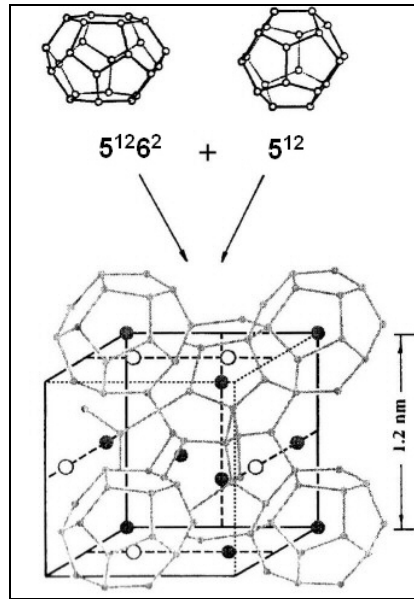


**Figure 2.4: Structure I (Sloan [1])**

The hydration number ( $N_H$ ) of Structure I hydrates ranges from 5.75 to 7.67 with an average of 6. Ideal hydrate number is 5.75 when all crystal units are occupied and 7.67 for large guest molecules that cannot fill small cages.

Pure methane, ethane, carbon dioxide or hydrogen sulfide usually forms Structure I hydrate.

**Structure II (sII):**

It is a combination of 1<sup>st</sup> and 3<sup>rd</sup> type crystal units; which has 8 large and 16 small cavities build by hydrogen bonding of 136 H<sub>2</sub>O molecules (Figure 2.5: Structure II).

The ideal unit cell formula for Structure II is:



Where;

X represents the guest molecule to fill in large cavities.

Y represents the guest molecule to fill in small cavities.

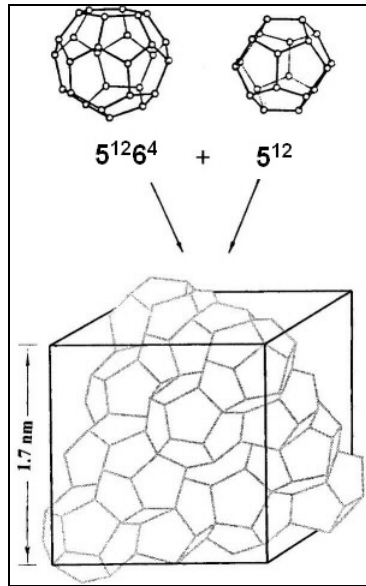


**Figure 2.5: Structure II (Sloan [1])**

Ideal hydrate number is 5.67 when all crystal units are occupied and 17 in case of large guest molecules that cannot fill small cages.

Structure II will form in the presence of even small quantities of heavier gases like propane or iso-butane. This reinforces the hydrate stability by lowering the dissociation pressure. As an outcome, Structure II hydrates are found in significantly wider range of geological P-T conditions than Structure I.

If all the cavities of either structure (SI or SII) are occupied, there will be 15 gas molecules per 85 water molecules.

**Structure H (sH):**

Structure H is initially discovered in a laboratory study by Ripmeester et al in 1987 and thought not to exist in nature until Sassen and MacDonald proved occurrence of Structure H hydrates in the Gulf of Mexico continental slope in 1994 (Sloan [3]).

This structure, when abundance of large molecules of hydrocarbon isomers demands existence of larger crystal units (such as  $5^{12}6^8$  found in Structure H), coexists with structure II in the temperature pressure conditions suitable for structure II formation.

In structure H hydrates, 34 water molecules correspond to 6 gas molecule and there are three  $5^{12}$ , two  $4^3 5^6 6^3$  and one  $5^{12}6^8$  crystal units in a unit cube (Figure 2.6: The three hydrate structures and associated crystal units).

Structure H is also called the “Double Hydrate” for 2 distinct guest species are needed for hydrate to be stable. One species fills in largest cavities of unit  $5^{12}6^8$  and other species fills in the smaller cavities.

The ideal unit cell formula for Structure H would be:



Where;

X represents the guest molecule to fill in large cavities ( $4^35^66^3$ )

Y represents the guest molecule to fill in small cavities ( $5^{12}$ )

Z represents the guest molecule to fill in largest cavity ( $5^{12}6^8$ )

Notice that while X and Y could be the molecules of the same component, Z should be the component with large molecules.

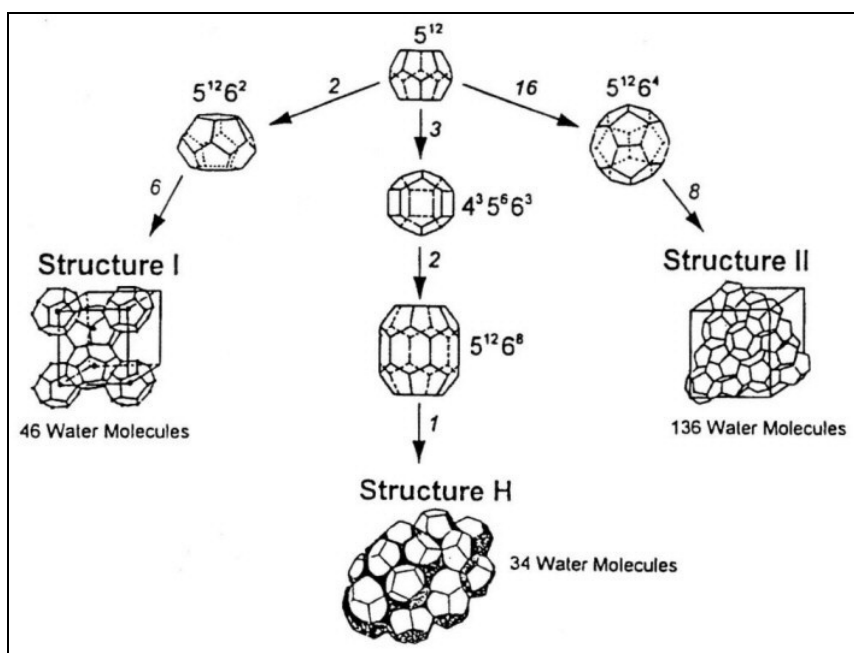


Figure 2.6: The three hydrate structures and associated crystal units (Sloan [3])

## 2.2 Properties of Hydrates

Most of the naturally occurring hydrocarbon gas hydrates involve more than 95% methane. One cubic meter of 90% saturated hydrate contains about 170 standard cubic meters of

methane while an empty container of same volume (1 m<sup>3</sup>) can contain 30-50 liters of methane at the same P-T with hydrate. Moreover hydrates contain more low solubility gases like methane than could be solved in water at the same temperature. Methane hydrate density at low pressure temperature region is about 0.9 g/cm<sup>3</sup>

Since hydrates consist of at least 85% water on molecular basis, most of its properties either resemble ice or approximates it. Nevertheless hydrates have a relatively lower thermal conductivity than water or ice (Thermal conductivity of hydrates is 0.49 W/mole/K at 263 K).

Approximately 10-20 kcal (63 kJ) of energy has to be added to one mole of hydrate in order to dissociate one mole of hydrocarbon gas.

### 2.2.1 Heat Capacity (Specific Heat)

The molar heat capacity of hydrates is computed from the Equation (2-8), Makogon [4]:

$$C_p = a + bT + cT^2 + dT^3 \quad (2-6)$$

Where;

C<sub>p</sub> in J/mole/K

T in K

a = 6.6

b = 1.454

c = -0.00364

d = 0.631\*10<sup>-5</sup>

### 2.2.2 Heat of Dissociation

Enthalpy of dissociation for hydrate is estimated using Clapeyron Equation (2-9) (Sloan [1]):

$$\frac{dP}{dT} = \frac{\Delta H}{T\Delta V} \quad (2-7)$$

Where;

$\Delta H$  is enthalpy (heat) of dissociation of hydrate could be either for formation from ice  $\Delta H_2$   
or from water  $\Delta H_1$ , in J

P is pressure in Pa

T is temperature in K

$\Delta V$  is the change in volume, m<sup>3</sup>

and

$$\Delta V_1 = V_{Hydrate} - [V_{Gas} + V_{Water}] \quad (2-8)$$

$$\Delta V_1 = V_{Hydrate} - [V_{Gas} + V_{Ice}] \quad (2-9)$$

For;

$$V_{Gas} \gg V_{Hydrate} \approx V_{Water} \approx V_{Ice} \quad (2-10)$$

$\Delta V_1$  and  $\Delta V_2$  can be approximated as:

$$\Delta V_1 \approx \Delta V_2 \approx V_{Gas} \quad (2-11)$$

$$V_{Gas} = \frac{znRT}{P} \quad (2-12)$$

$$\frac{dP}{dT} = \frac{\Delta H}{T \frac{znRT}{P}} \quad (2-13)$$

$$\frac{d(\ln P)}{dT} = \frac{\Delta H}{znRT^2} \quad (2-14)$$

$$\frac{d(\ln P)}{dT} = \frac{\overline{\Delta H}}{zRT^2} \quad (2-15)$$

Where;

R, gas constant 8.316, J/mole/K

z, compressibility (z) factor

$\overline{\Delta H}$ , molar enthalpy J/mole

$V_{Gas}$ , the volume of methane-water vapor mixture

It should be noted that here  $\overline{\Delta H}$  is the enthalpy of dissociation of hydrate which released 1 mole of methane and water vapor mixture in gas phase as a result of decomposition at equilibrium pressure P and equilibrium temperature T.

## CHAPTER 3

### HYDRATE RESERVOIRS

Natural Gas (more than 90% methane) comes into contact with water in sediments to form hydrates and hence hydrocarbon hydrate deposits exist where thermodynamic conditions are suitable for hydrate formation and there is enough water and hydrocarbon.

Hydrate occurrence is determined by both direct evidences like sample cores after drilling and indirect evidences such as well logging or seismic techniques.

Hydrates are wide spread in deep ocean crusts at outer continental margins (marked by numbers on the world map, Figure 3.1) where low temperatures and high pressures are available and in some portion of permafrost regions (marked by letters on the world map, Figure 3.1) where surface temperatures are extremely low hence temperature at any depth beneath the surface is also relatively low (Figure 3.2).

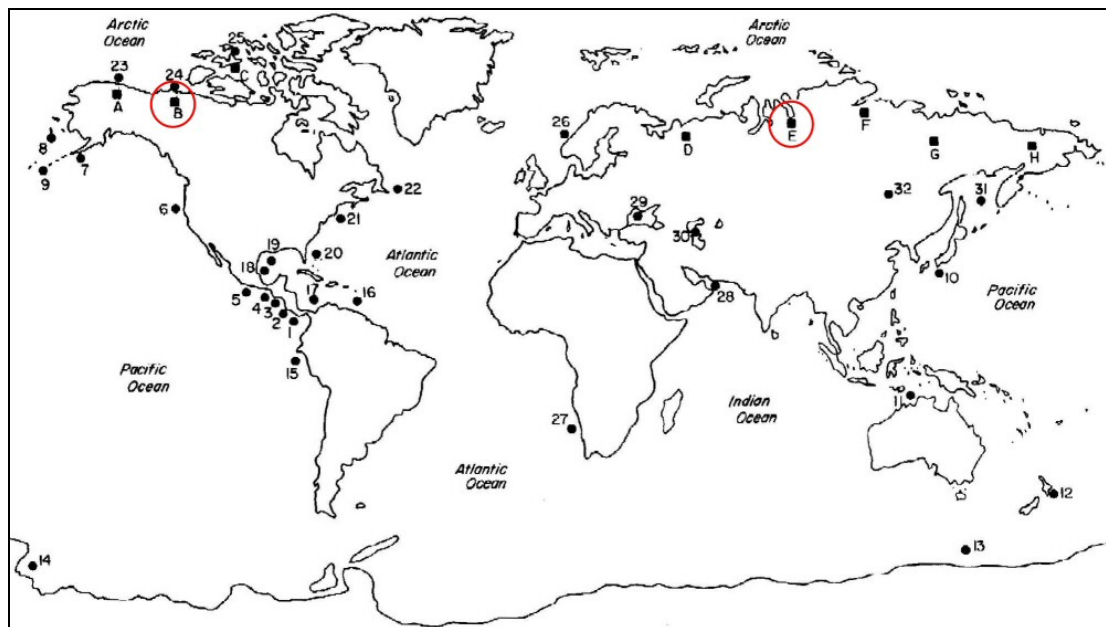
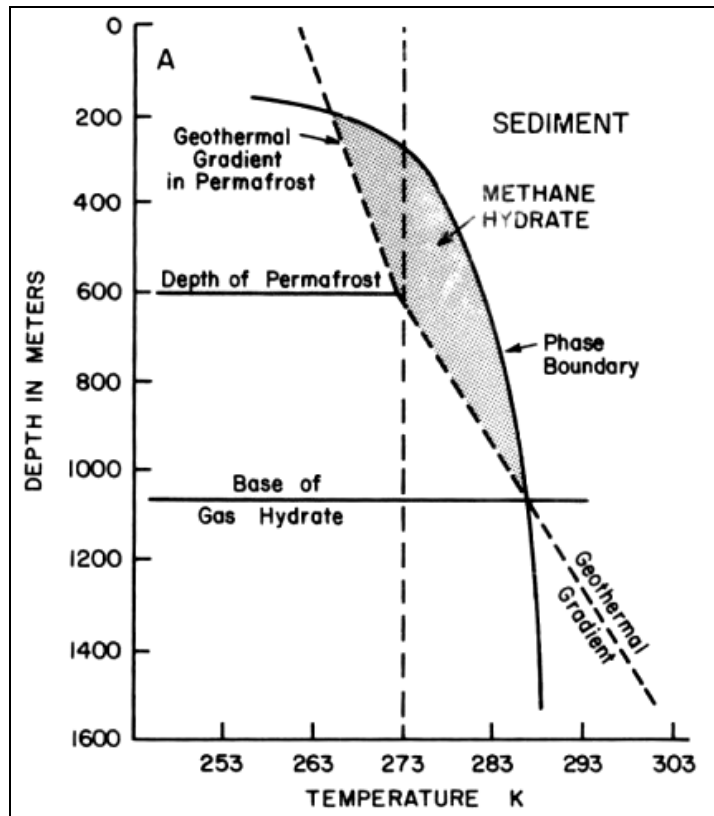


Figure 3.1: Hydrate deposit locations (Sloan [1])



**Figure 3.2: Hydrate window (Depth-Temperature diagram) for permafrost (Sloan [1])**

Hydrates even occur in the ocean sediments around equator where one might not anticipate ice-like compounds. However, as the *hydrate window* (depth – temperature diagram) (Figure 3.2 and Figure 3.3) suggest hydrates can form at temperatures above ice point at adequately high pressures.

The existence of naturally occurring hydrates has been verified in Alaska, Canada (McKenzie Delta), Siberia (Messoyakha, Vulyui fields), Gulf of Mexico and some other deep oceans.

Though the most common way the hydrates known to form is from liquid water and gaseous hydrocarbons, they can also form in the crude oil reservoirs when liquid water is in coexistence with liquid hydrocarbon. It has been shown that hydrates exist in top parts of conventional oil and gas reservoirs too.

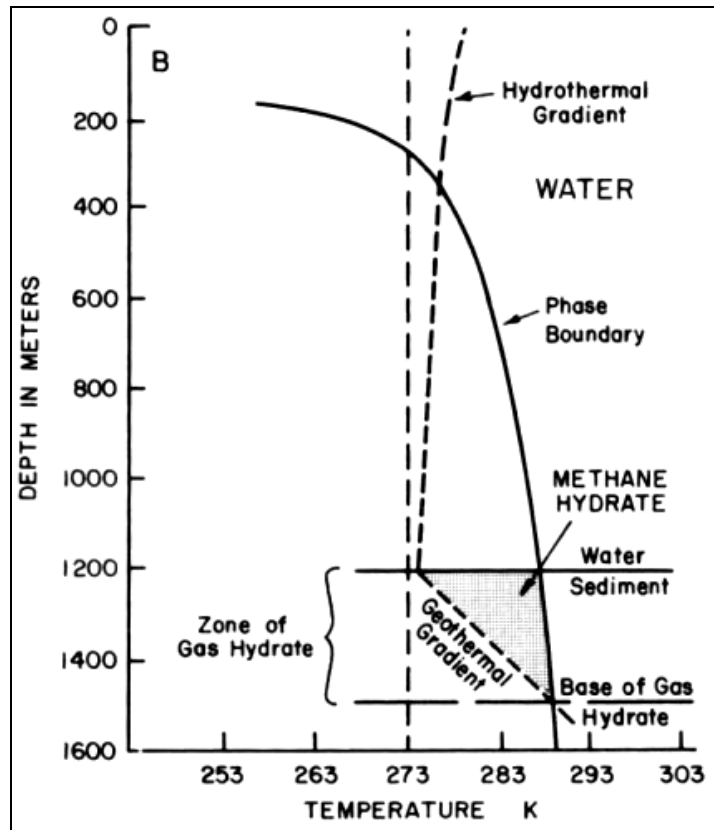


Figure 3.3: Hydrate window (Depth-Temperature diagram) for deep ocean (Sloan [1])

### 3.1 Origin of Gas in Hydrate Reservoirs

The gas trapped in hydrate reservoirs is considered to be of two origins (Sloan [1]):

#### Biogenic Origin:

Organic diagenesis of organic matter at low temperatures yields natural gas of mainly methane (more than 98%). Biogenic gases form Structure I hydrates due to lack of heavy compounds (being composed of mostly methane).

Because this gas is formed at low temperatures it may readily form the hydrate in the sediment (reservoir) where the gas itself is formed (the source rock). Therefore the hydrate of this origin is sometimes called “Recent in-situ hydrate”.

#### Thermogenic Origin:

At high temperatures, the catagenesis of organic matter results in natural gas richer in ethane and heavier hydrocarbon compounds. For they also involve molecules heavier than ethane, thermogenic gases form Structure II hydrates.

Since this type of gas is formed at high temperatures it should have migrated from deeper sediments (underlying hydrocarbon or coal reservoir as the source rock) to reservoirs at higher elevations. In these reservoirs that are in hydrate formation window (P-T envelope) the gas comes in contact with water to form hydrate.

It is also possible that thermogenic gases migrate into a pool of biogenic gases. Then one would expect both structure I and II hydrates in the same reservoir.

### 3.2 Occurrence of Hydrate in Reservoirs

Migrated or in-situ hydrocarbon gas, because it is lighter than water, moves upward in the reservoir. Hence there should be a seal rock at the top of reservoir. The permafrost layer may act as a seal too. About 90% of the pore water is converted to hydrate in the upper part of reservoir lying in hydrate formation window.

Experimental studies indicate the side factors influencing hydrate formation are (Sloan [1]):

- The degree of moisture saturation of the rock
- Gas water contact area
- Capillary radii of the pores, which causes vapor pressure of water to decrease and accordingly effects the hydrate formation pressure increase.

Mostly methane hydrates are found in earth at pressure ranges of 1 MPa to 50 MPa and temperature ranges of 264 K to 300 K. Beyond these ranges it is not only lower probability that hydrates will form but also it would be an insignificant amount.

Hydrates exist in 4 different distributions in the rock (Figure 3.4):

1. **Disseminated:** when hydrate size does not exceed pore size
2. **Nodular:** hydrate size exceed pore size but do not destroy pores.
3. **Layered:** size of hydrate varies from a few millimeters to several centimeters. Pore structure is destroyed and hydrates begin to act as concrete/cement.
4. **Massive:** extends many kilometers with several meters of thickness.

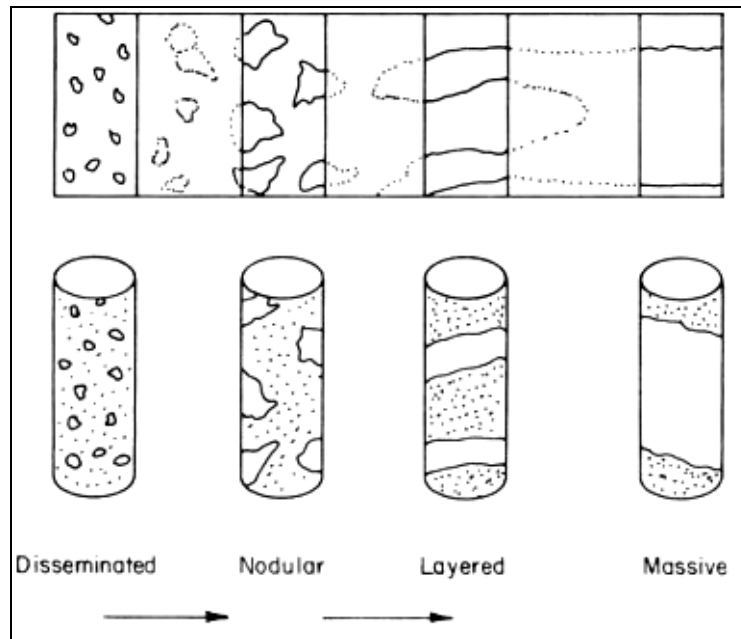


**Figure 3.4: Hydrate existence in reservoir (modified from Sloan [1])**

Actually these are the steps of evolution of hydrate. The initial formation of hydrates is in disseminated form. It then grows into nodules, then into layers and finally to massive hydrate. Similarly a reverse process may develop in the reservoir along many years. A massive hydrate may degrade into layered, nodular or disseminated ones with changing temperature and pressures during thousands of years.

### **3.3 Classification of Hydrate Reservoirs**

Apparently, hydrate reservoirs are subsurface occurrences of hydrates of natural gases; either in the pores of rocks or as a mass block. Hydrate reservoirs may be classified according to contents of porous medium (Moridis [6]):

**Class 1:** Hydrate above free gas zone, Figure 3.5

**Class 2:** Hydrate above free water zone

**Class 3:** Only hydrate zone in the reservoir, Figure 3.6

And Hydrate above free gas and water zones, Figure C. 2 (Combination Trap Reservoirs - Rose [7])

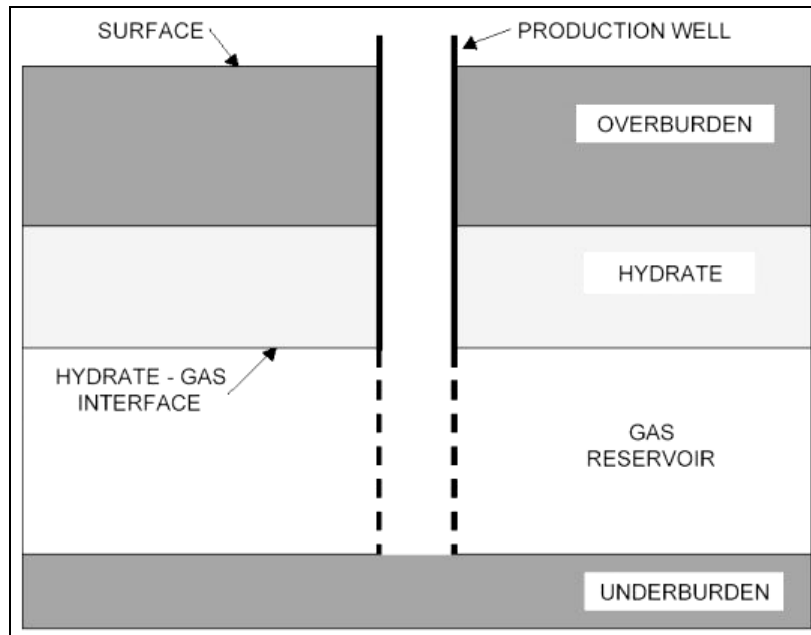


Figure 3.5: Hydrate reservoir Class 1 (Sawyer [5])

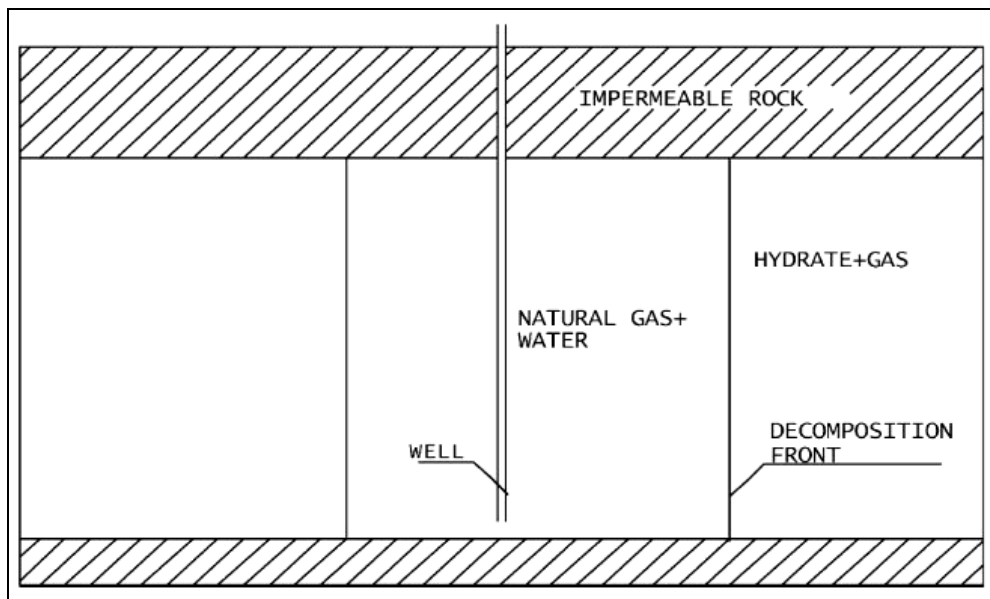


Figure 3.6: Hydrate reservoir Class 3 (Ji et al [8])

## CHAPTER 4

### GAS PRODUCTION FROM HYDRATE RESERVOIRS

Hydrates exist in solid state. Then they should be first dissociated into gas and water before gas can be produced conventionally through a regular well.

For hydrate dissociation there is some energy required to be added to the system because this is an endothermic process. This energy is supplied to the hydrate in two ways; it may be provided by the surroundings (surrounding fluid, hydrate, rock and formation), or it may be provided by means of some artificial source such as the thermal stimulation production scheme.

The energy required to dissolve hydrates in the reservoir is only approximately 10% of what the produced methane can give off (when heat losses are disregarded, Khairkhah [9]).

Hydrate decomposition does not happen in the whole hydrate volume in reservoir but at a surface where hydrate is initially exposed to the condition change. This surface is called the dissociating (decomposition) front.

Hydrates get colder when they decompose. Even though hydrate dissociation is an endothermic reaction, because the heat is partially supplied through the surrounding hydrate by conduction, these surrounding hydrates become colder naturally, resulting in a temperature gradient in the hydrate towards the dissociating front. Rate of hydrate decomposition is determined by the movement of this front or energy supplied to the front.

When a rapid dissociation is induced in a hydrate reservoir which is close to 3 phase equilibrium conditions, there could be local temperature drops causing hydrate (or ice) re-formation.

All known methods of dissociation of hydrates into gas and water, or in other words "methods of production", are based on shifting the reservoir conditions below the thermodynamic equilibrium and obtaining the energy required to decompose solid hydrate (Figure 4.1).

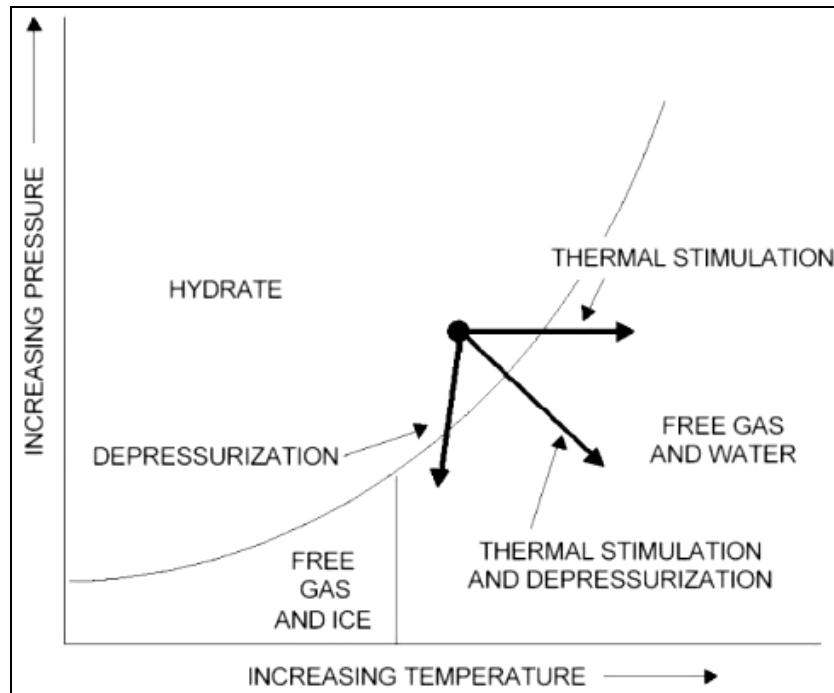


Figure 4.1: Production scheme effects on equilibrium (modified from Sawyer [5])

#### 4.1 Production Schemes

There are 3 main production schemes for hydrate reservoirs; thermal stimulation, depressurization and inhibitor injection (Figure 4.2).

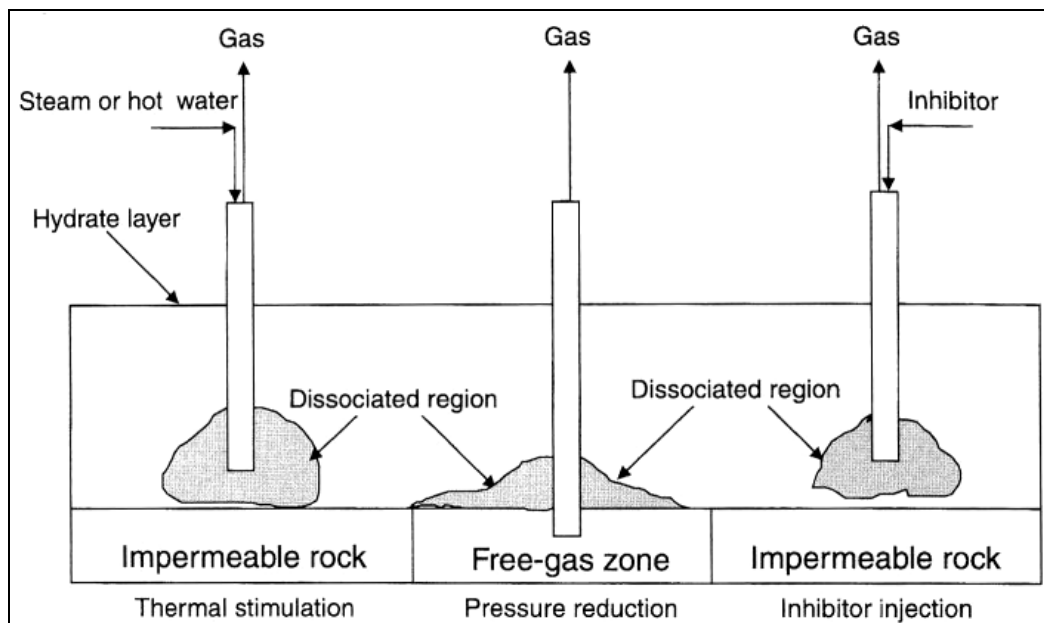


Figure 4.2: Production schemes (Khairkhah [9])

#### 4.1.1 Thermal Stimulation

Hydrate is somehow artificially heated above the dissociation temperature. Although the energy required to add to the hydrate for decomposition is only about 10% of its heating value when thermal injection models are used usually the heat losses to the surroundings is quite large, leaving the thermal models not a feasible choice for most of the hydrate reservoirs.

Thermal stimulation scheme includes:

- Steam injection (Figure 4.3)
- Hot liquid injection
- Fire sweeping
- Direct heating (using microwaves etc.)

Hot liquid injection is preferred over the steam injection because less heat loss occurs.

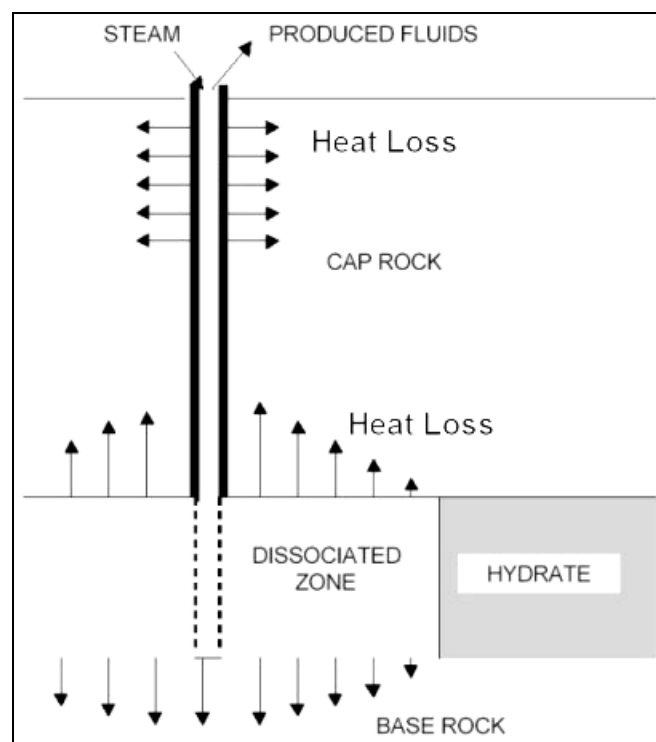


**Figure 4.3: Steam injection scheme (Sawyer [5])**

Rose [10], in 1982, has proposed a deep water hydrate production scheme involving utilization of geothermal water, which is usually found below the hydrate zone, as the hot liquid source for melting hydrate (Figure 4.4).

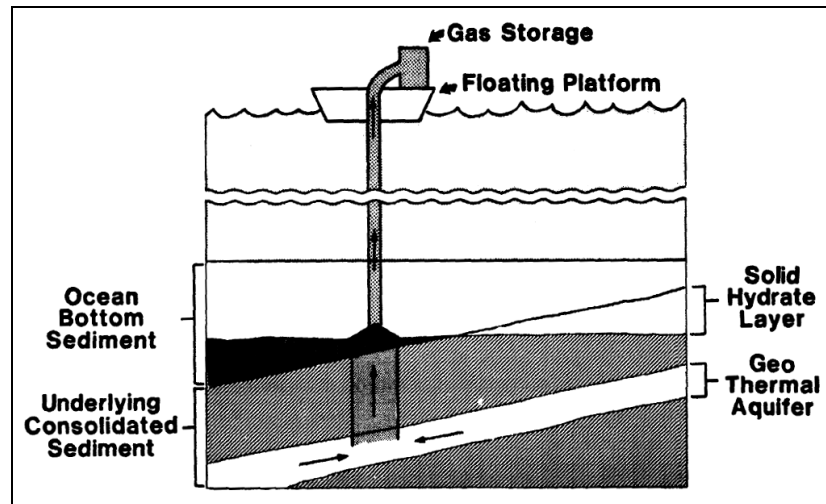


Figure 4.4: Production of deep water hydrates (Rose [10])

#### 4.1.2 Depressurization

The pressure on the hydrate is decreased below the equilibrium pressure by producing free gas (or water) below the hydrate.

Once it has begun by the lowering of pressure on it, decomposition of hydrate continues until vapor pressure on the hydrate is re-established by the dissociated gas for the new, colder temperature of reservoir. This new reservoir temperature is colder for required heat of decomposition is supplied from the sensible heat of reservoir and its contents.

The major drawback of this method is that the process is quite slow and may cause the dissociated water to cool down to ice phase resulting in the plugging of pores.

#### 4.1.3 Inhibitor Injection

An inhibitor, mostly methanol, is injected to the reservoir hence a shift in the Pressure-Temperature equilibrium is obtained.

Thermal stimulation alone is usually not favored. Because, although the energy required for gas hydrate to dissociate is about 10 % of its heating value, the hydrate reservoir location (especially the permafrost) brings the problem of extreme heat loss to the surroundings which in turn leaves the thermal stimulation scheme uneconomical compared to the other schemes or any combination of schemes (Khairkhah [9]).

## **4.2 Previous Experiences**

Though there have been extensive production tests carried out in the Mallik Field of Mackenzie Delta in Canada (indicated by letter “B” and a red circle on the left of Figure 3.1), the greatest field experience on hydrate gas production has been received by the engineers of former Soviet Union at Messoyakha field in Siberia (indicated by letter “E” and a circle on the Figure 3.1) where both industrial and scientific production had been continued about 19 years (Sloan [1]). See Appendices C for further information on Messoyakha field.

# CHAPTER 5

## PRODUCTION MODELING

Several studies on modeling of production from hydrate deposits have been published in the literature during the last 25 - 30 years. In the early modeling studies of former Soviet scientists, production of gas from hydrate reservoirs was assumed to occur isothermally. Hence their models did not consider heat changes or balance in the reservoir, leading weak estimations of production and contribution of trapped hydrate gas. Nonetheless, hydrate decomposition is significantly an endothermic process so, as Holder and Angert [11] pointed out, appropriate models should account for heat flow in the reservoir as well as fluid flow.

The studies on subject matter can be grouped according to:

- **Reservoir type (class)**
  - Class 1 - Holder and Angert [11], Burshears et al [15], Moridis [6]
  - Class 2 - Moridis [22]
  - Class 3 - McGuire [12], Durgut and Parlaktuna [18]
- **Production scheme**
  - Hot fluid injection - Holder et al [2], Iseux [16]
  - Depressurization - Holder and Angert [11], Moridis [22]
- **Number of wells and reservoir scale:**
  - Single well - Holder and Angert [11], Moridis [22]
  - Multiple well - McGuire [12], Swinkels and Drenth [14], Moridis [22]
- **Model of dissociation (equilibrium or kinetic):**
  - Equilibrium - Swinkels and Drenth [14], Moridis [22]
  - Kinetic - Moridis [23]
- **Method of analysis (analytical or numerical) considered:**
  - Analytical - Khataniar et al [13], Goel et al [20]
  - Numerical - Holder and Angert [11], Moridis [22]

### **Reservoir Type:**

Frequently studied reservoir types are solid state (only hydrate zone, Class 3) reservoirs and two phase (free gas zone below hydrate, Class 1) reservoirs. Although reservoir type does not necessarily restrict production scheme; usually thermal stimulation is associated with solid state reservoirs and depressurization is preferred in case of two phase reservoirs.

**Production Scheme:**

Apparently; the thermal stimulation and pressure reduction are the most studied schemes. These techniques are also coupled with reservoir fracturing in some studies (McGuire [12]) and thermal stimulation alone tested for cases of injection - production well patterns as well. Almost every author prefers depressurization over thermal stimulation wherever possible since thermal methods, due high heat losses to the surroundings, usually result in low energy efficiency ratios (E.E.R.), where energy efficiency ratio is defined as seen in Equation (5-1).

$$E.E.R. = \frac{G(t)H.V.}{Q(t)} \quad (5-1)$$

Where;

G(t): total production till time t

H.V.: total heating value of the gas

Q(t): total heat input to the system up to time t

**Single or Multi Well Schemes:**

Usually single well models in a cylindrical or rectangular reservoir section are studied. Nonetheless; for hydrate deposits to be considered for economical production, multi well models on a full reservoir scale should be presented.

**The Equilibrium Model of Dissociation:**

In the early studies, lack of information on hydrates limited authors to base their models on the equilibrium model of dissociation in which decomposition rate of hydrate is solely determined by amount and rate of heat transferred into it. Heat energy needed to melt certain volume of solid hydrate into water and gas can be known, say 'B' kJ energy is needed per kg of hydrate. If 'A' kilojoules of energy is supplied to the hydrate in 1 minute, then 'A/B' kg of hydrate decomposes in this 1 minute period.

**The Kinetic Model of Dissociation:**

Hydrate dissociation is controlled by kinetic parameters as well; meaning that for certain volume of hydrate to decompose some additional parameters such as hydrate surface area, dissociation activation energy and pressure differential on the hydrate also prevail.

After the study of Kim et al in 1987 (Khataniar [13]); the gas release from hydrates is obtained as shown in Equation (5-2):

$$\frac{dG_H}{dt} = K_o A \phi e^{-E/RT} (P_e - P) \quad (5-2)$$

Where;

$G_H$  is gas released from hydrate

$K_o$  is equilibrium constant

$A$  is hydrate surface area (reservoir area)

$E$  is hydrate dissociation activation energy

$P_e$  is hydrate decomposition equilibrium pressure

$P$  is actual pressure on the hydrate

$\phi$  is porosity

The values of  $K_o$  and  $E$  are determined empirically and absence of adequate data still leaves kinetic model to be applicable in a few cases if not applicable at all.

#### **Method of Analysis (Analytical or Numerical):**

Analytical analysis is adequate for simple porous flow, material and energy balance applications, and moving boundary approaches for the decomposing hydrate in the reservoir. Obtaining analytical solutions of the governing equations usually requires many simplifying assumptions to be made, causing a substantial decrease in accuracy. Besides, analytical analysis and models are usually applicable in single well cases.

Numerical analysis constitutes reservoir simulation studies in which the governing equations of material and energy balance are solved employing numerical methods. This method is utilized in order to obtain most accurate results with least simplifying assumptions.

Apparently, due to simplifying assumptions made in great extent during analytical analysis, these models are often insufficient as pointed out by Swinkels and Drenth [14] and therefore numerical models shall be the focus of attention.

### **5.1 Review of Previous Modeling Studies**

Holder et al [2] studied a basic energy balance approach for steam injection scheme (1980) and shown that from thermodynamic point of view hydrates have a good potential for production. They considered the change in the enthalpy of steam entering and leaving the reservoir volume to be simply equal to change in heat of reservoir matrix plus heat of

decomposition of hydrate and heat required to bring decomposed and initially free gas and water to the new reservoir temperature.

Holder and Angert [11] made the first non-isothermal simulation study for depressurization production from a reservoir containing hydrate and free gas layers (free gas below hydrate) in 1982. They have considered a rectangular reservoir section and a single production well. Along with being a pioneering work on this subject, as the authors agreed in the conclusion of article, major flaw of the study is that it considered decomposed water not to affect gas flow and the hydrate-free gas interface to be a planar surface. Actually a single phase gas simulator was modified to model the production. The work had yield that hydrate gas could contribute to gas production from 20% to 30% regardless of the production rate and thermal capacity of the reservoir was sufficient to supply heat of decomposition for hydrate.

McGuire [12], in 1982, has developed two simple thermal stimulation models and one depressurization model for hydrate gas production from reservoirs with no free gas zone. First model is a frontal-sweep model analogous to steam flooding in heavy oil reservoirs, where hot water is injected from a central well and decomposed water and gas are produced from the surrounding production wells. In the second model there is one well for hot water to be injected and it is connected to a single production well with a hydraulically fractured zone which was needed to increase permeability of the reservoir. For a hydrate reservoir with no free gas zone to be produced effectively by depressurization method; McGuire considered the single production well to be hydraulically fractured too. He concluded that thermal stimulation was not feasible while pressure reduction technique yield encouraging results.

Burshears et al [15] prepared a two-phase numerical model to study hydrate contribution to production by depressurization from a reservoir containing free gas below hydrate zone (1986). Though the evolved water was accounted for in the flow equations, the hydrate - free gas interface was again assumed to be a straight planar surface. Nonetheless model also considers hydrate or ice re-formation in the regions of reservoir where temperature pressure conditions are suitable.

Iseux [16]; in 1991, proposed another analytical thermal stimulation method involving hydraulic fracturing similar to McGuire's work in 1982 ([12]). The technique; Hot Solvent Stimulation after Hydraulic Fracturing, is similar to conventional acid fracturing where acid is replaced with the hot solvent. In this method an increase in the diffusivity of fluids is aimed for production from a single well but as mentioned earlier; McGuire had considered a two well scheme intending to increase reservoir permeability. Iseux also studied the economics of the model from points of view of Energy Efficiency Ratio and Production Cost.

Das and Srivastava [17] developed a finite-element numerical model for production of gas from a hydrate reservoir with hot fluid injection scheme (1993). Their two dimensional (2D, r-z) model accounted only for two dimensional heat conduction in a cylindrical reservoir section with a single production well at the center.

Durgut and Parlaktuna [18], in 1996, constructed a two phase simulator in order to model cyclic hot water injection into a hydrate reservoir at solid state and the rectangular deposit had a single well. They utilized a numerical scheme called IMPTES (Implicit Pressure-Temperature Explicit Saturation) and observed hydrate decomposition as a moving boundary.

Swinkels and Drenth [14], emphasizing the inadequacy of analytical models, carried out a comprehensive reservoir simulation study for production of gas from hydrate deposits by converting a conventional thermal reservoir simulator in 1999. According to Sawyer et al [5]; the only missing feature of this simulator is not being capable of handling hydrate dissociation kinetics. Based on the equilibrium model, the simulator could model any production scheme for any type of reservoir, well productivity and multiple well arrangements. Furthermore, thermal interaction with surrounding strata is considered.

Ji et al [8] conducted a parametric study on gas production by pressure reduction technique for a hydrate reservoir without a free gas zone, in 2000. Their model treats hydrate decomposition by depressurization method as a moving boundary problem. The utilized linearization scheme for the coupled equations removes the requirement of using numerical methods yet it causes heat conduction to be neglected in the entire reservoir. Ji et al [19], later (in 2002) repeated the same study with a finite difference numerical scheme instead of linearization. Comparing the result with previous analytical model of linearization scheme they concluded numerical model to be more accurate.

Goel et al. [20] analytically modeled production from cylindrical section of a solid state hydrate reservoir with radial decomposition front (2001). The dissociation kinetics was also incorporated into the equations by defining a rate equation for decomposition of hydrate.

Khataniar et al [13], in 2002, prepared an analytical model combining dissociation kinetics, inflow performance relationship and material balance equations. This study considered a depressurization scheme for a rectangular hydrate reservoir with free gas zone and a single production well in the center. The authors had created an economical analysis model as well to incorporate with production model. The economical model allowed sensitivity analysis by varying gas price and transportation cost. Moreover, the results of the analysis on hydrate

reservoir were compared with an equivalent only free gas reservoir in order to visualize contribution of hydrate zone.

The article of Sawyer et al [5] extensively reviews the most prominent studies on the subject matter and compares them from a point of real life applicability. The authors conclude that a “full featured hydrate simulator” should be capable of modeling any production scheme for single or multiple wells in field scale reservoir using either kinetic or equilibrium models of decomposition.

Moridis et al [21] developed an equation of state module (EOSHYDR) in 1998 for general purpose reservoir simulator TOUGH2 in order to model production of gas from hydrate deposits. The flexible and open structure of TOUGH2 is independent of grid geometry, number of phases as well as components and provides a variety of matrix solution schemes. This feature allows the EOSHYDR module to be capable of modeling production from cylindrical reservoir sections with a single well and whole reservoir with multiple wells in any arrangement (injection - production). The module accounts for all fluid phase flows both in pores and fractures, phase changes from hydrate to gas and water or vice a versa, and changes in hydrate formation conditions due to salt concentration. Plus, it is possible to use either the equilibrium or kinetic model of dissociation according to user's choice. Hence it is possible to model any production scheme in any reservoir structure. However, this first module considered only methane hydrates.

Moridis [22] later improved first module (EOSHYDR) to a newer, even more comprehensive version (EOSHYDR2) in 2002. The new module regards the existence of a secondary hydrate gas (such as ethane) and inhibitors. Furthermore it can keep track of initially free gas and later liberated gas distinctively; such a feature exhibits a great opportunity to observe instantaneous contribution of trapped gas to the production.

Moridis et al [23] published TOUGH-Fx/HYDRATE as the first member of TOUGH-Fx, the successor of TOUGH2. This new code includes both equilibrium and a kinetic model of hydrate formation and dissociation. It is capable to model the non-isothermal gas release, phase behavior and flow of fluids and heat under typical conditions of natural methane-hydrate deposits.

## CHAPTER 6

### STATEMENT OF THE PROBLEM

In this thesis, numerical modeling of gas production by depressurization from a theoretical hydrate reservoir using equilibrium model of dissociation is studied through utilization of TOUGH-Fx/HYDRATE code (Moridis et al [23]). Two different reservoir models, one with 30% gas in the hydrate zone and other one with 30% water in the hydrate zone are considered. In both reservoir models, the underlying free gas zone of hydrate zone is composed of 70 % gas and 30 % of water. The effect of well-bore heating is also investigated for both reservoir models.

In order to be able to compare modeling results with literature, the theoretical reservoir, fluid and production parameters were adapted from the article of Moridis [21] who also used the theoretical data from the earlier study of Holder [11]. When needed, these parameters are altered to the values estimated to create best approximate conditions.

With current information on hydrate reservoirs (Moridis et al [23]), the hydrate saturation and pressure-temperature conditions used by Holder [11] and adopted in this thesis are unrealistic for it is not possible to find hydrate reservoirs above 13-14 °C in permafrost and in deep water hydrate reservoirs hydrate saturation would not be as high as 70%.

# CHAPTER 7

## SOLUTION OF THE PROBLEM

### 7.1 Case Study

The studied 2 main cases are distinguished by the fluid content in the hydrate zone:

- Case 1: 30% gas in the hydrate zone
- Case 2: 30% water in the hydrate zone

Each case is further investigated with 2 different production schemes:

- a. With direct heat addition to the producing grids and a few other grids above these  
(Case 1a, Case 2a)
- b. Without any heat addition  
(Case 1b, Case 2b)

Direct heat addition was presumed to be necessary because of endothermic hydrate decomposition and Joule-Thomson cooling near the well-bore. The superposed effects of these processes is expected to cause hydrate formation at high saturations both at the producing and near well-bore grids, which would probably end up with shut-down of the well.

#### 7.1.1 Case 1: The Holder problem with 30% gas in the hydrate zone

There is 30% gas in the hydrate zone (70% hydrate) and 70% gas in the free gas zone (30% water). Though does not comply with field observation, such a distribution seems more natural at first sight since only gas phase (with a little liquid saturation as a result of capillary action) exists above the free gas zone and apparently it is easier to obtain as an initial condition.

The dissociation front, which is found practically in the middle of reservoir (vertically speaking), has a pressure of 20,684,250 Pa (~3000 psi) and a corresponding equilibrium (hydrate formation) temperature of 18.8757 °C.

### 7.1.2 Case 2: The Holder problem with 30% water in the hydrate zone

There is 30% water in the hydrate zone (70% hydrate) and 70% gas in the free gas zone (30% water). This saturation distribution is in accordance with the field observations and theory of formation of hydrate reservoirs. Because the gas is presumed to have migrated from deeper zones to a reservoir which is 100% water saturated initially, as well as the movement that is observed in the case of *ice lens* formation, it is the water component which is excess and resides with hydrate in the upper parts.

Difficulty of this problem is that a continuous column of approximately 30% water saturation has to be imposed as an initial condition in the reservoir, which practically means the existence of an only liquid saturated zone (in the 70% Hydrate zone) above a 70% gas saturated zone.

The dissociation front, which is found practically in the middle of reservoir (vertically speaking), has a pressure of 20,684,250 Pa (~3000 psi) and a corresponding equilibrium (hydrate formation) temperature of 18.8757 °C.

## 7.2 Reservoir Properties

A cylindrical, single well at the center, volumetric reservoir (Figure 7.1) is modeled with radial grids. Reservoir is 30 meters thick with a radius of 567.5 meters. In addition 1.001 meter thick intervals are added to the top and bottom of the reservoir to provide the necessary boundary conditions. Hence, height of the grid structure has been extended to 32.002 meters.

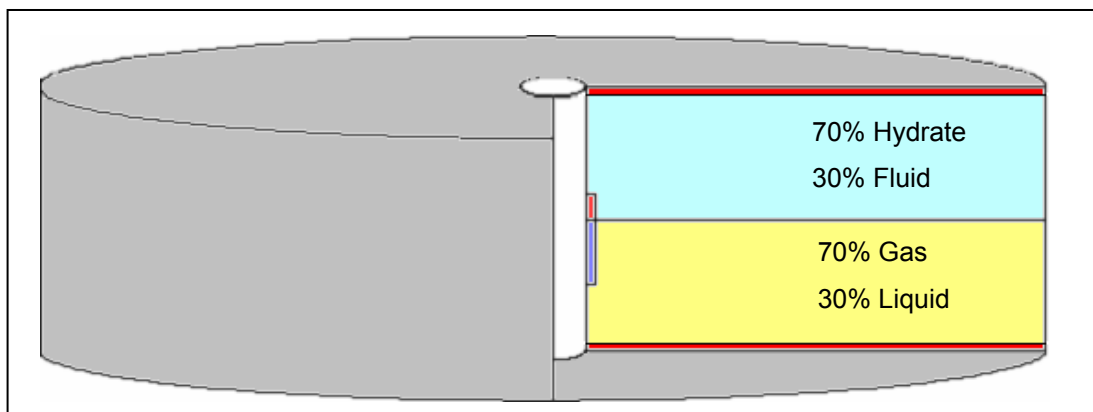


Figure 7.1: Schematic of theoretical reservoir (not to scale)

Reservoir rock is assumed to be sandstone with uniform porosity (30%) and permeability (44 md) in all directions. Reservoir rock properties are given in Table 7.1.

**Table 7.1: Reservoir rock properties (Moridis [21])**

<b>Reservoir Rock</b>	<b>Value</b>
Density	2600 kg/m <sup>3</sup>
Porosity	30%
Permeability	4.3425*10 <sup>-14</sup> m <sup>2</sup> (~44 md)
Specific heat	1000 J/kg °C
Heat conductivity	3.1 W/m °C (wet)
Heat conductivity	0.5 W/m °C (dry)
Pore compressibility	1.0*10 <sup>-8</sup> Pa <sup>-1</sup>

Upper half of the reservoir (top 15 meters) has 70% hydrate saturation while the lower half of the reservoir has a free gas saturation of 70% and 30% of liquid water, initially. Because the upper half of the reservoir is occupied by solid hydrate thus will not be significantly contributing to flow initially, it is presumed that well is completed in the top 10 meters of lower free gas zone.

### 7.3 Grid Structure

In case 1, Grid structure is composed of 77 radial elements with 48 layers in vertical direction, which makes a total of 3696 grids. In every layer, the radial distance between the first 4 consecutive grids is same and 0.5 meters. Then there are 73 grids with logarithmically increasing distance between them (Figure 7.2 and Figure 7.3).

In case 2, Grid structure is composed of 99 radial elements with 48 layers in vertical direction, which makes a total of 4752 grids. In all layers, the radial distance between the first two grids is 0.1 meter, and then 5 consecutive grids are the same with 0.2 meters. Afterwards there are 93 grids with logarithmically increasing distance between them (Figure 7.2 and Figure 7.3).

Layers have to be chosen as thin as possible to be able to accurately model and observe hydrate decomposition and saturation changes. 30 meters total thickness of reservoir is distributed in 42 layers while each of the top and bottom intervals representing boundary conditions were described by 3 layers (Figure 7.2 and Figure 7.3). The outermost layers at the top and bottom are very thin and are assigned the constant boundary temperatures. The following 2 layers are of 0.5 meters thick with no permeability and/or porosity for better description of heat flux to the actual reservoir. Layer data are given in Table 7.2.

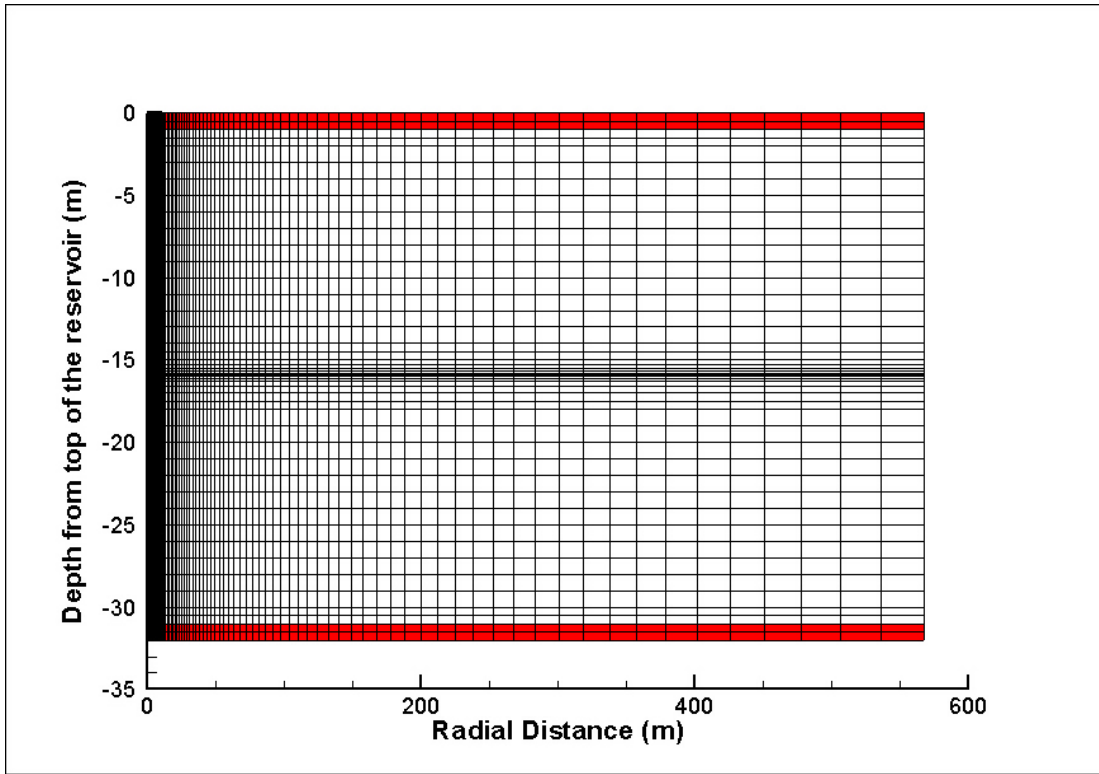


Figure 7.2: Grid structure of whole reservoir

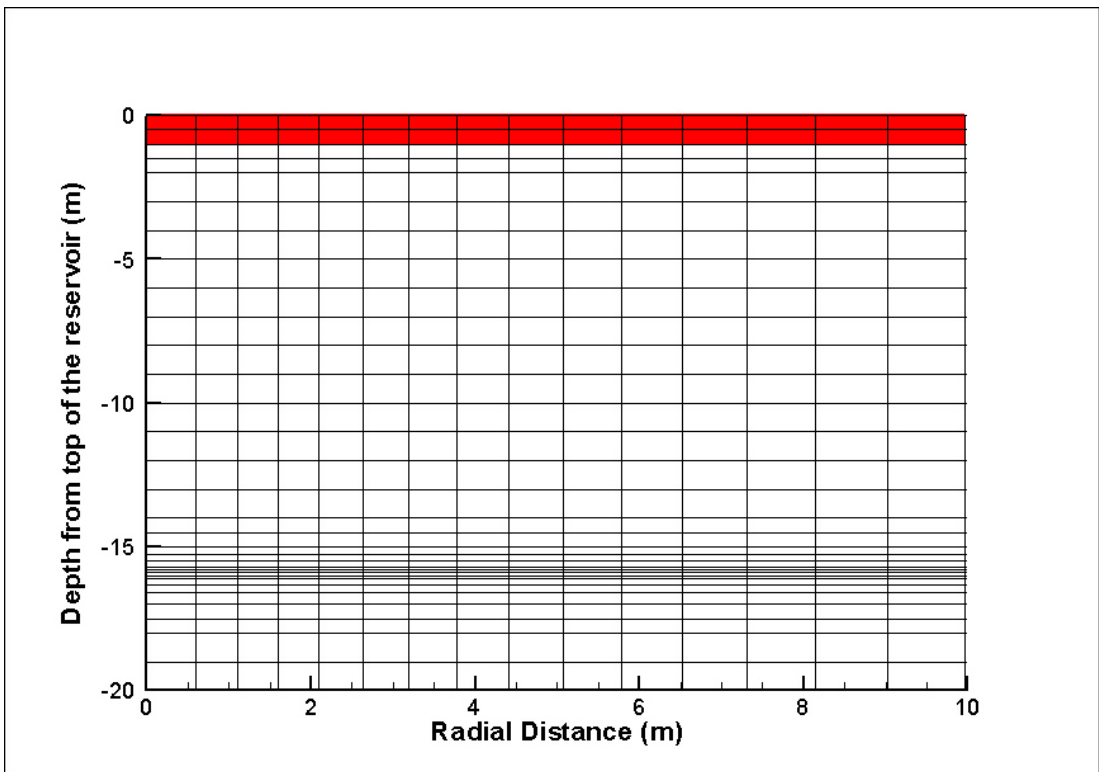


Figure 7.3: Grid structure near well-bore

### 7.3.1 Production Data:

A constant mass production rate of 0.555 kg/s (1137 MMCF/day equivalent) is specified. 30 year long production data was tried to be obtained as long as the physics allowed.

For all cases, constant mass production rate is rationed (according to grid volume) to the 1<sup>st</sup> column of small grids in the immediate vicinity of well bore which are indeed the inner most grids (14 layers, top 10 meters of free gas zone). The production data applied in all the cases is given in Table 7.3.

TOUGH-Fx computes fractions of components in the produced mass depending on the phase mobilities of producing grid elements (MOP(9) is 0). In other words, how much of which phase is produced in a grid is determined from the phase mobilities prevailing at that grid.

As mentioned earlier, some heat source was necessarily introduced along the column of producing grids and a few elements just above them (cases 1a & 2a). The distribution of heat sources to the column of inner most grids (for cases 1a & 2a) is given in Table 7.4.

**Table 7.2: Layer data**

# of layers	layer thickness Meter	total thickness meter	Explanation
1	0.001	0.001	Inactive constant P-T
2	0.500	1.001	for better description of heat flux No permeability
2	0.500	2.001	~70% Hydrate Saturation ~30% Liquid or Gas Saturation
12	1.000	14.001	
2	0.500	15.001	
2	0.250	15.501	
1	0.200	15.701	
2	0.100	15.901	
1	0.100	16.001	Dissociation Front
1	0.100	16.101	~70% Gas Saturation ~30% Liquid Saturation
1	0.200	16.301	
1	0.300	16.601	
1	0.400	17.001	
2	0.500	18.001	
12	1.000	30.001	
2	0.500	31.001	
2	0.500	32.001	
1	0.001	32.002	inactive constant P-T
<b>48</b>	<b>32.002</b>	<b>-</b>	<b>SUM</b>

**Table 7.3: Production data**

Layer	Depth (m)	Thickness (m)	Production (kg/s)
26	16.101	0.100	-5.55E-03
27	16.301	0.200	-1.11E-02
28	16.601	0.300	-1.67E-02
29	17.001	0.400	-2.22E-02
30	17.501	0.500	-2.78E-02
31	18.001	0.500	-2.78E-02
32	19.001	1.000	-5.55E-02
33	20.001	1.000	-5.55E-02
34	21.001	1.000	-5.55E-02
35	22.001	1.000	-5.55E-02
36	23.001	1.000	-5.55E-02
37	24.001	1.000	-5.55E-02
38	25.001	1.000	-5.55E-02
39	26.001	1.000	-5.55E-02
<b>Total:</b>			<b>-5.55E-01</b>

**Table 7.4: Heat source data**

Layer	Depth (m)	Thickness (m)	Heat addition (J/s)
20	15.251	0.250	5.00E+01
21	15.501	0.250	5.00E+01
22	15.701	0.200	4.00E+01
23	15.801	0.100	2.00E+01
24	15.901	0.100	2.00E+01
25	16.001	0.100	2.00E+01
26	16.101	0.100	2.00E+01
27	16.301	0.200	4.00E+01
28	16.601	0.300	6.00E+01
29	17.001	0.400	8.00E+01
30	17.501	0.500	1.00E+02
31	18.001	0.500	1.00E+02
32	19.001	1.000	2.00E+02
33	20.001	1.000	2.00E+02
34	21.001	1.000	2.00E+02
35	22.001	1.000	2.00E+02
36	23.001	1.000	2.00E+02
37	24.001	1.000	2.00E+02
38	25.001	1.000	2.00E+02
39	26.001	1.000	2.00E+02
<b>Total:</b>			<b>2.20E+03</b>

## 7.4 Simplifying Assumptions

Only methane is regarded as the hydrocarbon component. Though existence of other gases (excluding water vapor) even in small portions may dramatically change hydrate formation conditions, this is a reasonable assumption because in most of the hydrate reservoirs methane mass fraction in gas phase is about 99% (Sloan [1]).

Since only methane and water are considered to exist, structure I hydrates with an average hydrate number of 6.00 shall occur. Therefore mass fractions of methane (0.129) and water (0.871) in the hydrate body are constant values.

No salt or any other component other than water is considered; implying no inhibition of hydrate formation or any solid precipitation other than hydrate.

Trivial dissolution of methane in (liquid) water and existence of water vapor in gas phase is accounted through built-in capabilities of the code.

Phases in a grid element are decided solely by P-T couple on account of equilibrium model. For instance no hydrate should exist in a grid once P-T couple falls in the no hydrate zone. Ice formation in the pores is considered as it is inherent in the code.

Rock compressibility and associated change in pore volume are as well accounted by the code.

## 7.5 Governing Equations

For the reason that TOUGH-Fx is a compositional simulator and there are individual methane and water components, component mass balances have to be solved simultaneously:

$$\frac{\partial M^c}{\partial t} = -\nabla F^c + q^c \quad (7-1)$$

Where;

$M^c$  is mass accumulation of component c in the control volume (grid element)

$F^c$  is net mass flux of component c to the control volume (grid element)

$q^c$  is direct addition or removal of component mass (sink/source)

Mass accumulation of any component is computed from:

$$M^c = \phi \sum_{\beta} S_{\beta} \rho_{\beta} X_{\beta}^c \quad (7-2)$$

Where;

$\phi$  is porosity

$S_{\beta}$  is saturation of phase  $\beta$

$\rho_{\beta}$  is density of phase  $\beta$

$X_{\beta}^c$  is mass fraction of component c in phase  $\beta$

Mass flux of a component is calculated by adding contribution from phases:

$$F^c = \sum_{\beta} F_{\beta}^c \quad (7-3)$$

Where;

$F_{\beta}^c$  is the flux of component c in phase  $\beta$

Mass flux of component c in phase  $\beta$  is defined by Darcy equation:

$$F_{\beta}^c = -k \frac{k_{r\beta} \rho_{\beta} X_{\beta}^c}{\mu_{\beta}} (\nabla P_{\beta} - \rho_{\beta} \mathbf{g}) \quad (7-4)$$

Where;

$k$  is absolute permeability of rock

$k_{r\beta}$  is relative permeability to phase  $\beta$

$\mu_{\beta}$  is viscosity of phase  $\beta$

$P_{\beta}$  is pressure on phase  $\beta$

Because hydrate decomposition is substantially endothermic and thus a non isothermal reservoir is considered, energy equation has to be involved in solution as well:

$$\frac{\partial M^{heat}}{\partial t} = -\nabla F^{heat} + q^{heat} \quad (7-5)$$

Where;

$M^{heat}$  is heat content in the control volume (grid element)

$F^{heat}$  is net heat flux to the control volume (grid element)

$q^{heat}$  is direct addition or removal of heat (sink/source)

Heat content is described by:

$$M^{heat} = (1 - \phi)\rho_R C_R T + \phi \sum_{\beta} S_{\beta} \rho_{\beta} U_{\beta} \quad (7-6)$$

Where;

$\rho_R$  is density of rock

$C_R$  is rock specific heat

$U_{\beta}$  is internal energy of phase  $\beta$

Internal energy of a phase is calculated from component energies:

$$U_{\beta} = \sum_c X_{\beta}^c U_{\beta}^c \quad (7-7)$$

Heat flux accounting for both conduction and convection is expressed according to:

$$F^{heat} = -\lambda \nabla T + \sum_{\beta} h_{\beta} F_{\beta} \quad (7-8)$$

Where;

$-\lambda \nabla T$  is the conduction term

$\sum_{\beta} h_{\beta} F_{\beta}$  is the convection term

$\lambda$  is thermal conductivity of grid

$F_{\beta}$  is the mass flux of phase  $\beta$

$h_{\beta}$  is the specific enthalpy of phase  $\beta$

Specific enthalpy of a mobile phase (fluid) is computed from component enthalpies:

$$h_{\beta} = \sum_c X_{\beta}^c h_{\beta}^c \quad (7-9)$$

Enthalpy and internal energy are related to each other via Equation (7-10):

$$h_{\beta} = U_{\beta} + \frac{P_{\beta}}{\rho_{\beta}} \quad (7-10)$$

Thermal conductivity of a grid is calculated through the Equation (7-11) (MOP(10) is 0) which is derived by Moridis et al [23]:

$$k = k_{dry} + \left( \sqrt{S_A} + \sqrt{S_H} \right) (k_{wet} - k_{dry}) + \phi S_I \lambda_I \quad (7-11)$$

Where;

$k_{dry}$  is thermal conductivity of dry rock

$k_{wet}$  is thermal conductivity of wet rock

$S_A$  is liquid (aqueous) phase saturation

$S_H$  is hydrate saturation

$S_I$  is ice saturation

$\lambda_I$  is thermal conductivity of ice

Change in pore space is computed using the Equation (7-12):

$$\phi_f = \phi_i e^{C_r \Delta P} \quad (7-12)$$

Where;

$C_r$  is rock (pore) compressibility, pressure<sup>-1</sup>

$\phi_f$  is the final porosity

$\phi_i$  is the initial porosity

$\Delta P$  is the change in pressure

In all the above equations;

$\beta$  is for phases (solid, liquid and gas)

$c$  is for components (water and methane)

## 7.6 Numerical Solution of Equations

All conservation equations are strongly coupled and hence have to be solved simultaneously (no IMPES or SEQ method).

The non linear differential equations are first discretized and reduced to non linear algebraic equations before could be used in numerical computation.

TOUGH-Fx employs a fully implicit scheme for numerical solution of differential equations: both implicit in time discretization and implicit in linearization of coefficients of non-linear algebraic equations (which requires Newton-Raphson iteration).

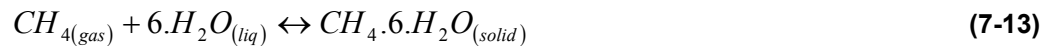
Interface density and phase mobilities are upstream weighted during the solution.

After the linearization, for solution of these linear algebraic equations a variety of matrix solvers are available in TOUGH-Fx. Nevertheless, during the simulation runs, conjugate gradient iterative method (Lanczos-type preconditioned bi-conjugate gradient solver) is kept as the default matrix solver for the code.

Differential equation discretization, remedy of non linearity by Newton-Raphson iteration for fully implicit scheme and simultaneous solution of linear equation's using matrix solutions are given in the TOUGH2 user's guide (Pruess [24]) and can be found in great detail in the text book Basic Applied Reservoir Simulation (Ertekin [25]).

## 7.7 Thermodynamic Properties

Since only methane and water are assumed to exist, structure I hydrates with an average hydrate number of 6 shall occur according to Equation (7-13):



Further more, this leads to constant mass fractions of components methane (0.129) and water (0.871) in the hydrate.

Hydrate formation (equilibrium) pressure for temperatures greater than 0 °C is computed using the equation derived by Moridis [1]:

$$\begin{aligned} \ln(P_e) = & -1.94138504464560 * 10^5 + 3.31018213397926 * 10^3 * T \\ & - 2.25540264493806 * 10 * T^2 + 7.67559117787059 * 10^{-2} * T^3 \\ & - 1.30465829788791 * 10^{-4} * T^4 + 8.86065316687571 * 10^{-8} * T^5 \end{aligned} \quad (7-14)$$

Where;

T is temperature in K

P<sub>e</sub> is equilibrium pressure in MPa

## 7.8 Hydrate properties

Hydrate thermal conductivity, specific heat and density are all considered to be constants and their values are presented in Table 7.5.

**Table 7.5: Hydrate properties**

Hydrate Density	920 kg/m <sup>3</sup>
Hydrate Specific Heat	2100 J/kg °C
Hydrate Heat Conductivity	0.45 W/m °C

Enthalpy change of solids is computed by the Equation (7-15):

$$dh = C_p(T) * dT \quad (7-15)$$

Where;

C<sub>p</sub> is the specific heat of substance, usually a function of temperature

Therefore hydrate enthalpy is computed by the Equation (7-16):

$$h_H = \int_{T_0}^T C_p(T) * dT \quad (7-16)$$

Hydrate decomposition enthalpy is estimated from Clapeyron equation (Equation 7-17) as stated earlier in section 2.2.2:

$$\frac{d(\ln P)}{dT} = \frac{\Delta H}{znRT^2} \quad (7-17)$$

Where;

P is system pressure, Pa

T is system temperature, K

R, gas constant 8.316, J/mole/K

z, gas compressibility factor

$\Delta H$  , dissociation enthalpy, J

It should be noted that here  $\Delta H$  is the enthalpy of dissociation of hydrate which released n moles of methane and water vapor mixture in gas phase as a result of decomposition at equilibrium pressure P and equilibrium temperature T.

Then, decomposition enthalpy is included in the main energy equation as if it was an additional sink/source term (Equation 7-18). This way, the expected cooling due to

endothermic nature of decomposition can be introduced to all the components and rock matrix present in the grid when dissociation occurs:

$$q^{heat} = q^d + \sum_{k=A,G} H_{\beta} q_{\beta} + \phi (dS_H) \rho_H \Delta H^0 \quad (7-18)$$

Where;

$q^d$  is direct addition or removal of heat via microwave etc.

$H_{\beta}$  is enthalpy of produced or injected fluid phase  $\beta$

$q^{heat}$  is mass addition or removal rate of mobile phase  $\beta$

$\phi$  is porosity

$dS_H$  is the change in hydrate saturation

$\rho_H$  is hydrate density kg/m<sup>3</sup>

$\Delta H^0$  is the hydrate decomposition enthalpy, J/kg

Liquid and gas phase enthalpies are computed using the routines available in TOUGH-Fx.

## 7.9 Phase Behavior

Existence of water vapor in the gas phase and negligible amount of methane dissolution in water are all accounted by the TOUGH-Fx/Hydrate code. An equilibrium model is employed for decomposition of hydrate. Therefore phases present in a grid are determined according to pressure and temperature of grid. If grid pressure-temperature couple is in the no-hydrate zone than there is water and gas in the pores. If P-T couple is in the hydrate zone than there is solid hydrate and excess gas (or excess water). Hydrate, water and gas may co-exist in a grid only if pressure and temperature are equilibrium values or in other words P-T couple is on the equilibrium line. Shall reservoir conditions ever cross the ice formation line, ice would form in the grids as it is also accounted by the code.

Phase changes are described by **variable switching (variable substitution)** technique in TOUGH-Fx/Hydrate, as it is in TOUGH2.

## 7.10 Problem Initialization

What is meant by problem initialization is the establishment of stabilized initial conditions along with boundary conditions. It is important to assign correct boundary conditions, indeed temperatures, and capillary pressure - relative permeability data to maintain the dissociation front at the desired depth, at steady-state.

As you shall read in detail the method of initialization in the following paragraphs, assigned boundary temperature at the top is not necessarily what corresponds to geothermal gradient. This is simply because, in the applied method here, one has to consider the heat flux to the dissociation front and should obtain same amount of heat flux from upper and bottom parts of the reservoir to the dissociation front in order to keep the location of front stable. When high saturation and higher thermal conductivity of hydrate in the upper part is recalled, it is obvious that a temperature value higher than the geothermal gradient should be assigned for the sake of obtaining steady-state initial conditions.

#### **7.10.1 Method of Initialization**

To prepare a hydrate reservoir which will be at steady-state, one should begin with separating the reservoir into upper and lower sections. These sections are individually prepared and after obtaining equal rates of heat flux to the decomposition front they are joined back. The layer, which is going to accommodate decomposition front properties, is where the reservoir is separated into 2 parts. Also, this layer should be included in both parts of the reservoir before they are united again to form actual reservoir, since it is going to act as an intermediate boundary condition. Moreover, during preparation of each part, the heat flow to this layer is needed to be equalized.

##### **Lower section:**

The layer for decomposition front is now the top layer of lower section and it is assigned to be inactive (constant boundary condition) with equilibrium P-T values as well as same hydrate and gas (or liquid) saturation as desired to be obtained in the upper section. The layer at the bottom is also assigned to be inactive with a temperature value corresponding to geothermal gradient. The 2 layers just above this last layer are not inactive but have 0 (zero) porosity and permeability implying that these 2 (and thus the bottom layer) have no contribution to flow and their pressure values do not matter. However, they are required for a better description of conduction heat flow from underlying strata to the reservoir. Table 4 gives the lower section layer data in details.

Rest of the layers are assigned the same P-T values as top layer (decomposition front). Their liquid and gas saturations are initially assigned to be exactly equal to what is desired in the lower region. Afterwards, a simulation without any sink/source term is carried out for this section and expected to reach steady state with new pressure, temperature and saturation distributions. Rate of heat flux to the dissociation front is noted for later comparison to the value obtained in the upper section.

**Table 7.6: Lower section layer data**

# of layers	layer thickness m	total thickness m	Explanation
1	0.100	0.100	Dissociation Front
1	0.100	0.200	~70% Gas Saturation ~30% Liquid Saturation
1	0.200	0.400	
1	0.300	0.700	
1	0.400	1.100	
2	0.500	2.100	
12	1.000	14.100	
2	0.500	15.100	
2	0.500	16.100	
1	0.001	16.101	Inactive (constant P-T) Temperature according to geothermal gradient
<b>24</b>			<b>SUM</b>

**Upper section:**

This time the layer for decomposition front has become the bottom layer of upper reservoir section. It is assigned to be inactive (constant boundary condition) with equilibrium P-T values as well as same hydrate and gas (or liquid) saturation as desired to be obtained in the upper section. The layer at the top is also assigned to be inactive, first with a temperature value corresponding to geothermal gradient. The 2 layers just below this layer are not inactive but have 0 (zero) porosity and permeability implying that these 2 (and thus the top layer) have no contribution to flow and their pressure values do not matter. However, they are required for a better description of conduction heat flow from overlying strata to the reservoir.

Rest of the layers are assigned the same P-T values as bottom layer (decomposition front). Their hydrate and gas (or liquid) saturations are initially assigned to be exactly equal to what is desired in the upper section. Later, a simulation without any sink/source term is carried out for this section and expected to reach steady state with new pressure, temperature and saturation distributions. Table 5 gives the upper section layer data in details.

When the simulation result is examined, the heat flux to the dissociation front is found to be different than the one obtained for the lower section. To make both equal, the simulation for upper section is repeated with different temperature values at the top, till same heat flux as lower section is obtained.

**Table 7.7: Upper section layer data**

# of layers	layer thickness m	total thickness m	explanation
1	0.001	0.001	Inactive (constant P-T)
2	0.500	1.001	for better description of heat flux no permeability
2	0.500	2.001	~70% Hydrate Saturation  ~30% Liquid or Gas Saturation
12	1.000	14.001	
2	0.500	15.001	
2	0.250	15.501	
1	0.200	15.701	
2	0.100	15.901	
1	0.100	16.001	Dissociation Front
<b>25</b>			<b>SUM</b>

Once the same heat flux is got for the upper and lower sections they are joined together and the layer for decomposition front is assigned to be active now (P-T and saturations may vary with time). A simulation run without any sink/source term has to be carried out again for the whole reservoir, before beginning the simulation of production. This is to make sure that reservoir is truly at steady-state in the absence of intermediate boundary condition which was temporarily assigned at the layer of decomposition front when the reservoir was divided into sections.

After this final run made in order to ascertain steady-state, when initial temperature distribution in the whole reservoir is observed, the deviation from the geothermal gradient (0.03 °C/m) can be clearly seen for Case 1 (a&b) in Figure 7.4 and for Case 2 (a&b) in Figure 7.5.

In Figure 7.4 and Figure 7.5, the observed divergence from geothermal gradient in the last meter of reservoir (between 31-32 meters interval) is because of no porosity layers (the two 0.5 meter thick layers). Apparently thermal conductivity is high in these layers, as it is in the upper section (hydrate zone).

When initial P-T values are plotted on a hydrate equilibrium line graph (Figure 7.6), it is easily observed that top portion of reservoir in case 1 remains in the hydrate formation zone. While almost lower half of the upper section in case 2 corresponds to a 3 phase (hydrate-liquid-gas) zone with some small gas saturation.

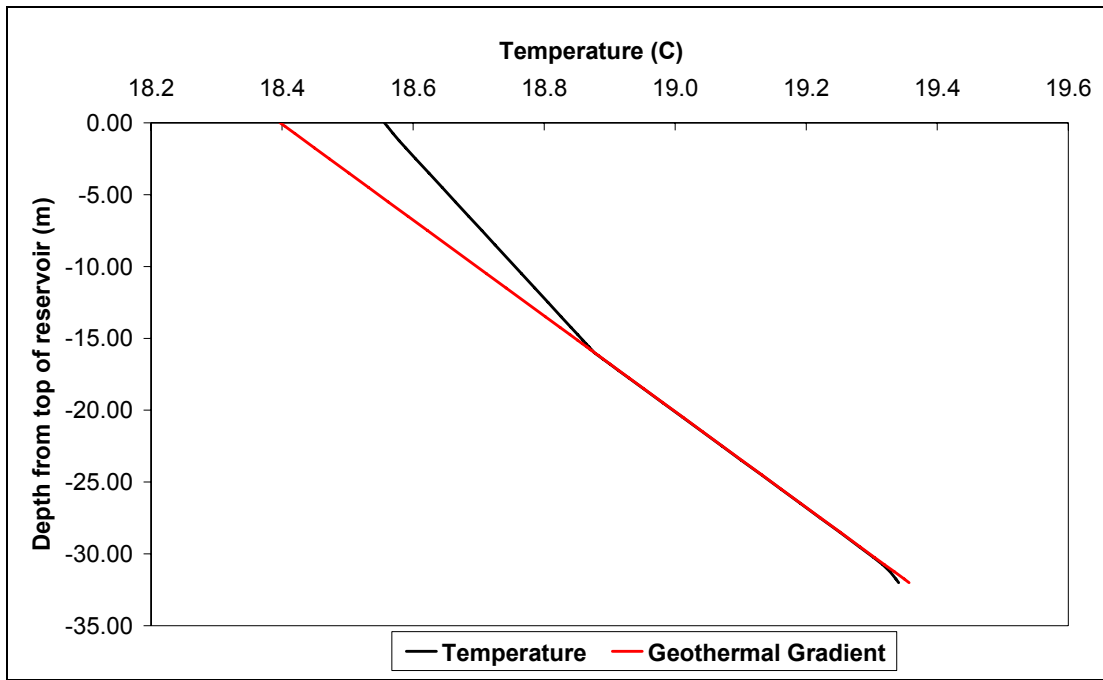


Figure 7.4: Initial vertical temperature distribution for Case 1.

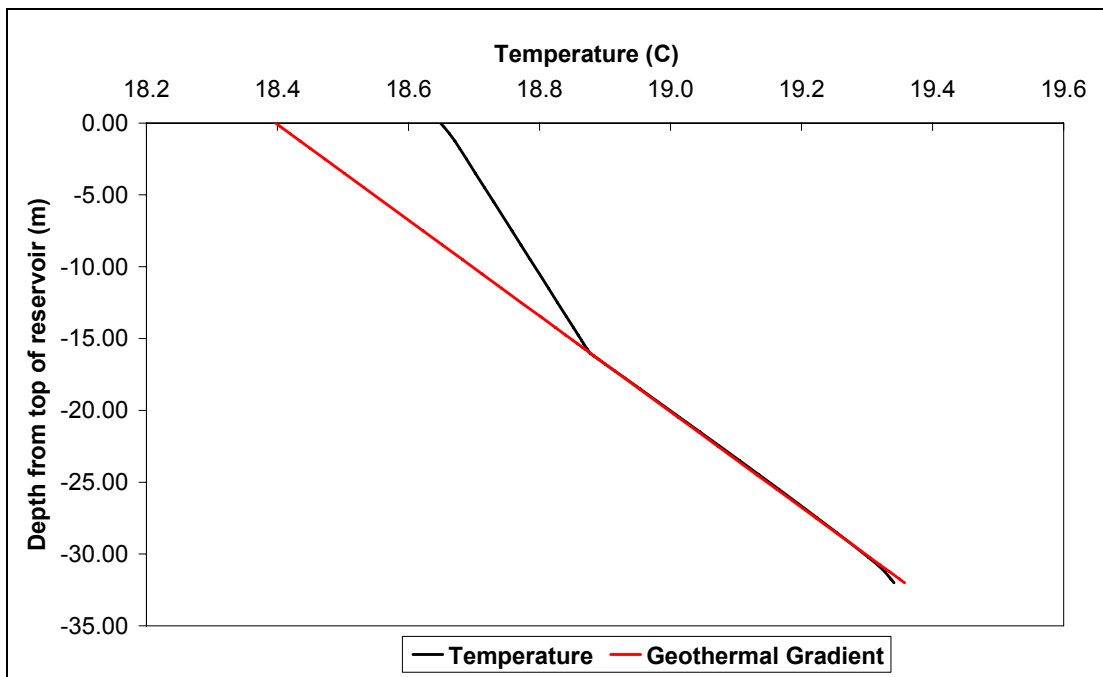


Figure 7.5: Initial vertical temperature distribution for Case 2.

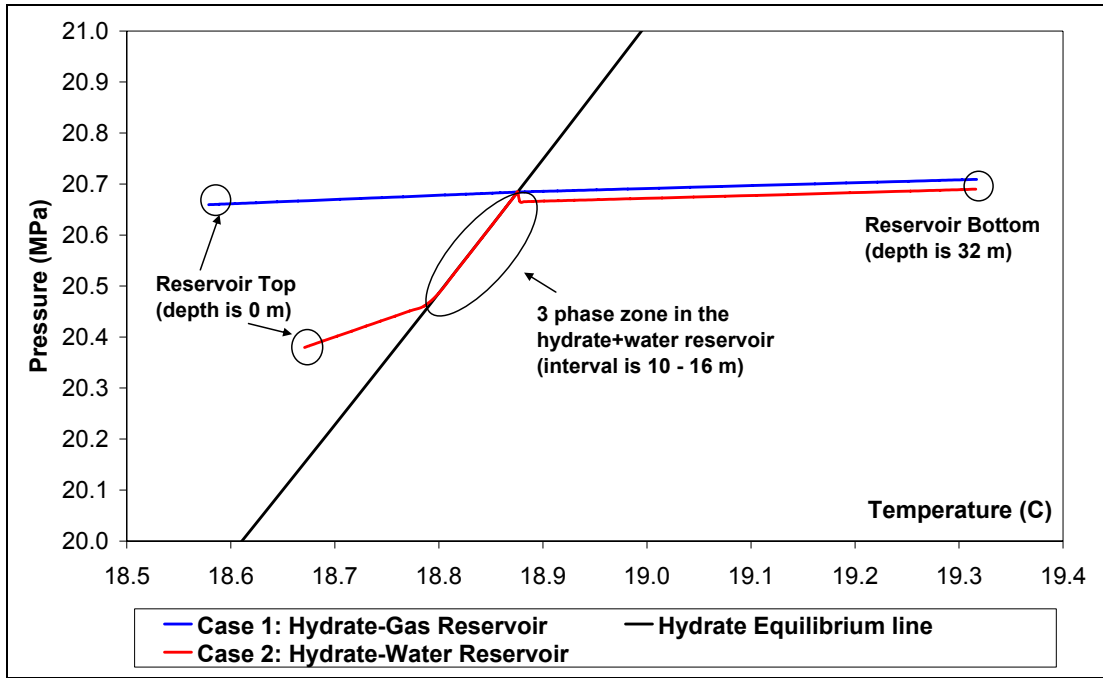


Figure 7.6: Initial Pressure-Temperature diagrams of Case 1 and Case 2.

### 7.11 Rock Properties:

Changes in porosity due to solid formation (or dissolution) can be easily calculated straight forward. However; changes in permeability is quite a complex issue to model accurately, because low porosity alterations may lead high permeability changes through clogging of pore throats.

Available “Original Porous Medium” (OPM) model in TOUGH-Fx is applied in this study to account for changes in permeability due to solid precipitation/formation in pore space.

The model does not bring any additional permeability reduction factor and in essence benefits from the fact that effective permeability to a phase is a function of the phase saturation and with increasing solid saturation there is an inevitable reduction in the saturation of mobile phase. Hence absolute permeability reduction is introduced within relative permeability changes.

$$k_{\beta} = k_0 k_{r\beta} \tag{7-19}$$

$$k_{r\beta} = k_{r\beta}(S_{\beta}) \tag{7-20}$$

Where;

$k_0$  is the absolute permeability

$k_\beta$  is the effective permeability to phase  $\beta$

$k_{r\beta}$  is the relative permeability to phase  $\beta$  as function of phase saturation according to original pore space.

### 7.11.1 Relative Permeability:

Stone's model (Moridis [23]) is chosen to accommodate relative permeability changes in all studied cases.

Gas relative permeability:

If  $S_g \leq S_{gr}$  then  $k_{rg} = 0$

If  $S_g > S_{gr}$  then;

$$k_{rg} = \min \left\{ \left[ \frac{(S_g - S_{gr})}{(1 - S_{lr})} \right]^n, 1.0 \right\} \quad (7-21)$$

Liquid relative permeability:

If  $S_l \leq S_{lr}$  then  $k_{rl} = 0$

If  $S_l > S_{lr}$  then;

$$k_{rl} = \min \left\{ \left[ \frac{(S_l - S_{lr})}{(1 - S_{lr})} \right]^n, 1.0 \right\} \quad (7-22)$$

Where;

$S_{lr}$  is irreducible liquid saturation

$S_{gr}$  is irreducible gas saturation

n is a constant

**Table 7.8: Parameters for relative permeability function**

Parameter	Value
n	3.00
$S_{lr}$	0.25
$S_{gr}$	0.02

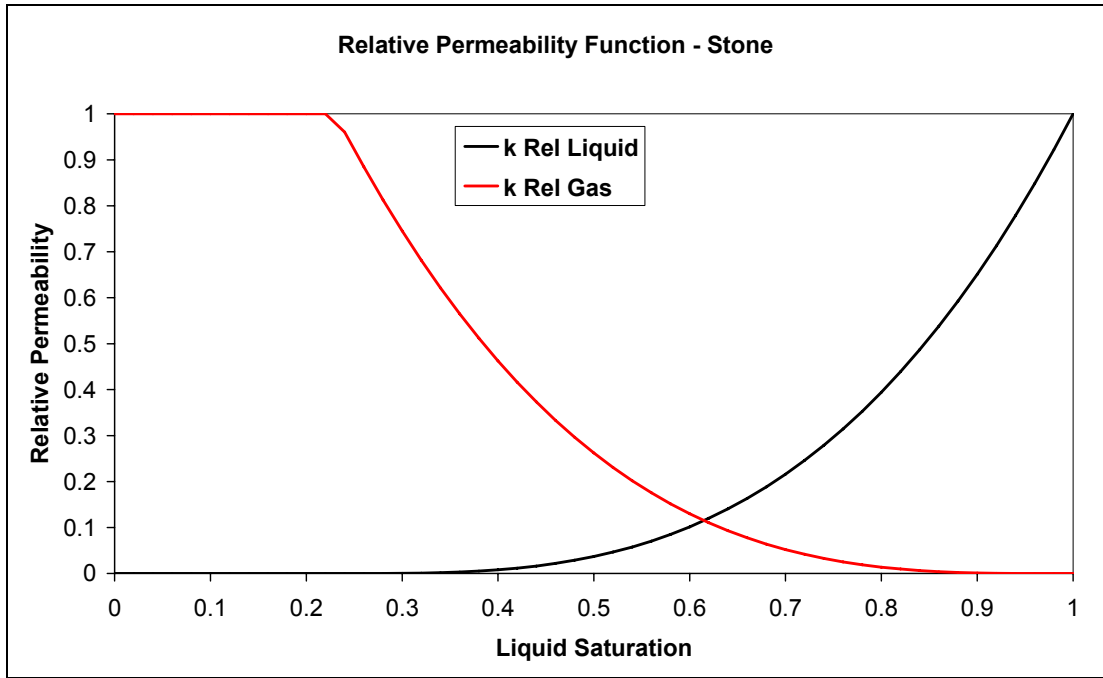


Figure 7.7: Relative permeability function - Stone

#### 7.11.2 Capillary Pressures:

In case 1 (with 30% gas in the hydrate zone) capillary pressure is modeled using the **van Genuchten** function (Pruess et al [24]).

$$P_{cap} = -P_0 \left( [S^*]^{1/\lambda} - 1 \right)^{1-\lambda} \quad (7-23)$$

Where;

$P_0$  is the strength coefficient

$$S^* = (S_l - S'_{lr}) / (S_{ls} - S'_{lr}) \quad (7-24)$$

$S'_{lr}$  is irreducible liquid saturation

and  $-P_{max} \leq P_{cap} \leq 0$

The irreducible liquid saturation in the capillary pressure function should be chosen smaller than the same parameter in the relative permeability equation ( $S'_{lr} < S_{lr}$ , Pruess et al [24]).

In Case 2, the need for using two distinct capillary pressure functions in the upper and lower sections has risen in order to retain the approximately 30% liquid saturation (which is significantly above irreducible saturation of ~25%) all along the upper and lower sections. Indeed, this means that two different porous medium are defined in the reservoir.

**Table 7.9: Capillary pressure function parameters of Case 1**

Parameter	Value
$\lambda$	0.60
$1/P_0$	$5.3 \cdot 10^{-4}$ Pa
$P_{\max}$	$1.0 \cdot 10^6$ Pa
$S'_{lr}$	0.245
$S'_{ls}$	1

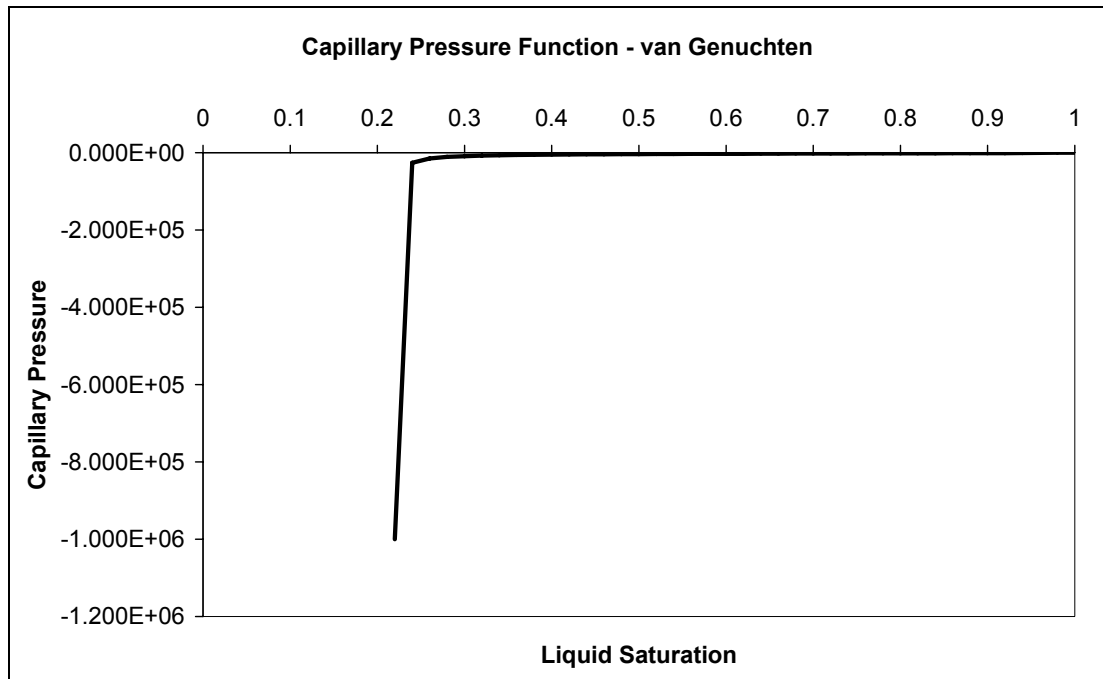


**Figure 7.8: Capillary pressure function of Case 1**

There is actually the problem of keeping a mobile liquid saturation trapped above a free gas zone. This might have been established by a different method such as by defining irreducible liquid saturation as a function of solid saturation where  $S_{lr}$  increases with increasing solid saturation. However, this would result in a completely immobile liquid saturation which would be contradictory to field observations. The discussion shall be detailed in the results and discussion chapter.

For the lower section of case 2, again the **van Genuchten** function (Pruess et al [24]) is employed with the parameters specified in Table 7.10.

**Table 7.10: Capillary pressure function parameters of Case 2, lower section**

Parameter	Value
$\Lambda$	0.50
$1/P_0$	$2.5 \times 10^{-4}$ Pa
$P_{\max}$	$5.0 \times 10^6$ Pa
$S'_{lr}$	0.249
$S'_{ls}$	1

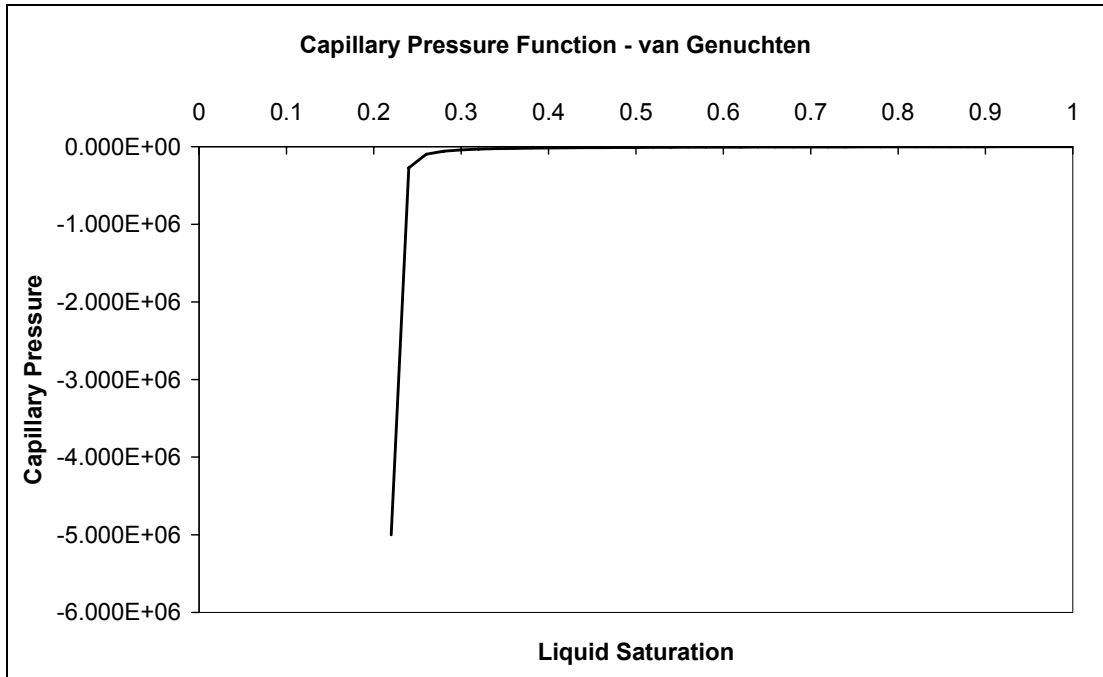


**Figure 7.9: Capillary pressure function of Case 2, lower section**

While a *van Genuchten* type capillary pressure is suitable for lower section, to be able to sustain ~30% liquid saturation initially in the hydrate zone (~70% hydrate), a function which gives high capillary pressures even at high liquid saturations is required. Therefore; for the upper section of case 2, a modified (continuous at  $S_l = 1.0$ ) **Brooks - Corey** function was defined in TOUGH-Fx/Hydrate (Moridis [23]). With this Equation (7-24) though the liquid in the hydrate zone is initially hold in place, it can be moved with adequate pressure difference.

$$P_c = -P_e * S_e^a * erf(60 * (1 - S_l)) \quad (7-25)$$

Where;

$P_e$  is the gas entry pressure

$S_e$  is defined by  $S_e = (S_l - S'_{lr}) / (1 - S'_{lr})$

$a$  is function of grain distribution, its value is in the range  $-1 < a < 0$

$S'_{lr}$  is irreducible liquid saturation

$erf(60*(1 - S_l))$  is an error function added to correct discontinuity present in the original equation.

**Table 7.11: Capillary pressure function parameters of Case 2, upper section**

Parameter	Value
$P_e$	$1.55 \times 10^5$ Pa
$a$	-0.350
$S'_{lr}$	0.249

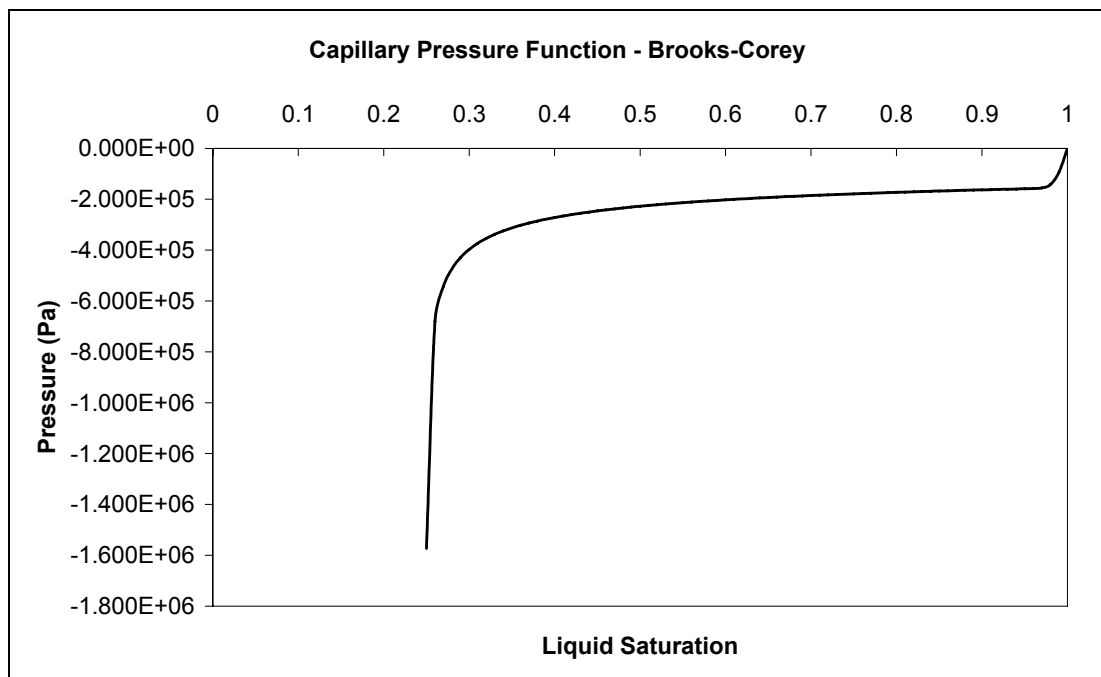


**Figure 7.10: Capillary pressure function of Case 2, upper section**

## CHAPTER 8

### RESULTS AND DISCUSSION

Even though the reservoir is 3 dimensional, because it is symmetric, pressure, temperature and saturation distributions obtained in simulation runs are carried to and shown on a 2 dimensional (Radial-Depth, R-Z) cross section from well-bore to outer radius (Figures 8.1 to 8.14).

Though a production period of 30 years was intended, it was not possible to obtain the data in all the cases. For instance; in case 2b the simulation stopped very early at 0.8 year. This was due to high amount of hydrate formation in a producing grid. The hydrate saturation was so high that it did not allow any fluid flow into or out of the element, so the well, hence the simulation was shut down.

Compared to pressure profiles of case 1 (Figure 8.23 and Figure 8.24) in case 2 (Figure 8.25, Figure 8.26, Figure 8.27 and Figure 8.28) there developed a high temperature zone in the interval of 13 - 16 meters as hydrate formation pressure lines indicate a large increase.

This large increase in temperature is due to high capillary pressure existing in the upper section. As dissociating hydrate absorbs heat it retains its temperature and so does the liberated water and gas. Because capillary pressure was not too high in case 1, released water and off course the gas could flow easily and carry away their heat. However, in case 2, liberated water could not move away that easily due to this high capillary pressure and consequently temperature of this interval is kept high.

#### 8.1 Hydrate Saturation Distributions

When hydrate saturation distributions for the studied cases are considered (Figure 8.3, Figure 8.11), it is apparent that 2 distinct dissociation patterns arise for the hydrate with gas (case 1) and hydrate with water reservoirs (case 2).

In the hydrate zone of cases 1a and 1b, there forms a structure resembling **flow channels** with low hydrate saturations. They are clearly visible beginning from year 5 or 6 (Figure 8.3). These pseudo **flow channels** are slanted as if they coincide with streamlines of flow. While hydrate saturation is lowered along these channels, they are separated by inclined layers of

high hydrate saturation because heat has to be supplied to the channels in order to decompose them. As separating layers cool and retain high hydrate saturation, pressure increases. Size (aperture) of channels should be a function of grid structure.

There is a large portion of hydrate decomposition taking place at the top of hydrate zone in addition to dissociation front. This is attributed to the fact that the hydrate zone cools while supplying heat to the dissociation front. The zone gets colder than the top constant temperature boundary which is always supplying heat to the system. Also, pressure drop is observed in the hydrate zone due to production (gas can easily flow). However, because of cooling, zone remained at the equilibrium conditions till the top constant temperature boundary supplied enough heat to the layer just below itself and caused it to decompose. This can be seen from the pressure profiles (Figure 8.23, Figure 8.24, Figure 8.25, Figure 8.26 and Figure 8.27) and temperature distributions of cases 1a and 2a (Figure 8.2, Figure 8.4, Figure 8.10 and Figure 8.12) .

What is happening here is hydrate equilibrium pressure line (which is an indicator of system temperature) is initially below system pressure at the hydrate zone (Figure 8.23 and Figure 8.25). As production continues, pressure drop is observed all over the hydrate zone. But, the place experiencing the greatest pressure drop and where decomposed gas can freely flow is the dissociation front. Therefore, hydrate zone cools not only because of general dissociation taking place all over the zone, but also layers transfer heat to the front where cooling is more. Then, initially the top layers can receive the heat from constant temperature boundary found above. Hence another dissociation front is created at the top. And this second front shows similar characteristics to the actual front.

After 4<sup>th</sup> year of production, formations which resemble an inverse *ice lens* structure began to form at the top of hydrate zone in case 2a (Figure 8.9 and Figure 8.11). These are lateral low saturation hydrate layers followed by thinner high saturation hydrate layers. The reason of such successive low-high hydrate saturation bands can be deduced from the pressure profiles for case 2a (Figure 8.26 and Figure 8.27).

Initially, in Figure 8.26, hydrate equilibrium line is below the system pressure in the hydrate zone. Later, there develop decreasing pressure and temperature gradients in the hydrate zone (because of production). Starting with year 3, hydrate equilibrium line meets the system pressure and decomposition is initiated in the top layers of hydrate zone because of heat supplied from the constant temperature boundary above the reservoir. When the text output of the simulation is examined for these layers, it is seen that at 3<sup>rd</sup> year 2 of the upper most layers (interval 1-2 meters) are both decomposing. After a very short while (at 3.5 years), only the top layer continues to decompose as opposed to the layer just below it where

hydrate saturation begins to increase (at equilibrium conditions). Increasing hydrate saturation seals the 2<sup>nd</sup> layer and decreases the flow from these 2 layers. There builds a no flow boundary acting only as a heat conducting strata because water saturation decreased below irreducible with increasing hydrate amount. So, a similar horizontal low-high hydrate saturation structure begins to develop in the following 2 layers and this chain of low-high saturation bands extent to the dissociation front during rest of the production (Figure 8.27).

Then, the reason why two different hydrate saturation patterns occur in the reservoirs is because of very high capillary pressure acting on the liquid phase in case 2. In case 1, gas and released water can easily flow towards producing grids without being impeded by high capillary pressure keeping water stagnant. Yet, in case 2, water remained in the grids due to high capillary pressure and this further prevented released gas from easily flowing (by reducing relative permeability to it). When released water and gas could not be moved from their initial locations, they caused an increase in the pressure and thus re-formation of hydrate.

In case 2a, around year 9 (Figure 8.11), the low saturation hydrate layer at 10 meter depth started to be evacuated of hydrates because the cavity in hydrate zone near the well-bore has grown so large that there established a gap of no hydrate grids (Figure 8.11, year 12) where liberated gas in the layer at 10 meter could easily flow through to the producing elements (Figure 8.9 years 18 and 20).

## **8.2 Effect of Well-bore Heating**

Effect of well-bore heating is very obvious when hydrate saturation distributions of case 1a and case 1b, case 2a and case 2b are compared (Figure 8.3, Figure 8.7, Figure 8.11 and Figure 8.13). Formation of hydrate at and near the top producing grids is clear. Also, it is understood that in cases 1a and 2a, the cavity forming near the well-bore due to dissolution of hydrate should be solely due to this heating.

One important point here is, in case 1b (hydrate-gas in the upper section) the saturation of newly formed hydrate around the production grids is low enough to permit a continuous flow, thus it was possible to obtain more than 20 years long production with out heating. Moreover, because in case 1b some of the water is captured in hydrate form near and at the producing elements and permeability to water has decreased due to solid saturation, amount of produced water is less than case 1a.

On the other hand, in case 2b (hydrate-water in the upper section) the amount of new hydrate formation near the producing grids is too high and restrict the flow. The reason of

hydrate formation at high saturations is the existence of enough water and gas to form hydrate. In case 2, there is water in the hydrate zone and when it drains towards producing grids in the free gas zone (lower section), it meets high amount of gas at an adequate temperature to form high amounts of hydrate. Eventually, the simulation is shut-down when fluids can no longer be supplied to producing elements at the specified rates.

Apparently, the rate of production and depth of completion (location of production) determines whether well-bore heating is required for the depressurization scheme. Producing elements had better be placed as far as possible from the dissociation front.

### 8.3 Replenishment of Produced Methane

Contribution of released methane to the free gas in the reservoir is termed **replenishment** in this text. This means how much of the produced free methane was restored back into the reservoir through dissolution of hydrate. From Figure 8.16, Figure 8.17 and **Error! Reference source not found.** it is apparent that replenishment in cases 1a and 1b are same, suggesting it was not necessary to apply heating and main contribution to the methane release is coming from the dissociation fronts but especially from the new front developed at the top of hydrate zone, as hydrate saturation distributions imply.

The great take off in the replenishment plot of cases 1a and 1b after 2<sup>nd</sup> year of production is evidently attributed to development of the second dissociation front at the top of hydrate zone (Figure 8.16).

The large rate decrease at years 6 and 8 (Figure 8.16) in the replenishment graphs of cases 1a and 1b are due to complete depletion of hydrates in the layer where the second (upper) dissociating front is. This should be because; the layer below the second front is initially colder and it takes sometime before decomposition could be re-initiated in this new layer of dissociation front. Following continuous rise in the graph during a long period of time shows how decomposition rate increases with decreasing hydrate in the layer.

Same thing applies for the case 2a. The drops in methane release, which is a result of wiping out of hydrate in the layer of dissociation front, are quickly restored by the initiation of decomposition in the new layer of front.

Acute increases in methane release rate observed in cases 2a and 2b ( ) are attributed to the fact that a high pressure drop is felt all over the reservoir and in the hydrate zone. Because compressibility of water is quite low compared to gases, the pressure drop due production is

sensed in the whole hydrate zone and therefore decomposition induced in all of the upper section.

Compared to case 2a, it takes a longer period to reestablish the rapid rate of decomposition in case 1. Because gas released from the second (upper) front can expand only to the space left by previously emptied layer and released water has to move down. But in case 2a, because the main contribution is from the primary front and released water and gas can expand more freely, the rate is quickly restored.

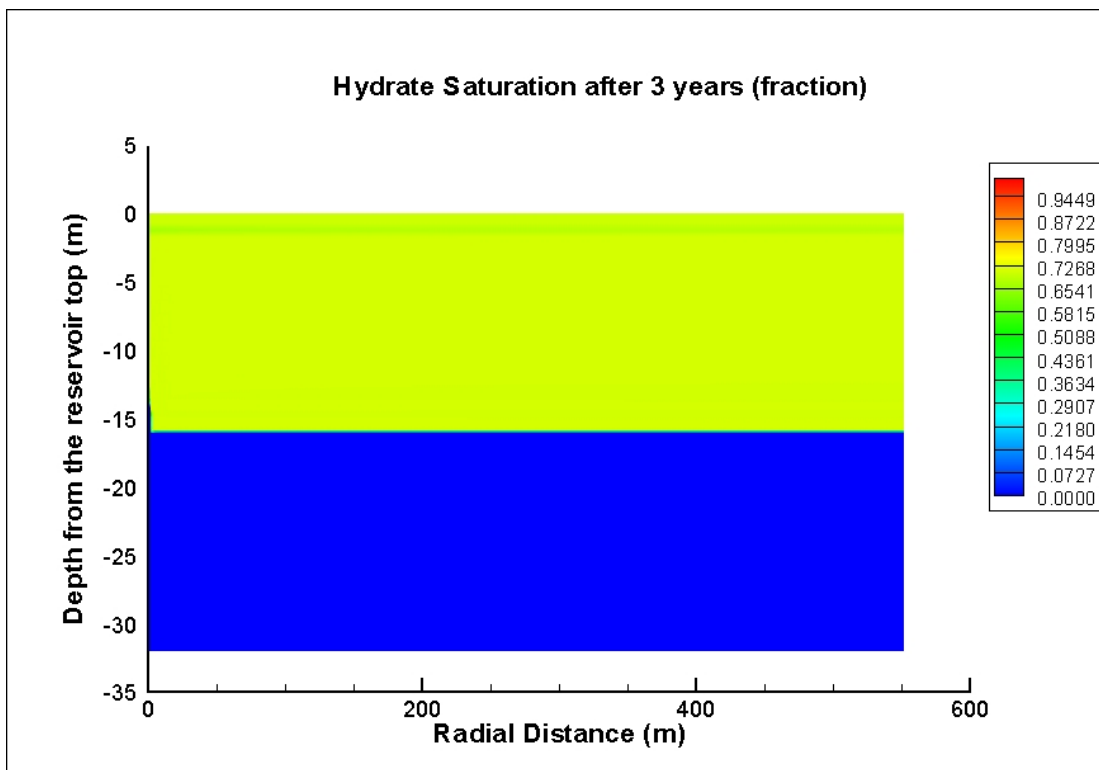
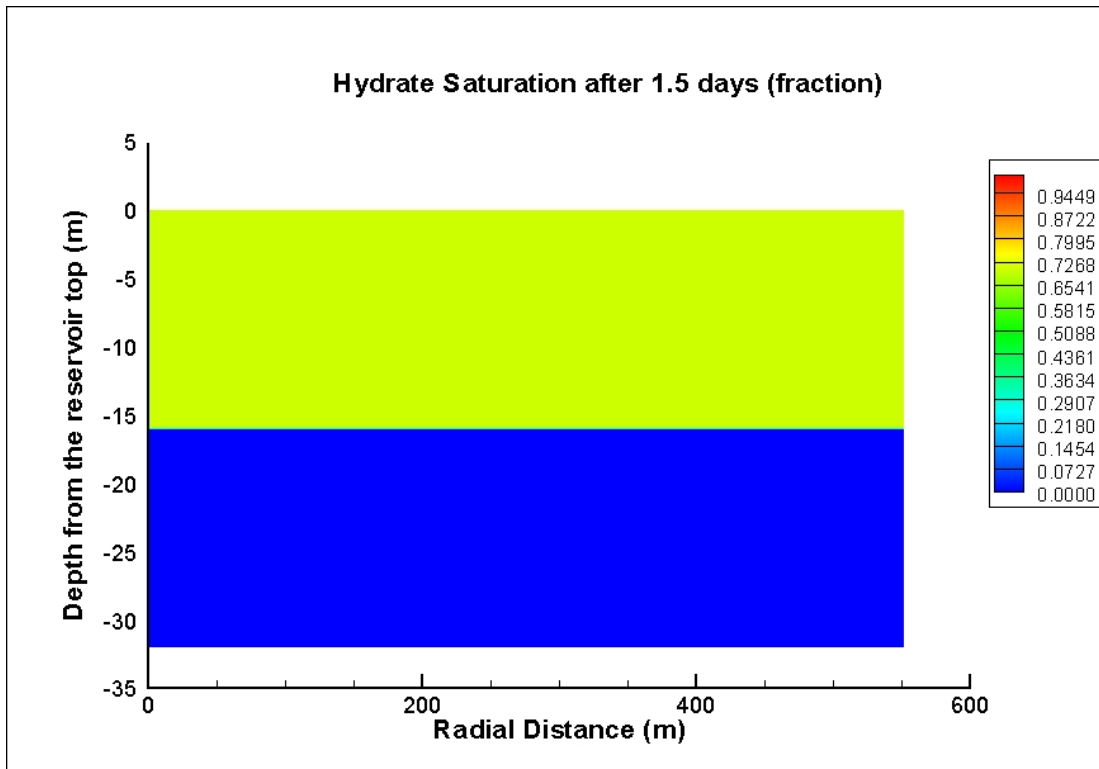


Figure 8.1: Hydrate saturation distribution for whole reservoir, Case 1a

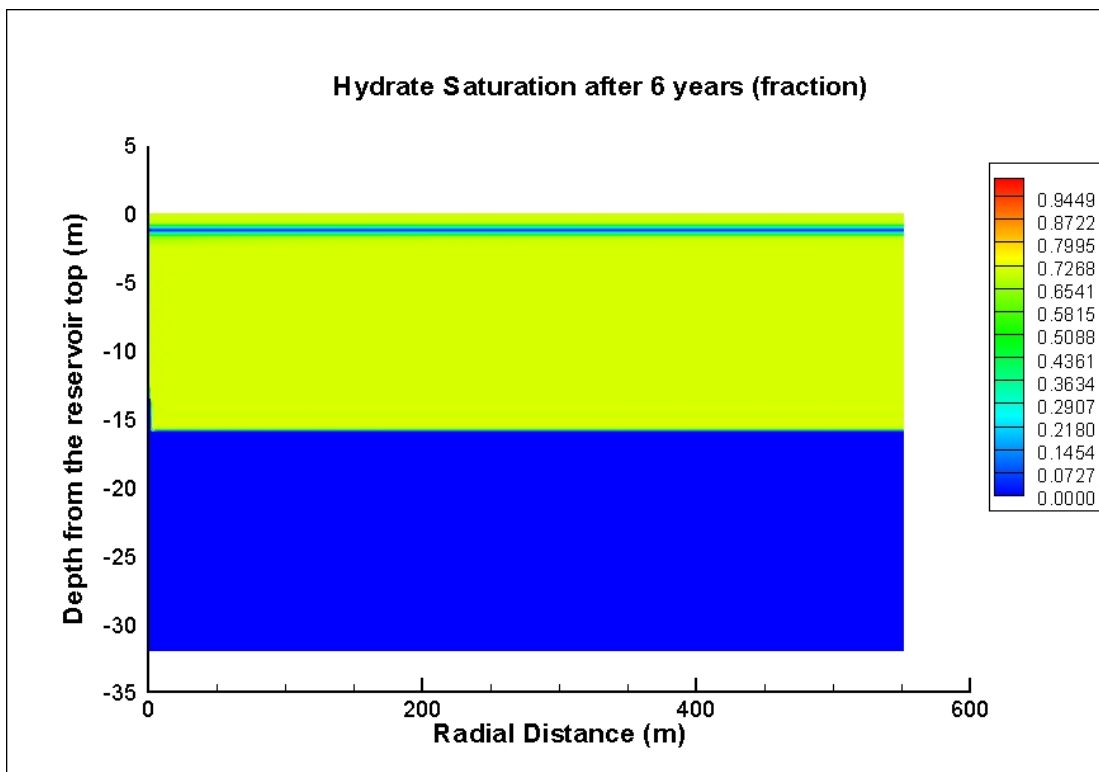
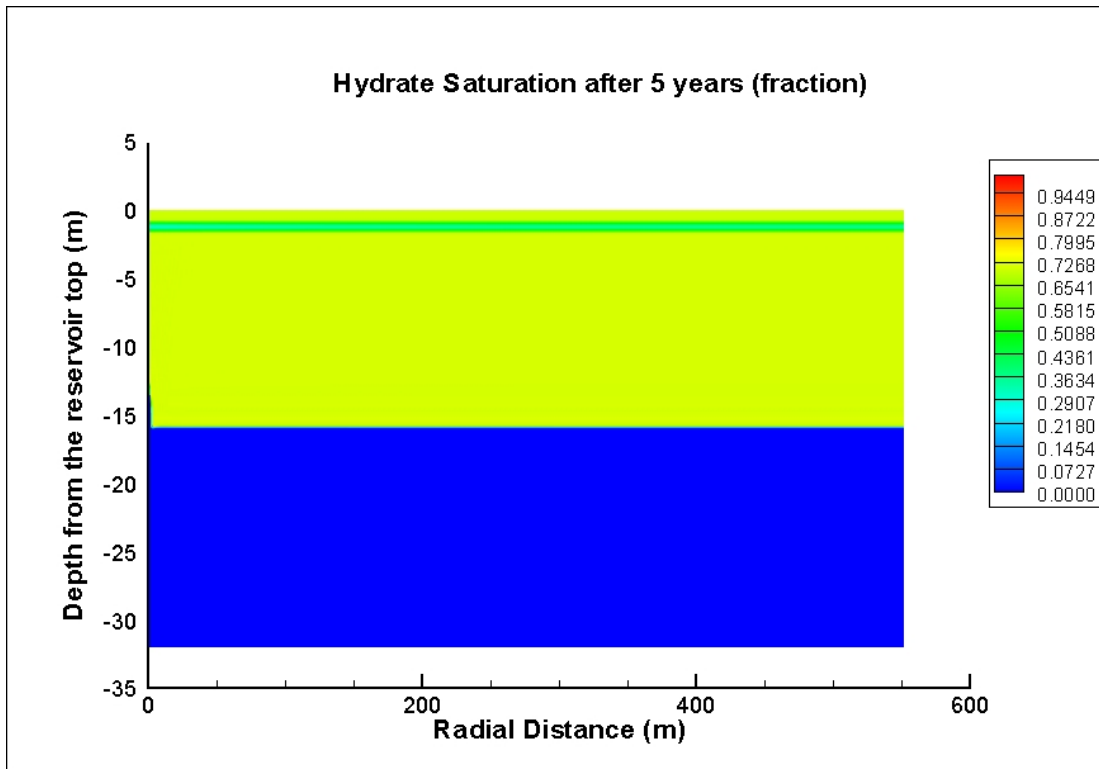


Figure 8.1 (Continued)

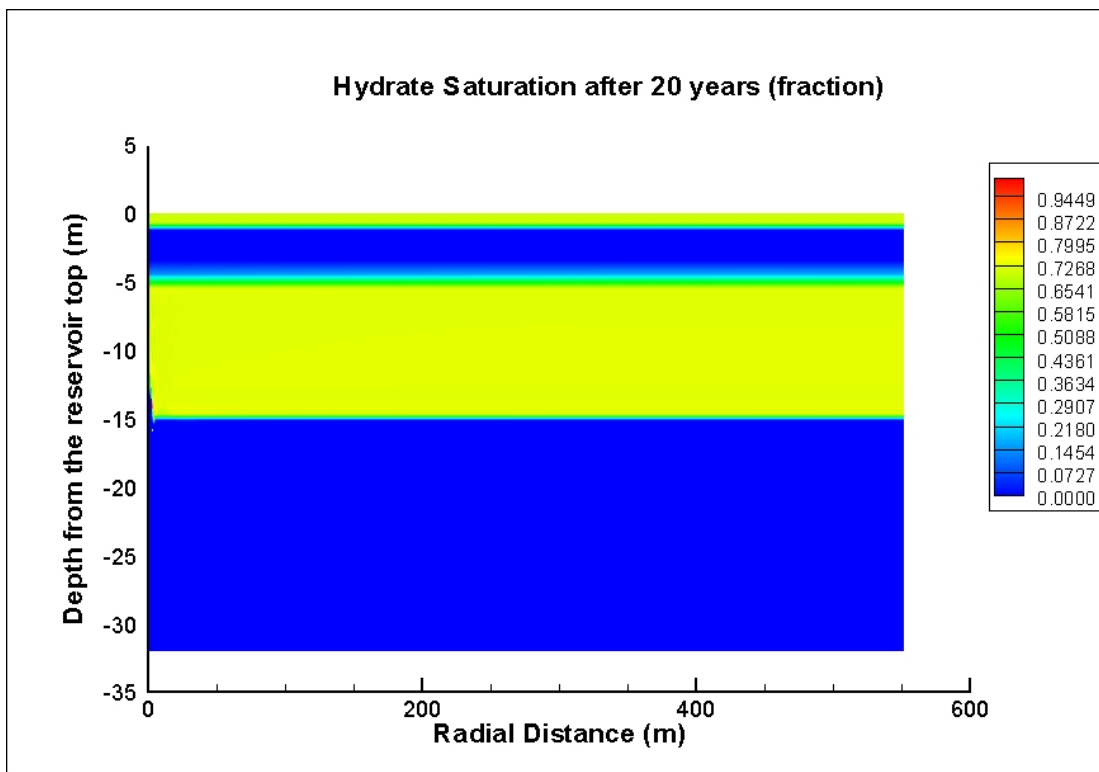
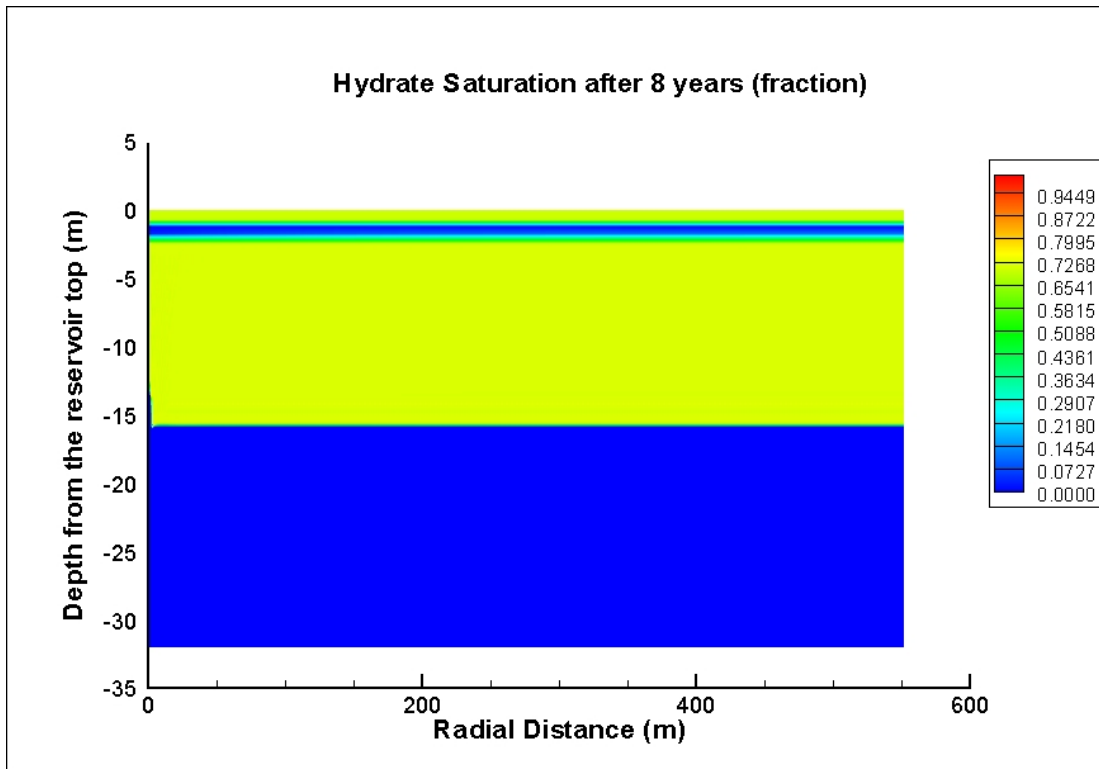


Figure 8.1 (Continued)

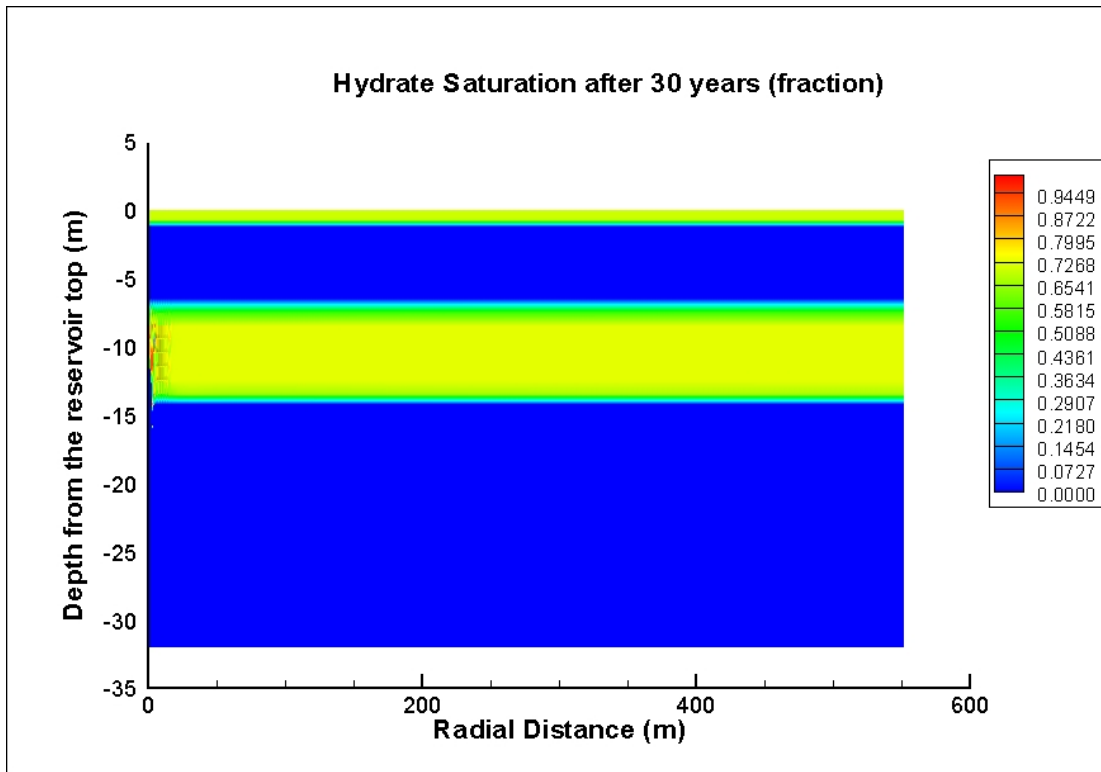


Figure 8.1 (Continued)

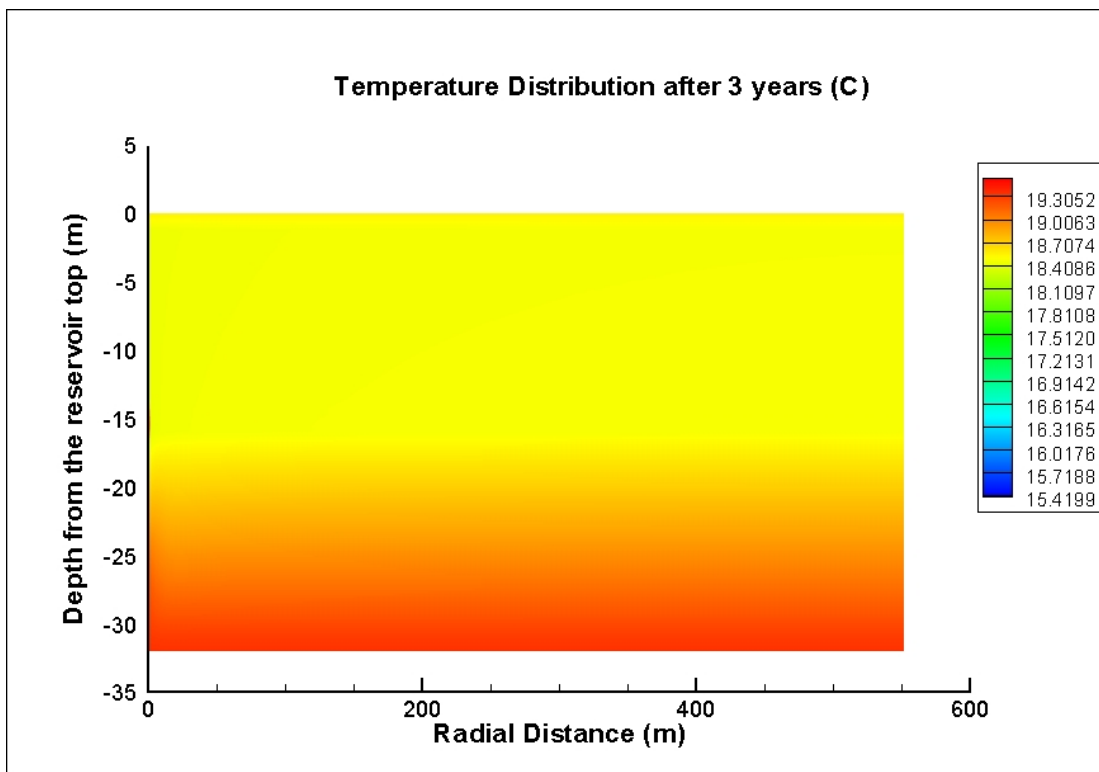
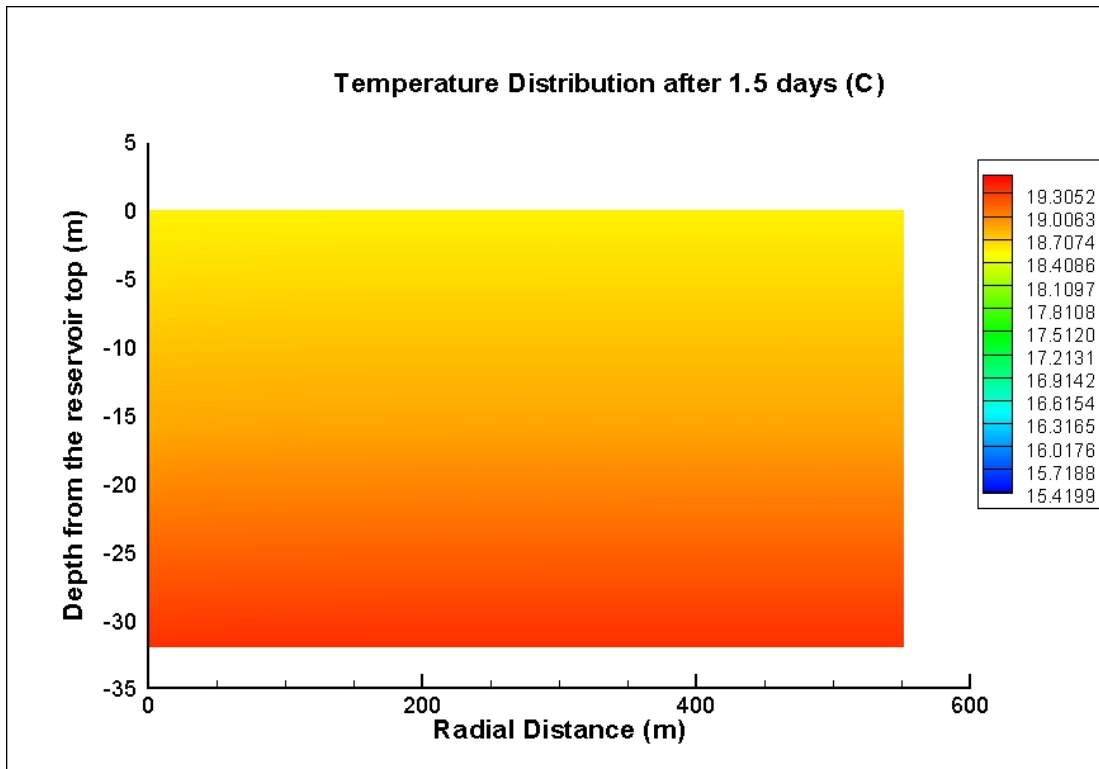


Figure 8.2: Temperature distribution for whole reservoir, Case 1a

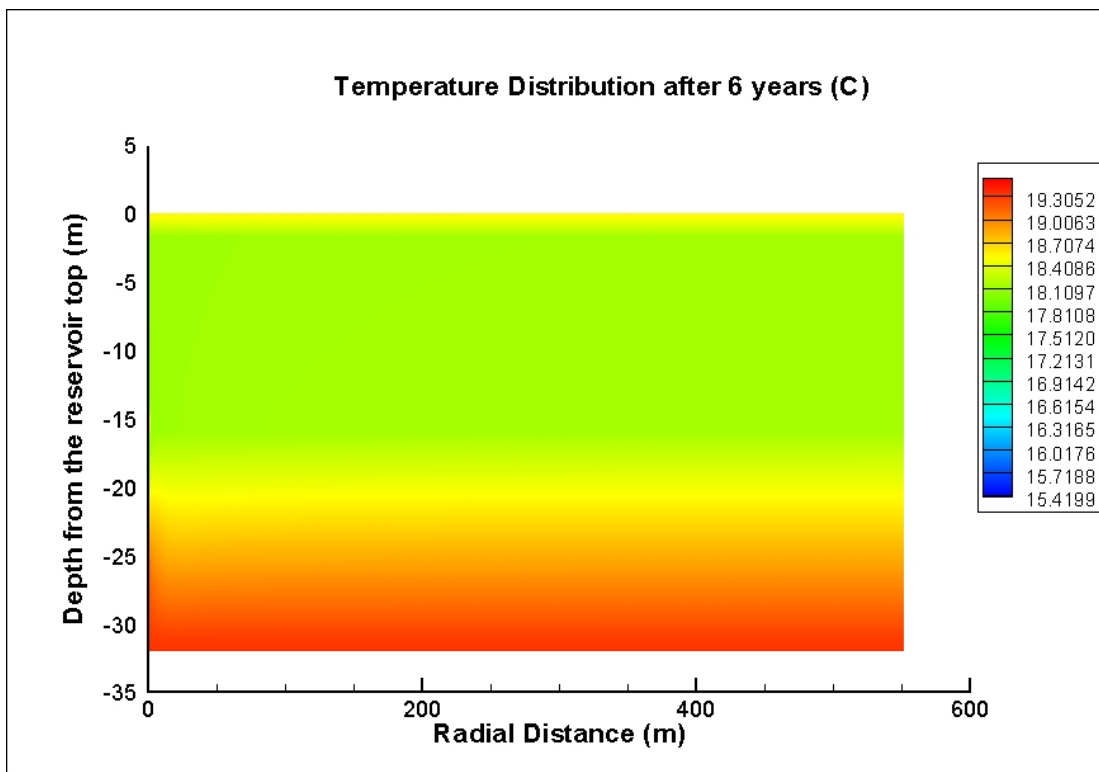
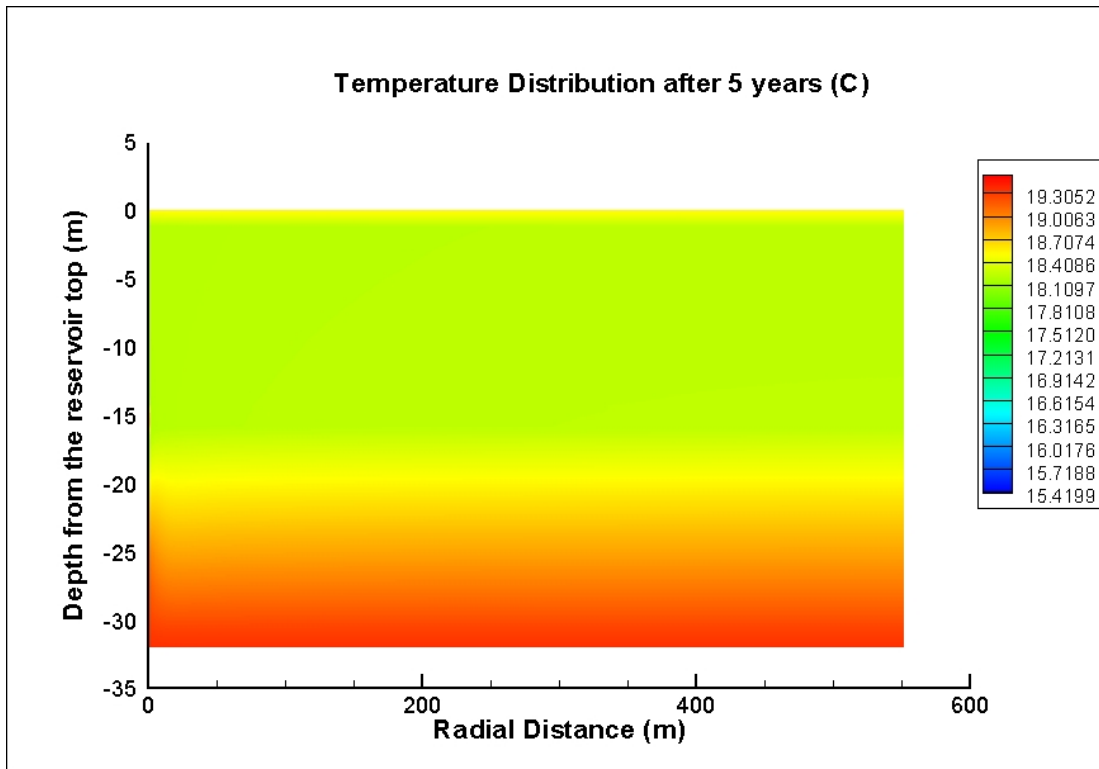


Figure 8.2 (Continued)

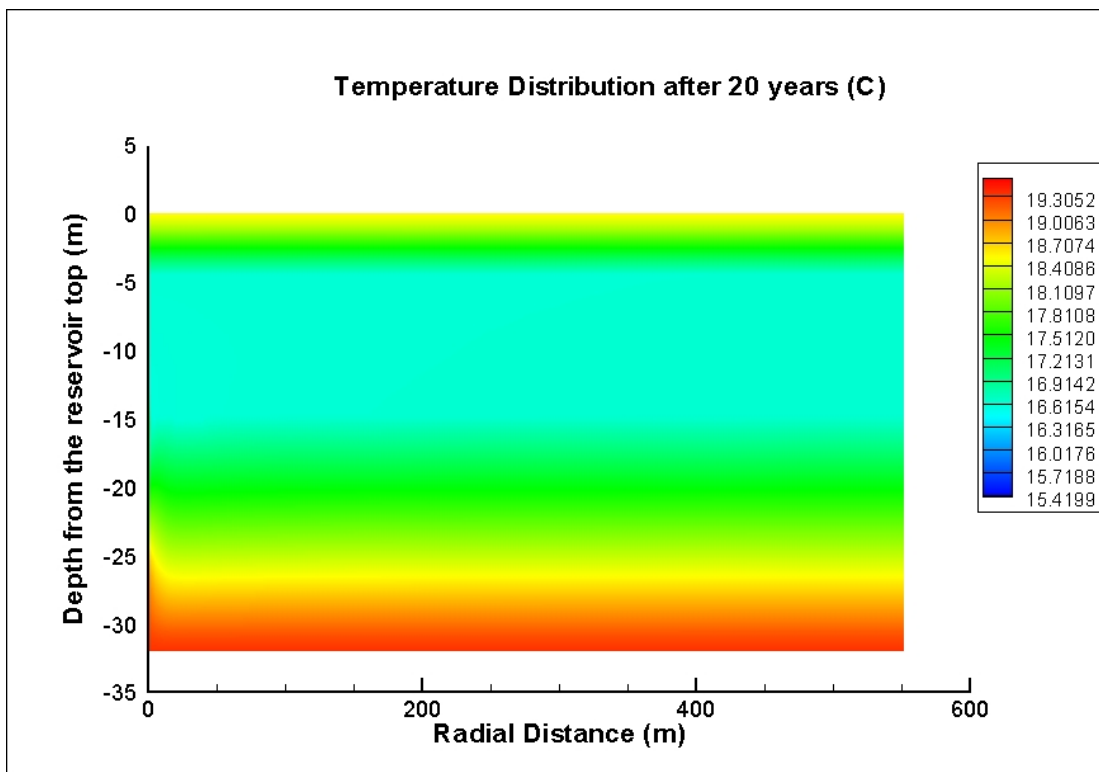
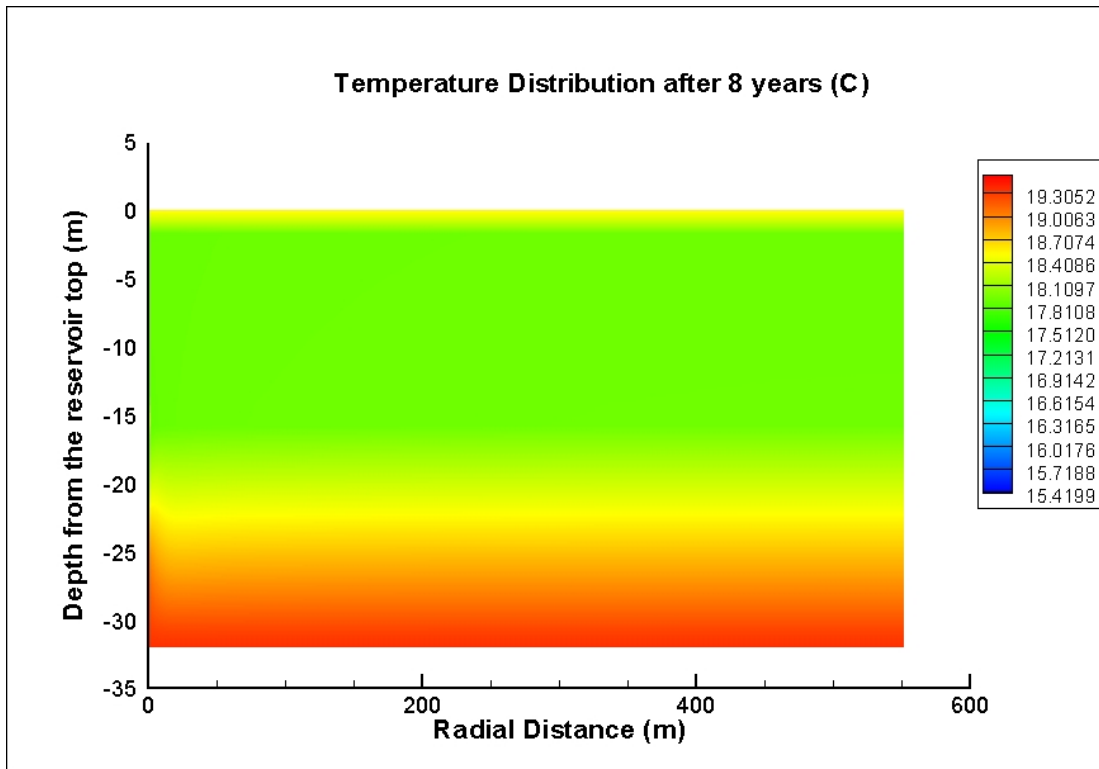
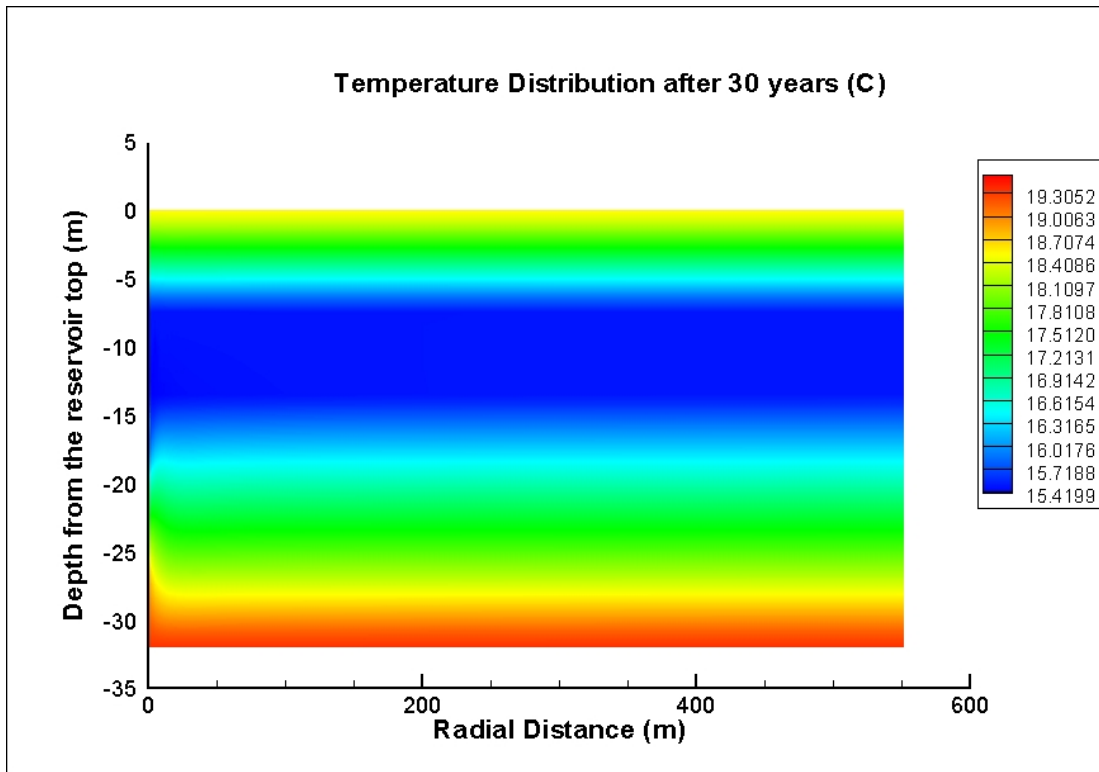


Figure 8.2 (Continued)



**Figure 8.2 (Continued)**

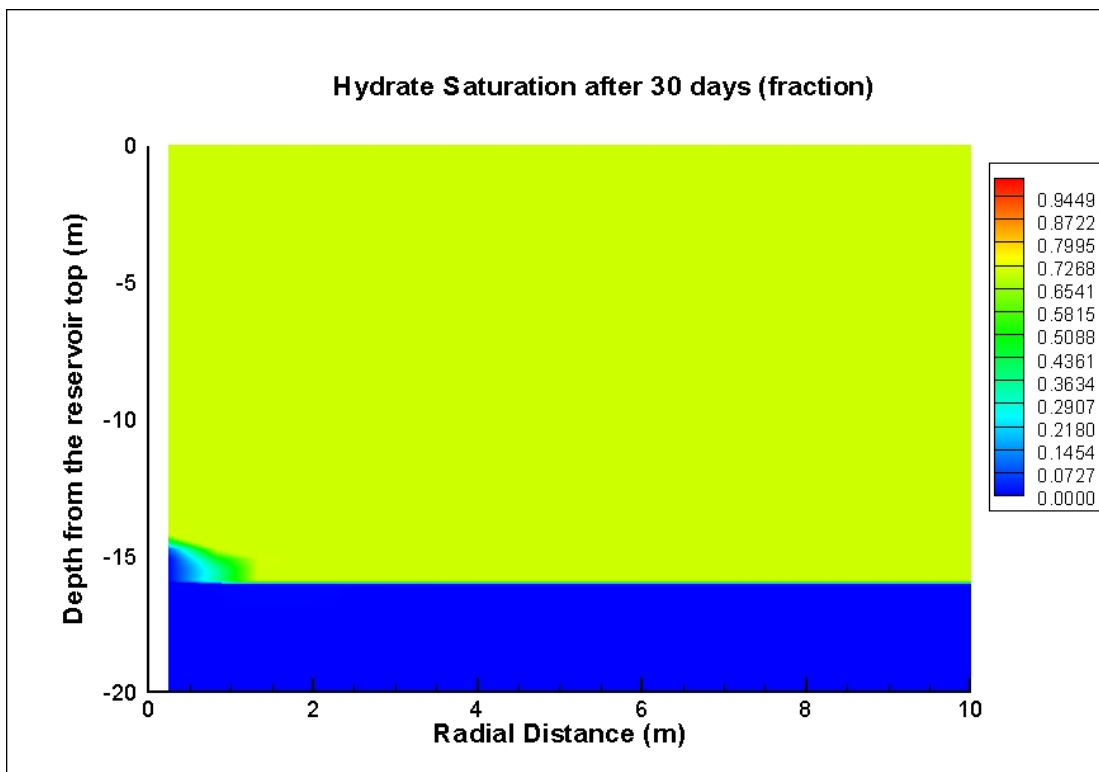
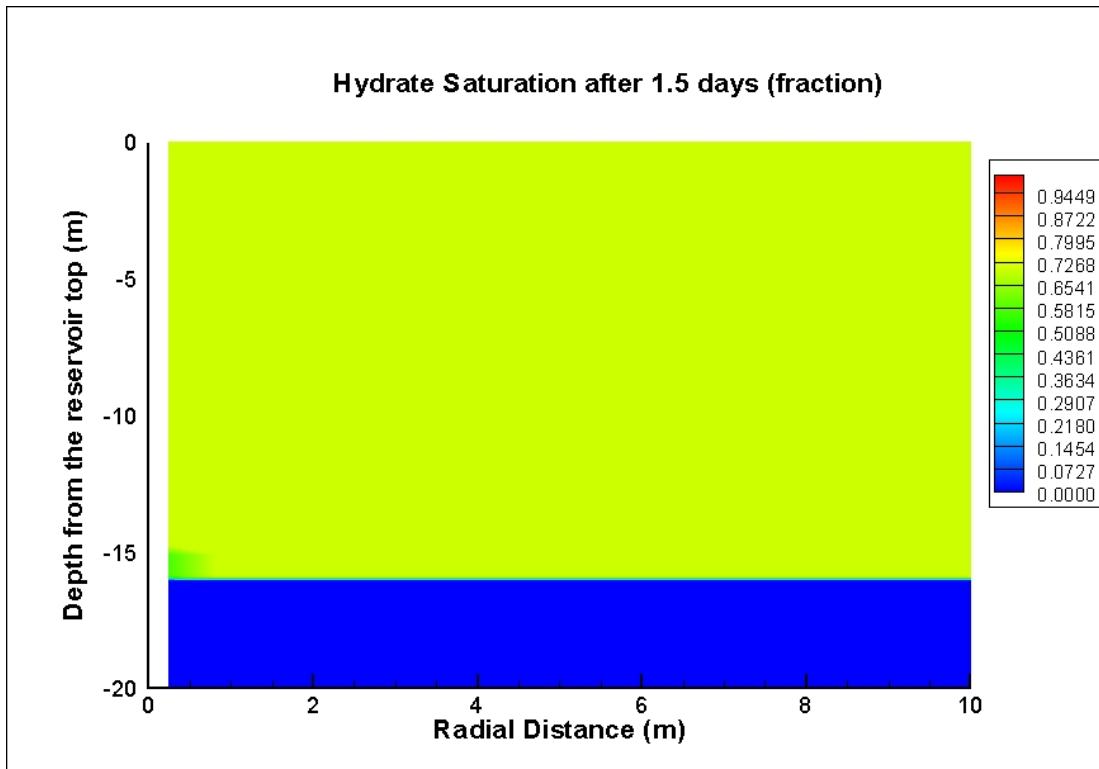


Figure 8.3: Hydrate saturation distribution near well-bore, Case 1a

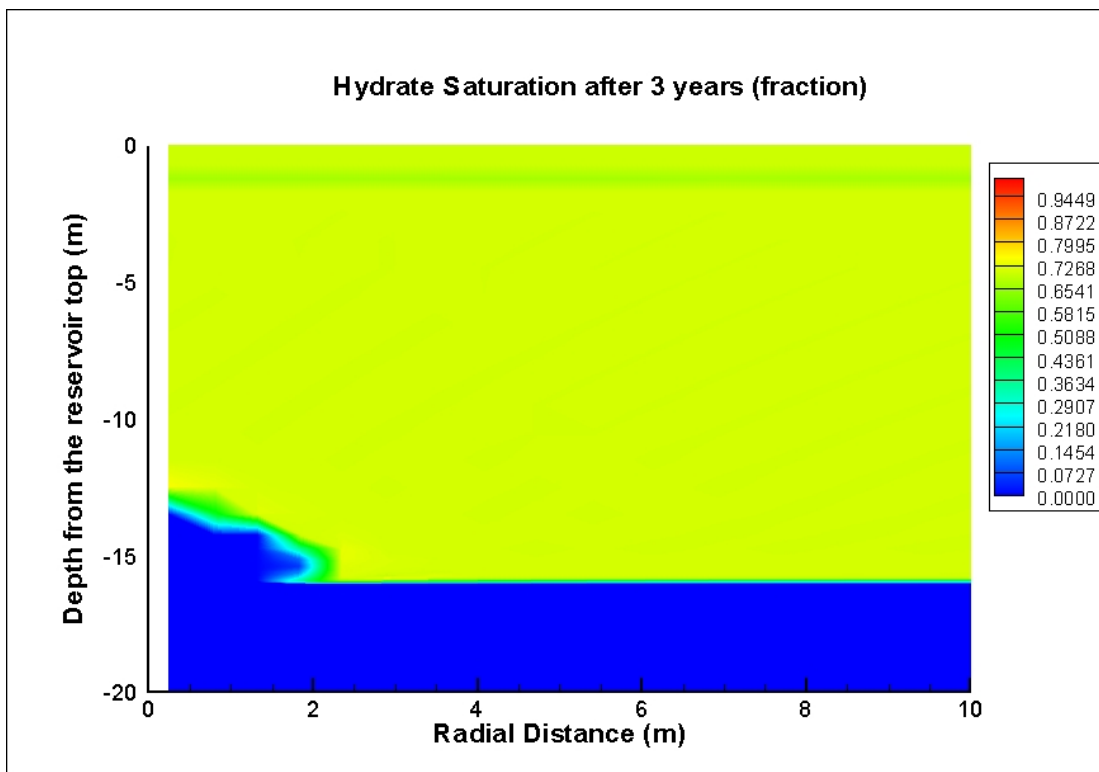
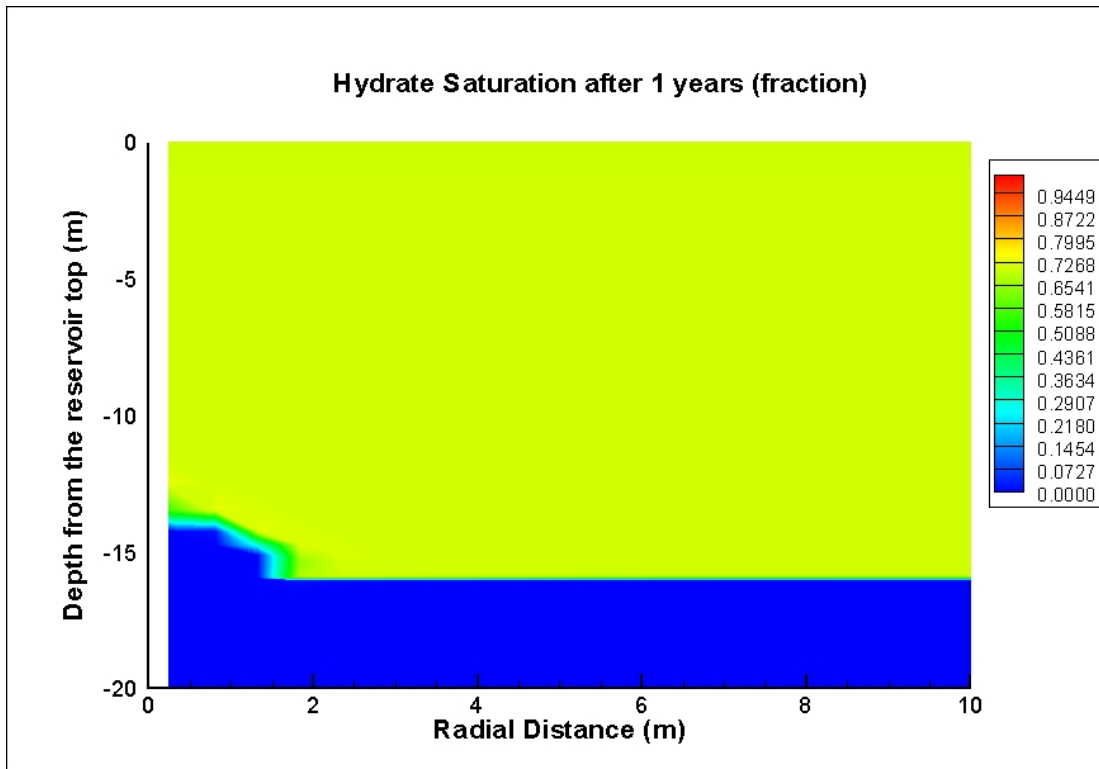


Figure 8.3 (Continued)

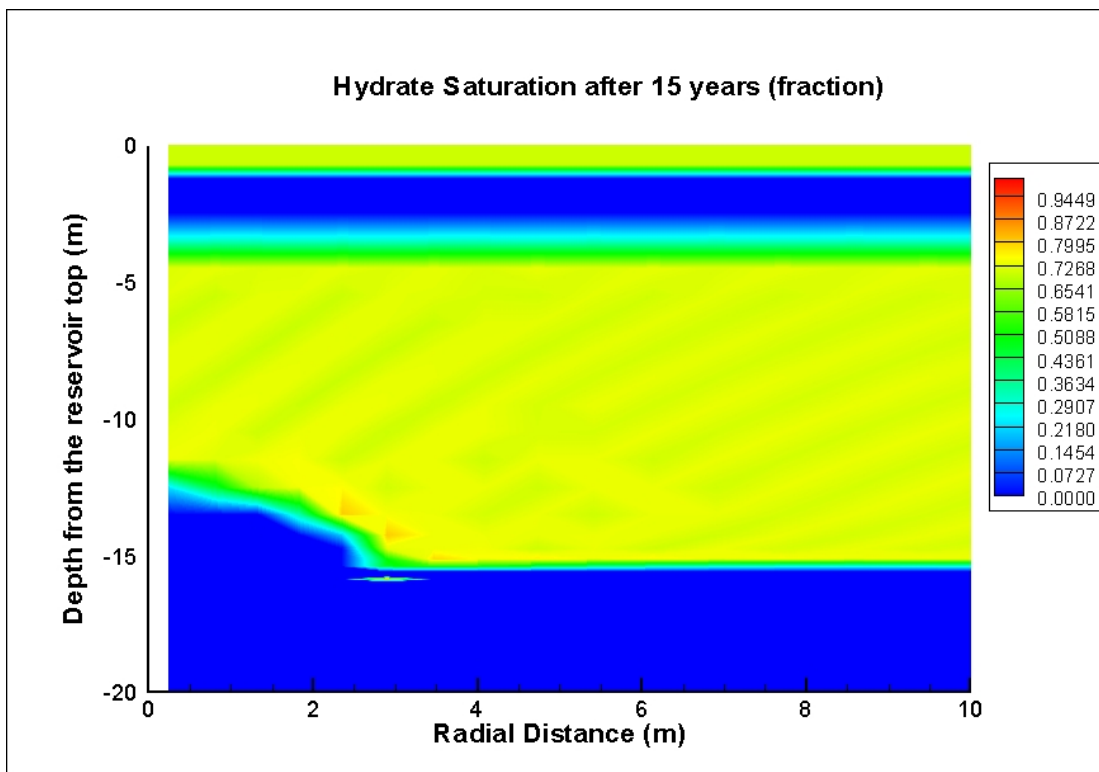
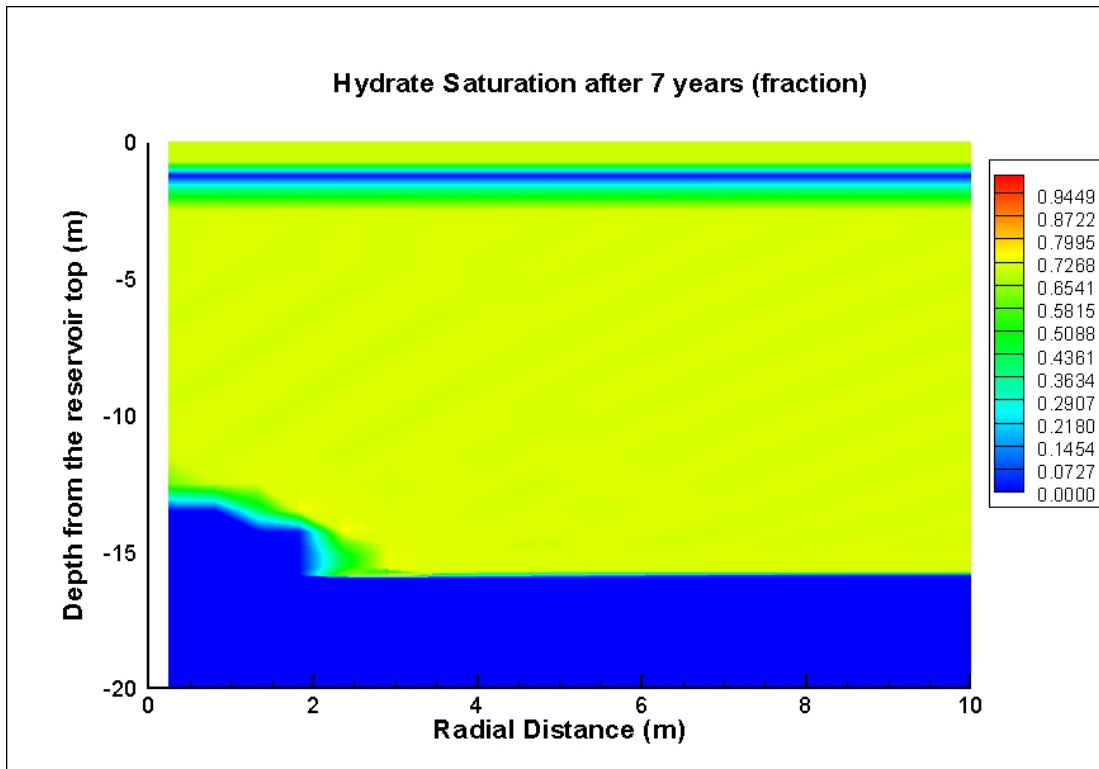


Figure 8.3 (Continued)

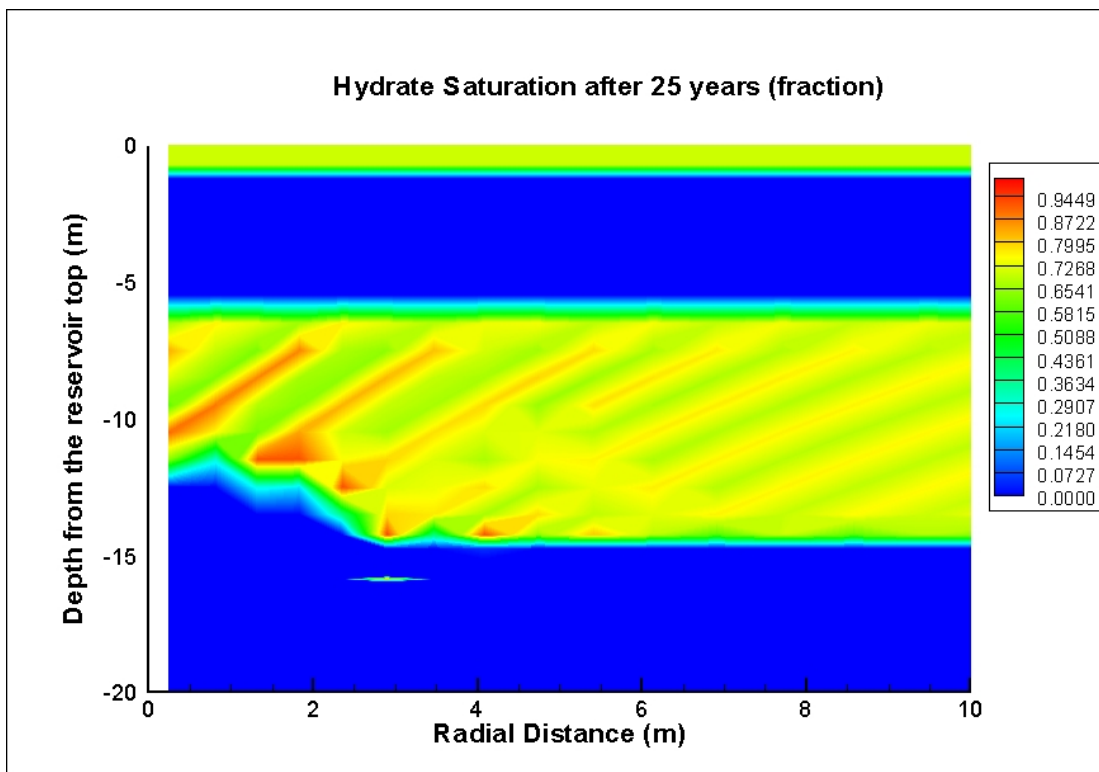
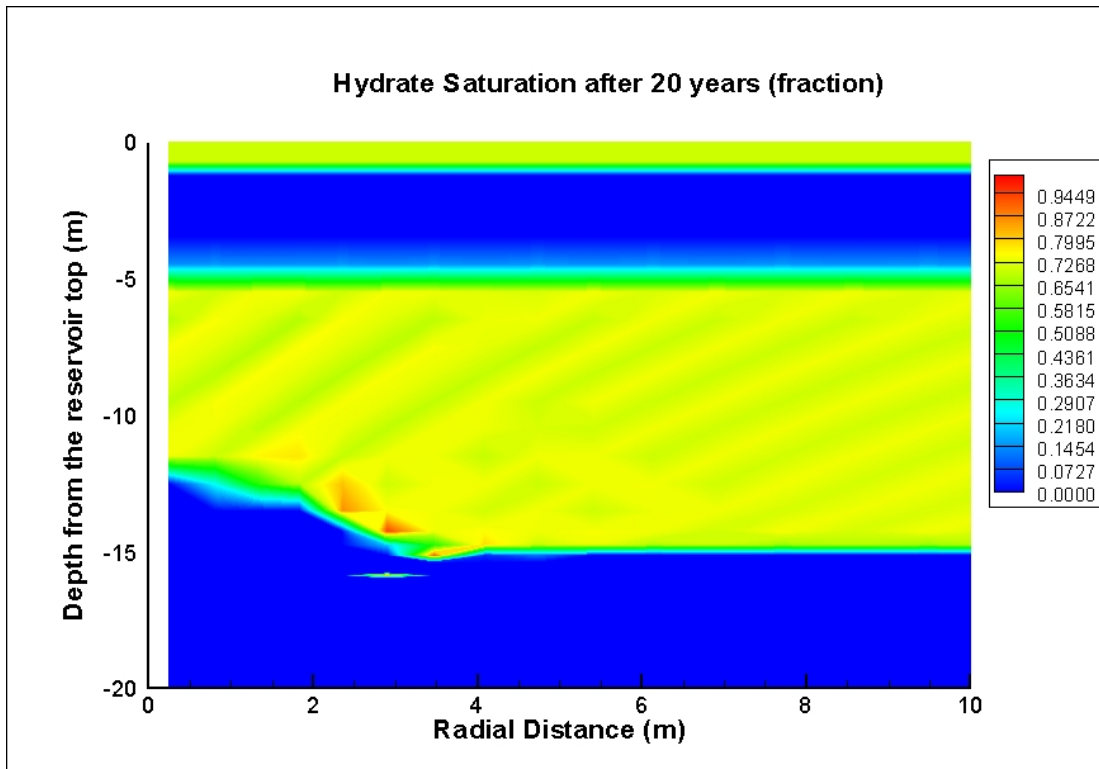
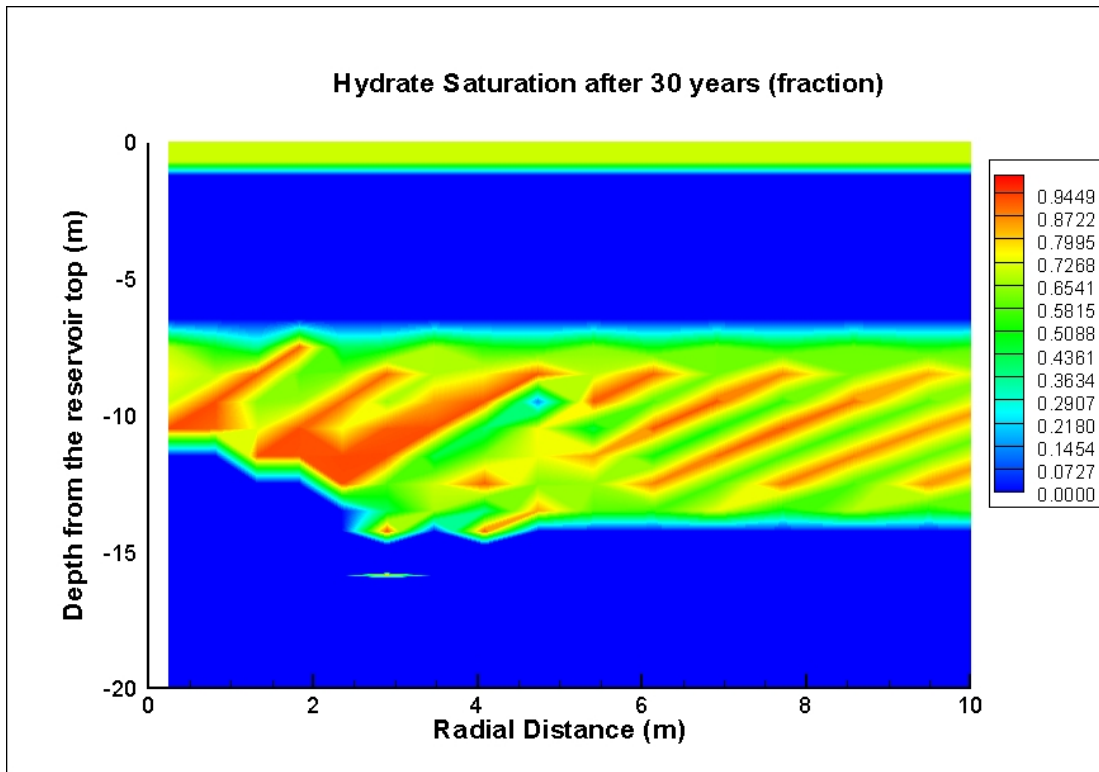
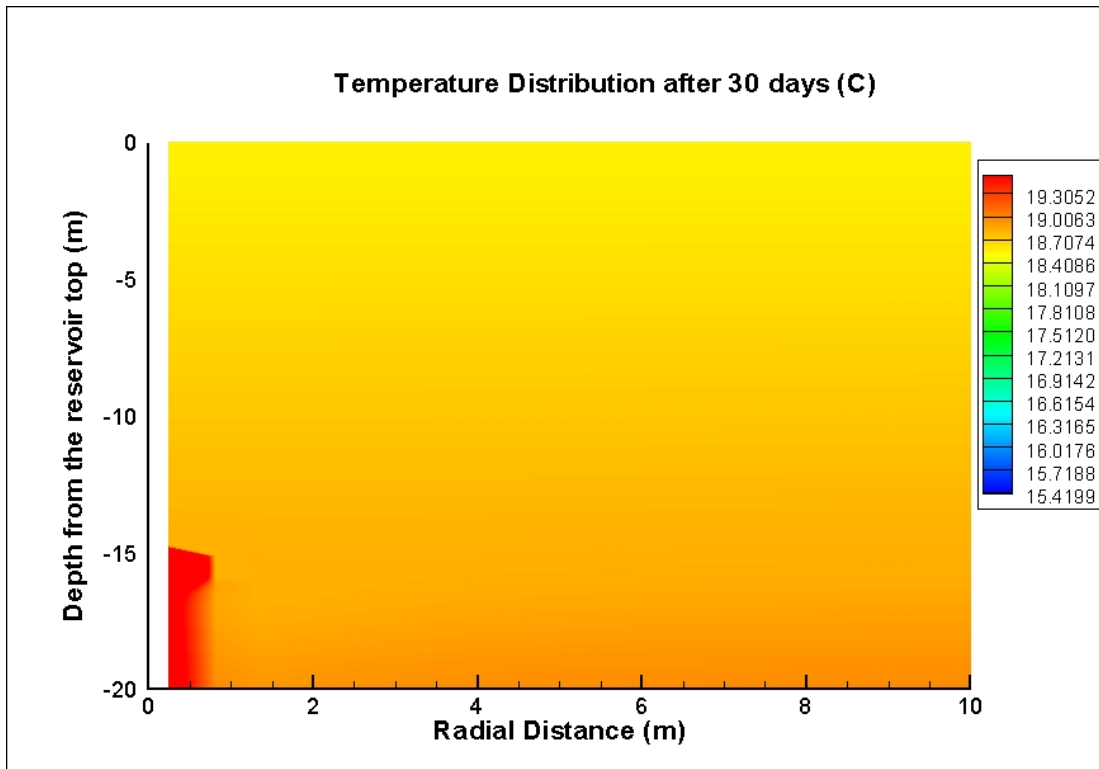
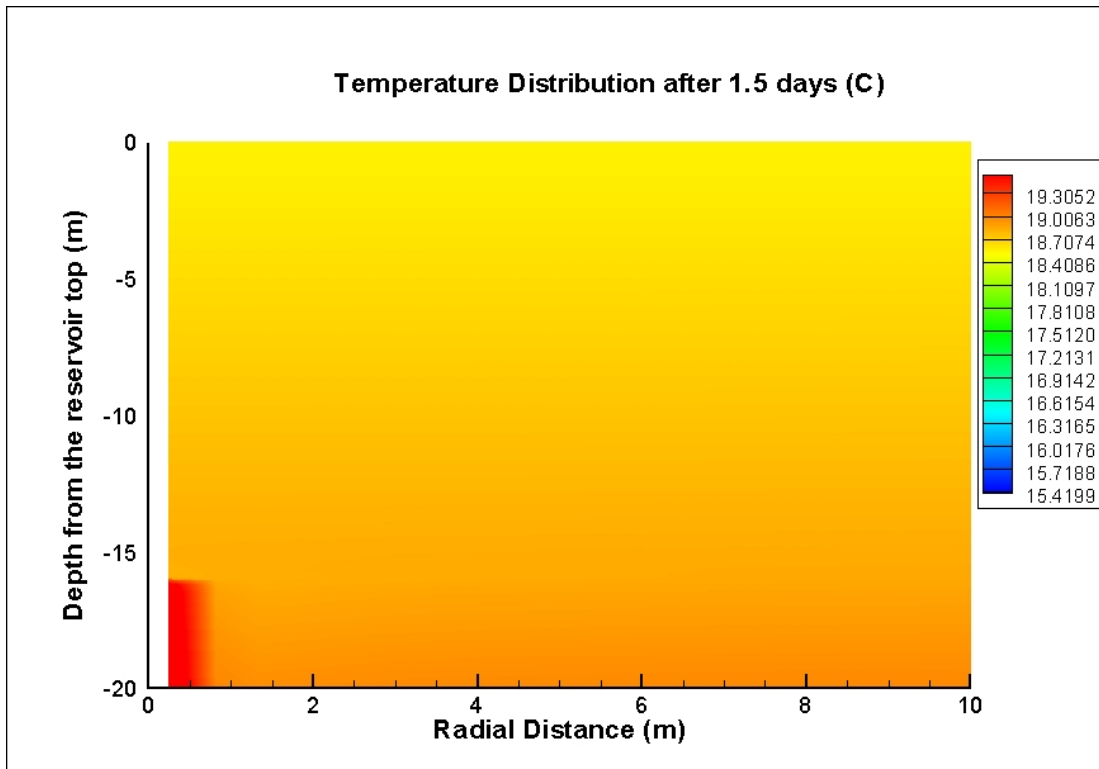


Figure 8.3 (Continued)



**Figure 8.3 (Continued)**



**Figure 8.4: Temperature distribution near well-bore, Case 1a**

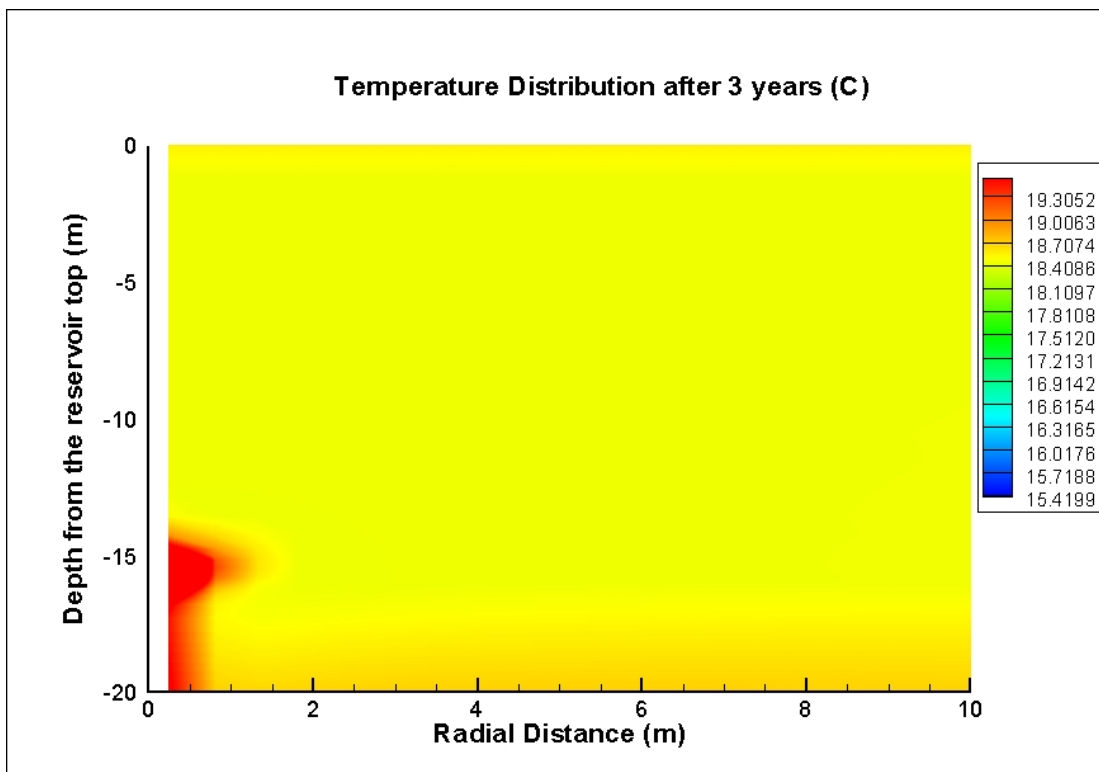
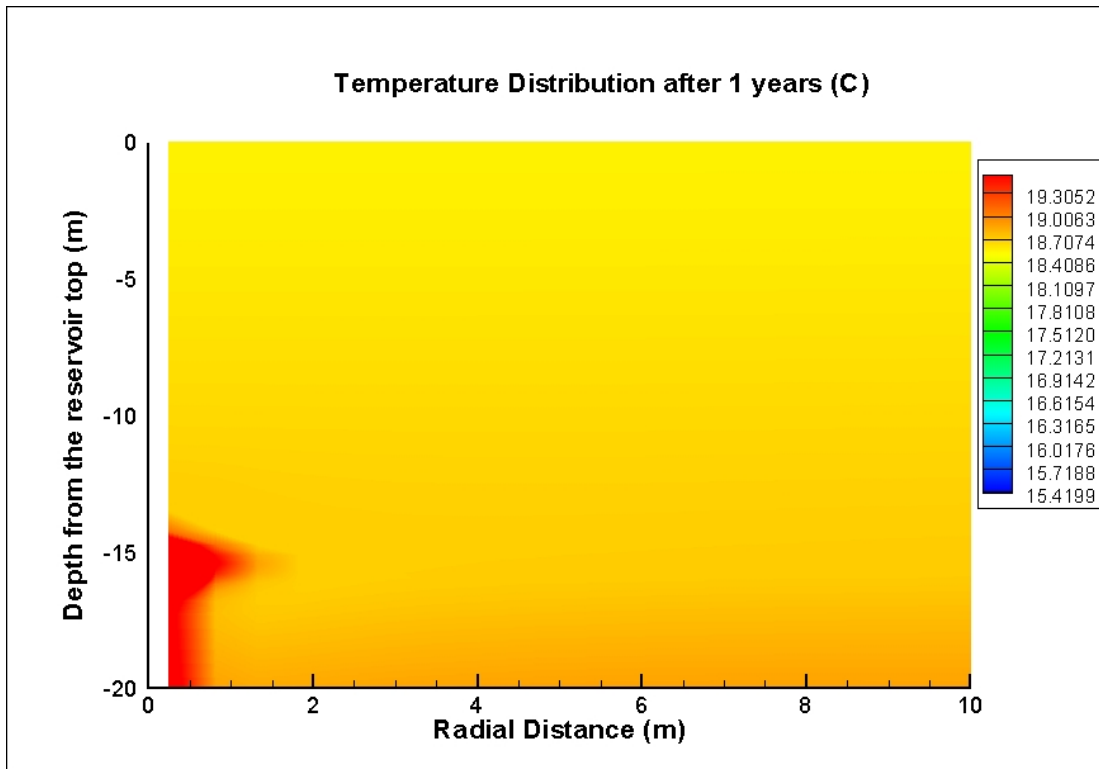


Figure 8.4 (Continued)

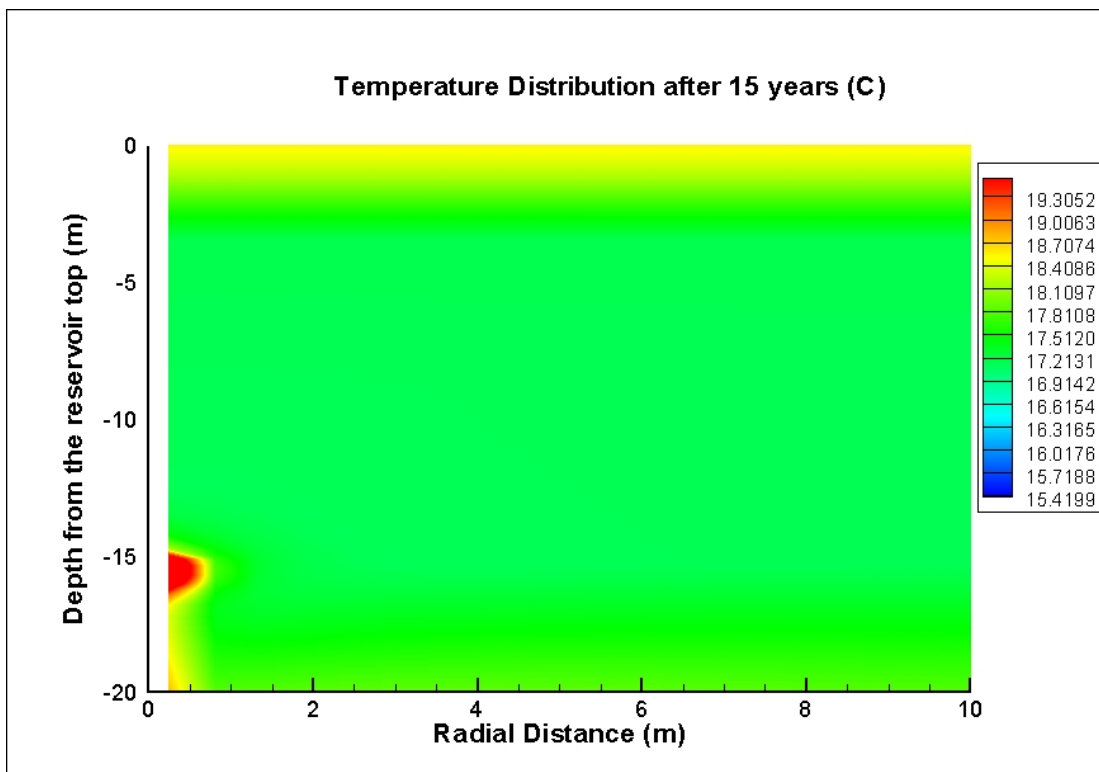
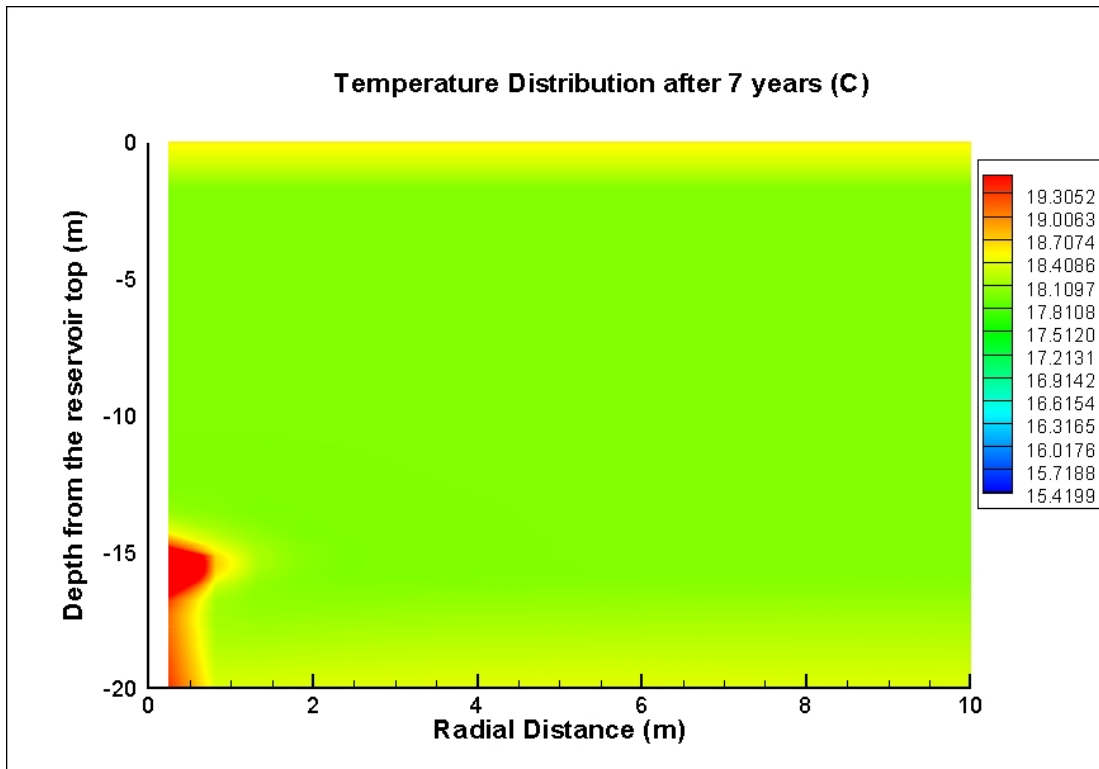


Figure 8.4 (Continued)

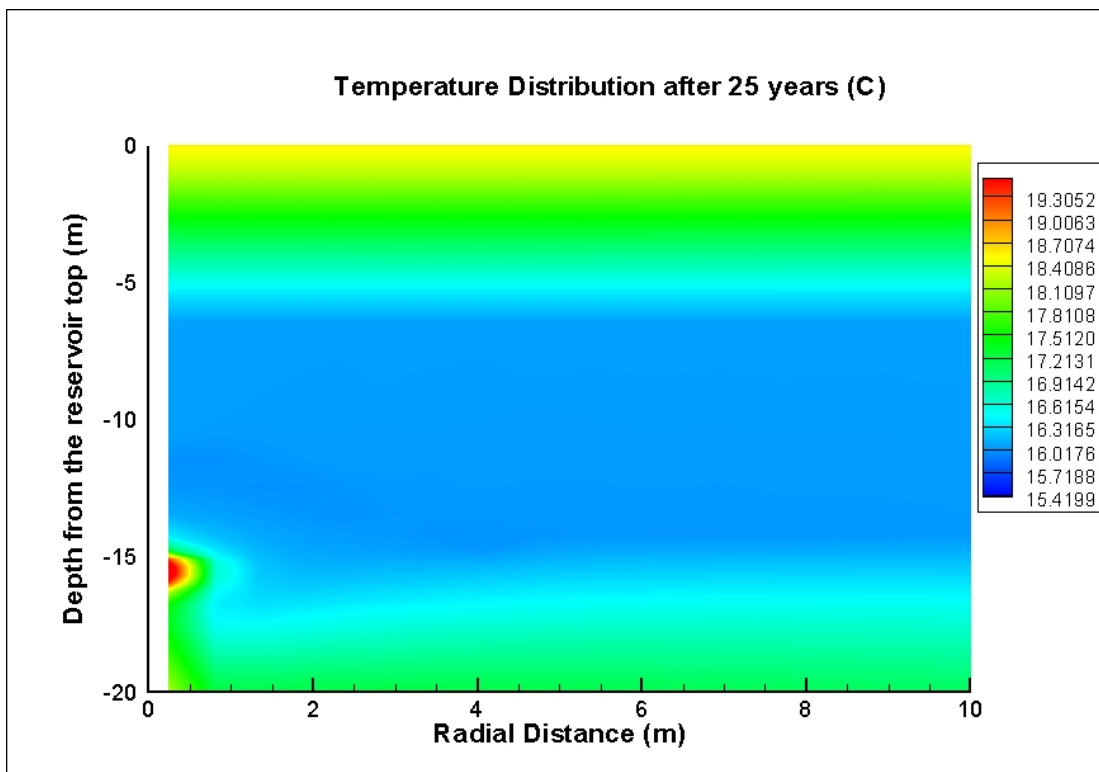
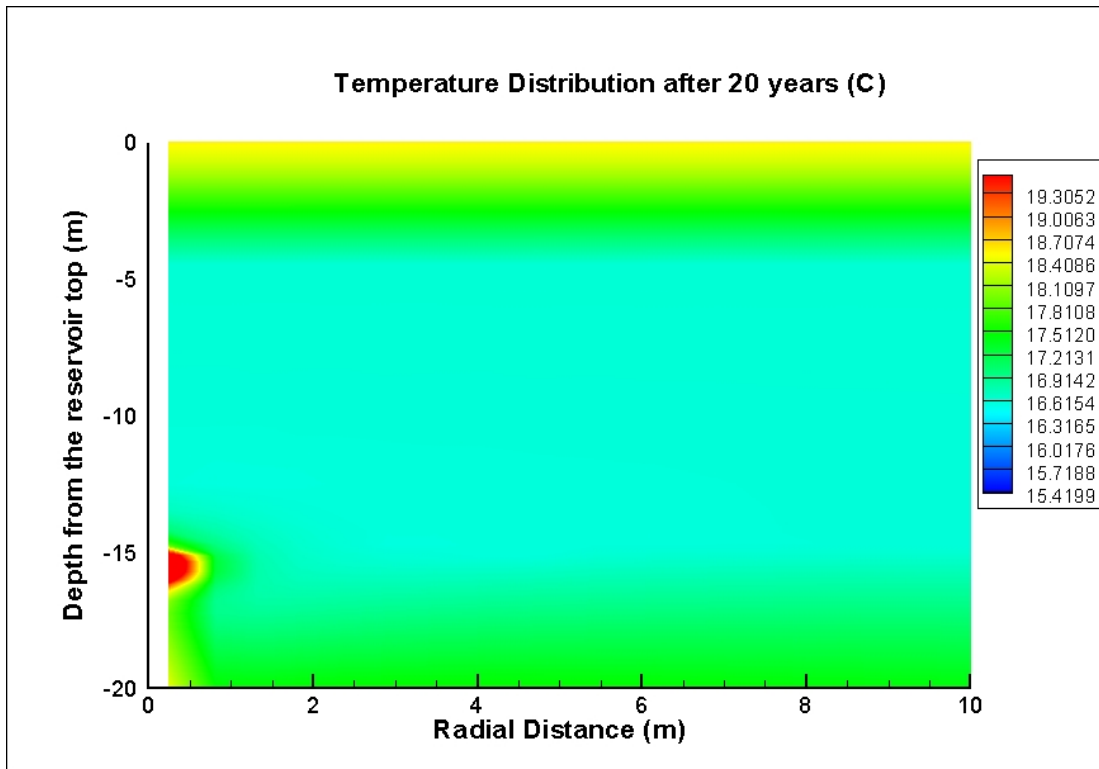
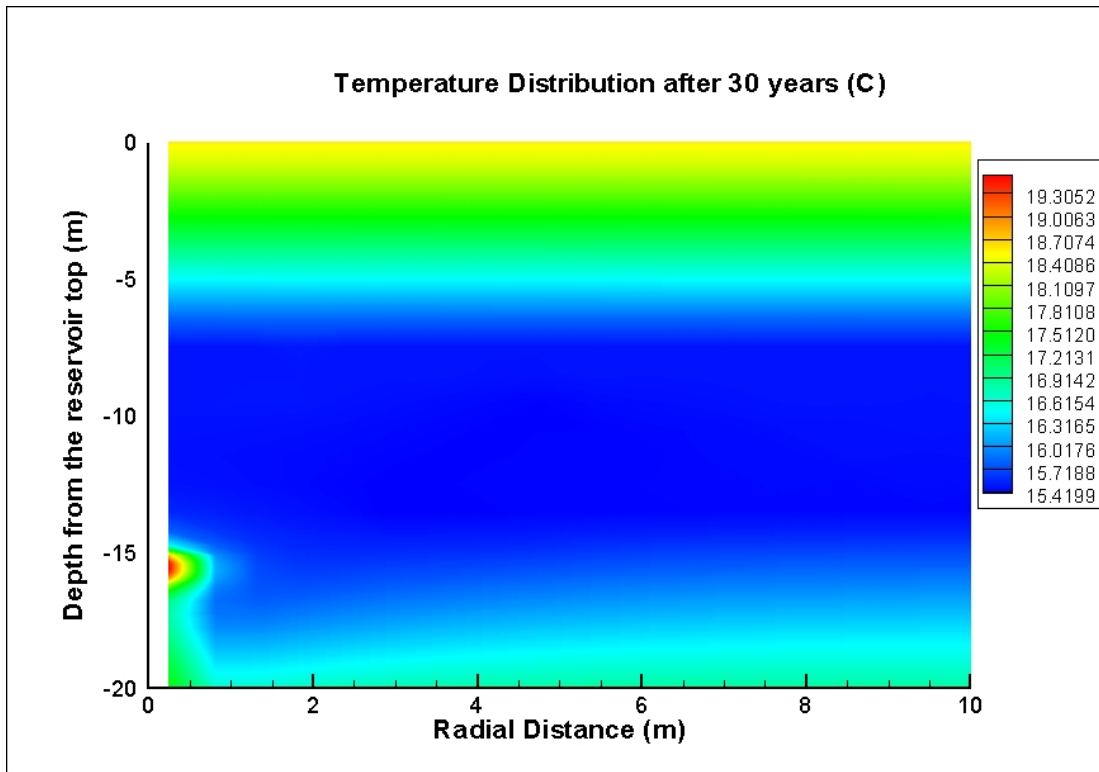


Figure 8.4 (Continued)



**Figure 8.4 (Continued)**

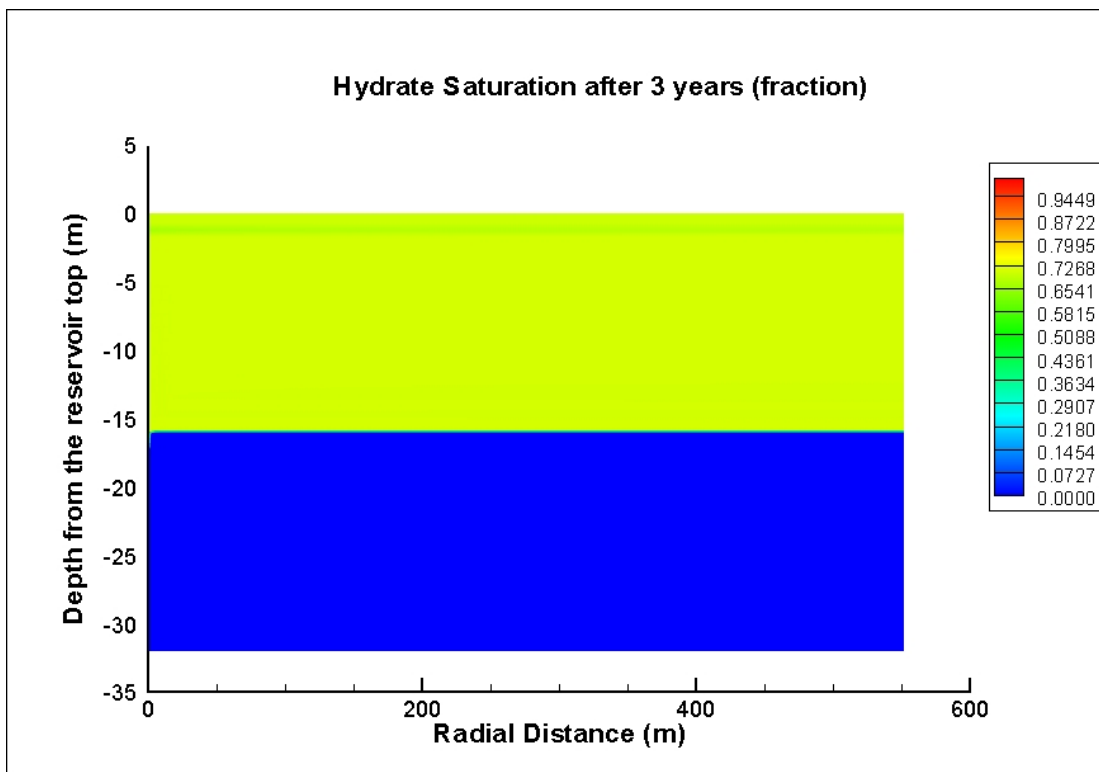
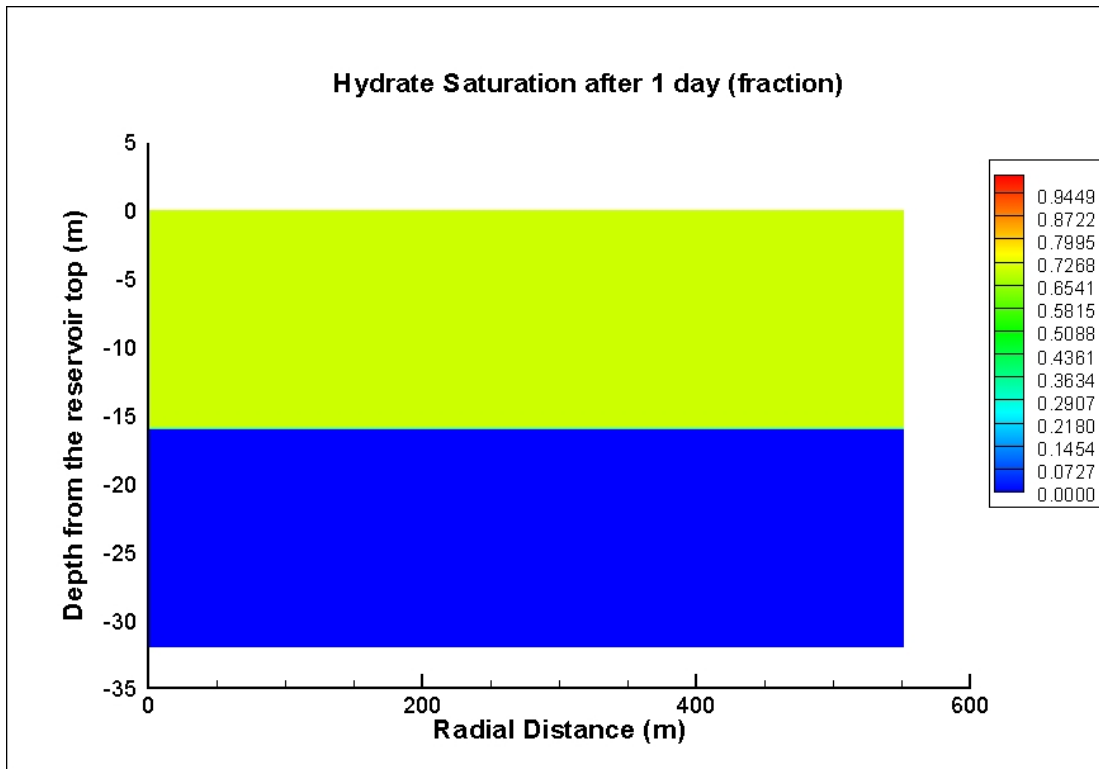


Figure 8.5: Hydrate saturation distribution for whole reservoir, Case 1b

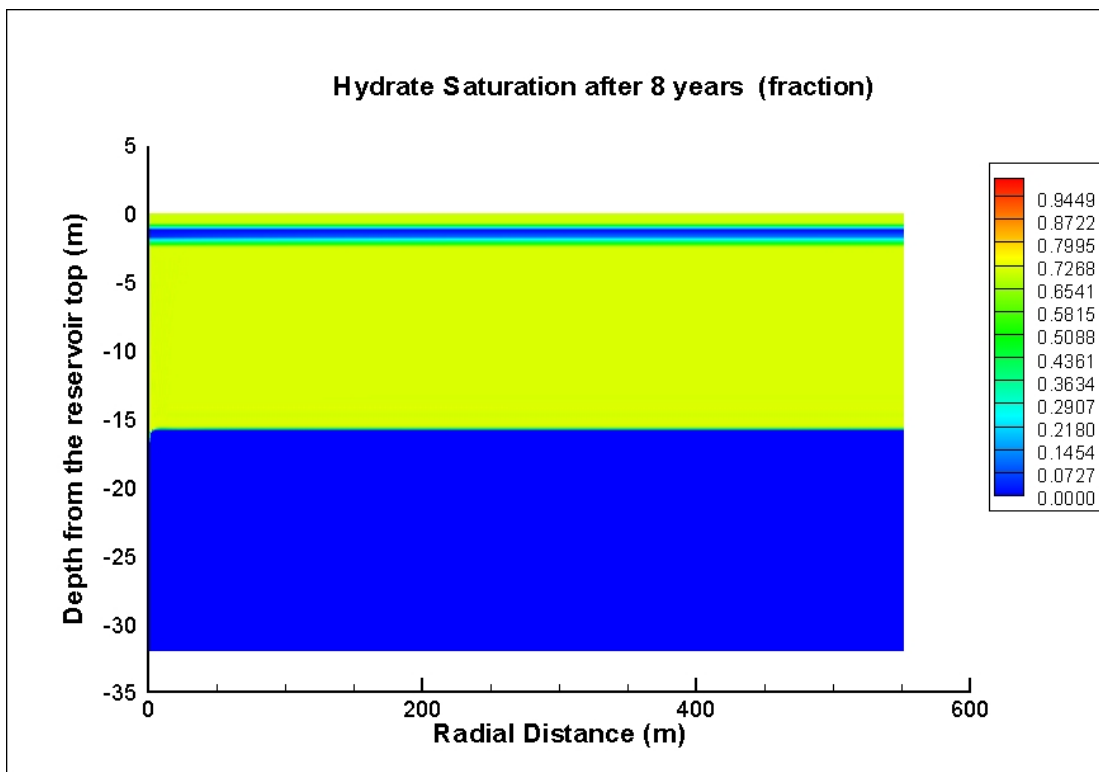
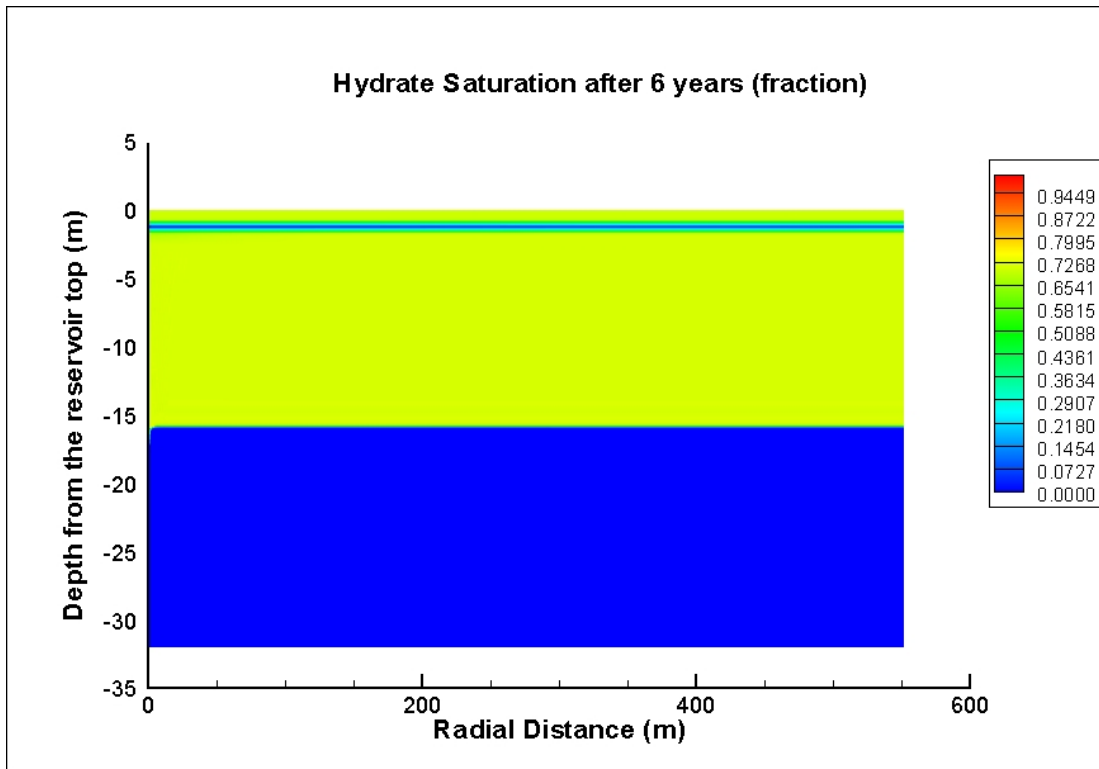


Figure 8.5 (Continued)

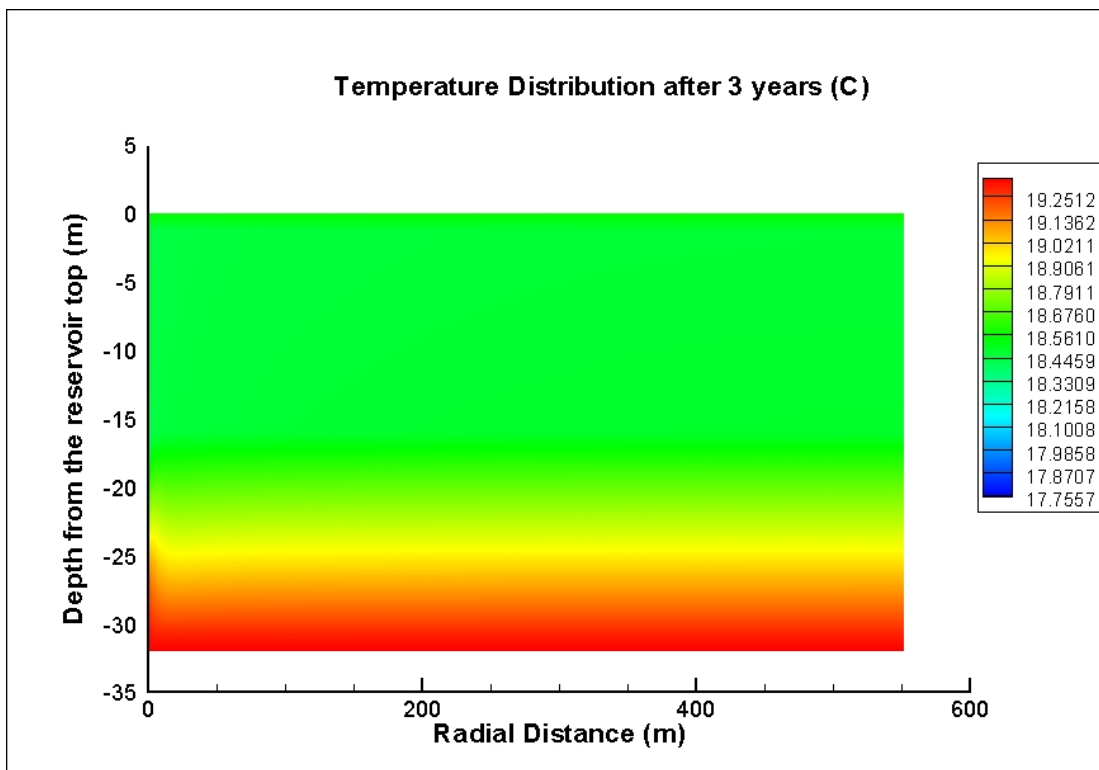
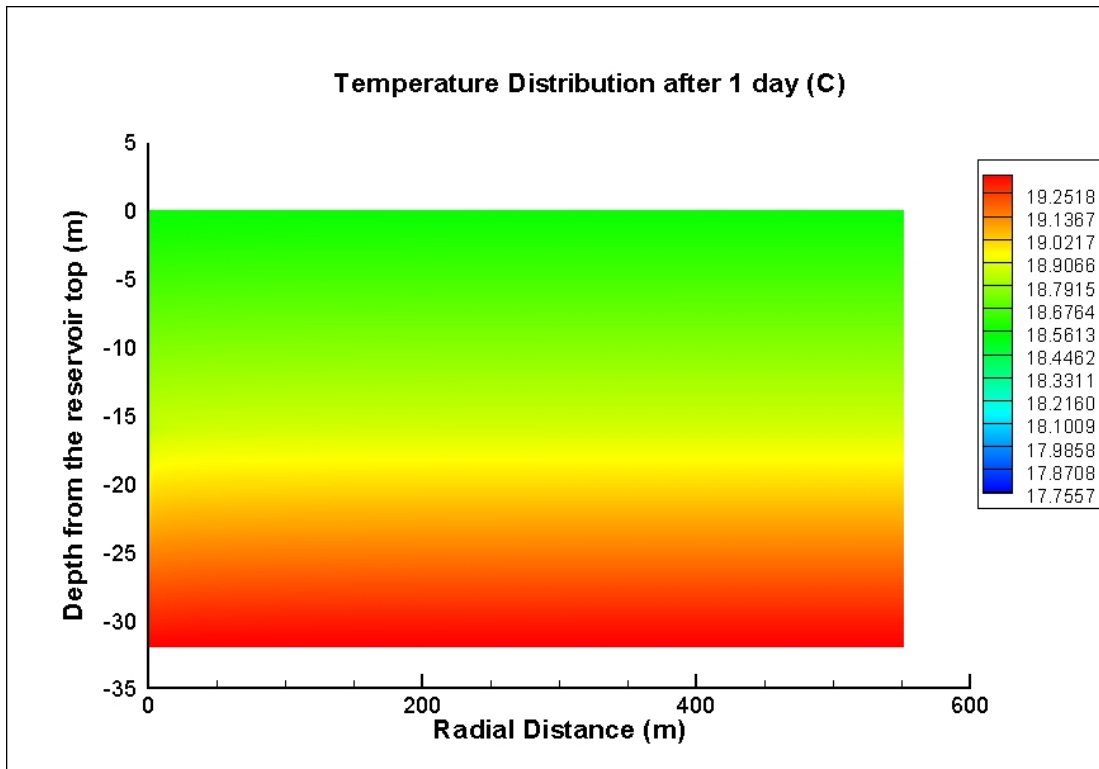


Figure 8.6: Temperature distribution for whole reservoir, Case 1b

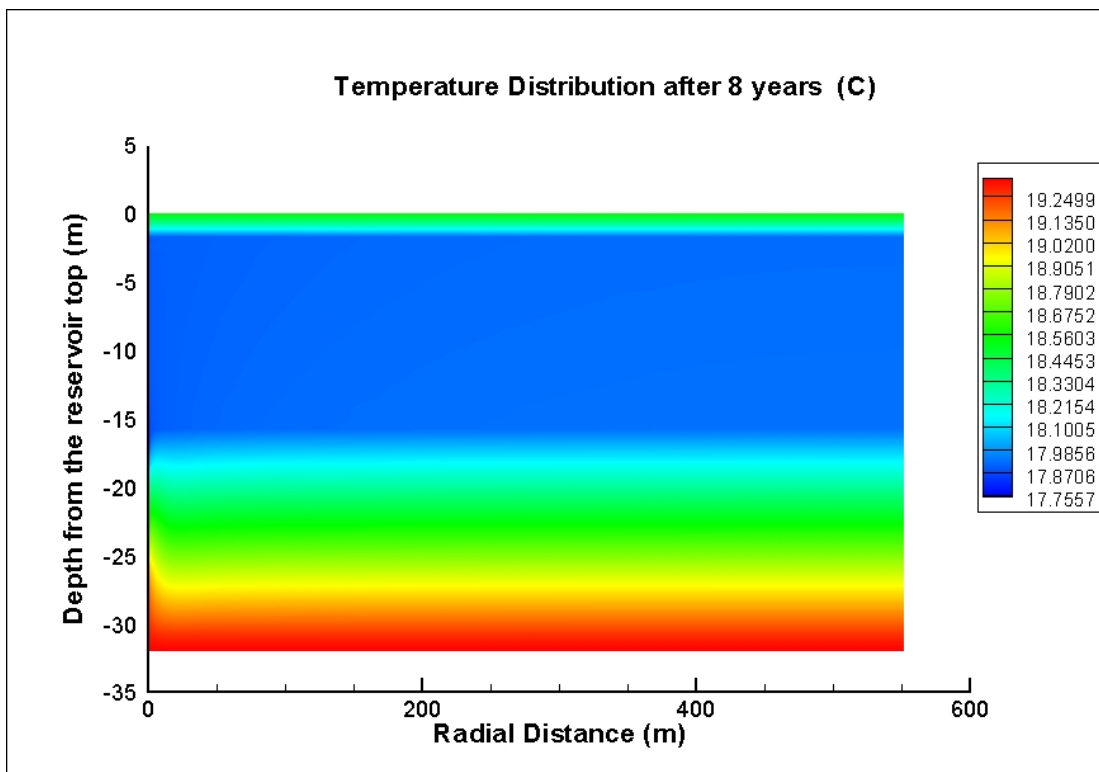
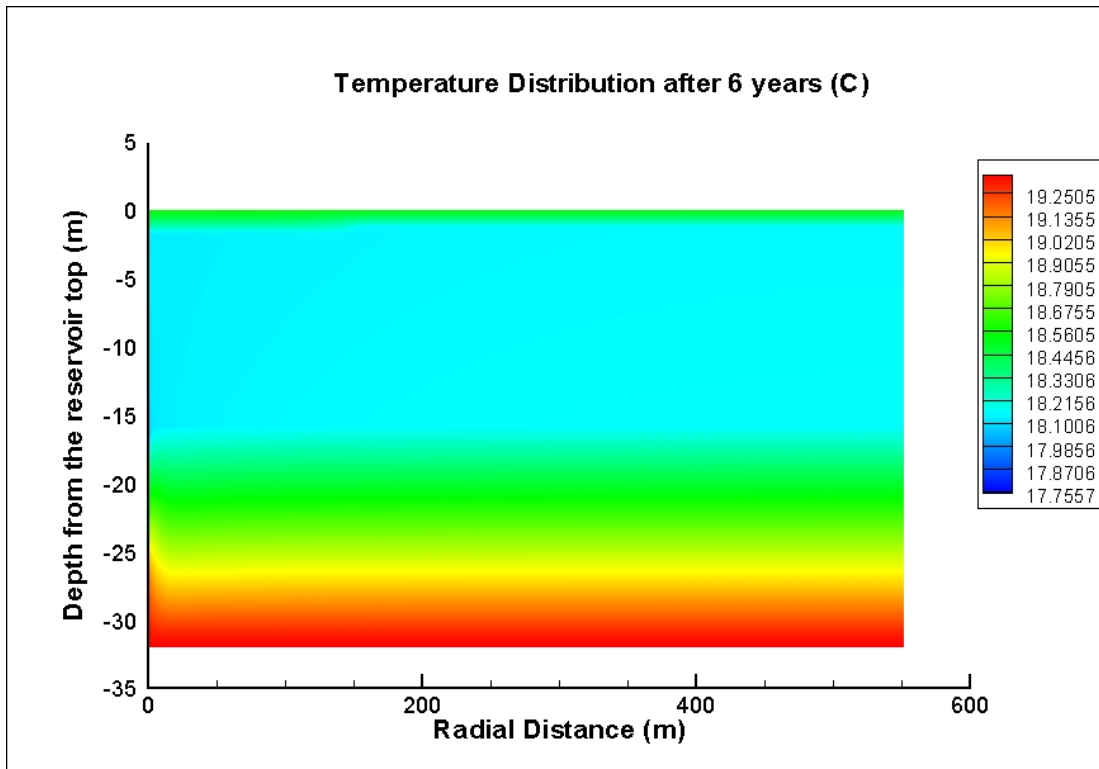


Figure 8.6 (Continued)

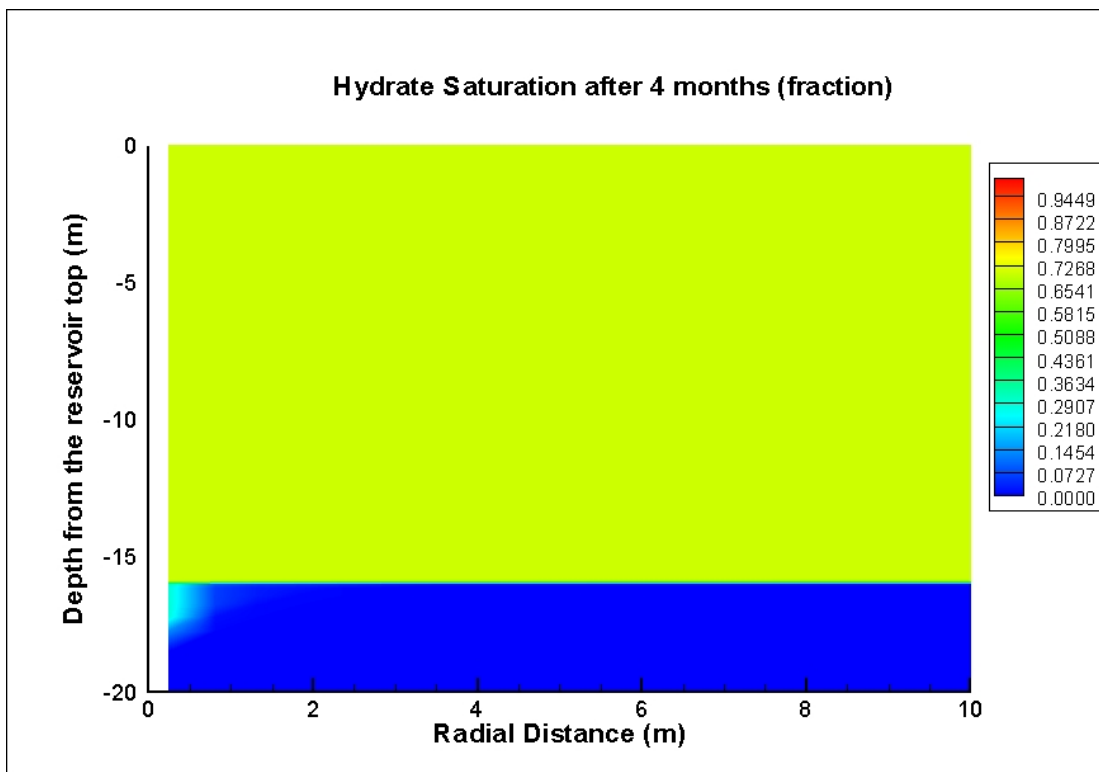
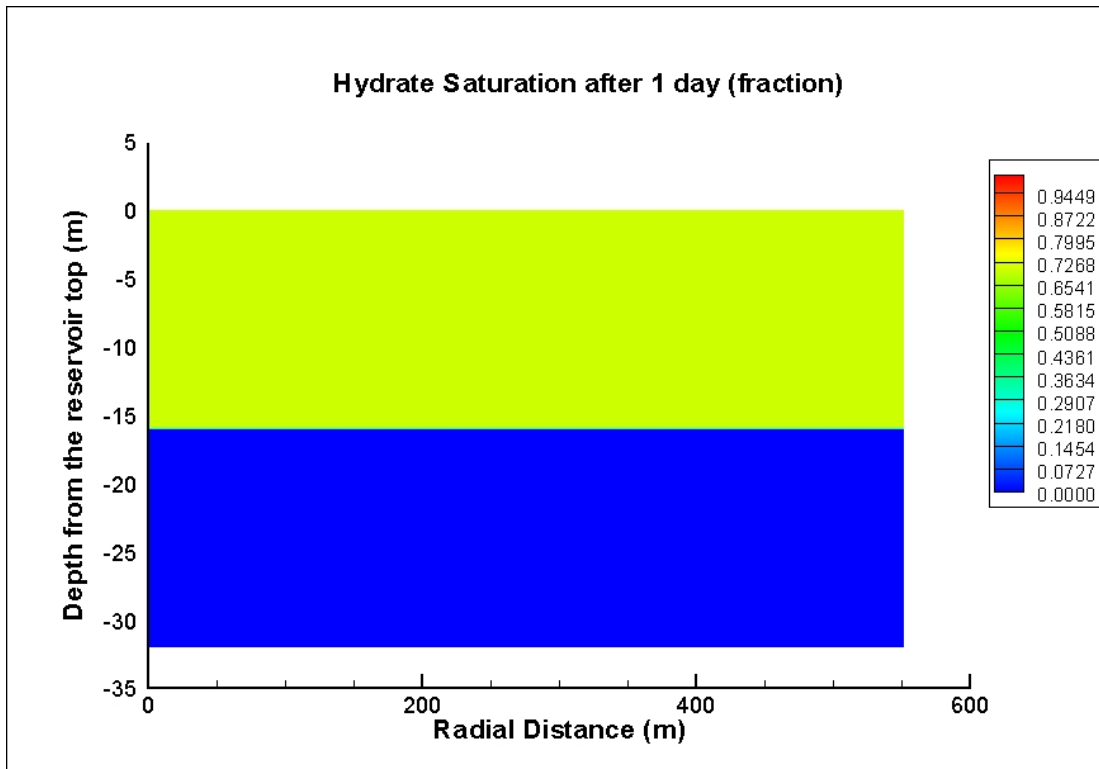


Figure 8.7: Hydrate saturation distribution near well-bore, Case 1b

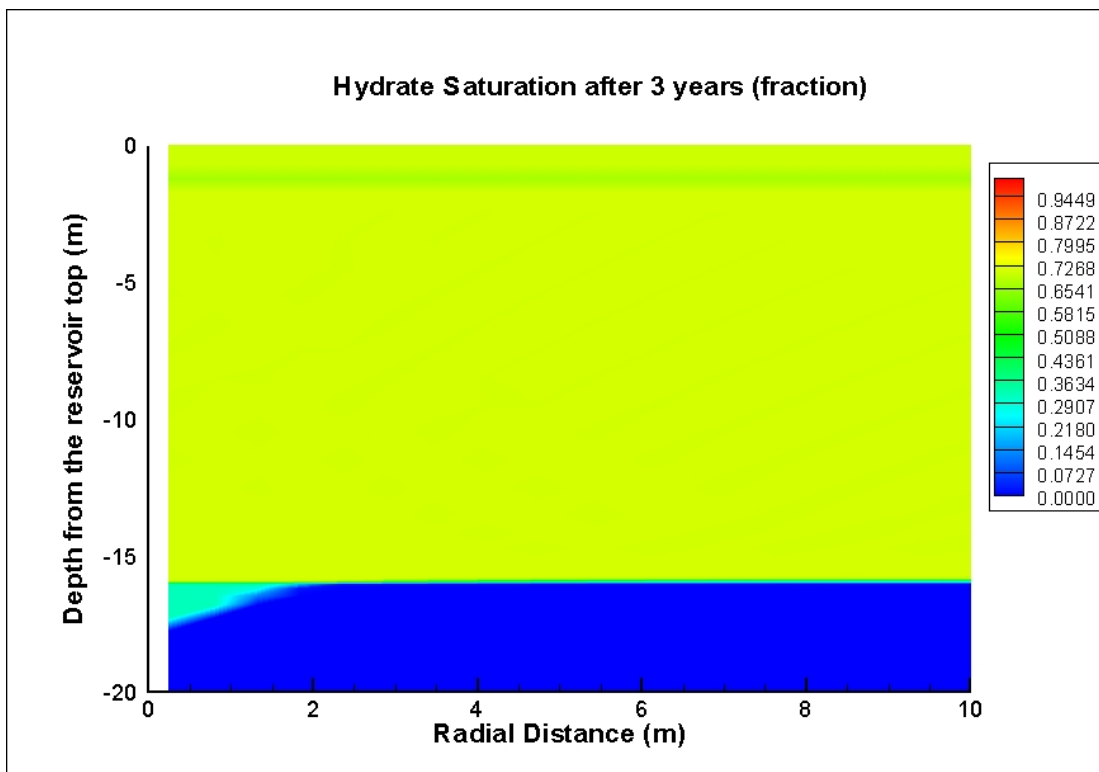
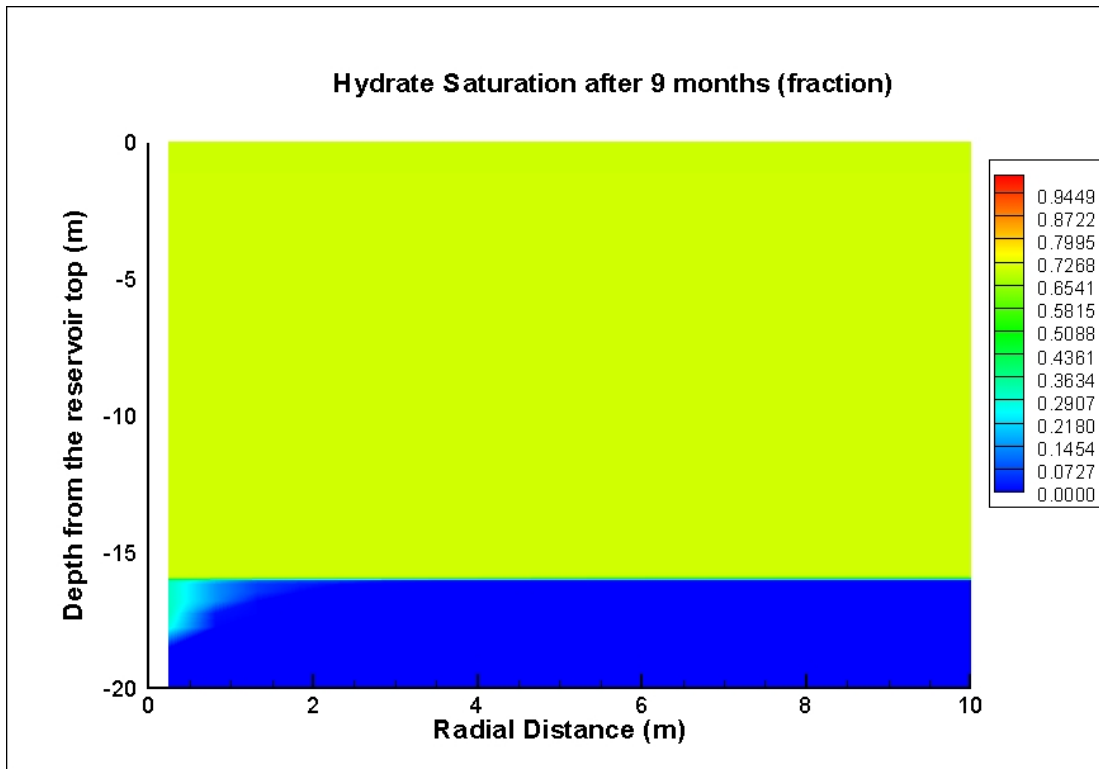


Figure 8.7 (Continued)

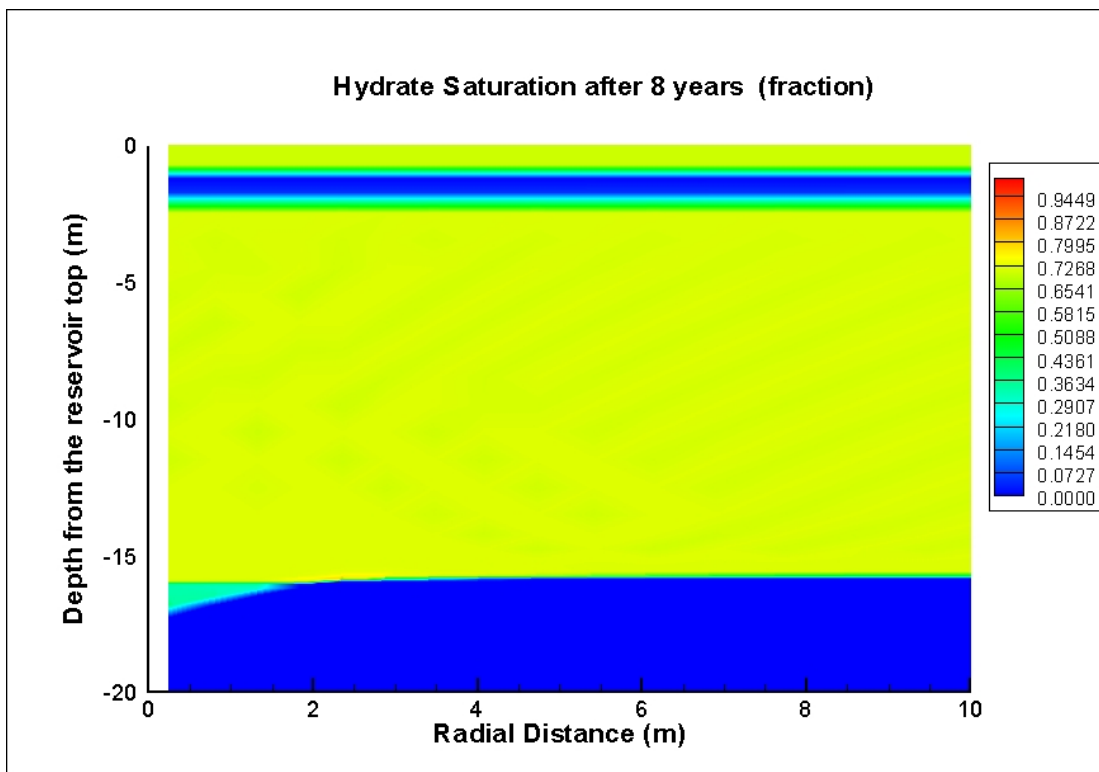
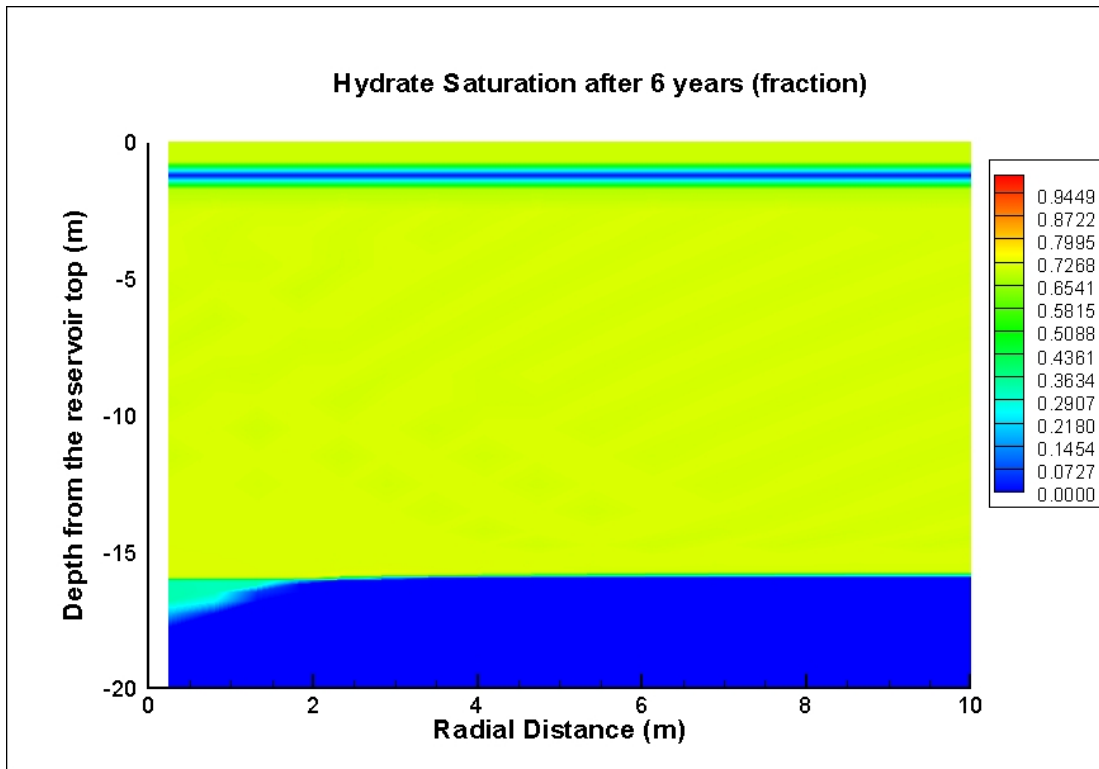
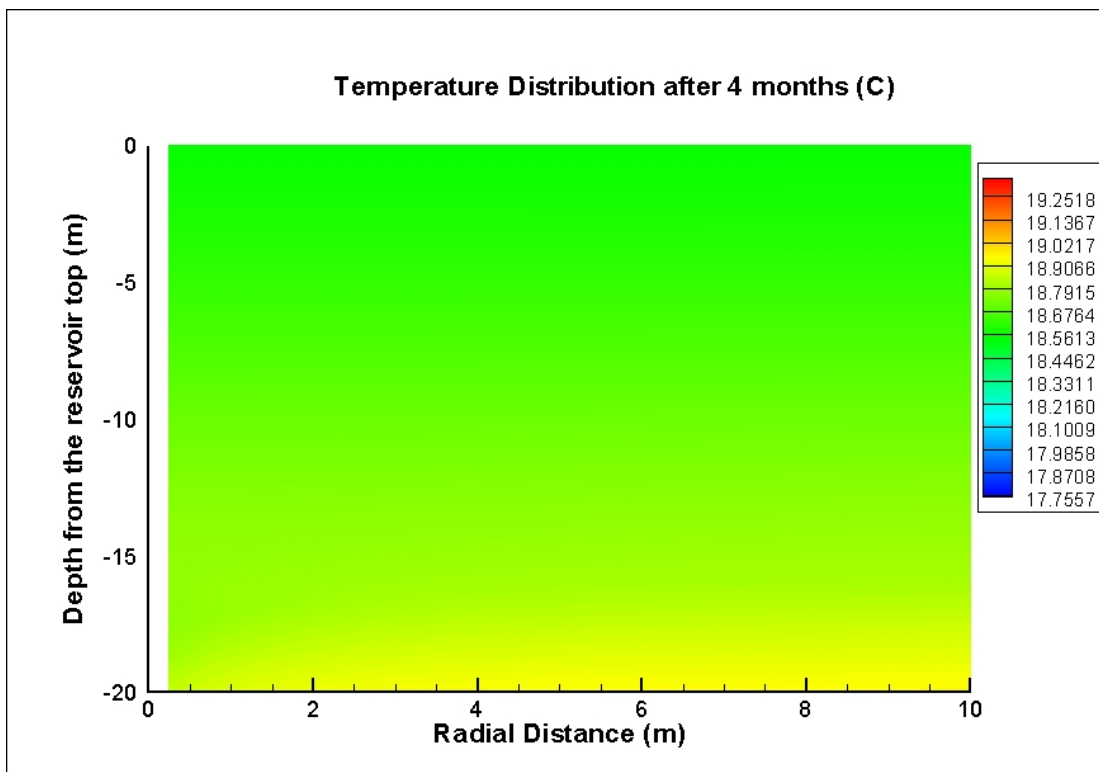
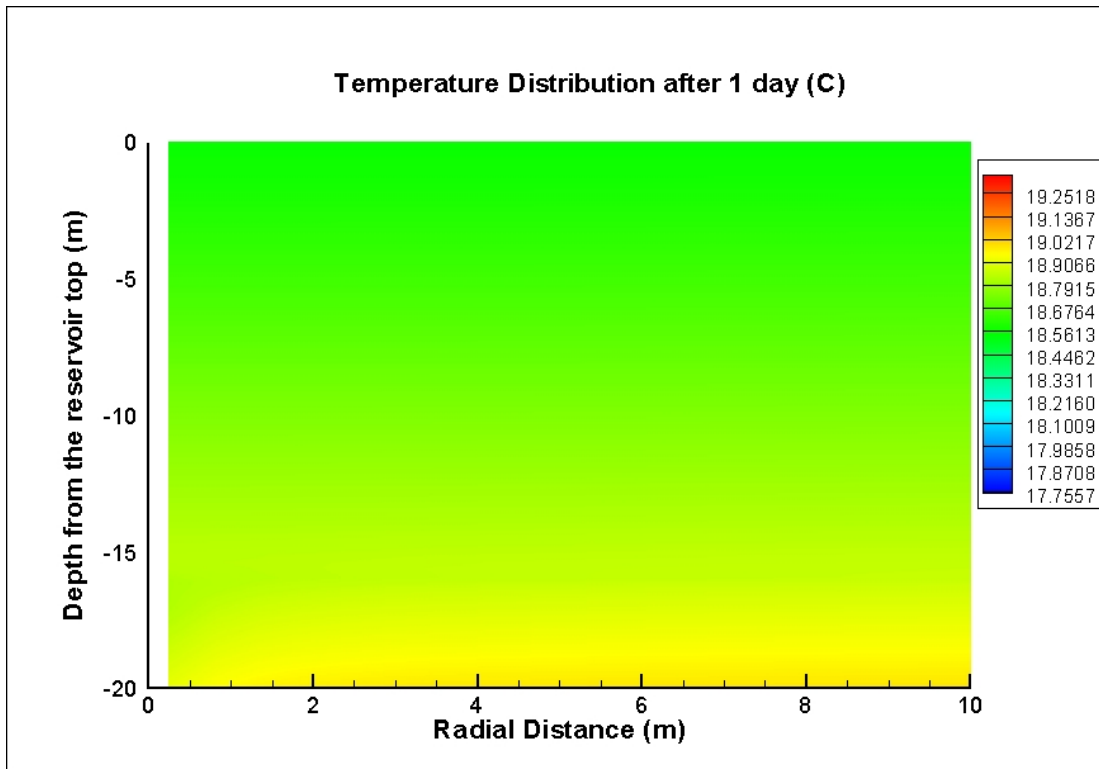


Figure 8.7 (Continued)



**Figure 8.8: Temperature distribution near well-bore, Case 1b**

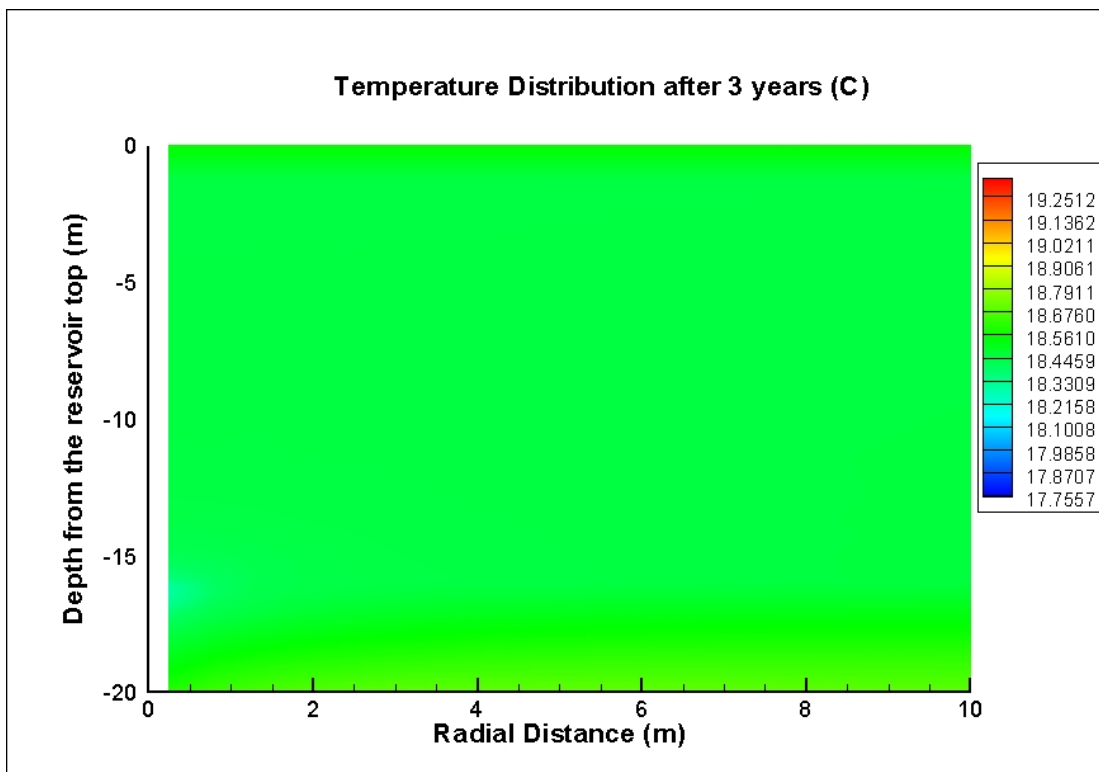
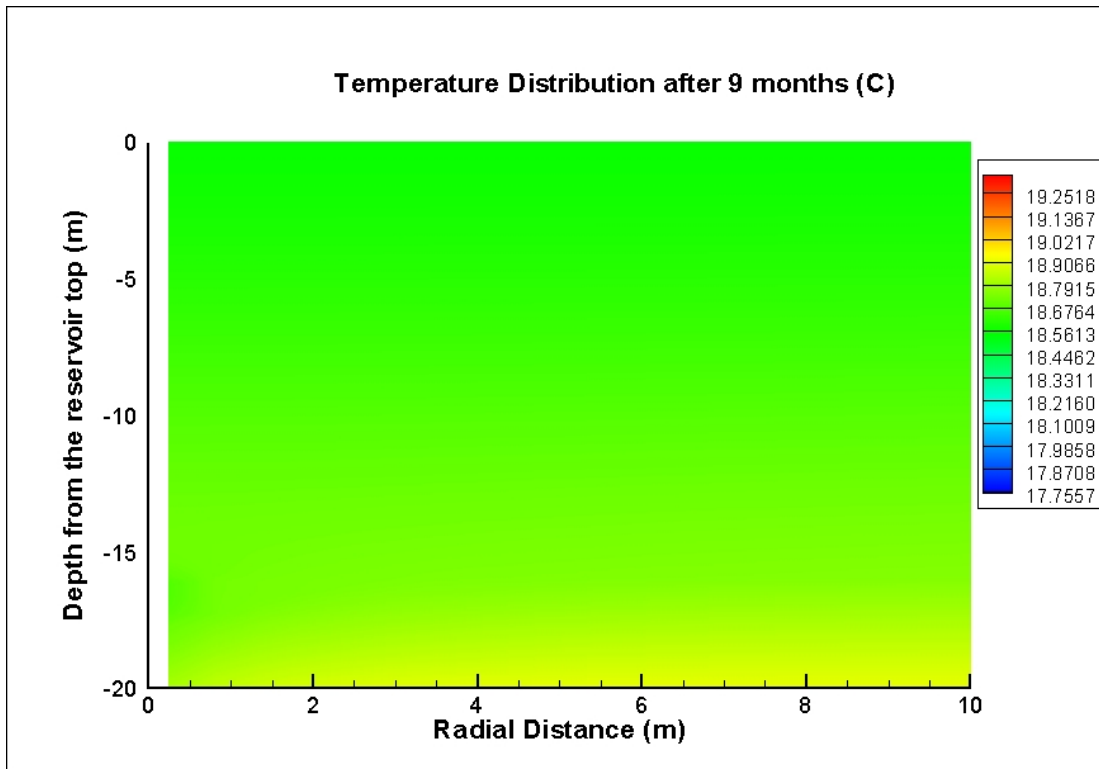


Figure 8.8 (Continued)

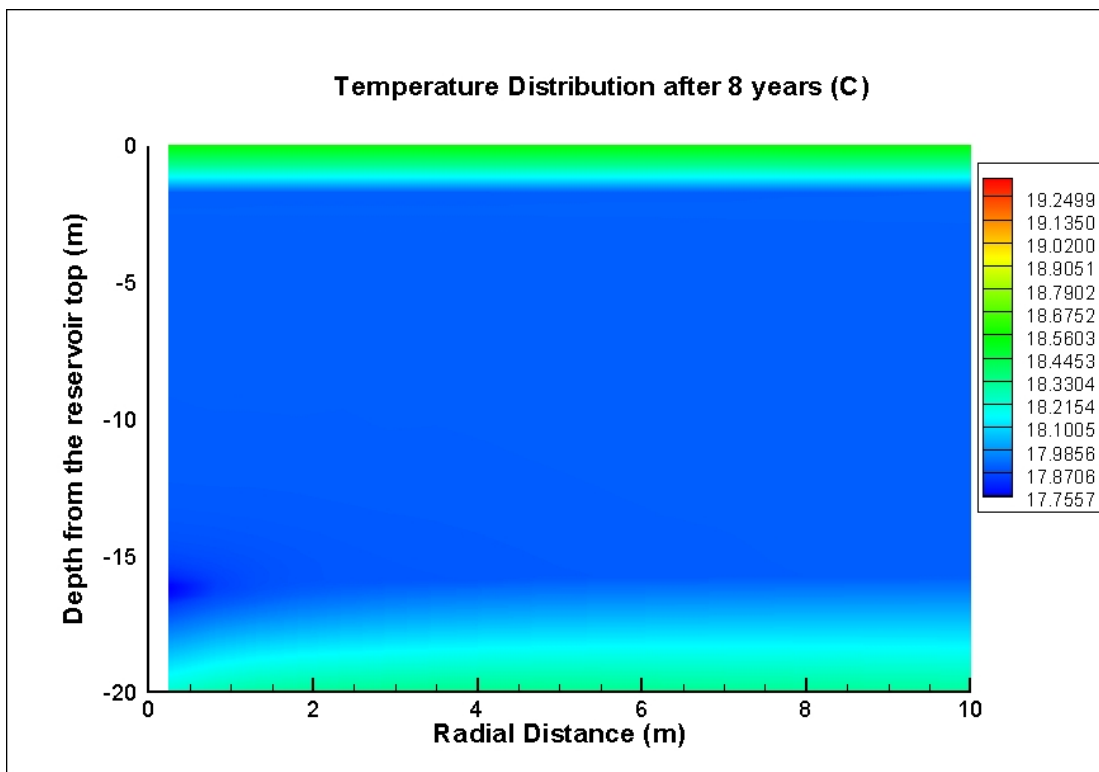
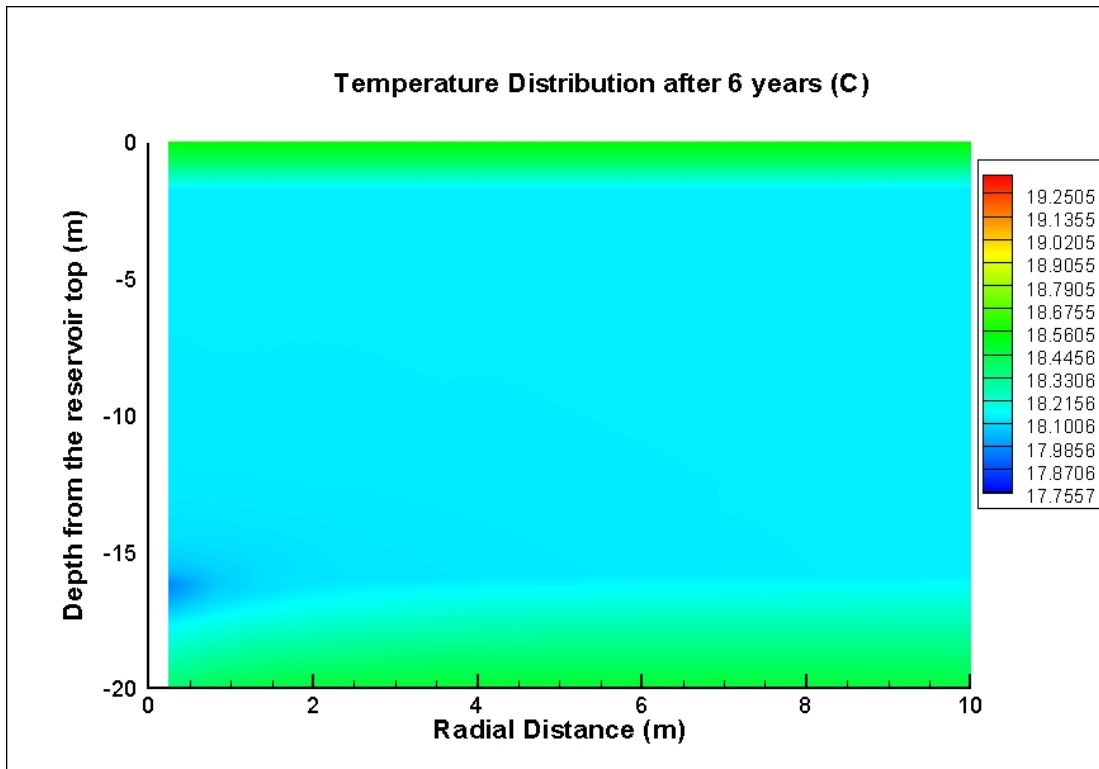


Figure 8.8 (Continued)

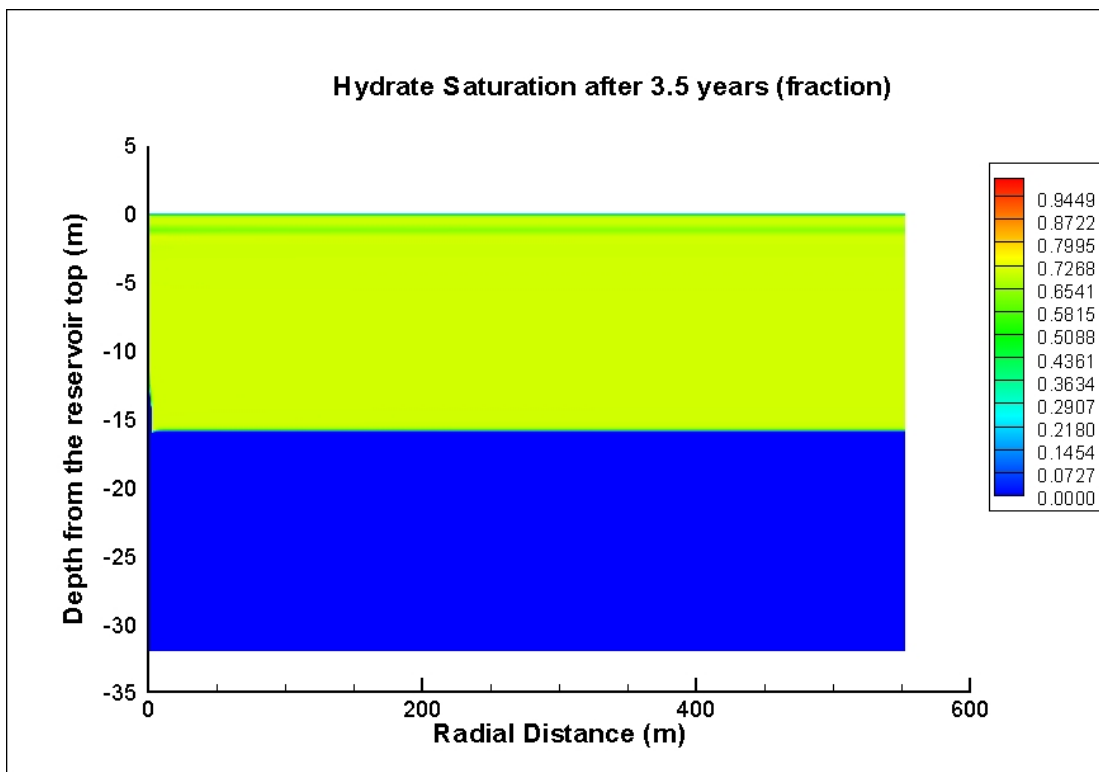
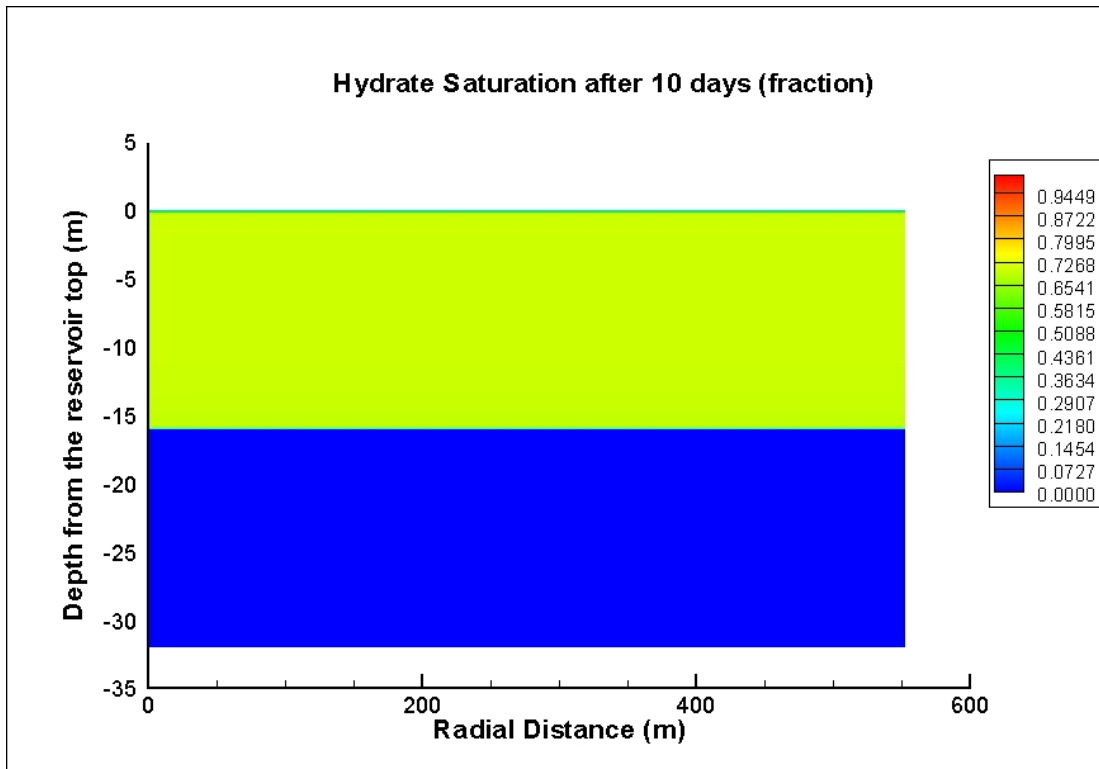


Figure 8.9: Hydrate saturation distribution for whole reservoir, Case 2a

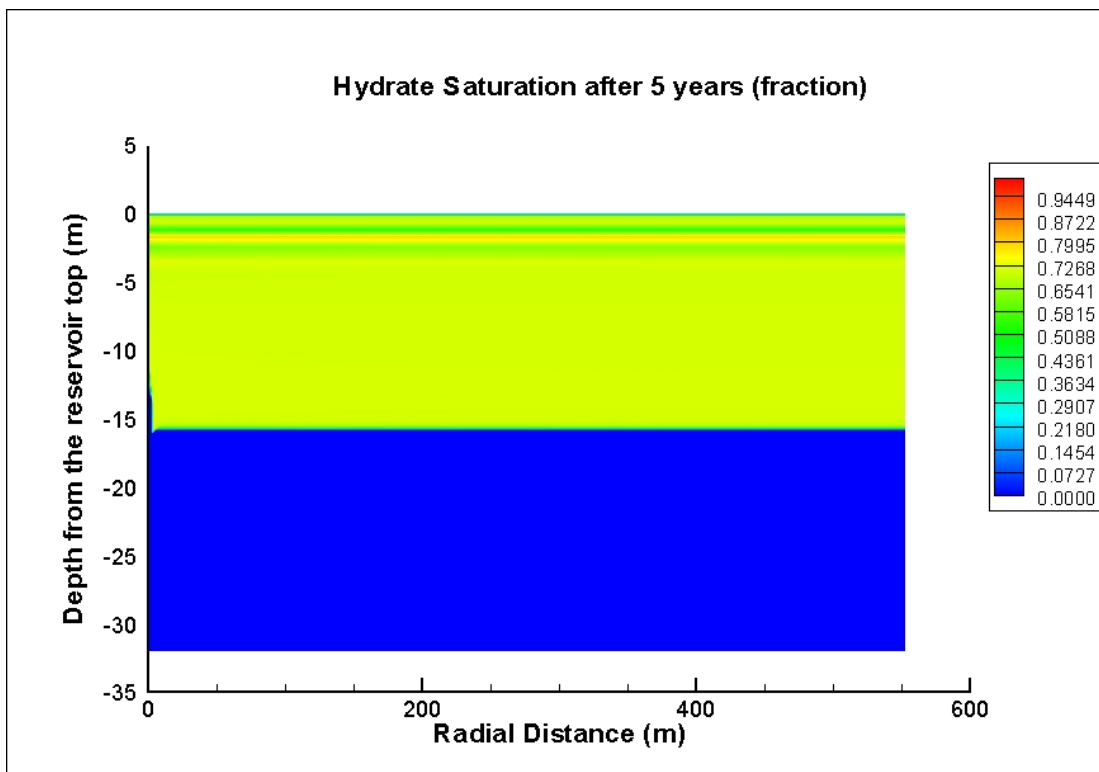
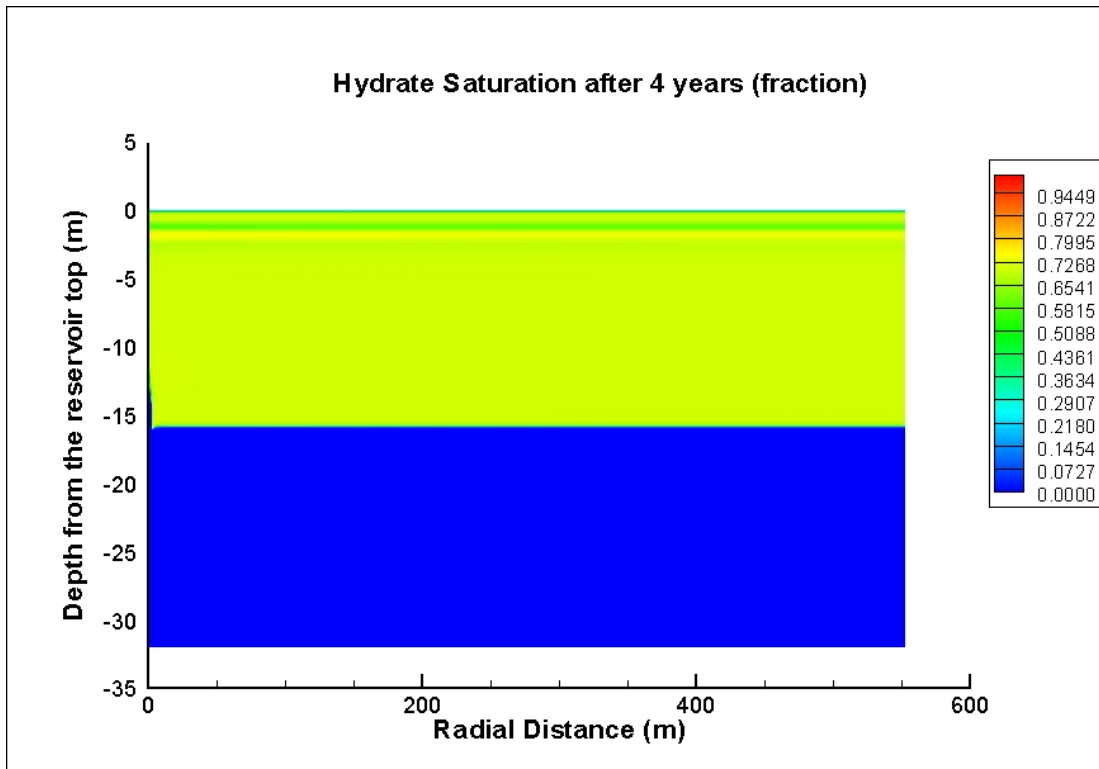


Figure 8.9 (Continued)

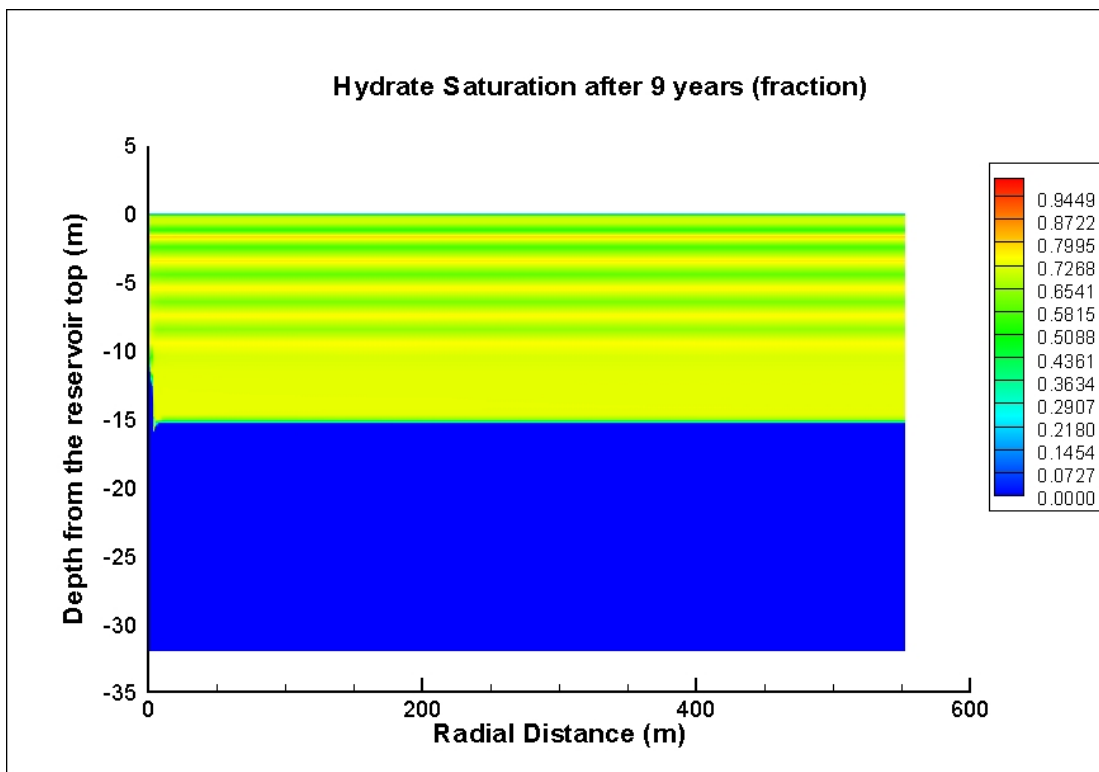
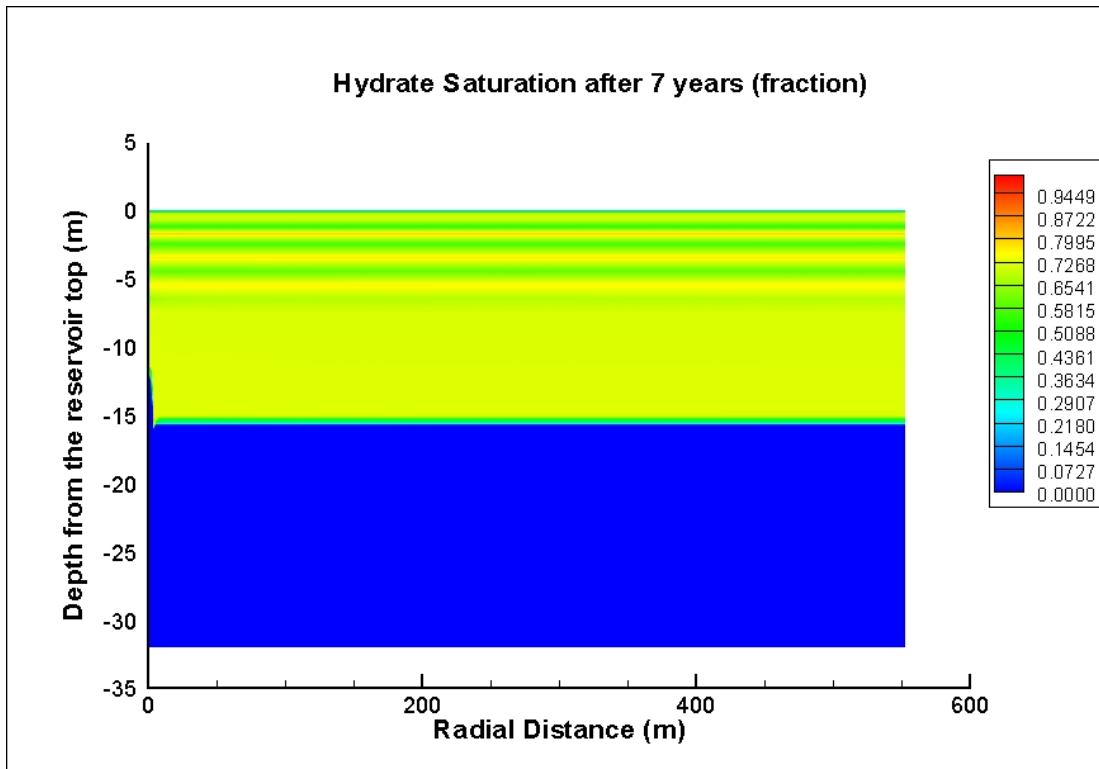


Figure 8.9 (Continued)

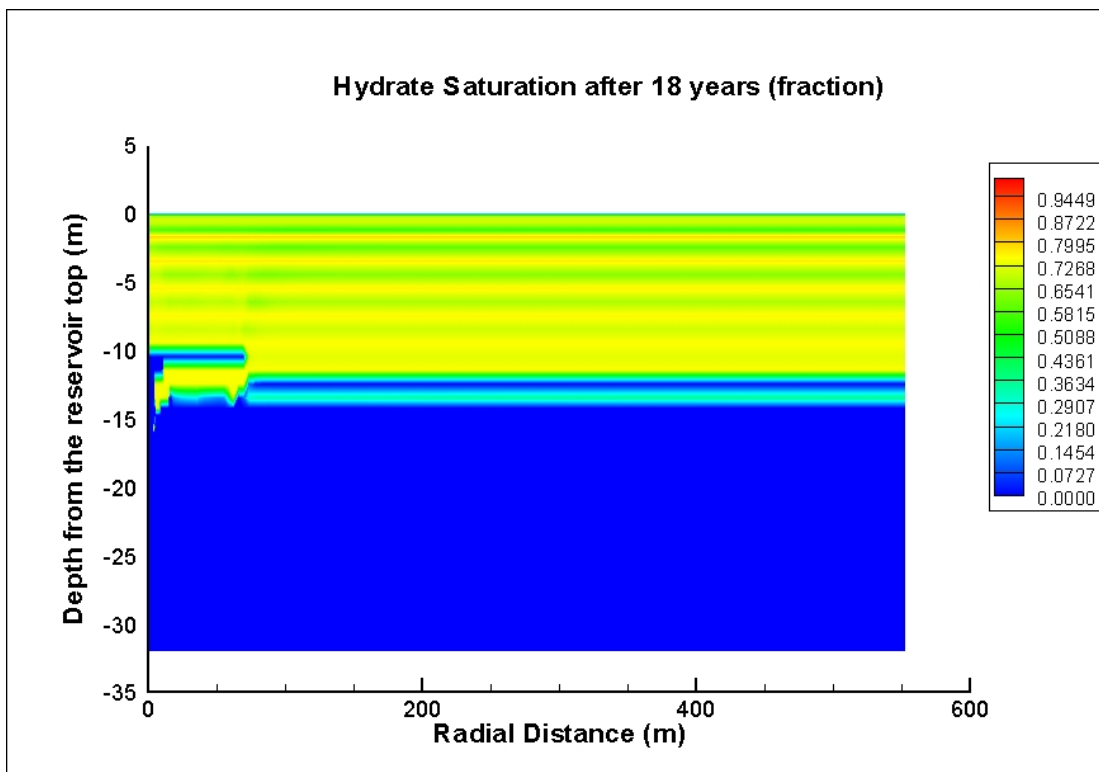
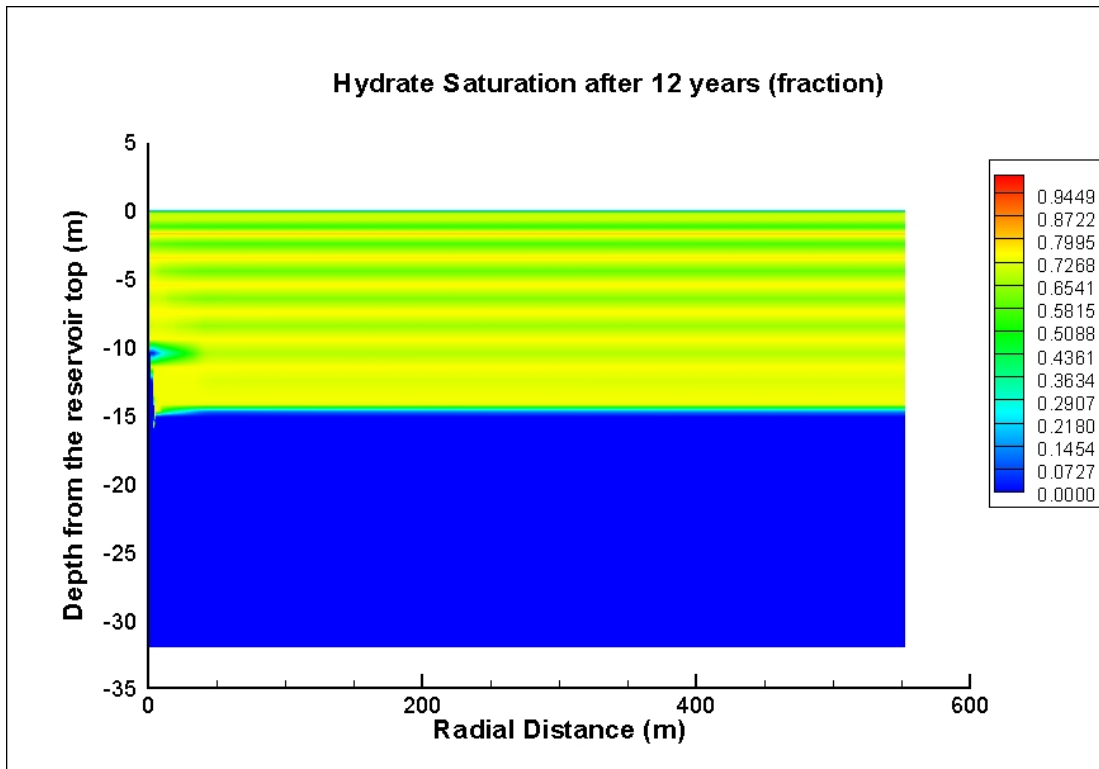
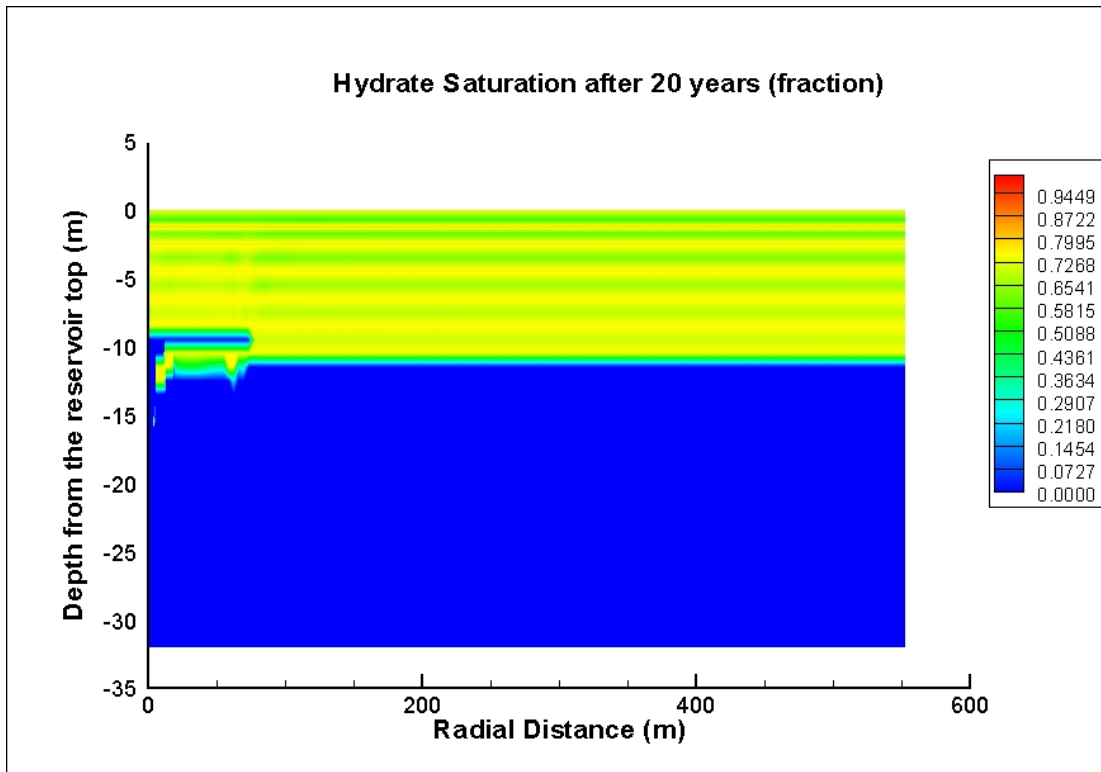


Figure 8.9 (Continued)



**Figure 8.9 (Continued)**

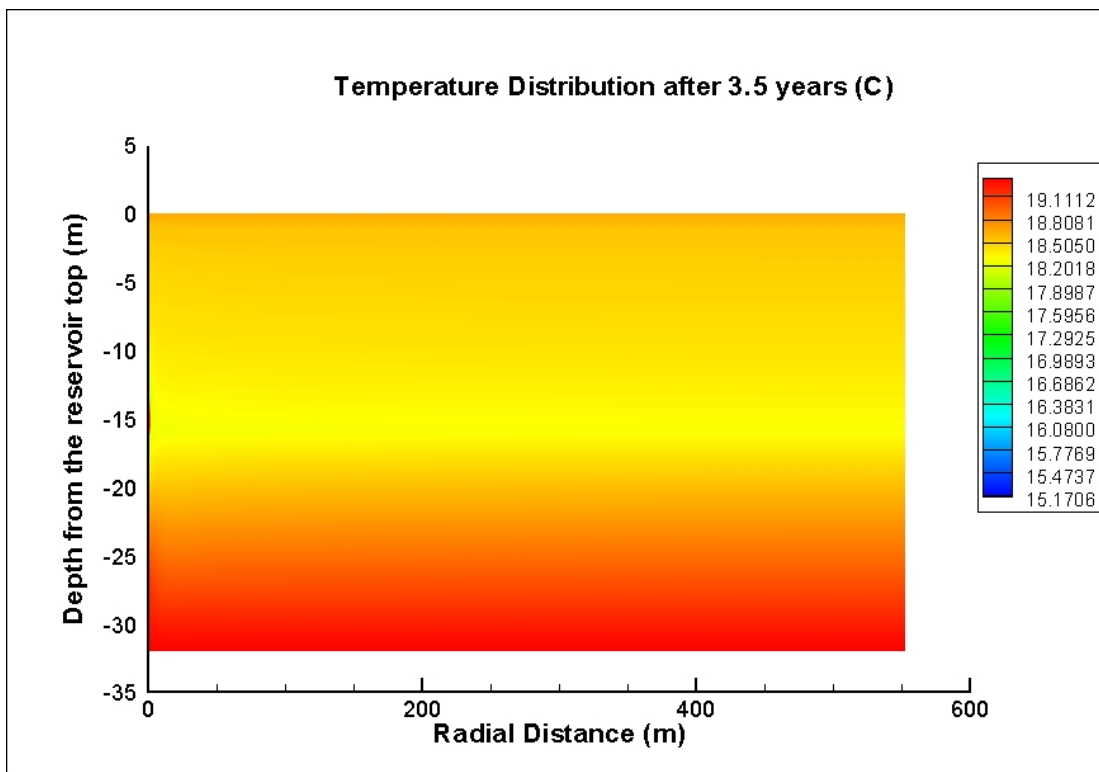
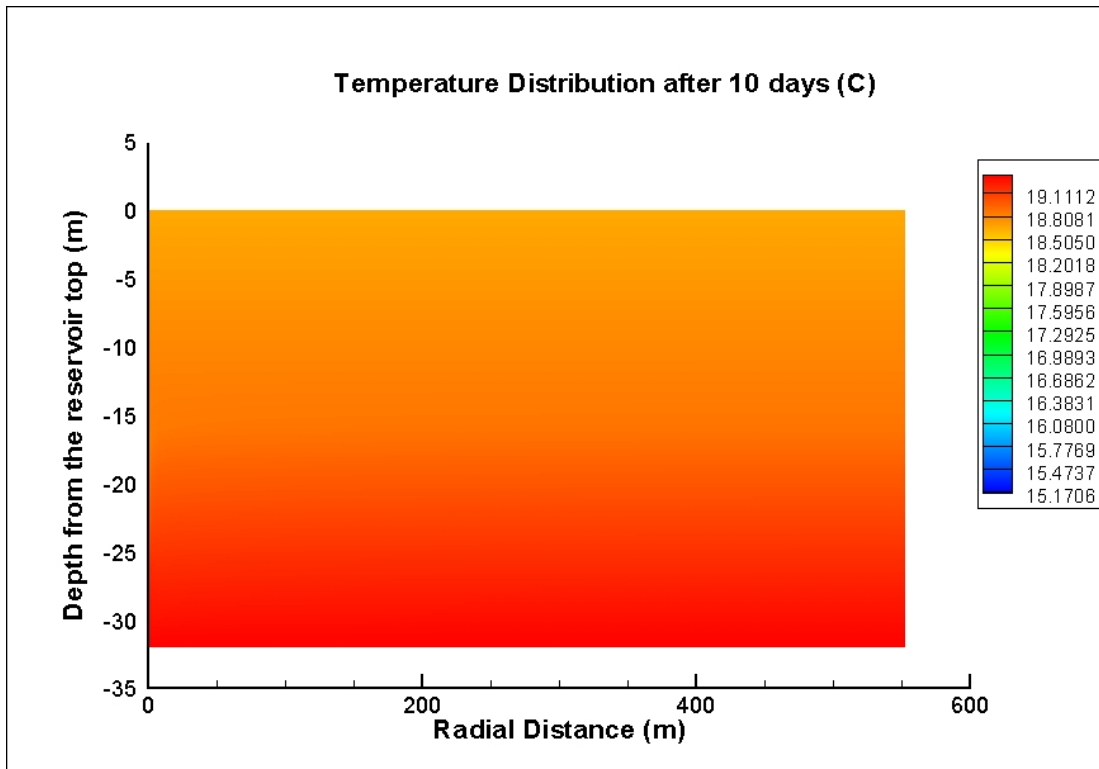


Figure 8.10: Temperature distribution for whole reservoir, Case 2a

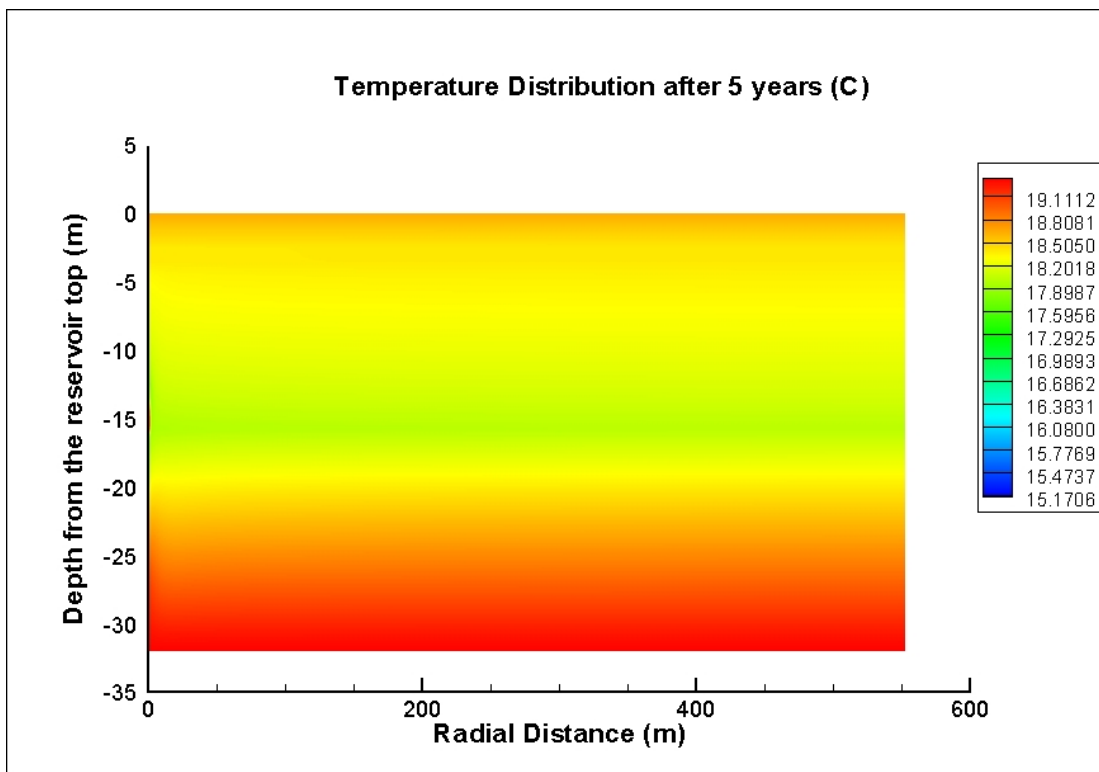
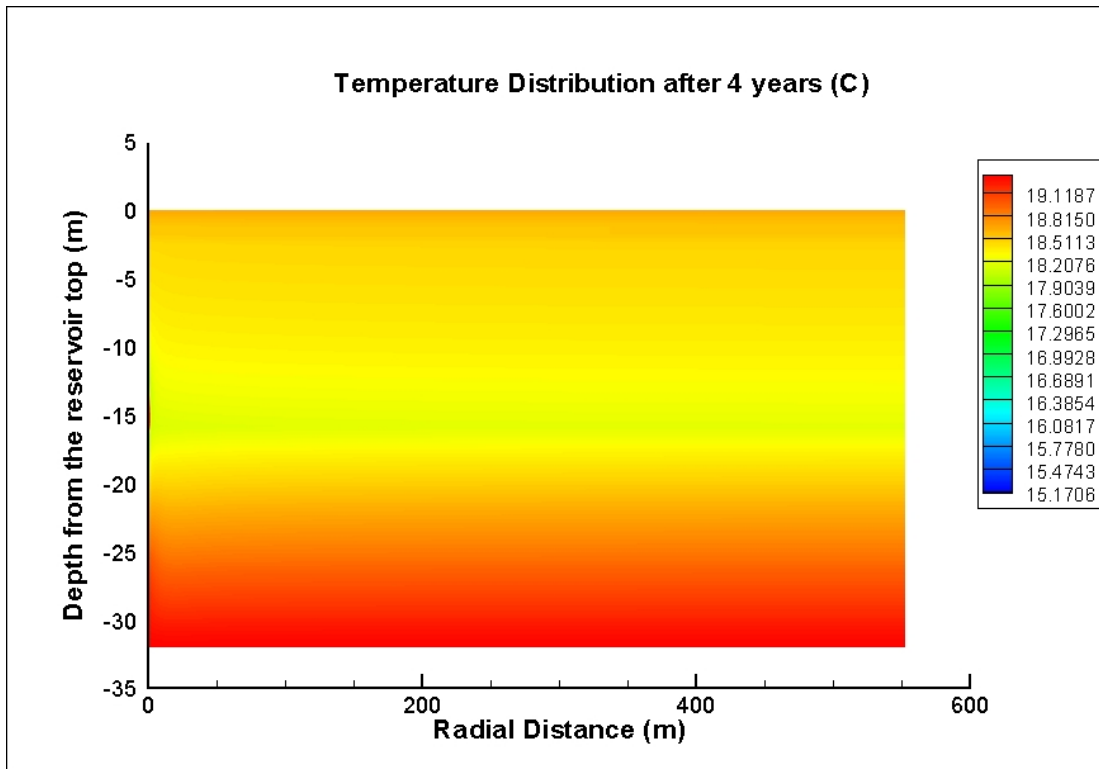


Figure 8.10 (Continued)

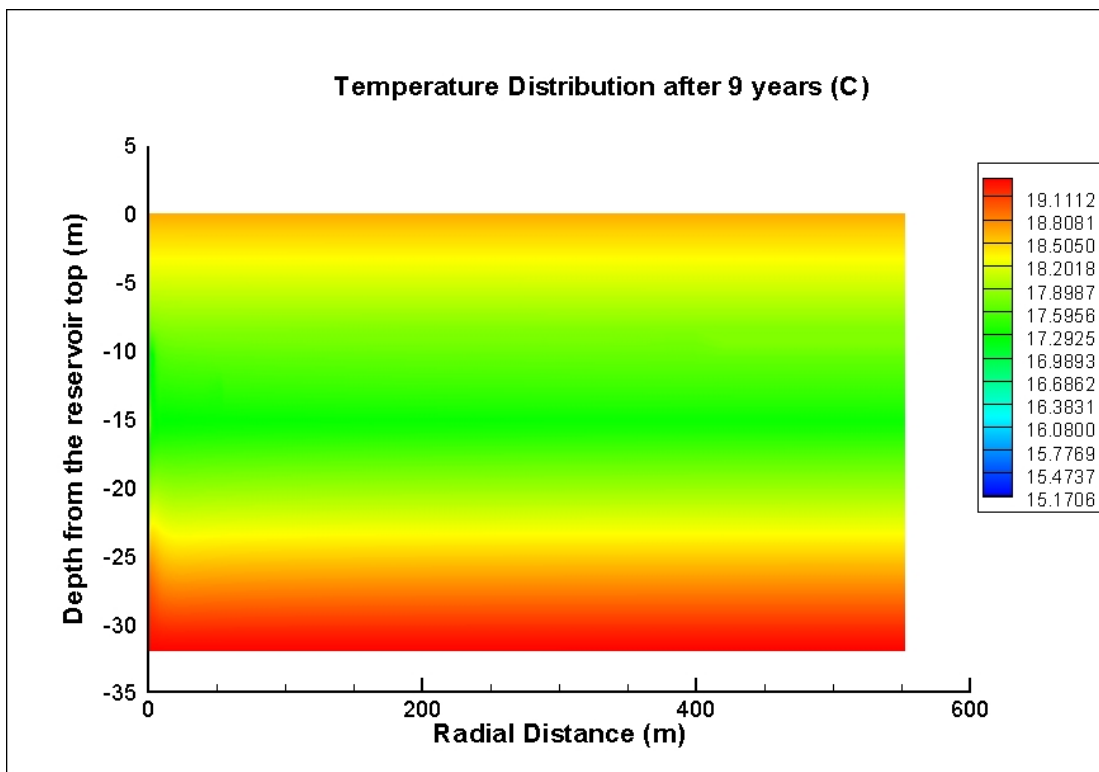
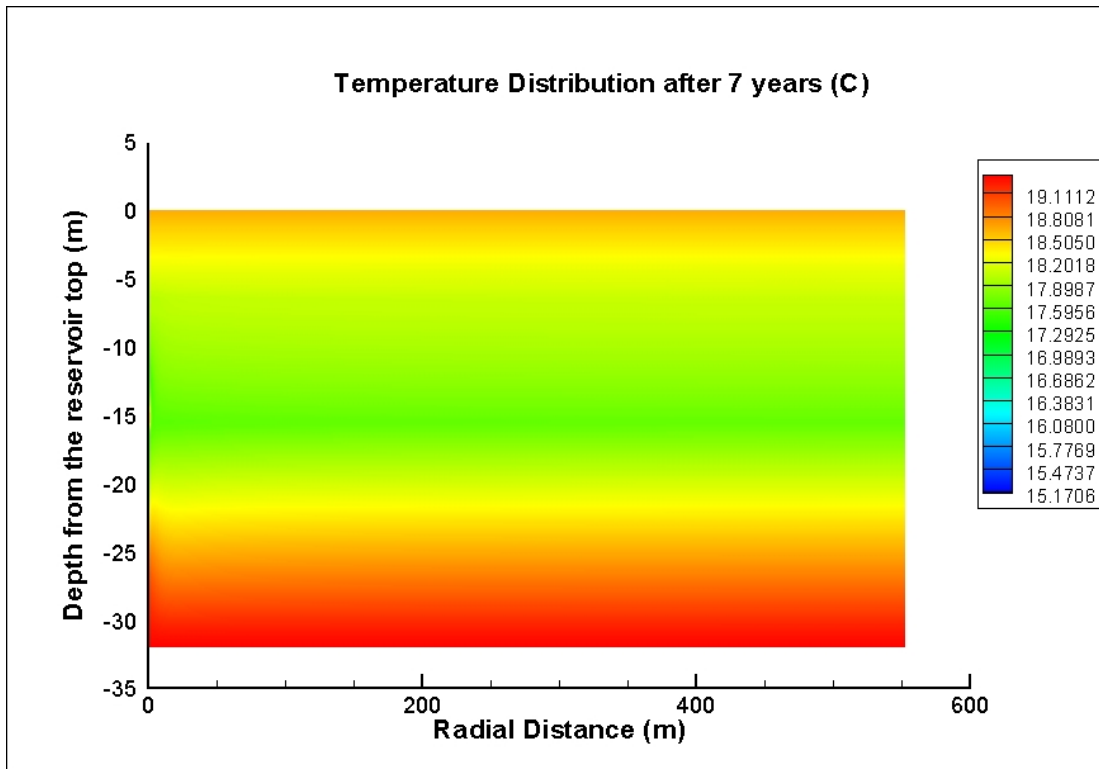


Figure 8.10 (Continued)

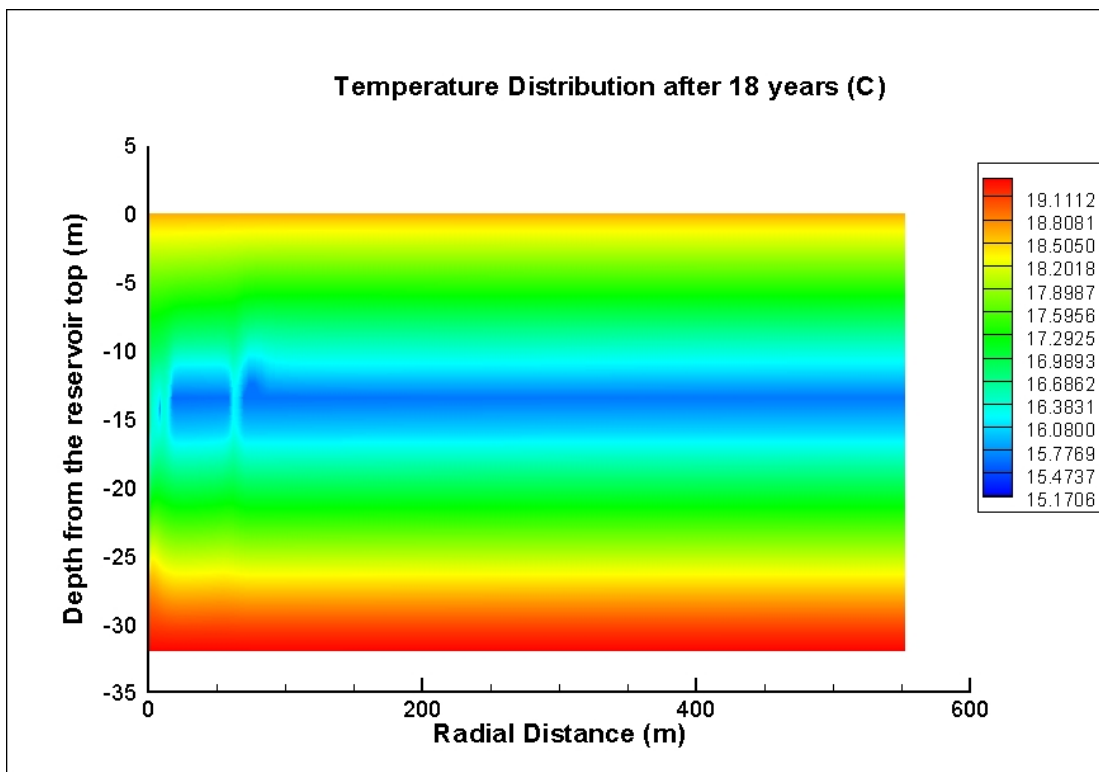
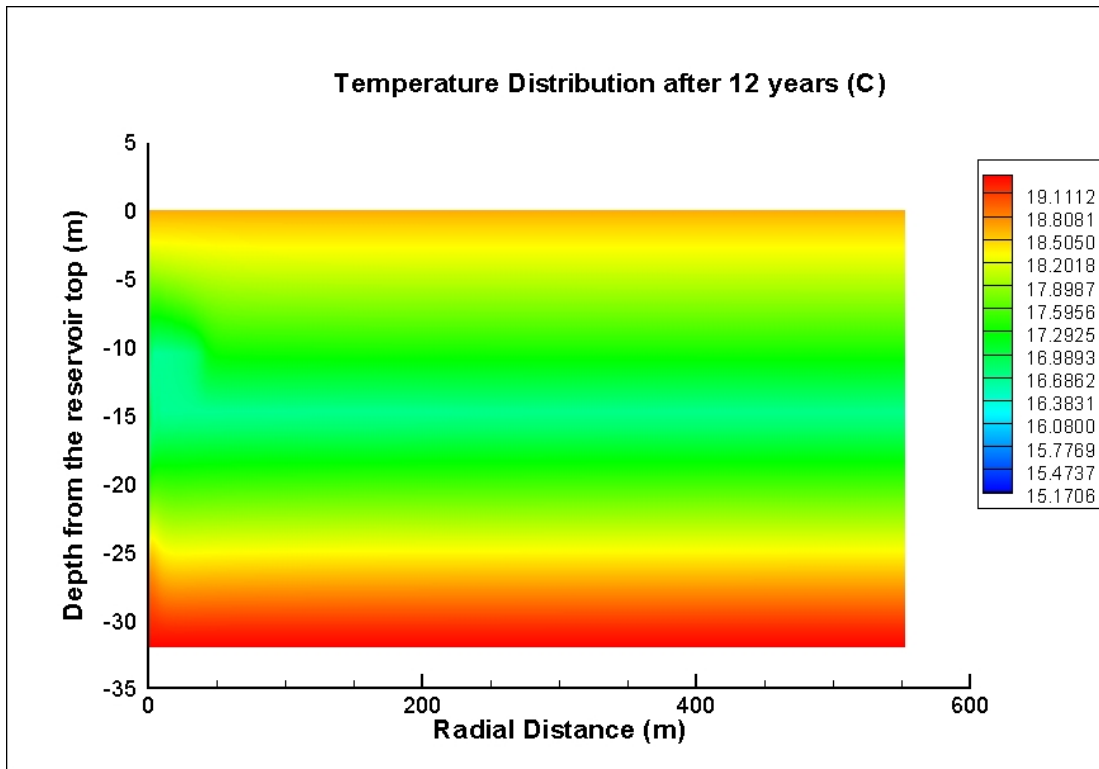
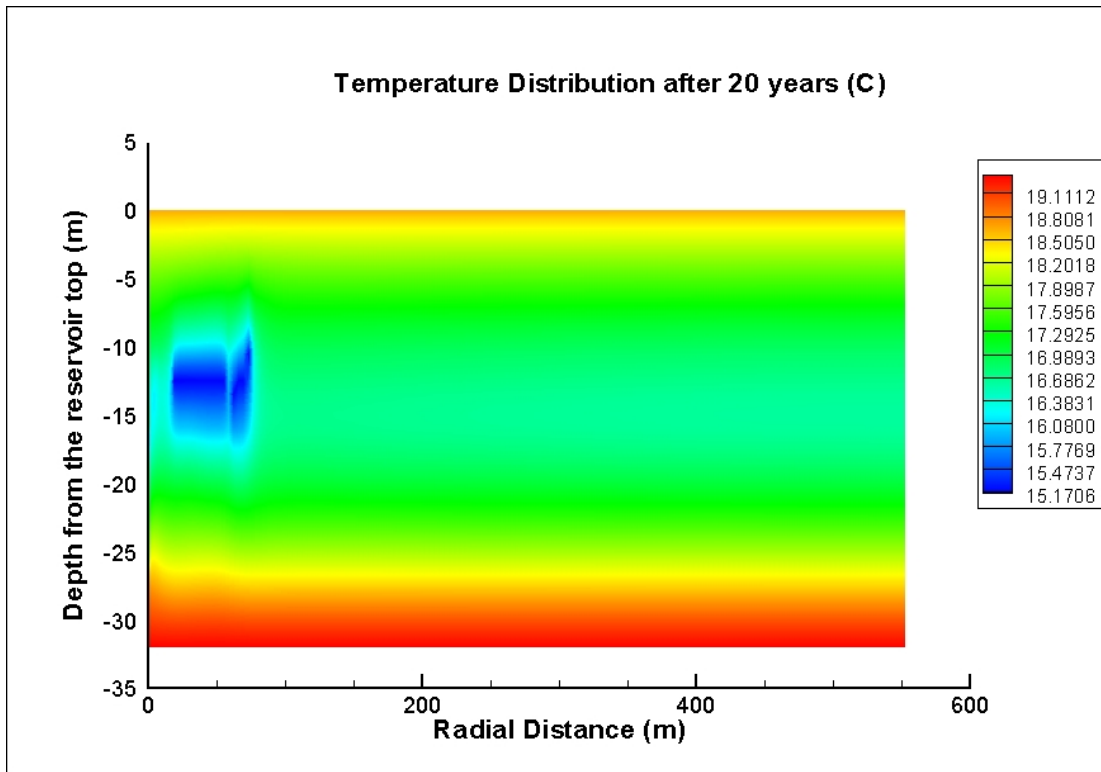


Figure 8.10 (Continued)



**Figure 8.10 (Continued)**

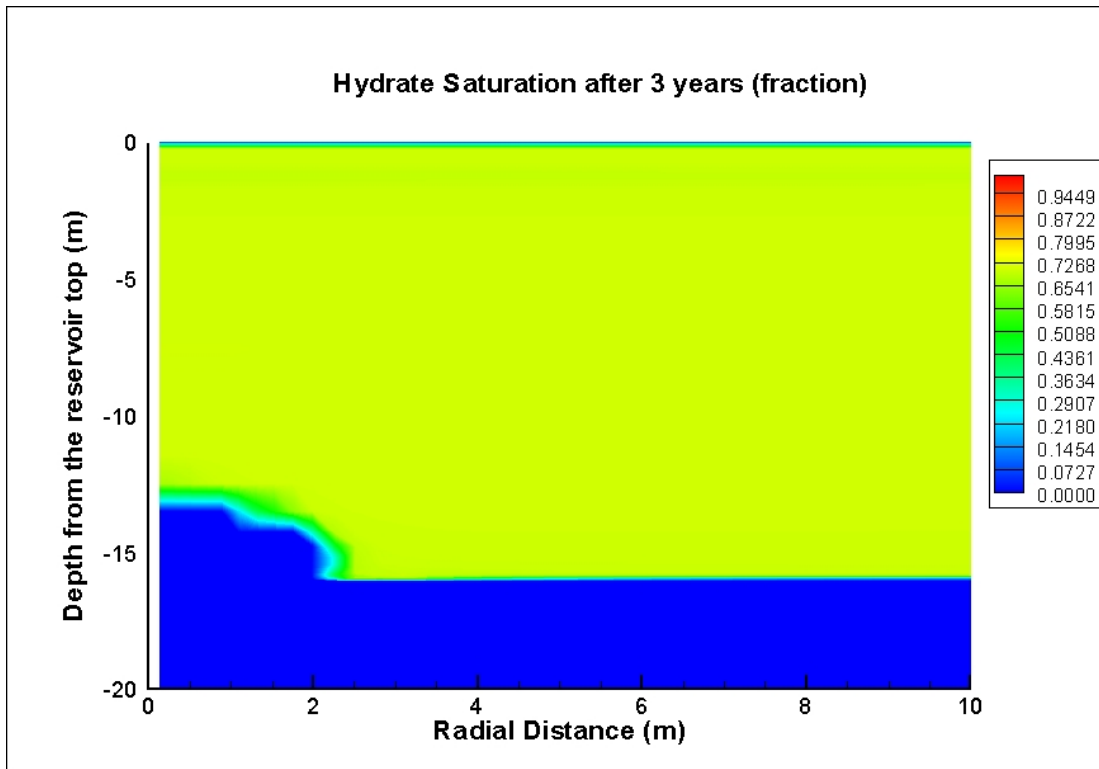
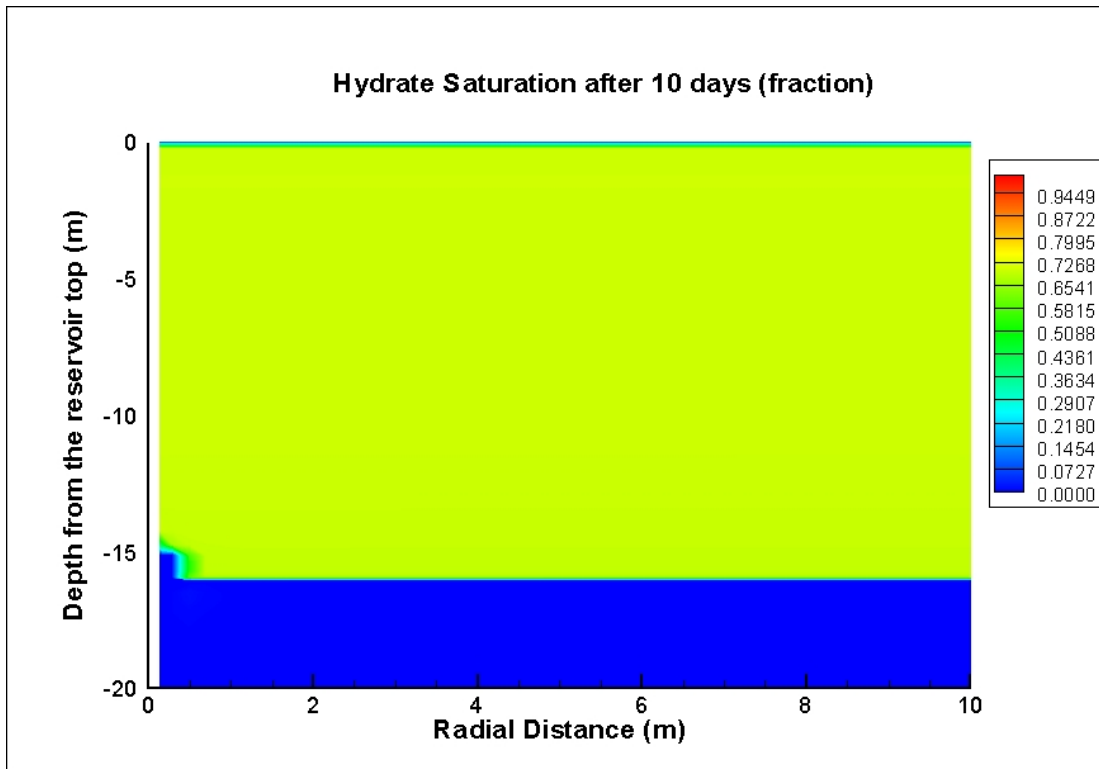


Figure 8.11: Hydrate saturation distribution near well-bore, Case 2a

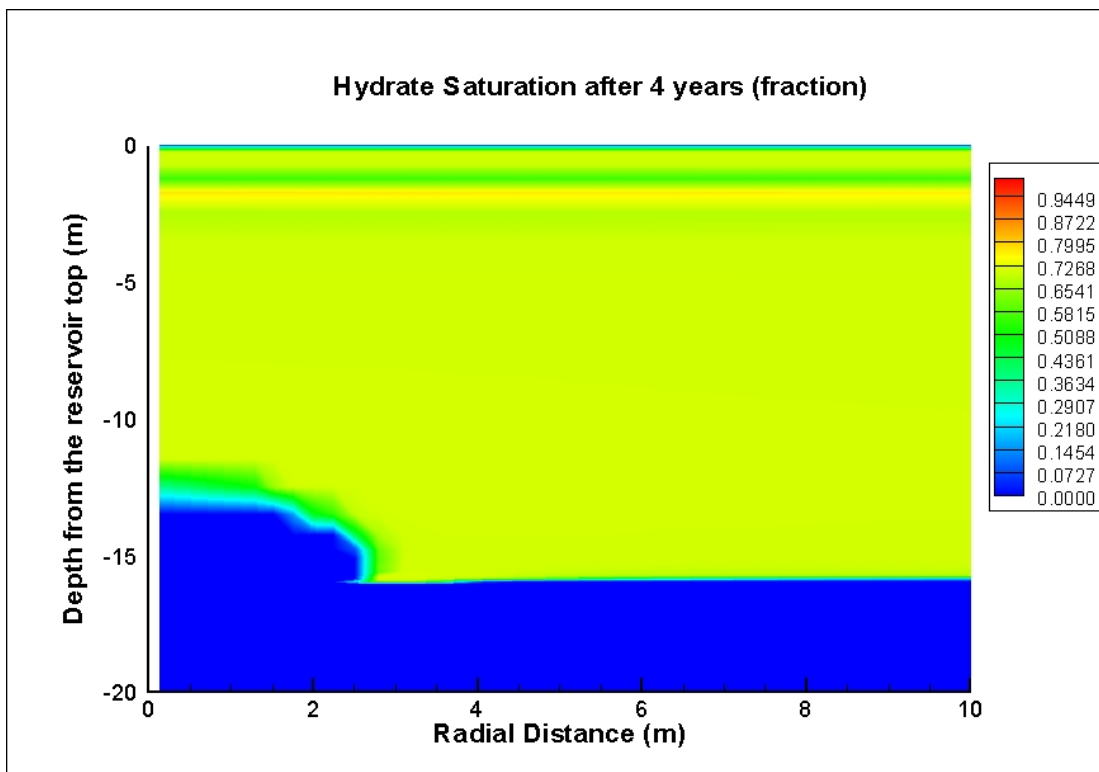
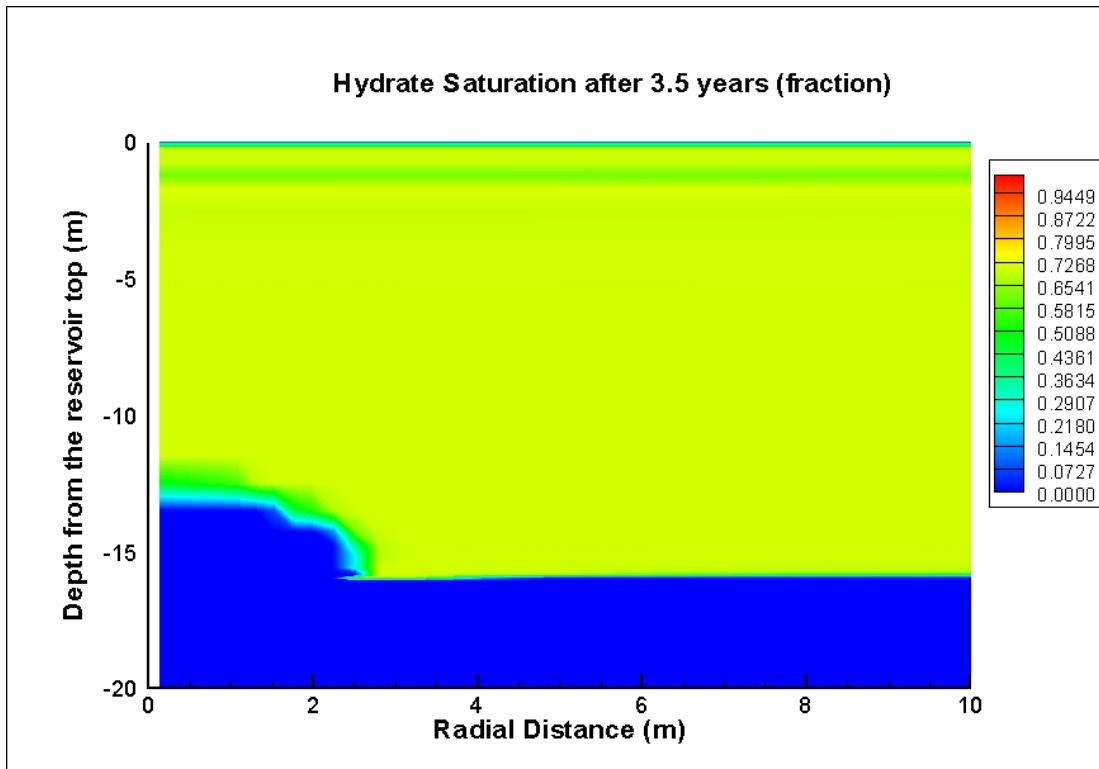


Figure 8.11 (Continued)

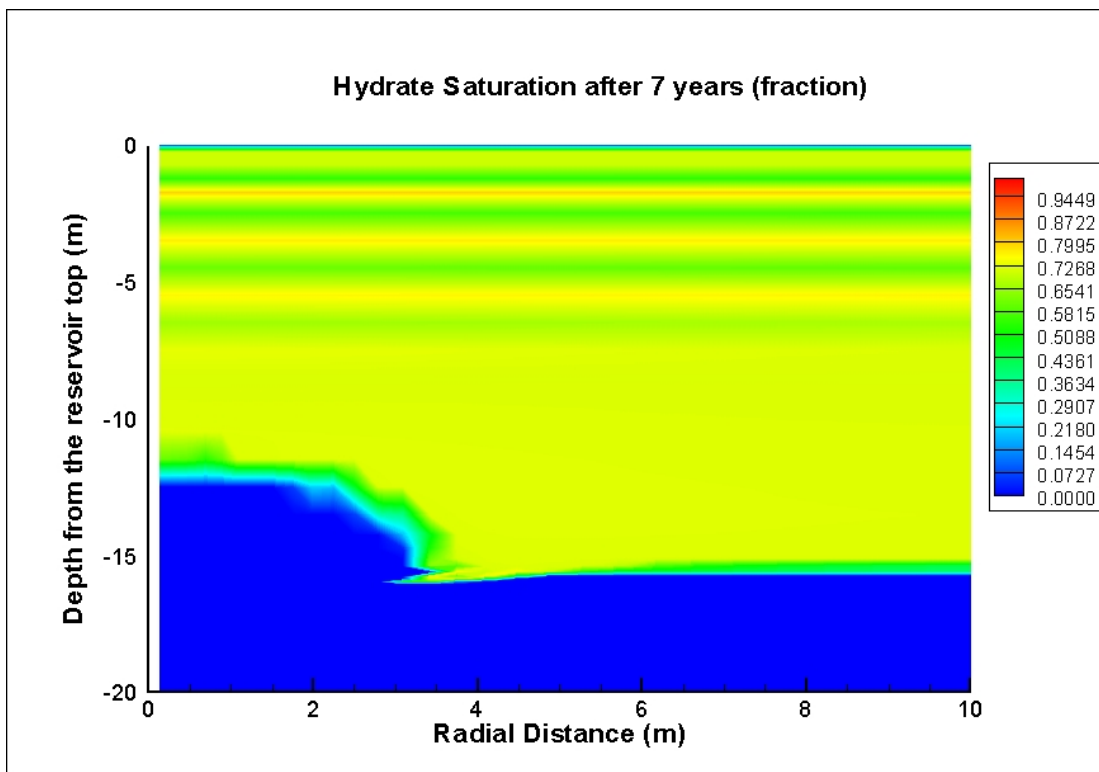
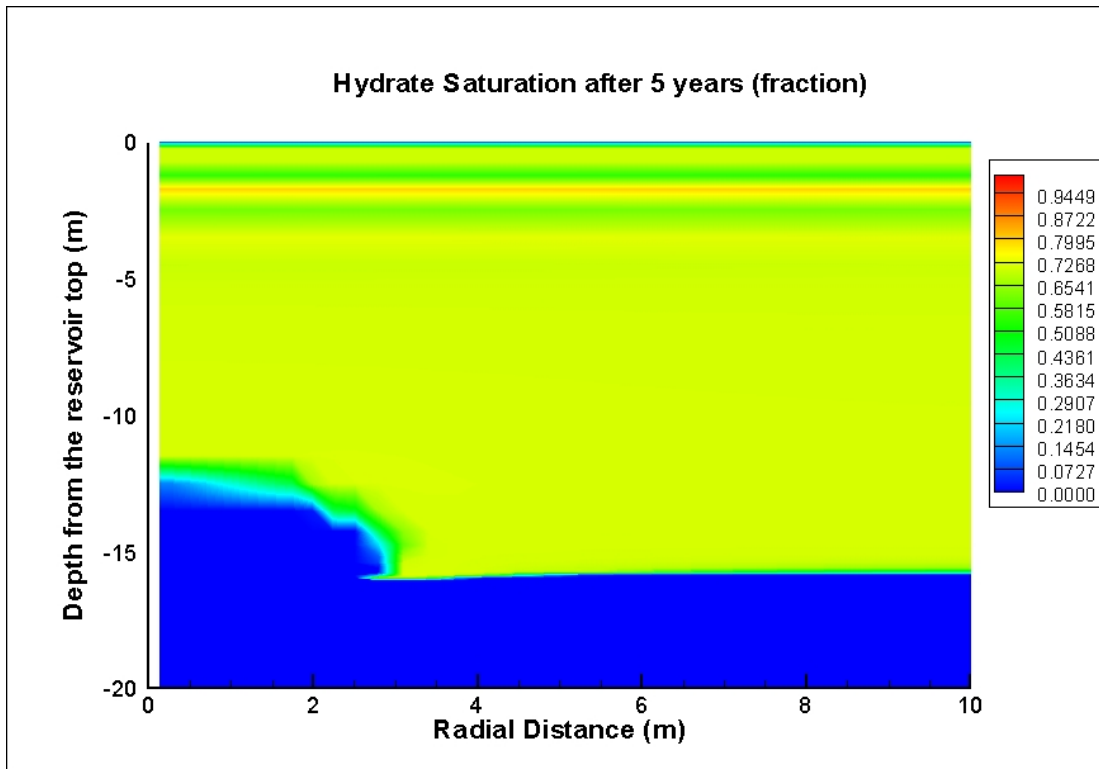


Figure 8.11 (Continued)

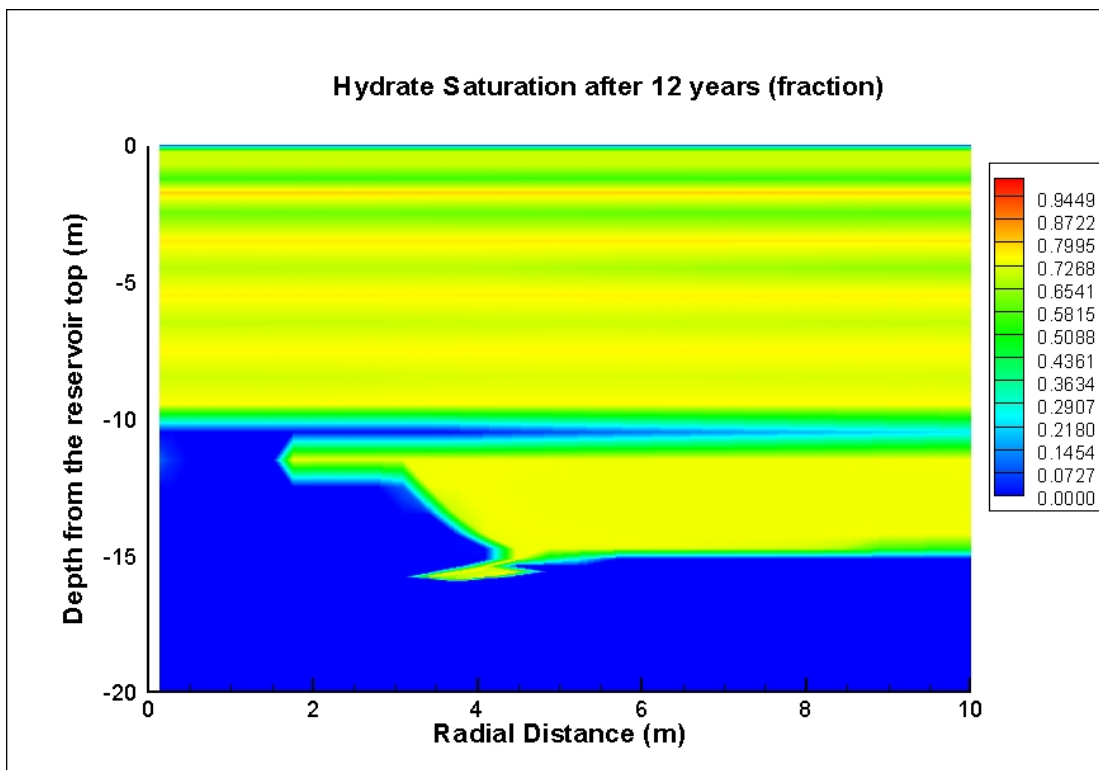
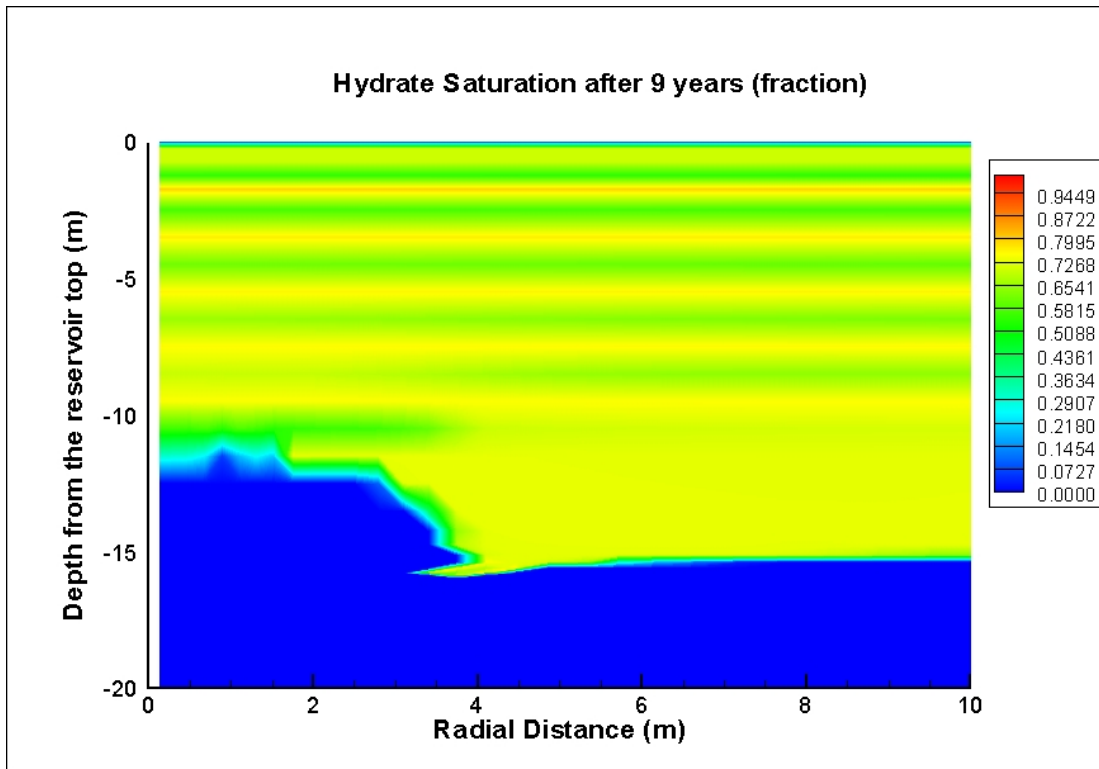


Figure 8.11 (Continued)

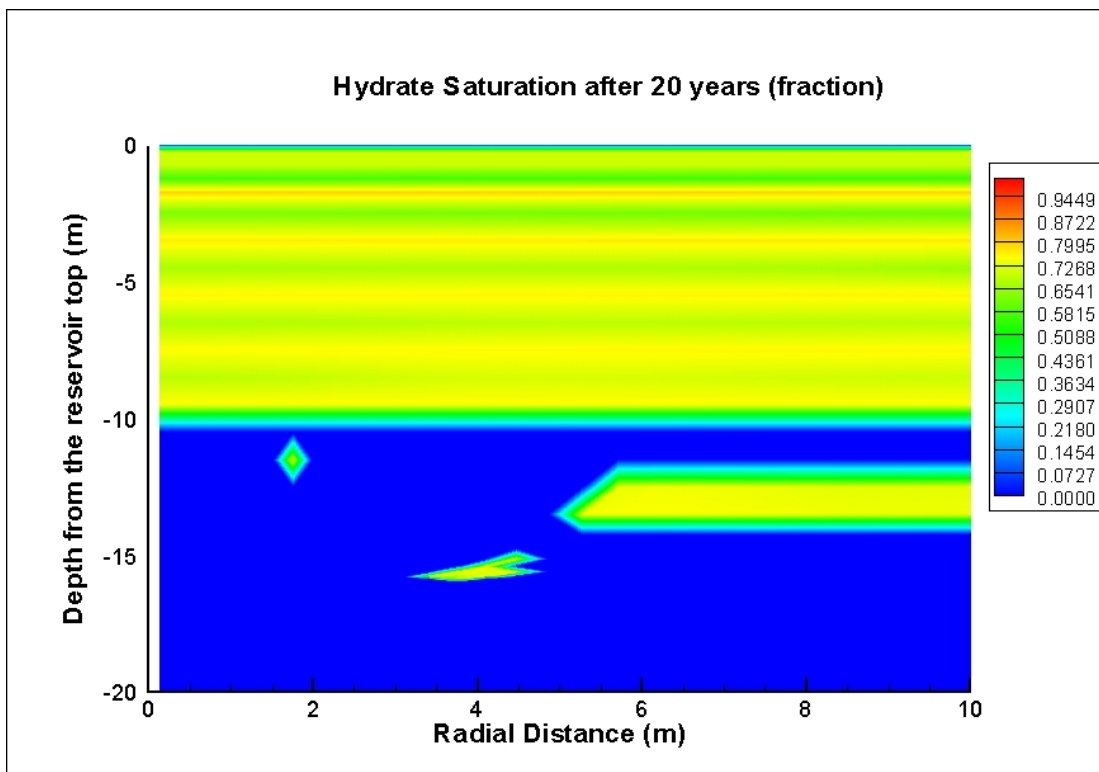
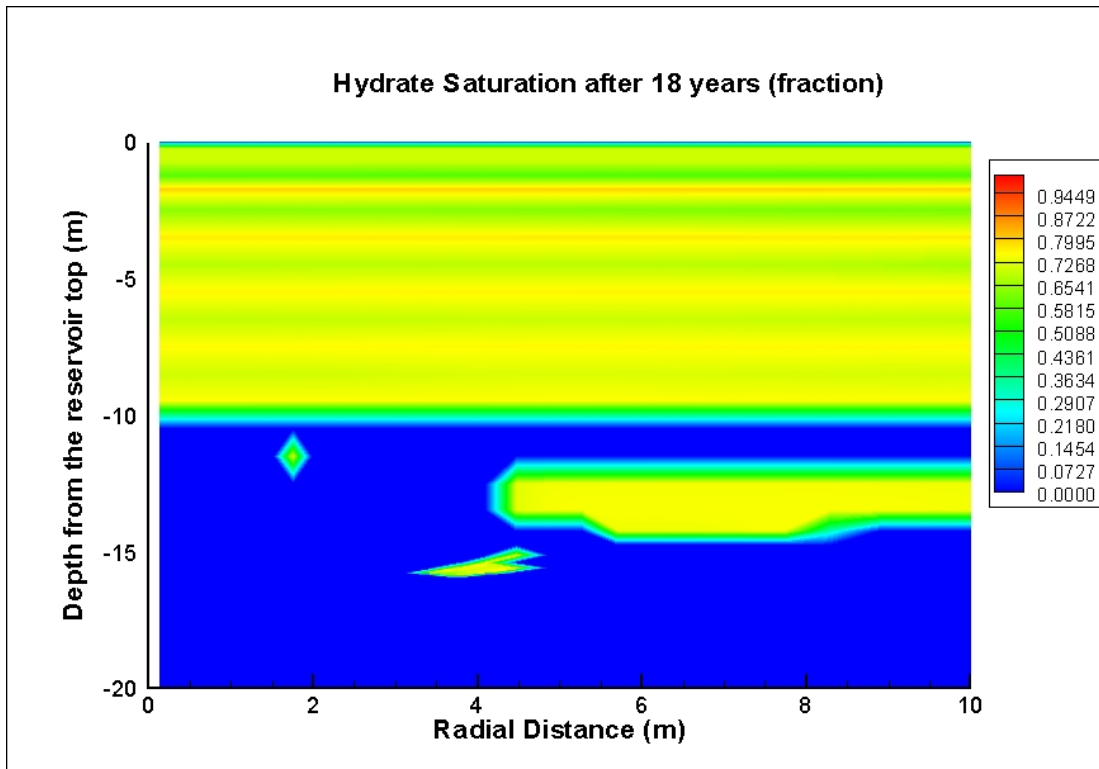


Figure 8.11 (Continued)

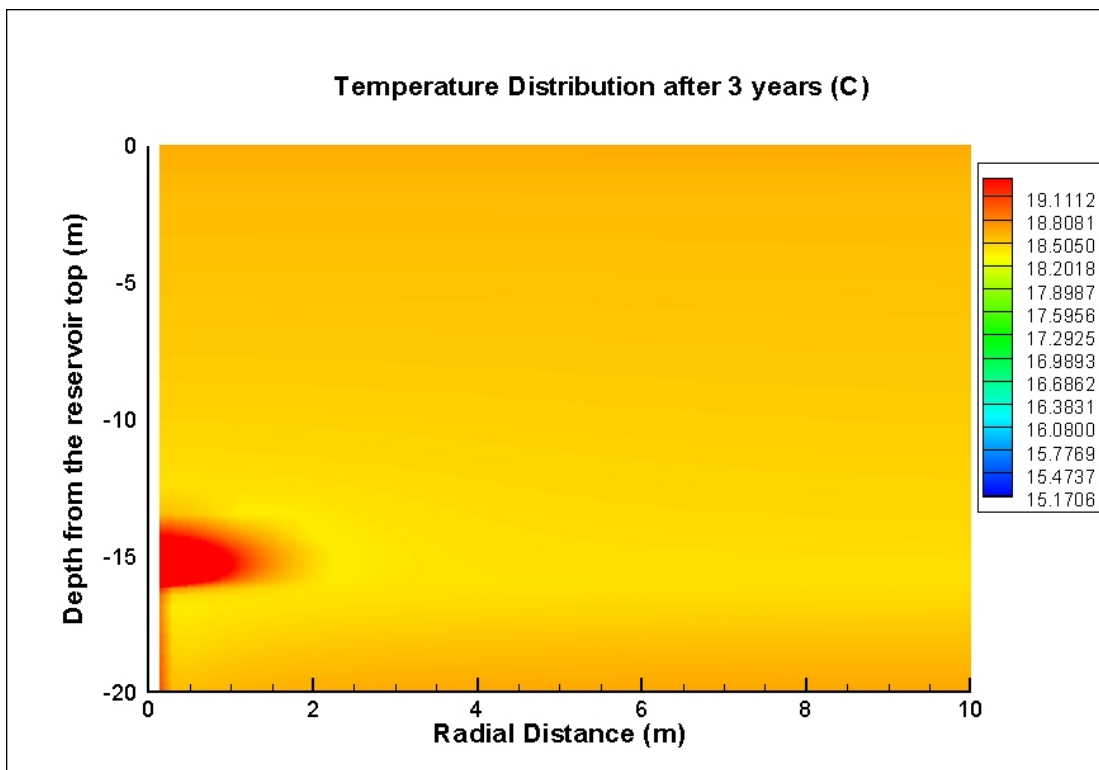
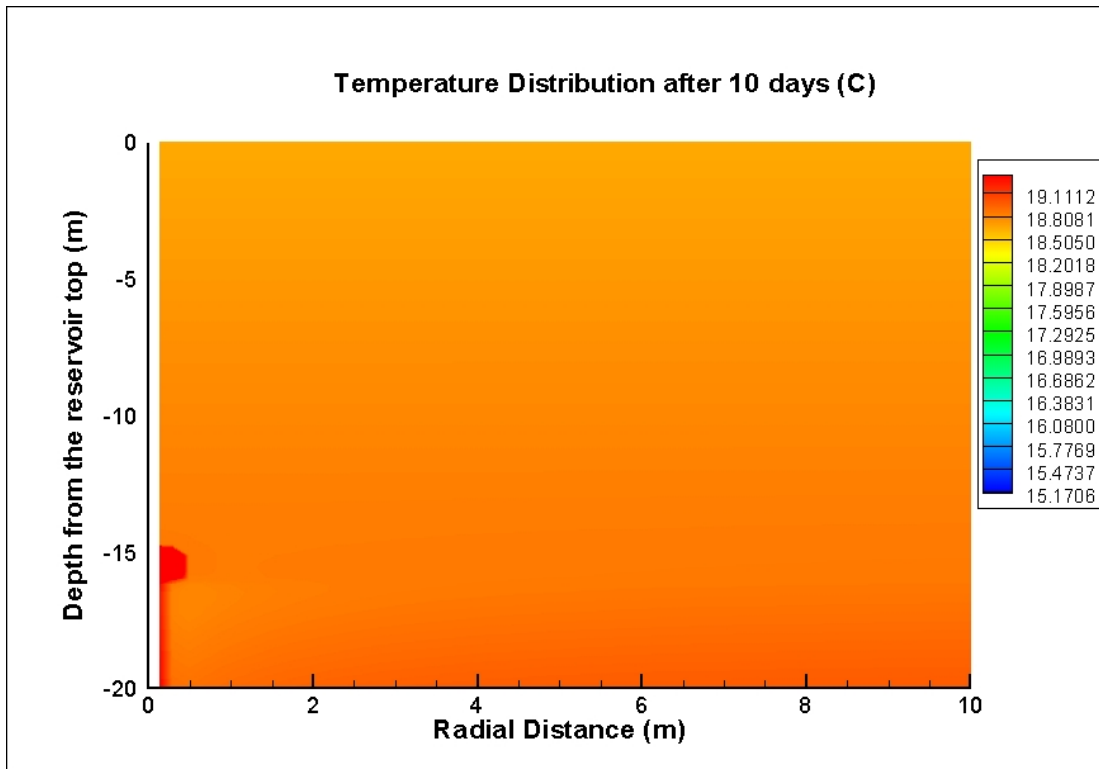


Figure 8.12: Temperature distribution near well-bore, Case 2a

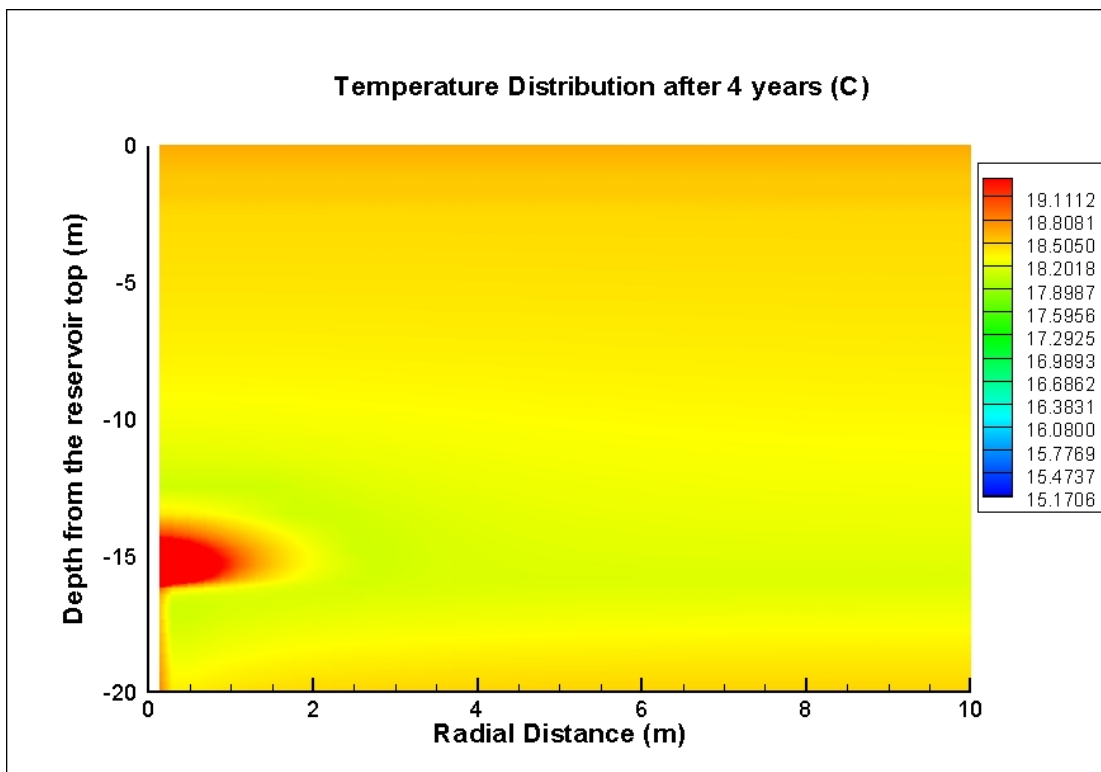
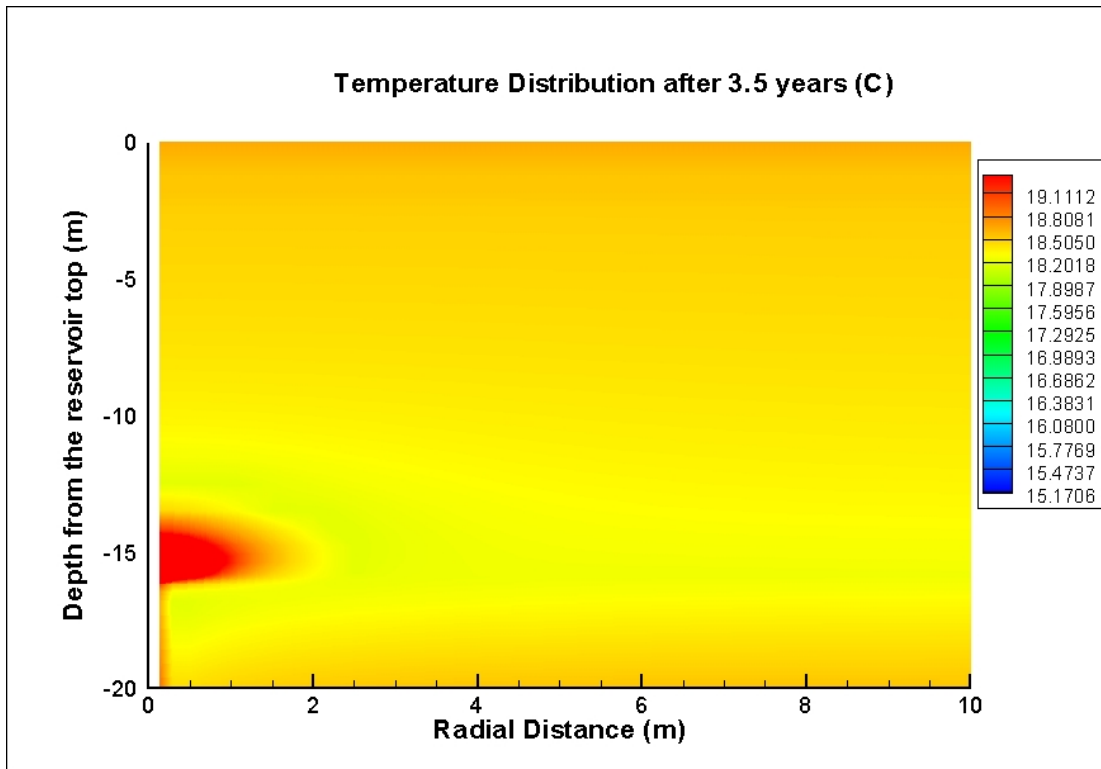


Figure 8.12 (Continued)

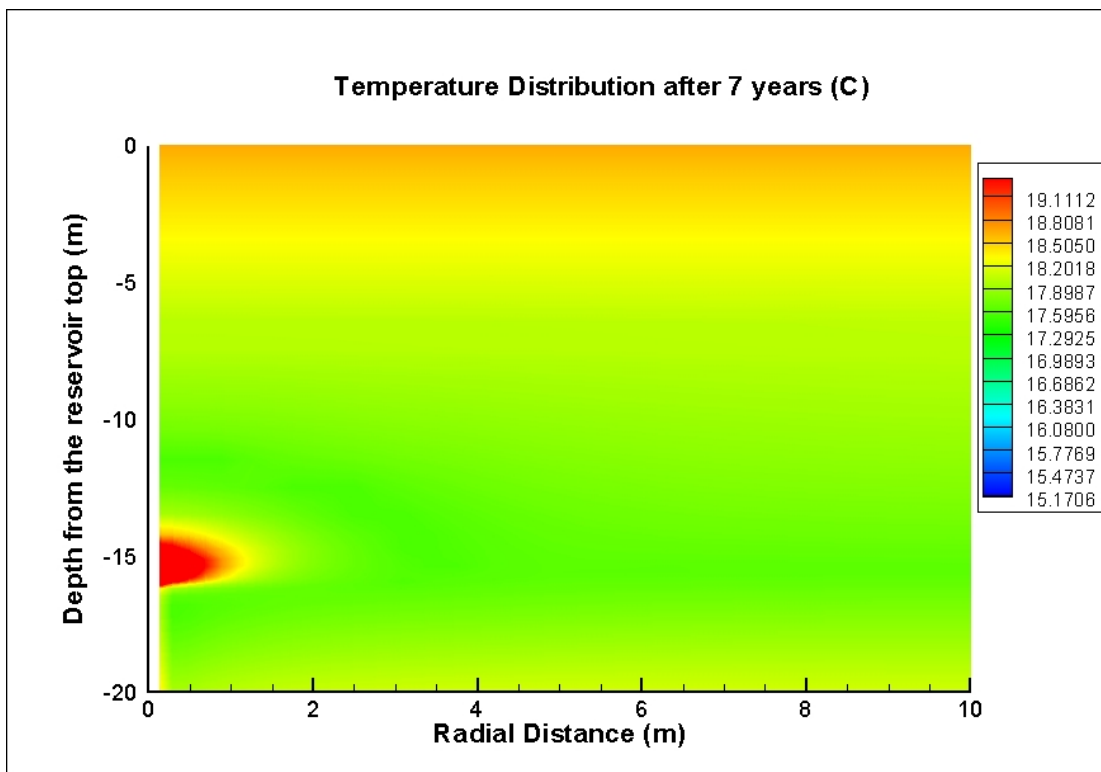
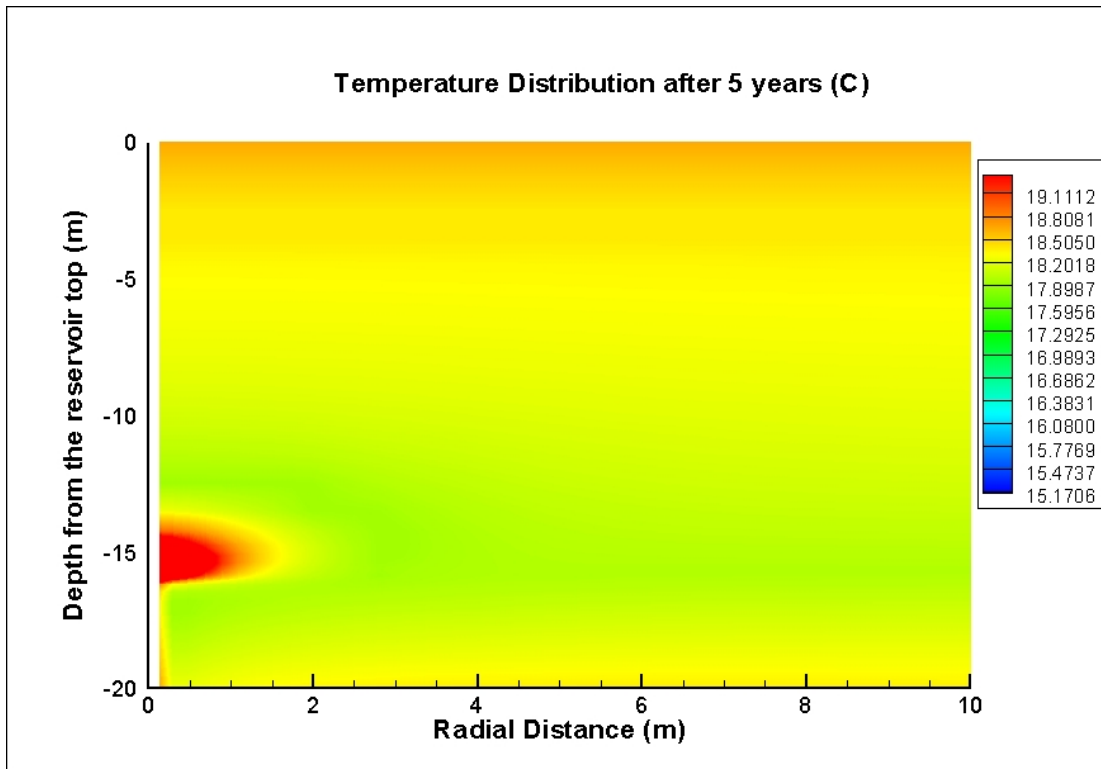


Figure 8.12 (Continued)

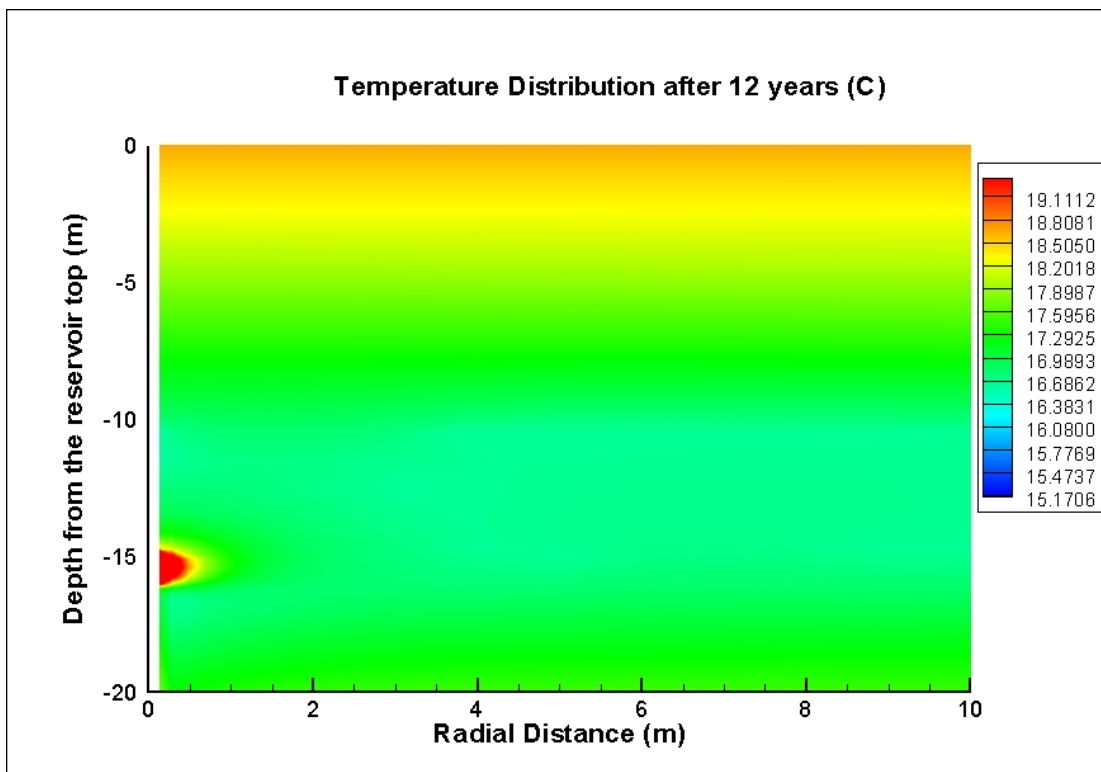
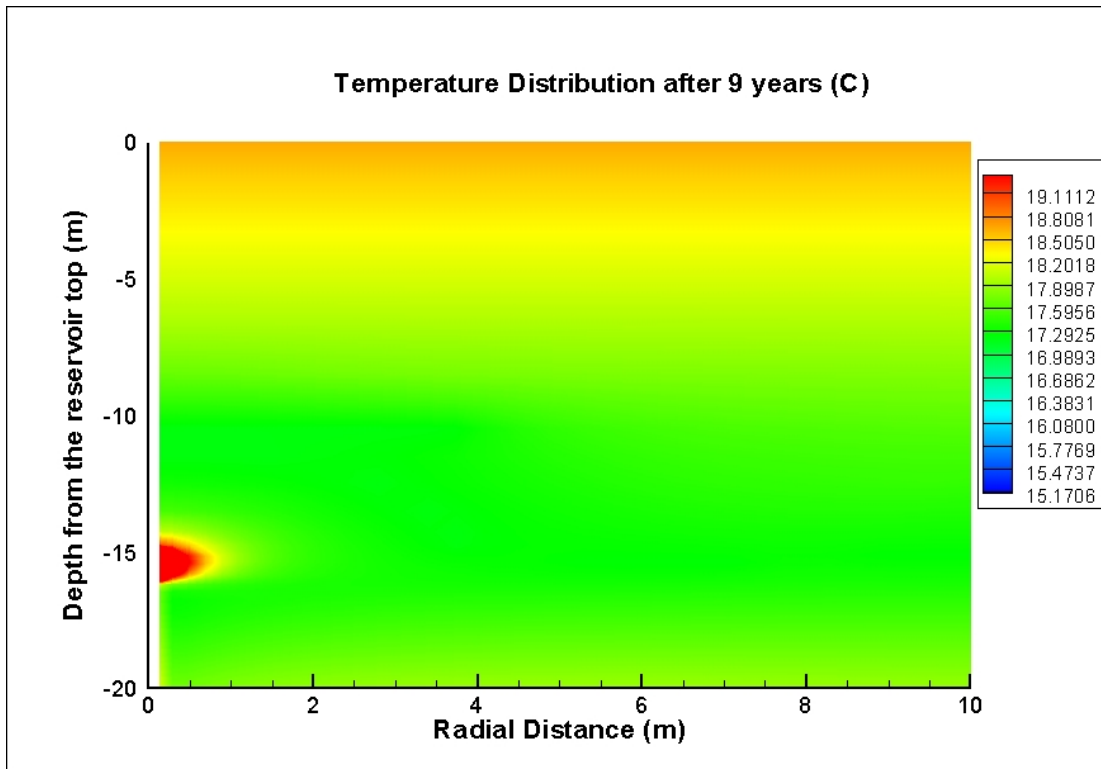


Figure 8.12 (Continued)

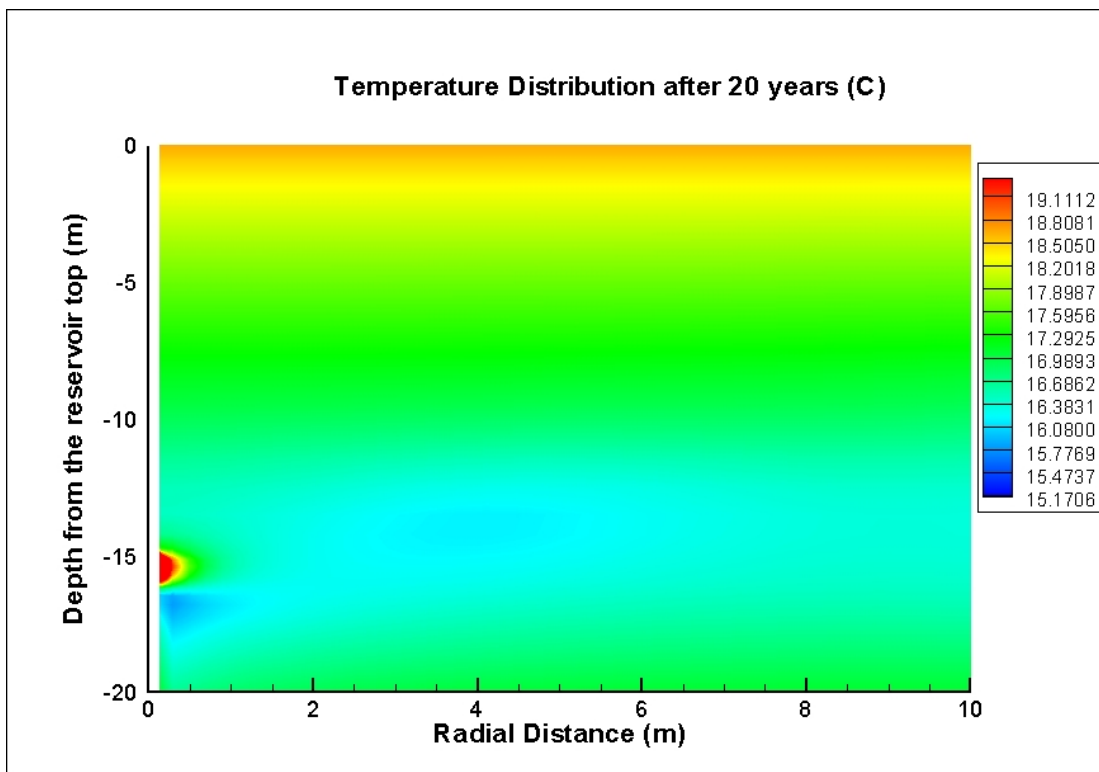
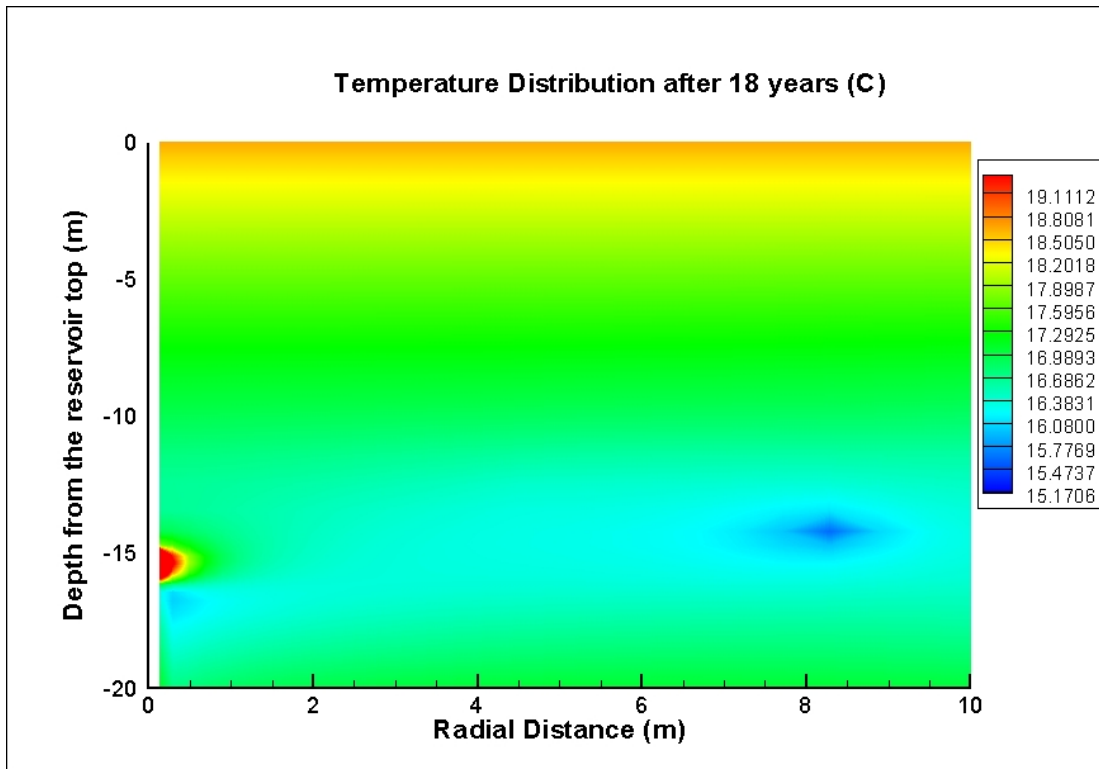


Figure 8.12 (Continued)

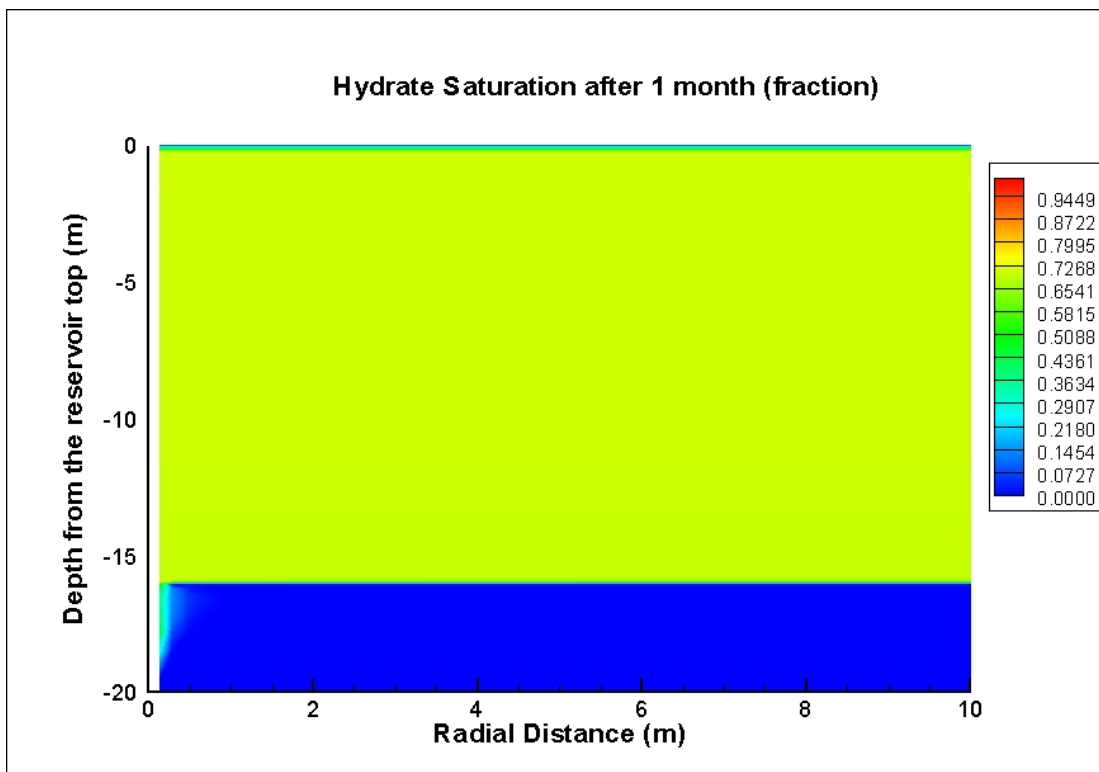
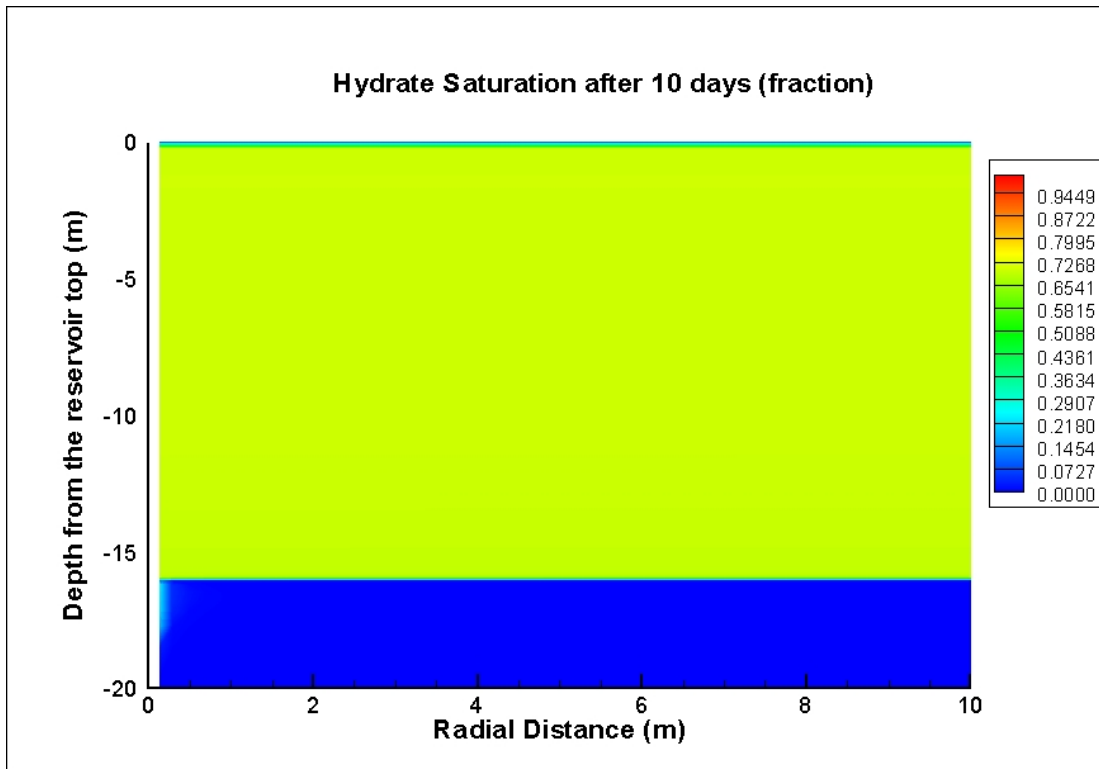


Figure 8.13: Hydrate saturation distribution near well-bore, Case 2b

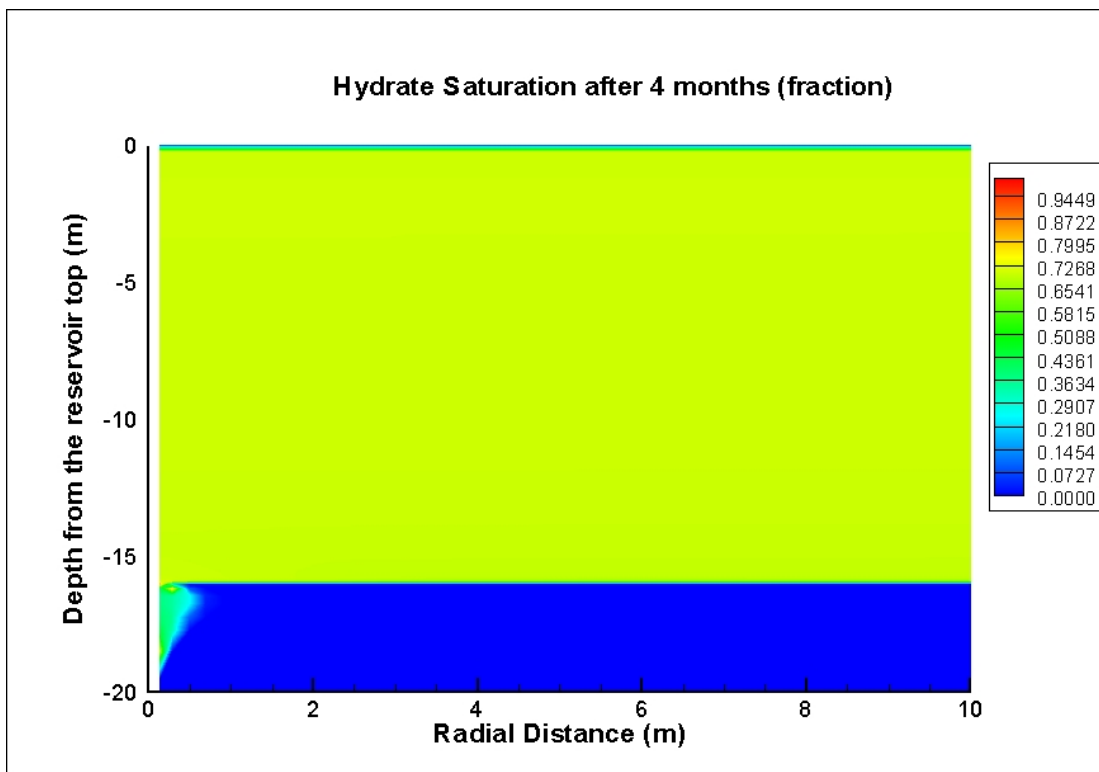
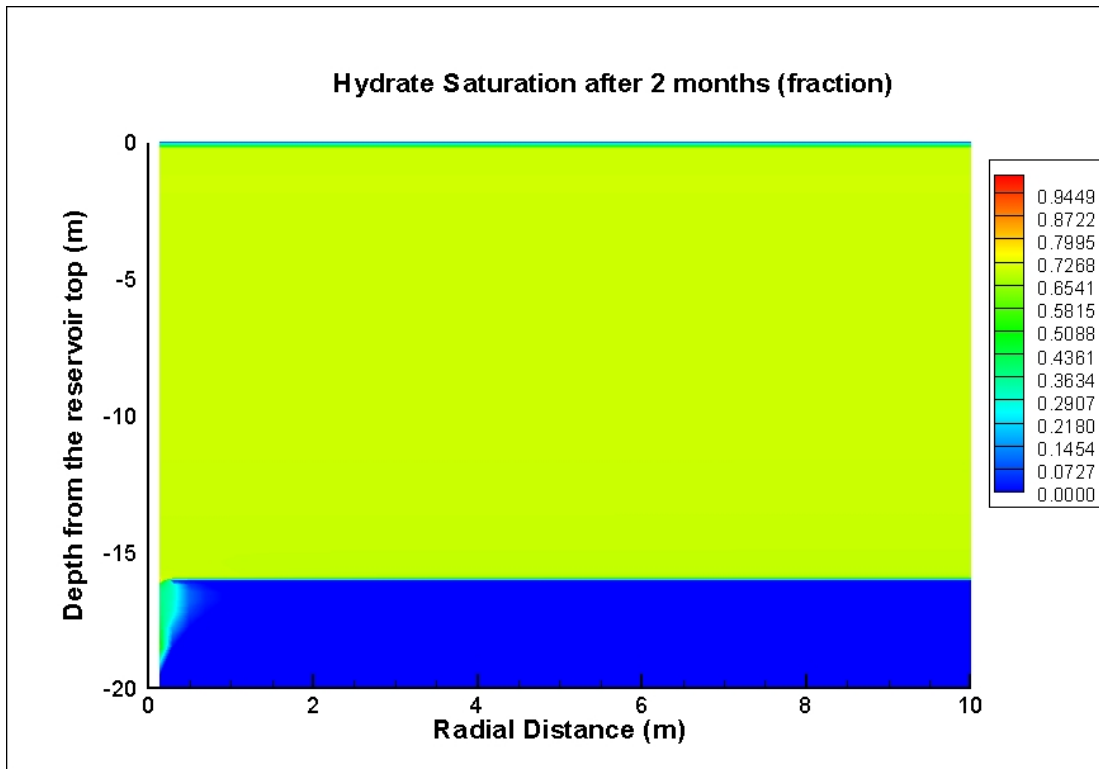


Figure 8.13 (Continued)

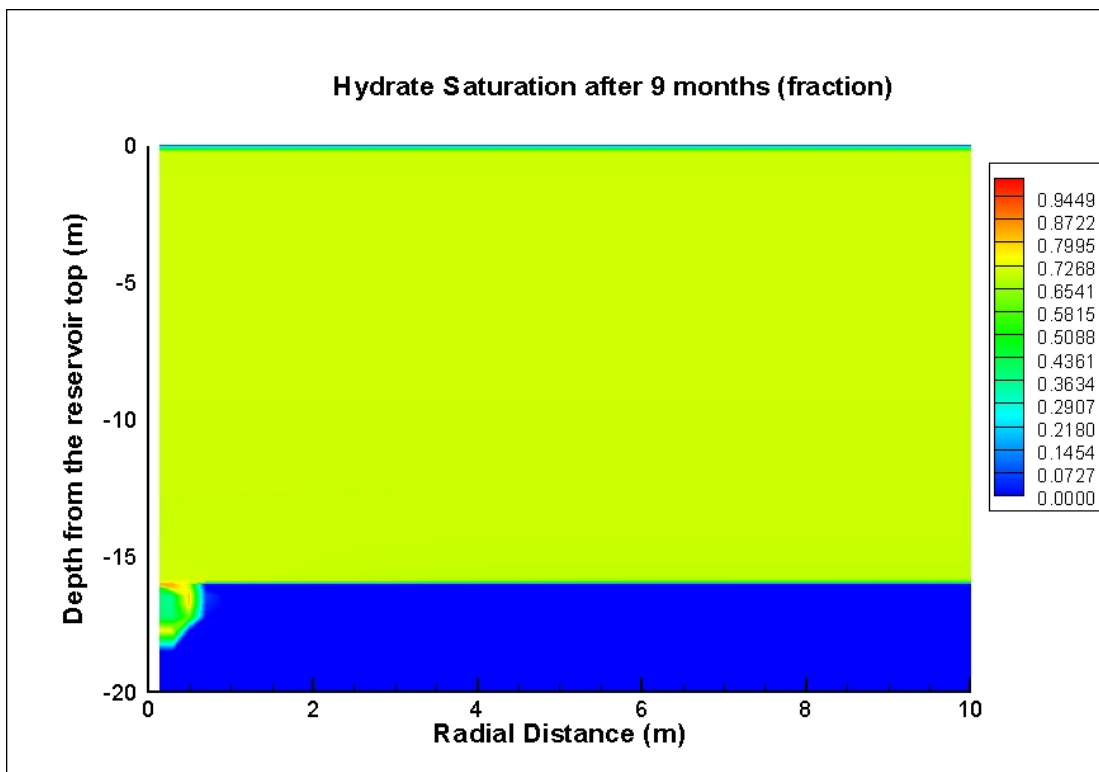
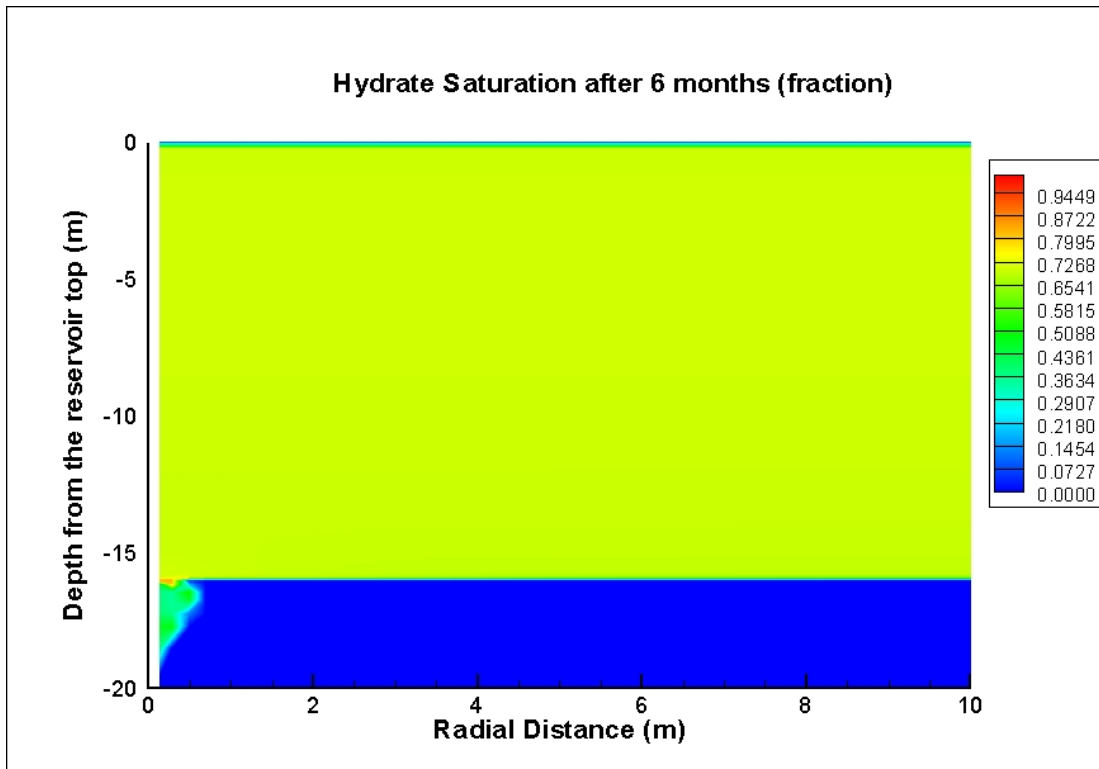
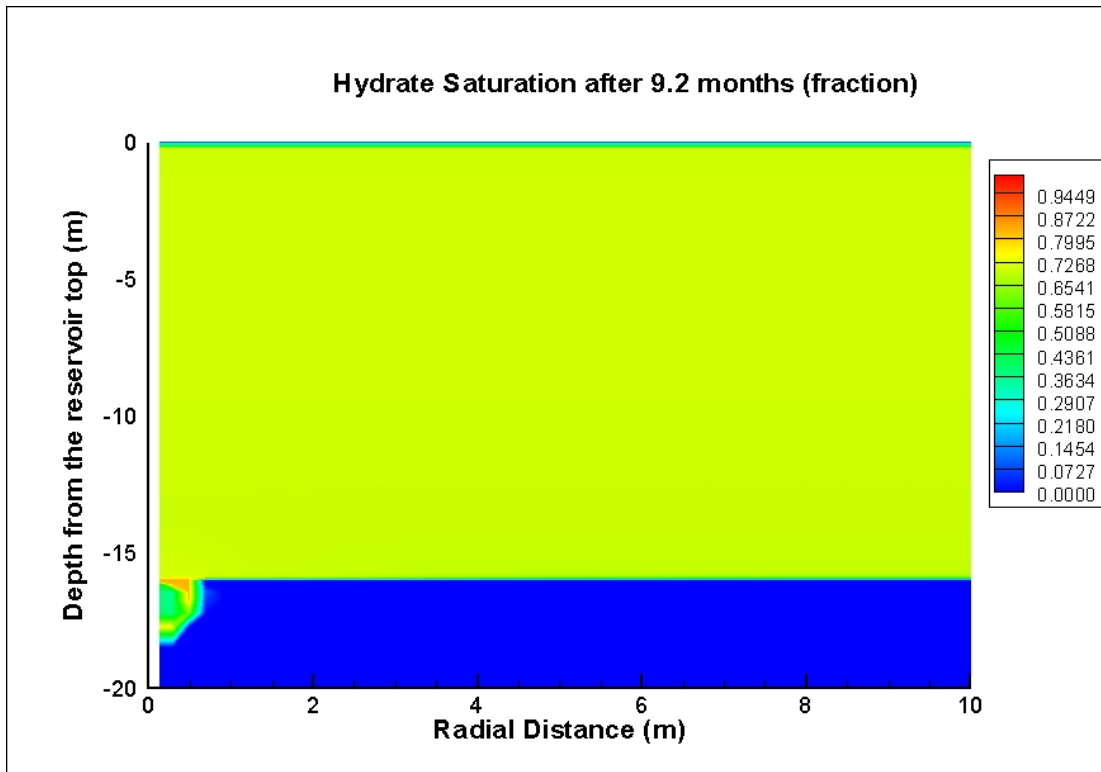


Figure 8.13 (Continued)



**Figure 8.13 (Continued)**

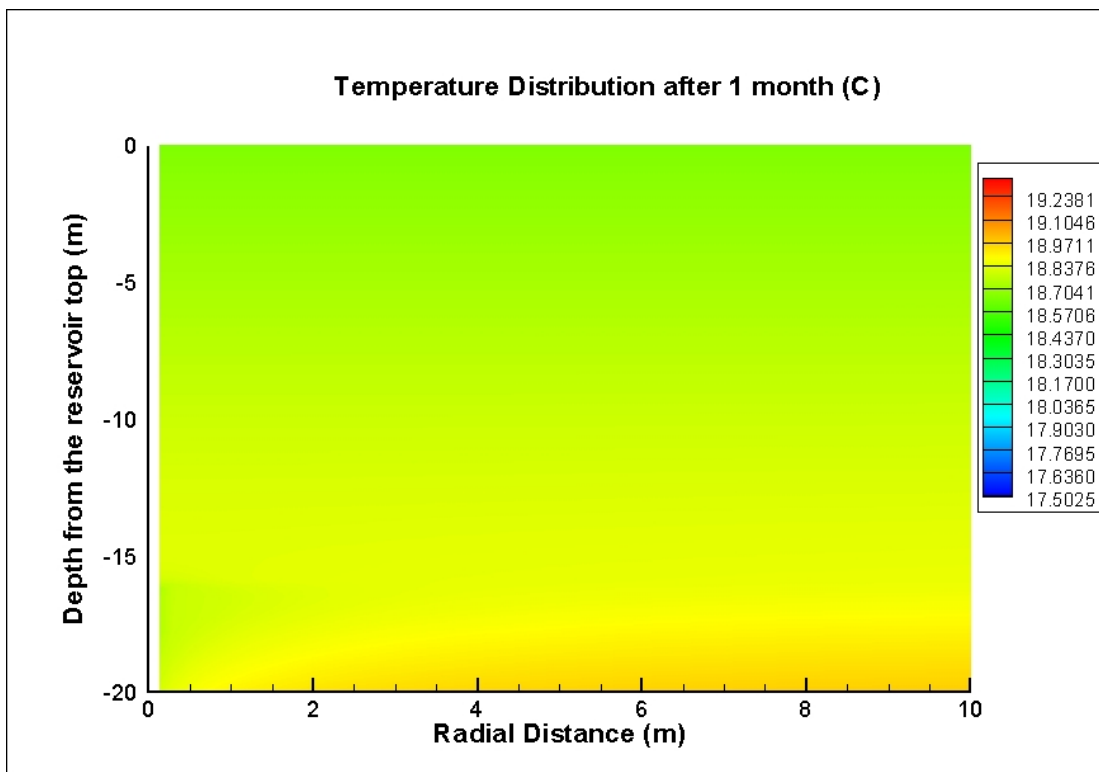
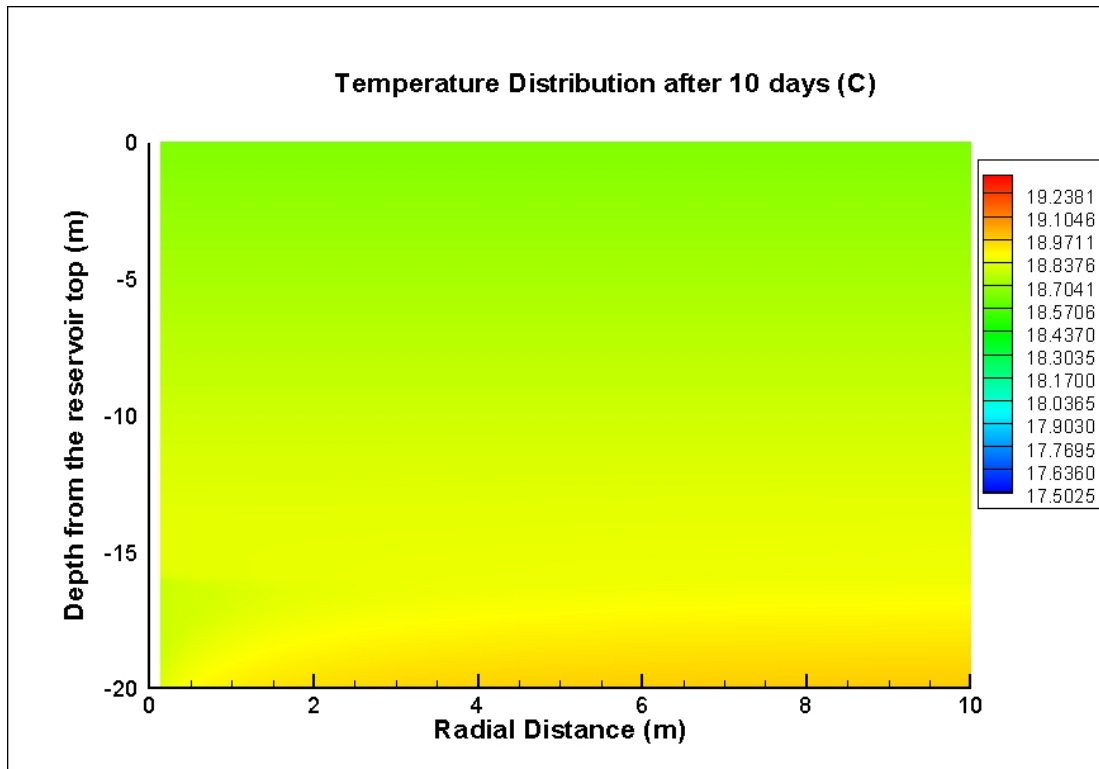


Figure 8.14: Temperature distribution near well-bore, Case 2b

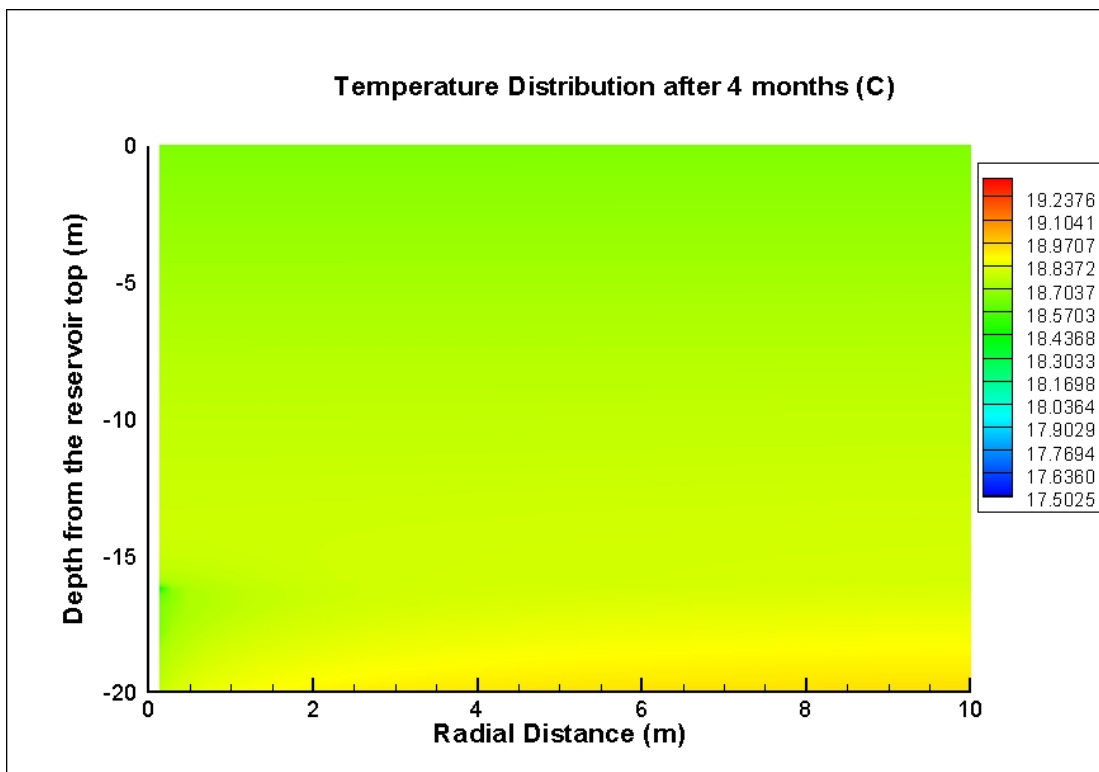
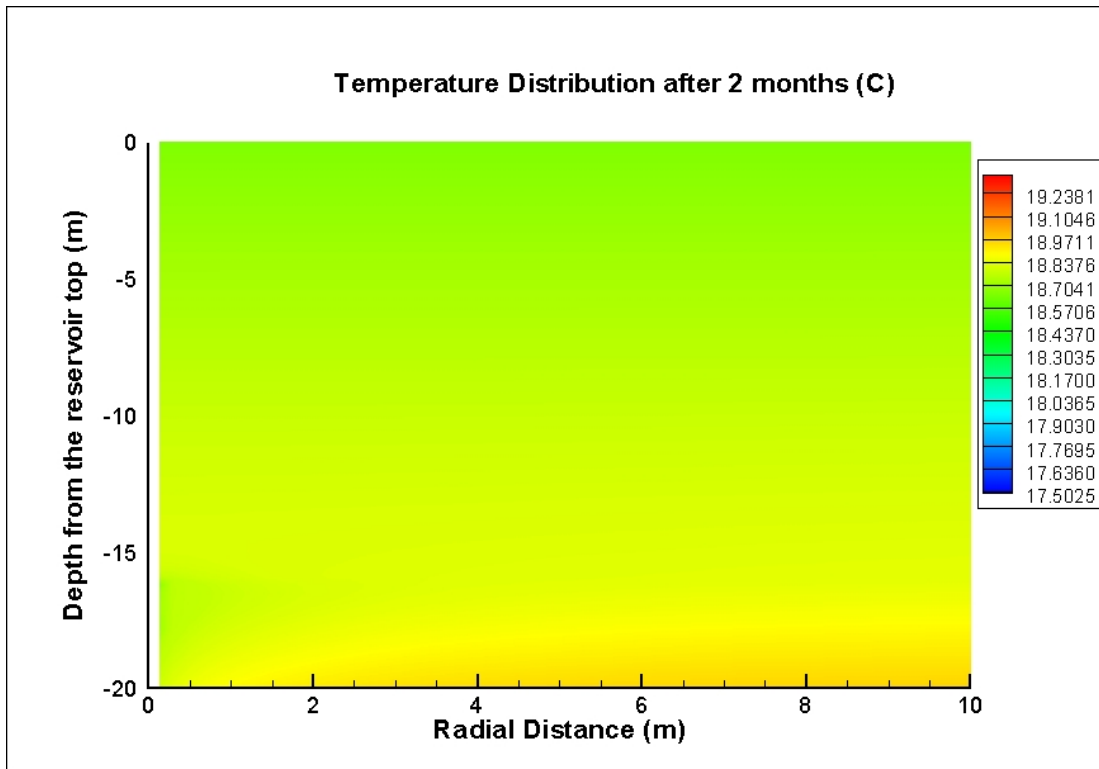


Figure 8.14 (Continued)

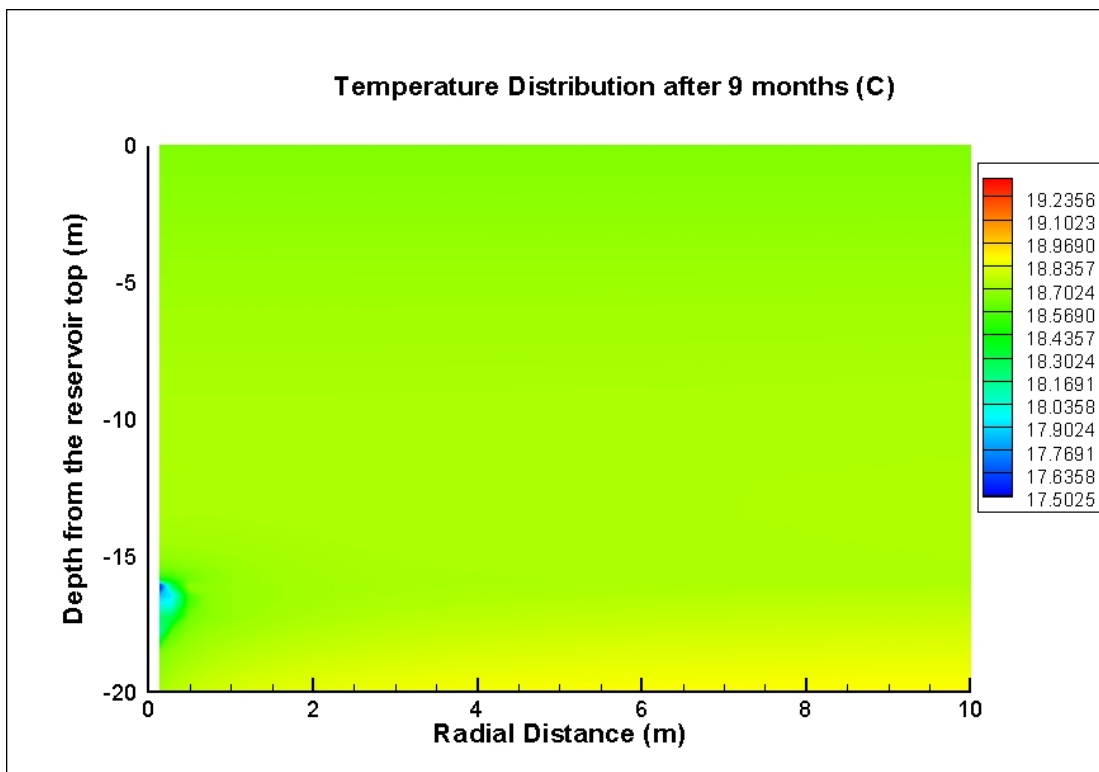
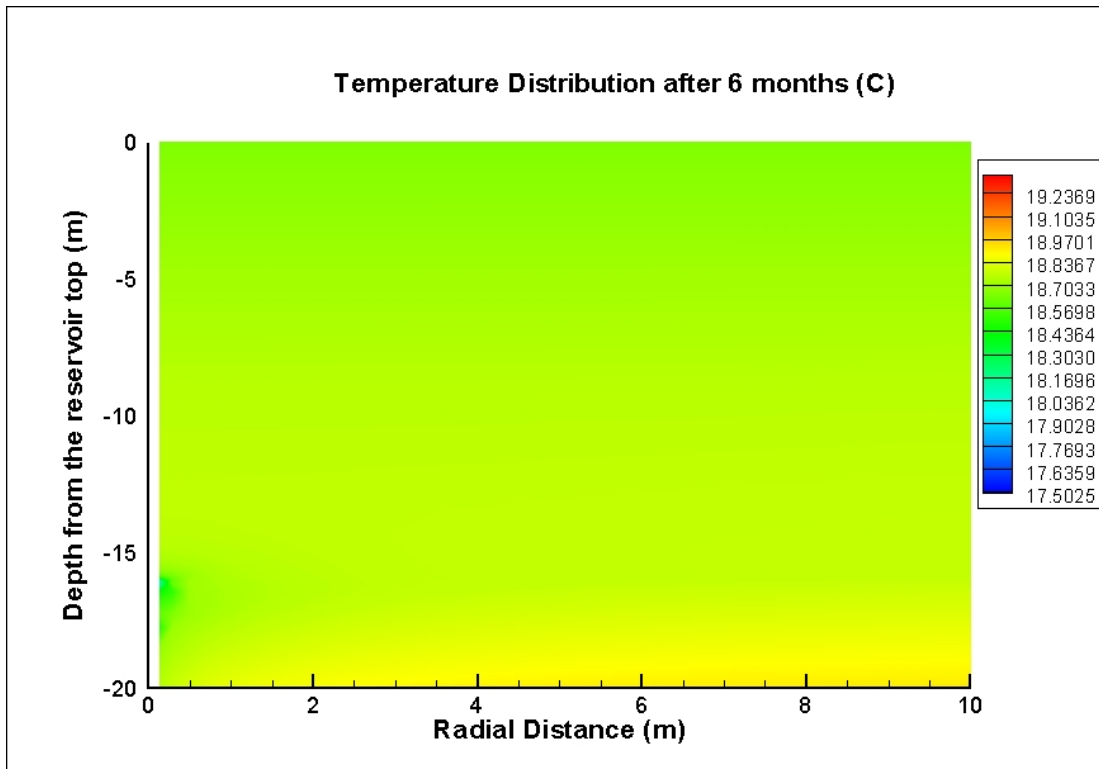
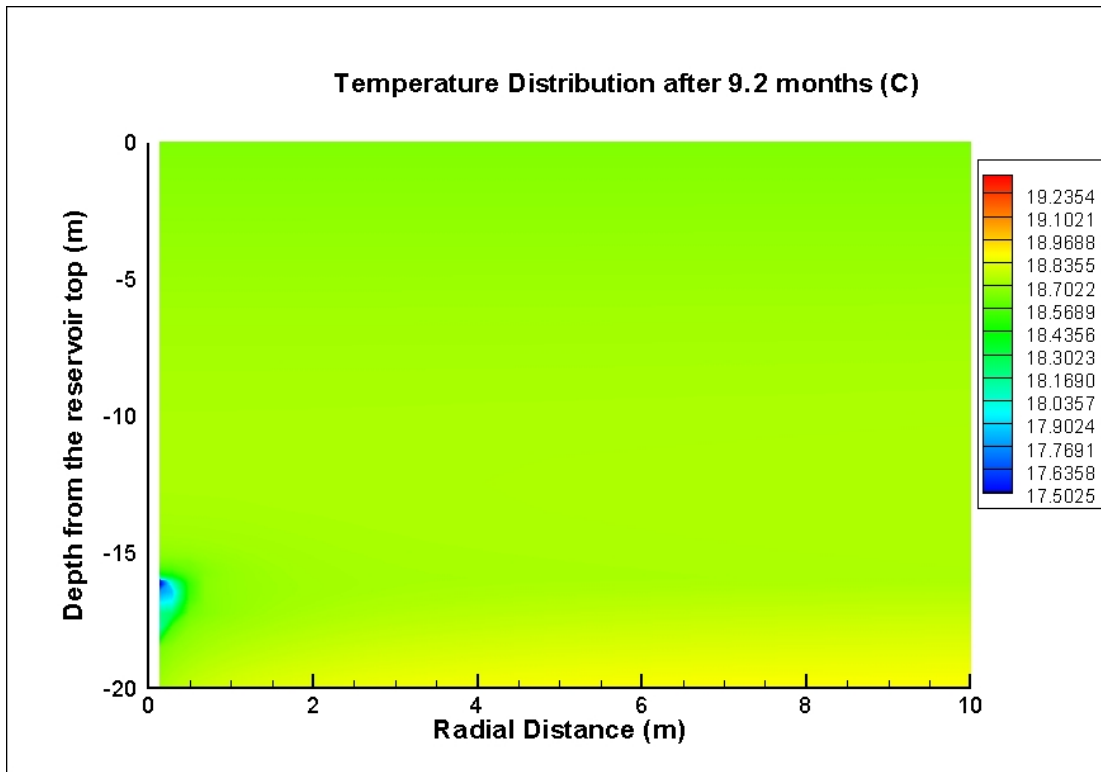


Figure 8.14 (Continued)



**Figure 8.14 (Continued)**

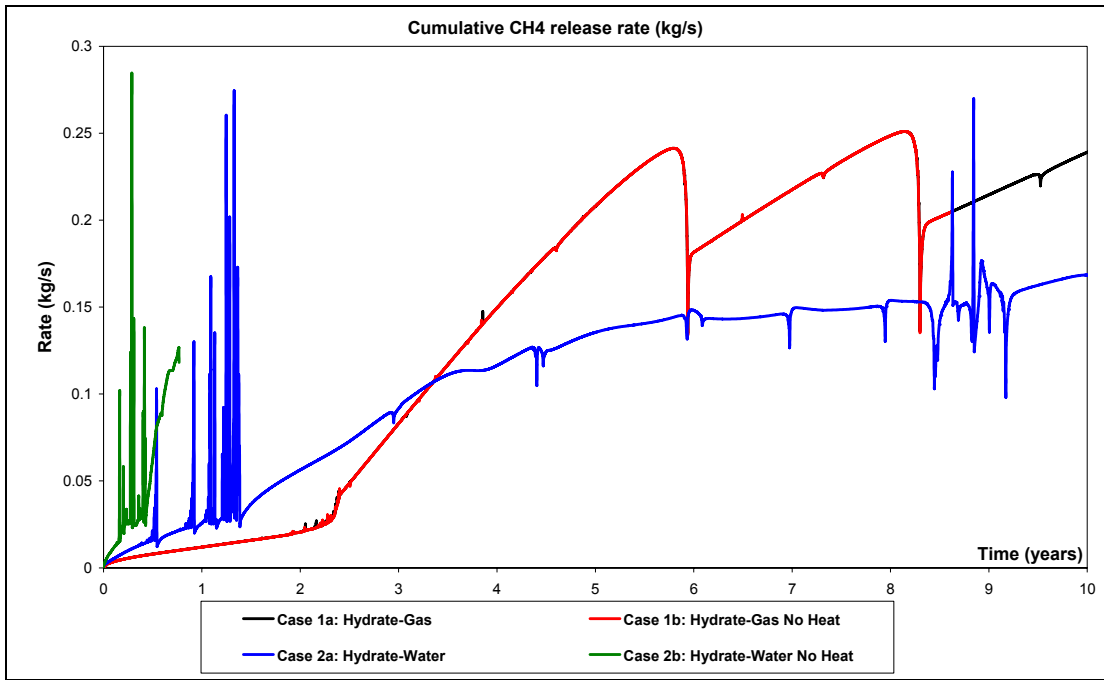


Figure 8.15: Cumulative methane release rate

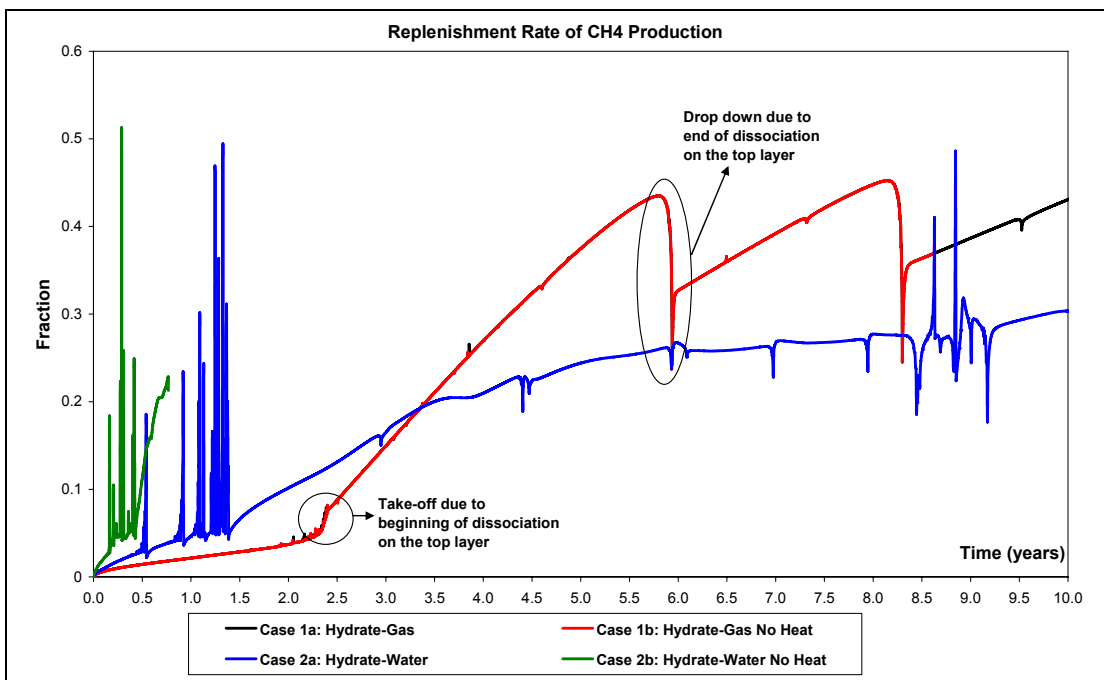


Figure 8.16: Replenishment rate of methane production, 10 years

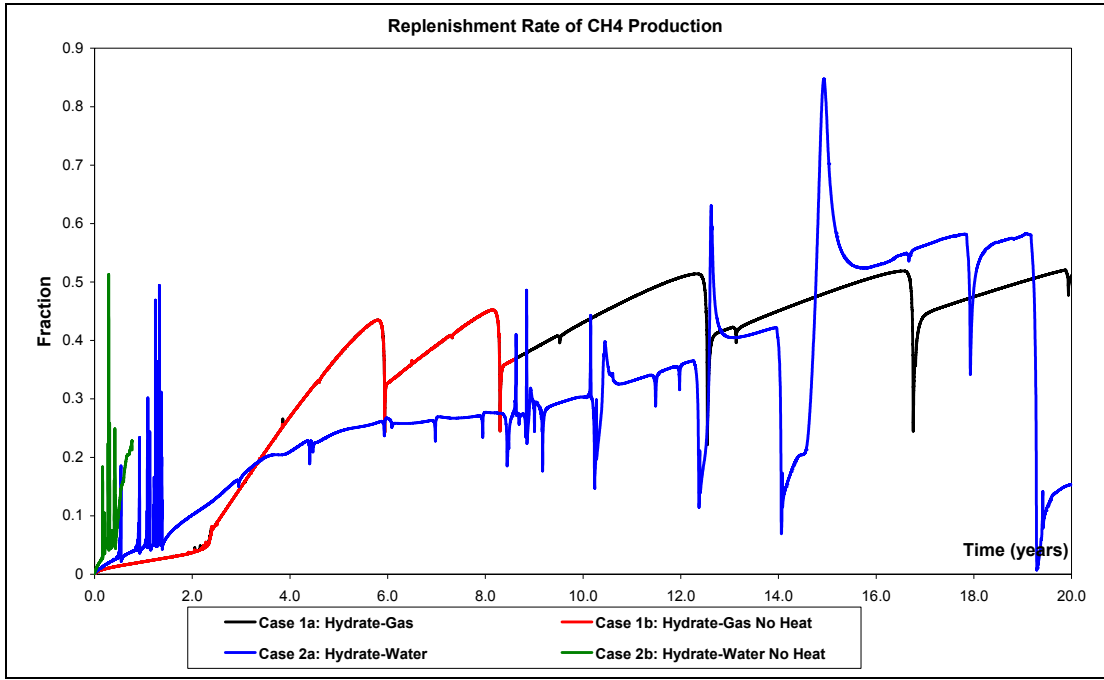


Figure 8.17: Replenishment rate of methane production, 20 years

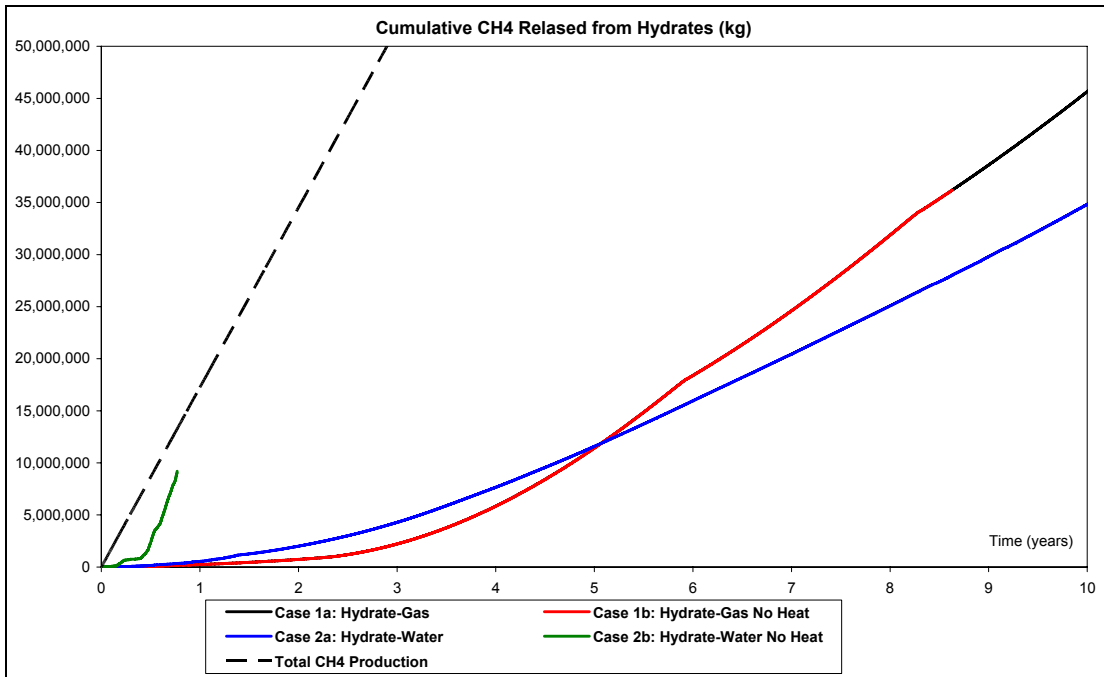


Figure 8.18: Cumulative methane release from hydrates

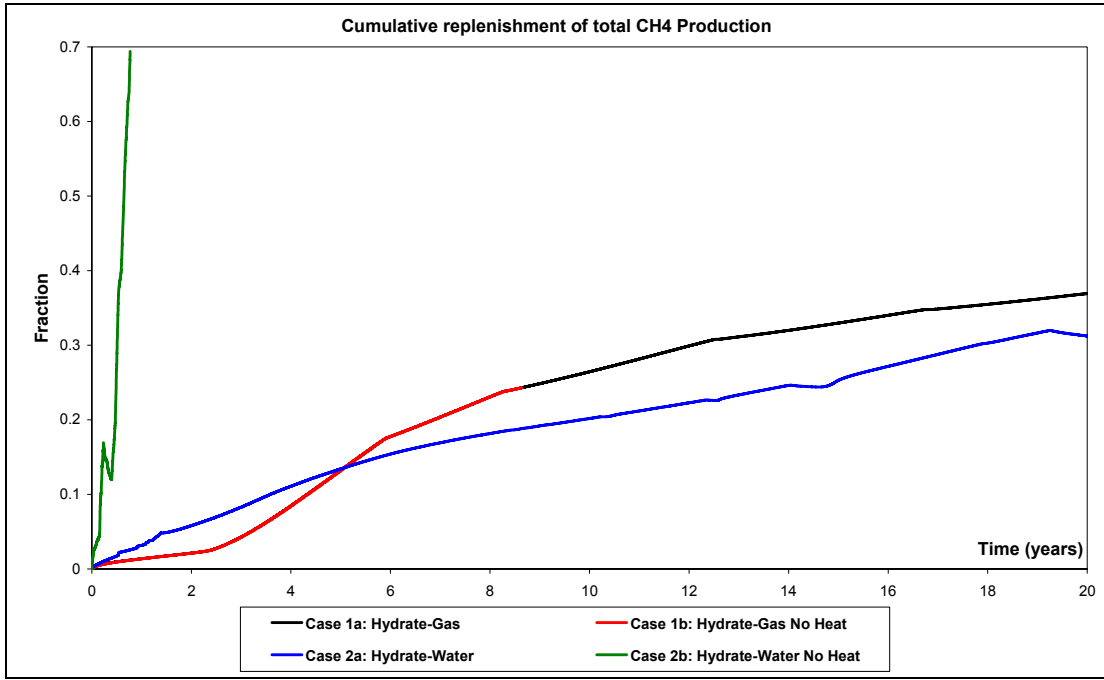


Figure 8.19: Cumulative replenishment of methane production, 20 years

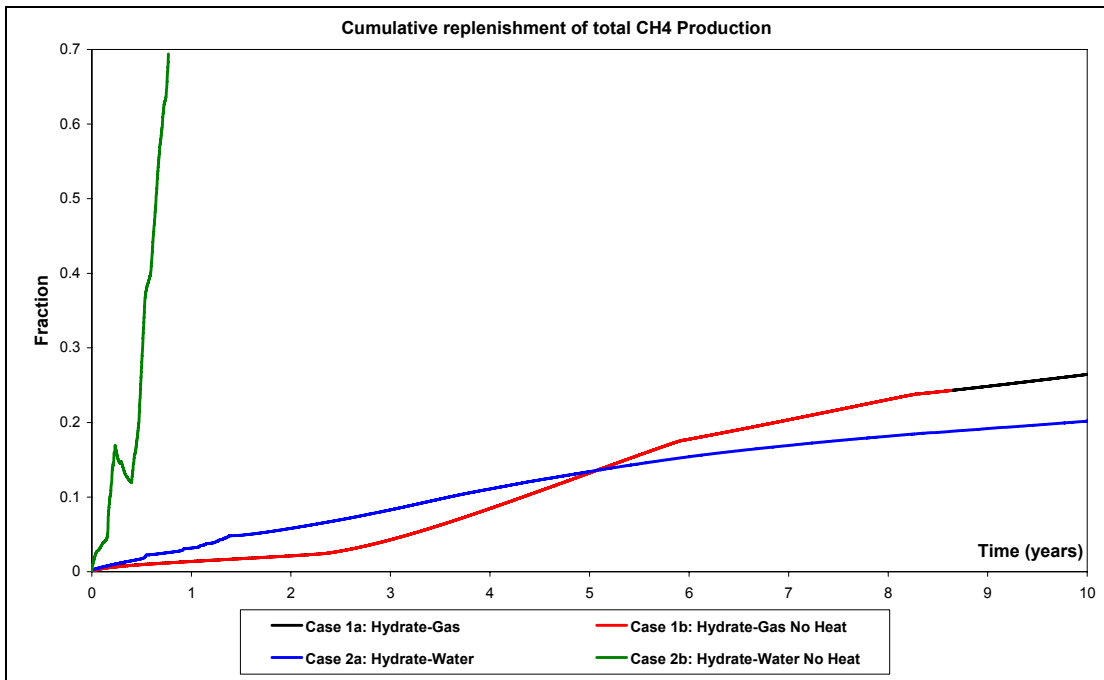
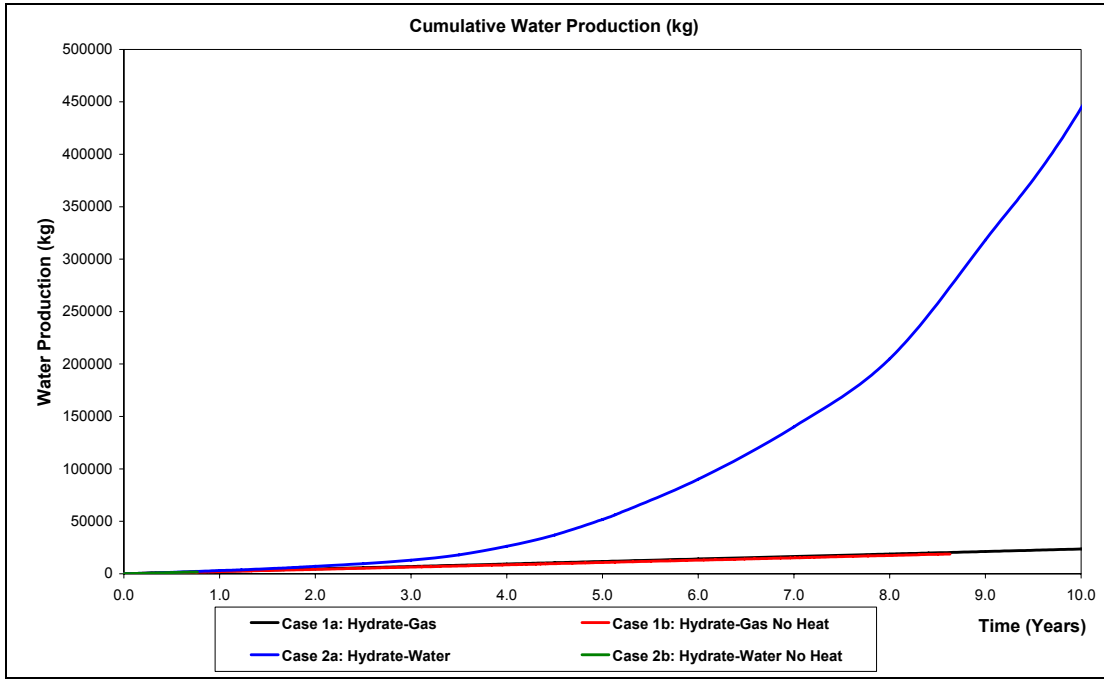
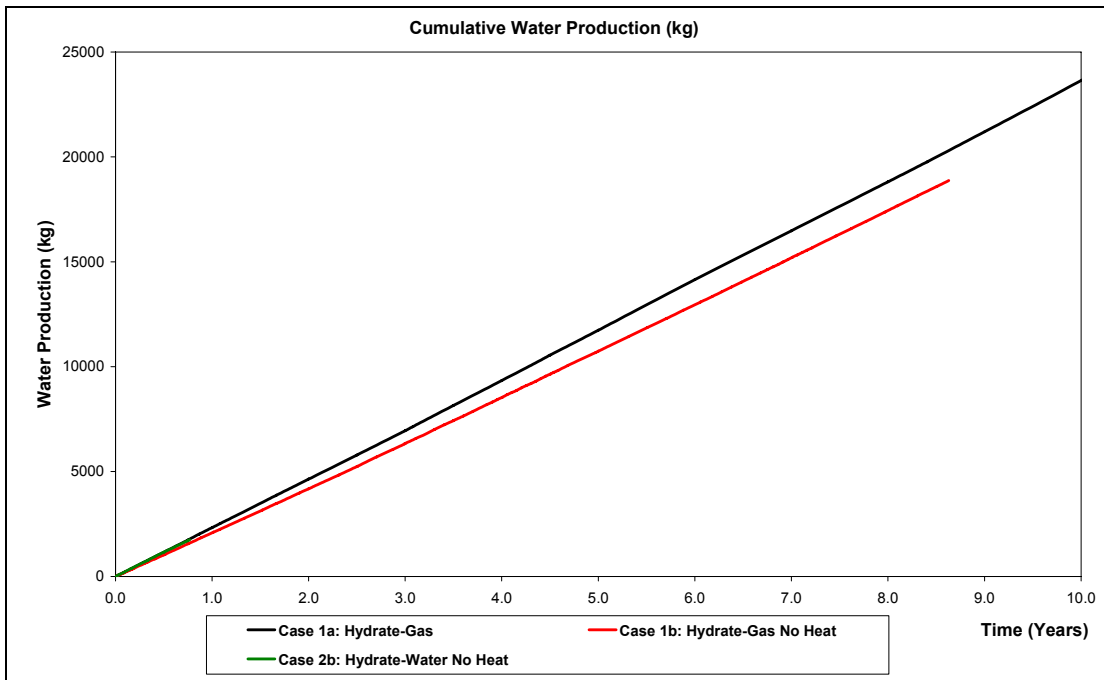


Figure 8.20: Cumulative replenishment of methane production, 10 years



**Figure 8.21: Cumulative water production, 1**



**Figure 8.22: Cumulative water production, 2**

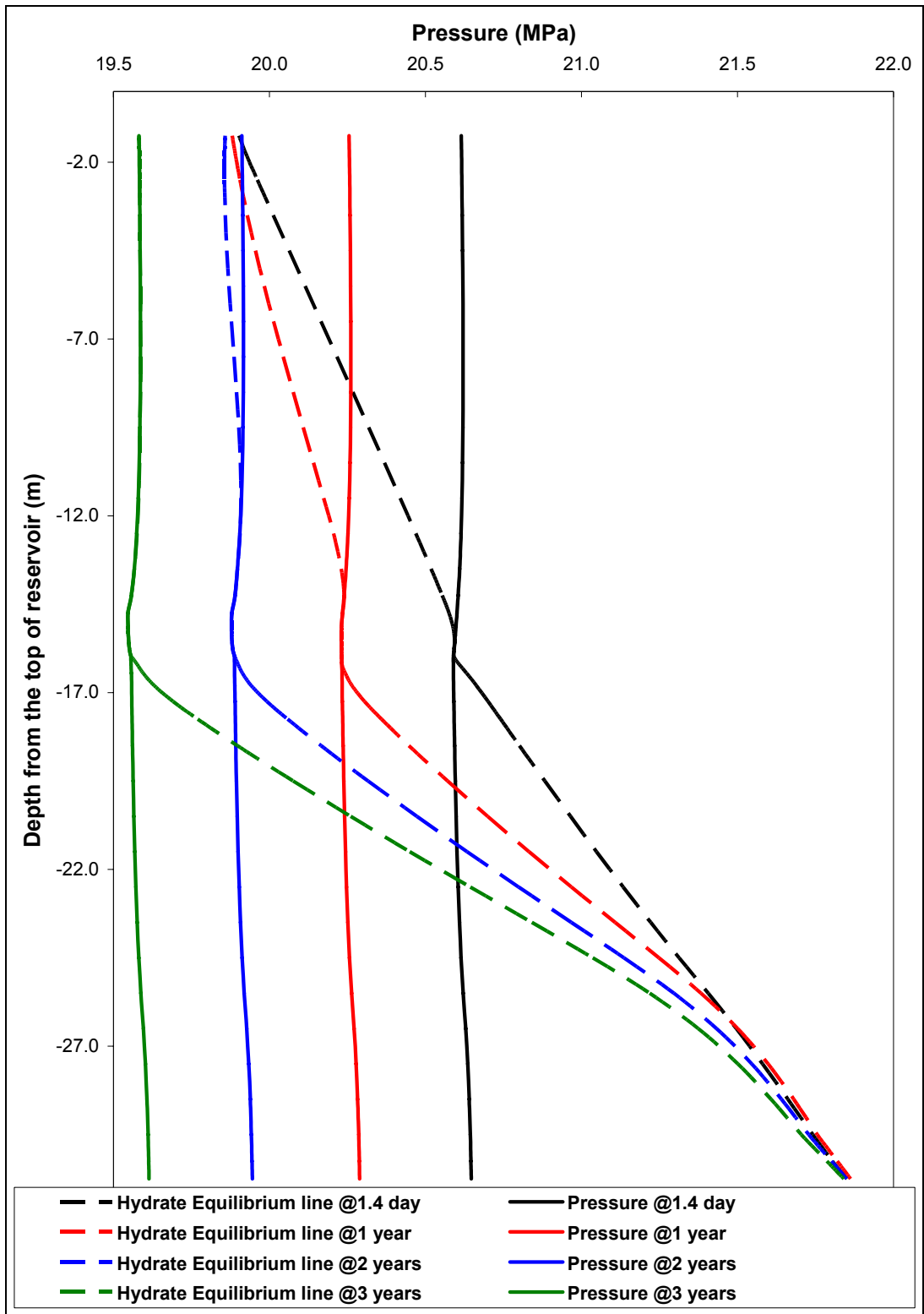


Figure 8.23: Pressure profile for case 1a, 3 years

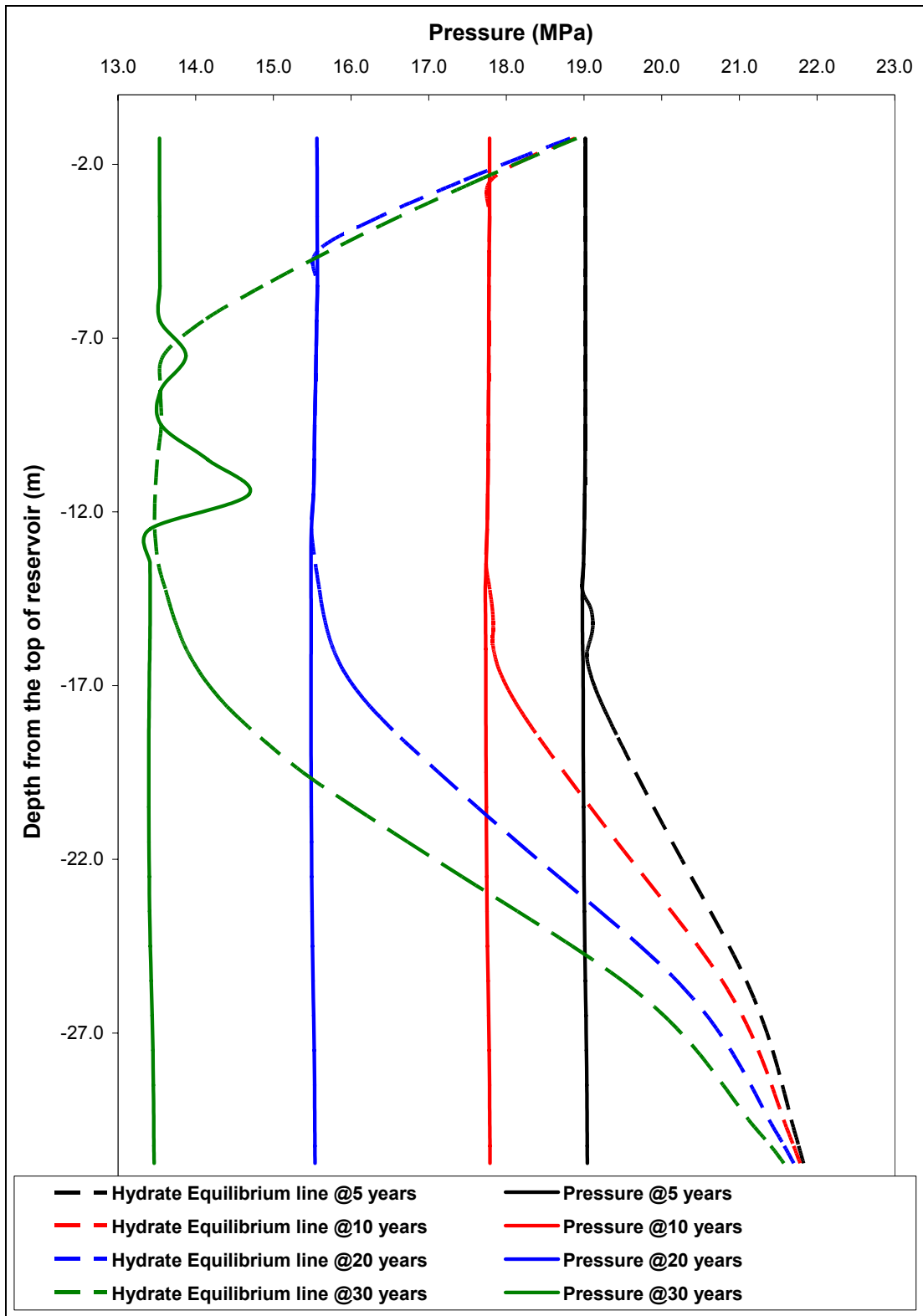


Figure 8.24: Pressure profile for case 1a, 30 years

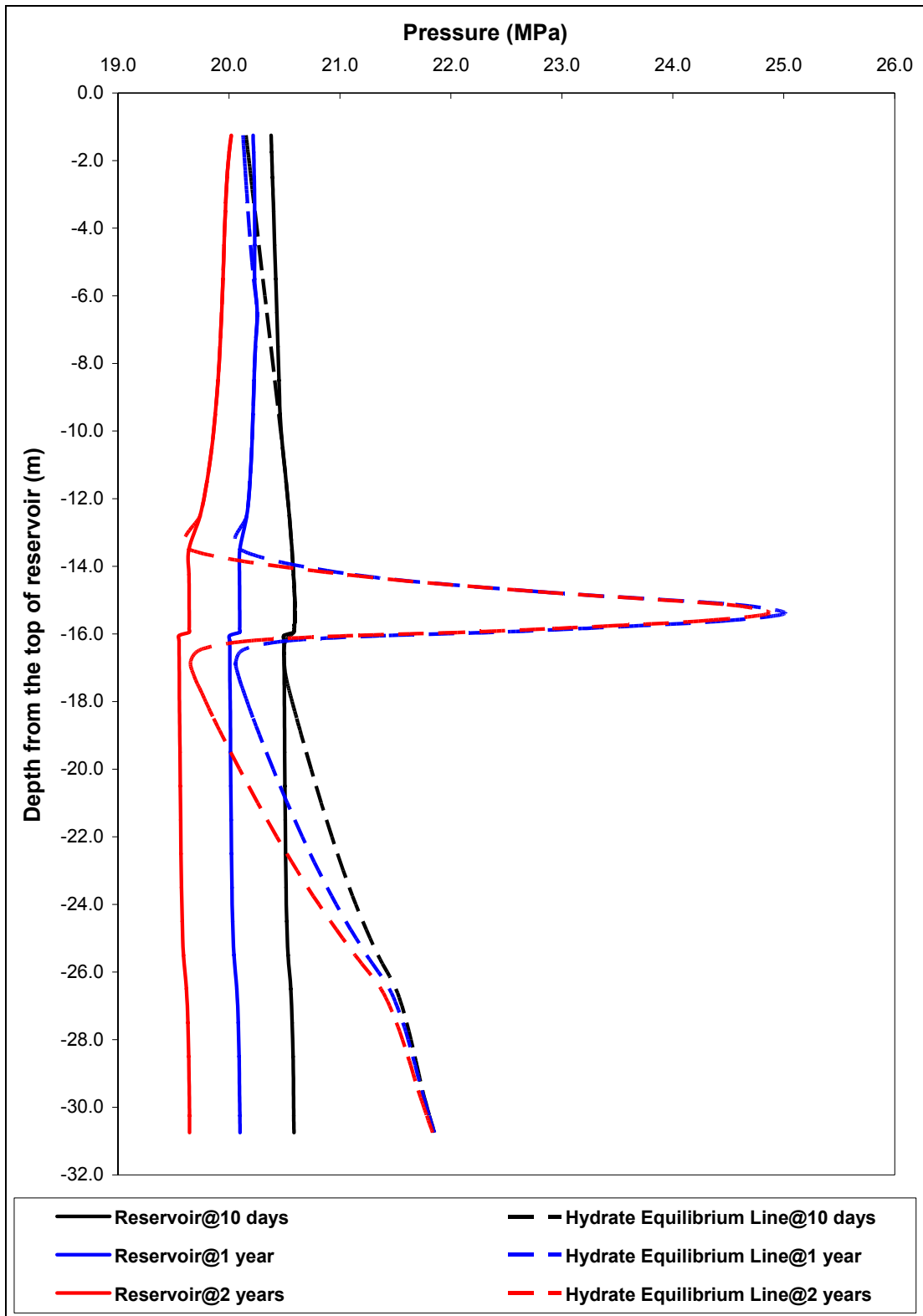


Figure 8.25: Pressure profile for case 2a, 2 years

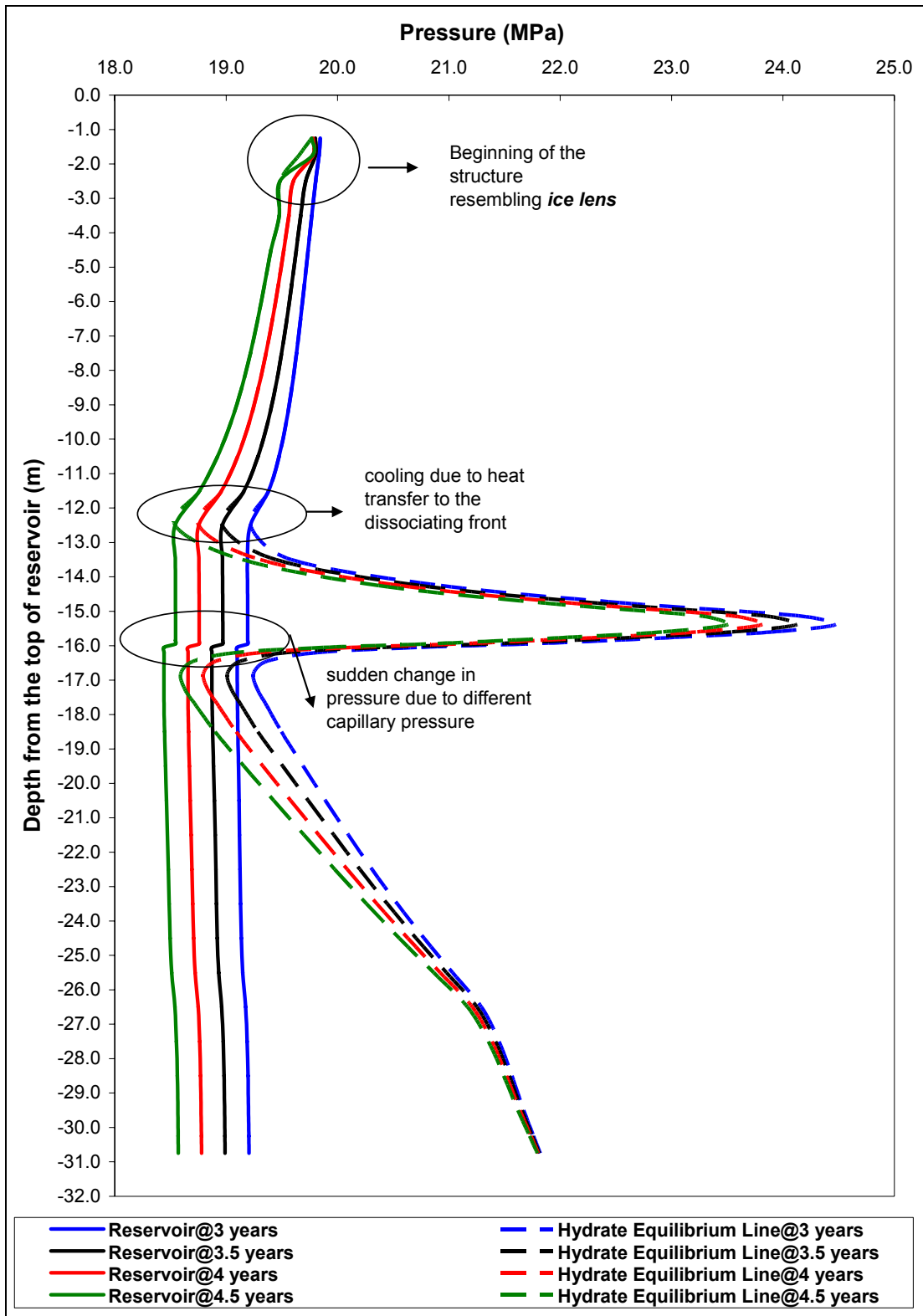


Figure 8.26: Pressure profile for case 2a, 4.5 years

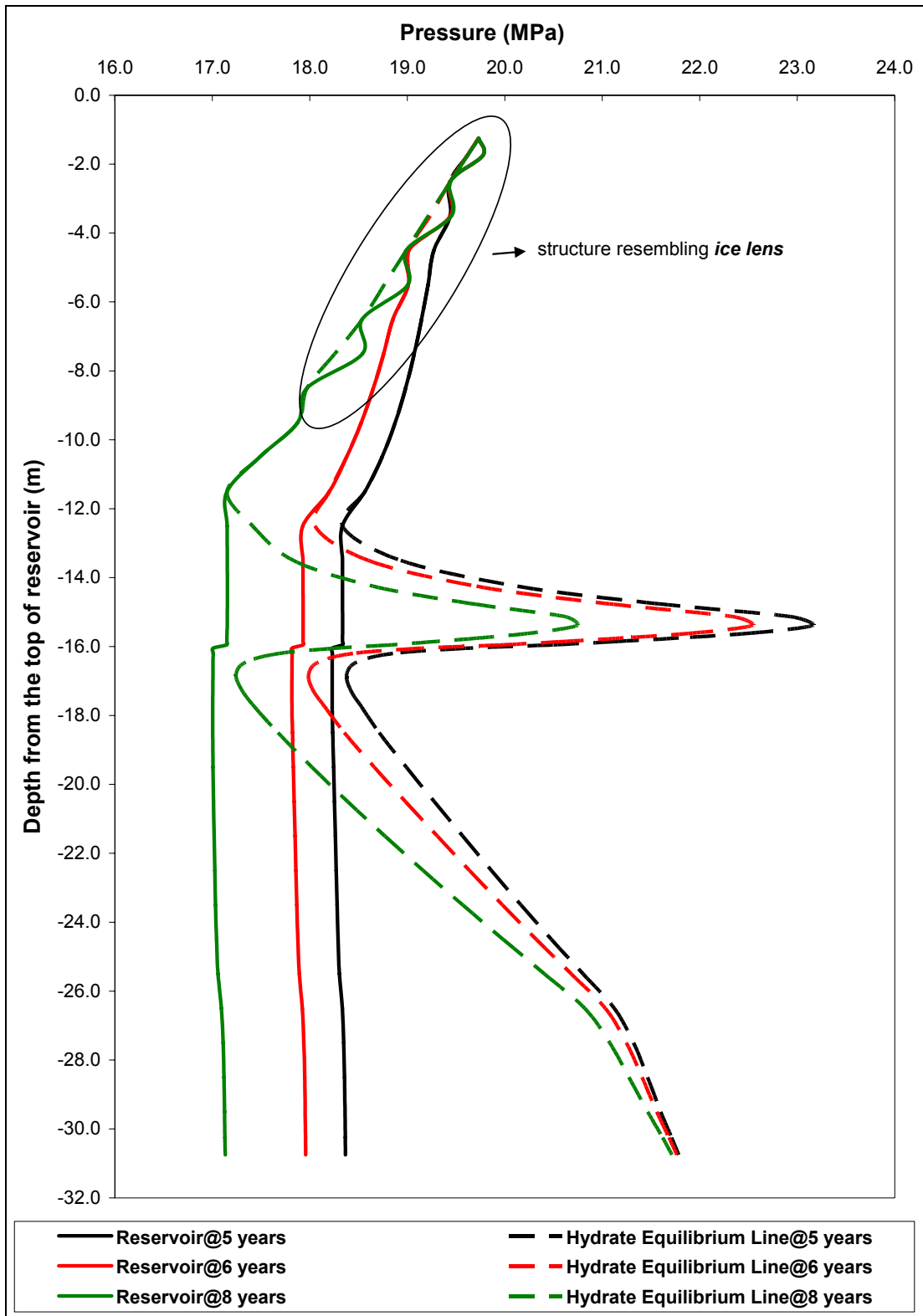


Figure 8.27: Pressure profile for case 2a, 8 years

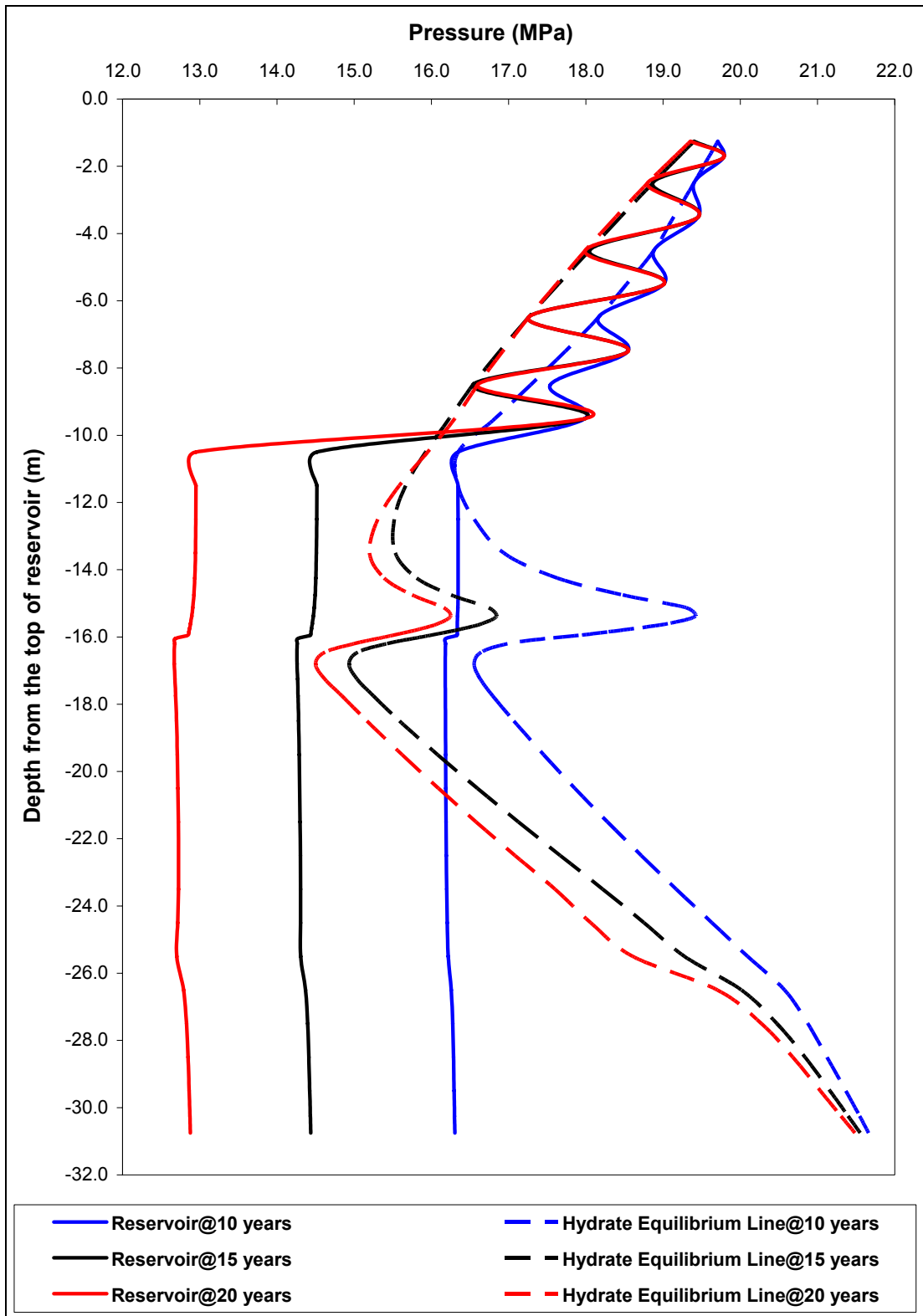


Figure 8.28: Pressure profile for case 2a, 20 years

## 8.4 Comparison with Previous Work

In the articles of Holder [11] and Moridis [22], amount of released gas contribution within the first 3 years of production is as high as 21% (triangular data points in Figure 8.29) and 72% (Figure 8.30) respectively and it is not mentioned in the texts that any ice lens formation or secondary dissociation front at the top of hydrate zone is observed.

In this study, contribution of released gas for the first 3 years has been around 10% (Figure 8.19, case 2a), significantly lower than previous studies and this is attributed mainly to the fact that a very strong capillary pressure has been assigned in the upper section of reservoir causing the least release from hydrates by preventing water from draining (actually, Holder [11] assumed a linear, smoothed dissociation front acting as a moving boundary of impermeable hydrate zone). Therefore, though this result is a pessimistic one, should further encourage the studies on hydrate gas production with better description of capillary pressure function.

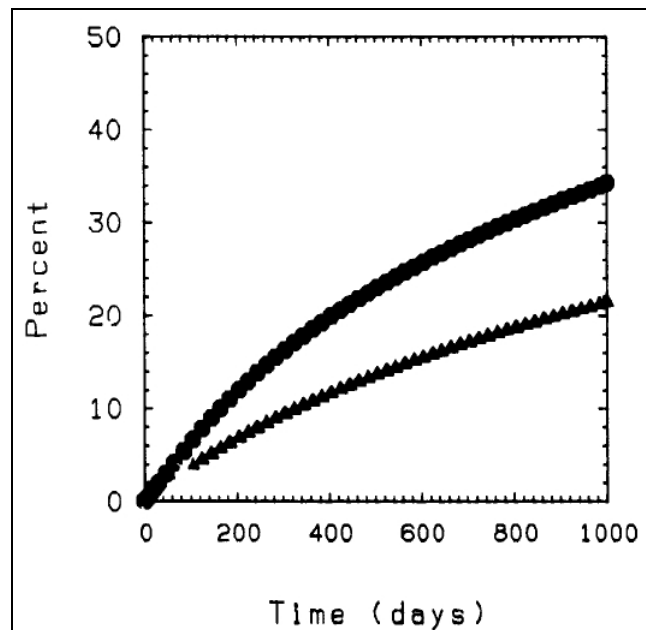


Figure 8.29: Contribution of released methane, Holder [11]

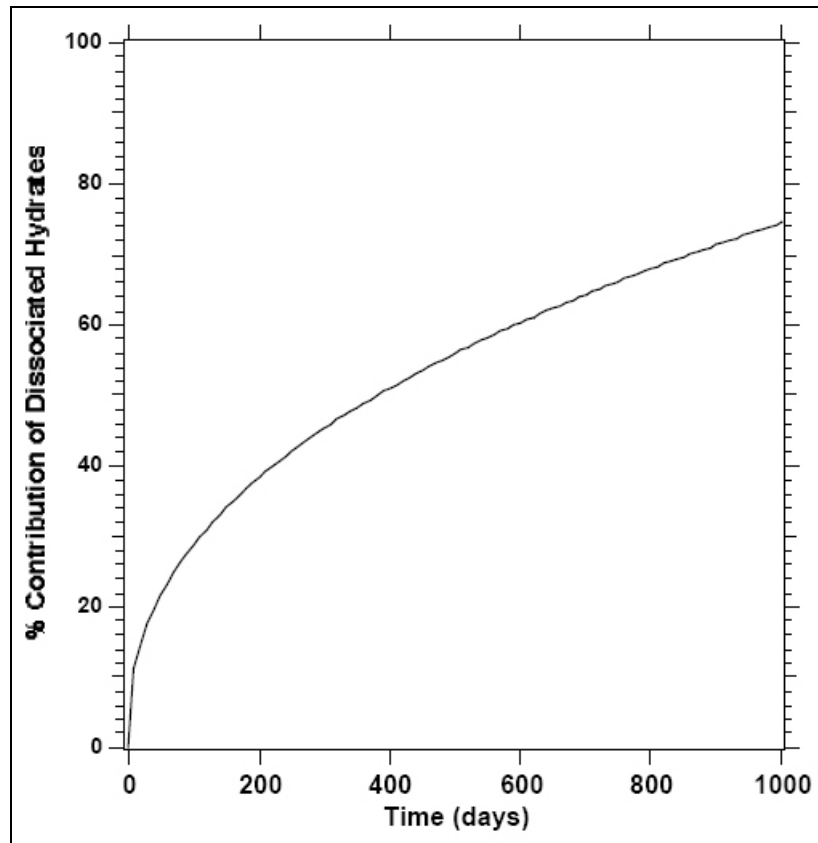


Figure 8.30: Contribution of released methane, Moridis [22]

## CHAPTER 9

### CONCLUSION

As stated in the beginning chapter, production of gas from hydrate reservoirs is a subject that should be considered seriously today for it could well be the next source of fossil fuels regarding the decline predictions made about reserves of conventional reservoirs. In addition, with today's increasing oil prices it is an even more attractive investment.

In this study, simulation modeling of gas production using depressurization scheme for a single well, class 1 hydrate reservoir with hydrate-gas (case 1) and hydrate-water (case 2) zones above free gas zone were carried out.

To be able to study case 2, to keep mobile water (%30 saturation) initially in place in the hydrate zone above a zone of 70% gas saturation, a different capillary pressure function, thus a different medium, is assigned for the upper section of the reservoir. Although this has served very well for the purpose of problem initialization, it for sure introduced some error during the rest of production simulation. This high value capillary pressure kept initial and dissociated water from draining to the lower section and created a horizontal high saturation water barrier in the middle of reservoir which accordingly reduced gas release and transfer from the hydrate zone. Hence, contribution of released methane in case 2 is for a worst case scenario and indeed this approach caused a significant loss of accuracy in the results. Then, it is necessary to fully identify the physics behind the full water occupancy in the rest of pore space with in the hydrate zone in case 2.

For the solution of problem, altering the relative permeability or irreducible water saturations may result in an unexpected way for in order to decrease pressure in a layer, water should be mobile. Nevertheless, a new capillary pressure definition which is also a function of solid saturation would be suitable (Moridis [23]).

The results of this study indicate that:

- In case 1, second dissociation front develops at the top of hydrate zone and has the most substantial contribution in replenishment.
- In case 2 (hydrate-water in the hydrate zone), because the second dissociation front could not fully develop due to high capillary pressure acting on liquid phase, a structure similar to ice lens formation (inverse) is observed.

- Initial cumulative replenishment (first 5 years in Figure 8.19) and the replenishment rate (first 3.5 years in Figure 8.16) are higher for case 2 because, production pressure drop is felt all over the reservoir due to low compressibility of water and more hydrate is decomposed.
- Well-bore heating may not be necessary if production is not close to dissociation front. And less water is produced in no well-bore heating case 1b compared to case 1a (Figure 8.22)
- Compared to previous works of Holder [11] and Moridis [22], amount of released gas contribution within the first 3 years of production is significantly low which is primarily attributed to the specified high capillary pressure function.

## CHAPTER 10

### RECOMMENDATIONS

Definition of a new capillary pressure function in which capillary pressure increases with increasing solid saturation is apparently necessary for accurate modeling of gas recovery from hydrate reservoirs.

Building up of inverse ice lens structure suggests that an extensive study of causes of ice lens formation in nature and their associated introduction in the code may be needed for it is known that in nature not only the capillary pressure and cooling are in effect during the development of this structure but also the surface forces acting between the ice and water. However; probably introduction of the new capillary pressure function would already account for this effect.

Because a second dissociation front develops at the top of hydrate zone in case 1, and due to inverse ice lens sequence at the top of hydrate zone in case 2, this region should as well be modeled using finer (thinner) layers.

The number of no porosity layers, which are provided at the top and bottom of reservoir in order to describe heat flux from surrounding strata, should be significantly increased so that the constant temperature boundaries are placed away from the reservoir. This way, the strata (no porosity layers) above the reservoir may remain colder during the production period along with a more realistic heat flux to the reservoir and development of second dissociation front as well as the inverse ice lens sequence would likely be delayed.

Since decomposition of hydrate at the top would cause great trouble in reservoirs where the hydrate zone itself acts as the impermeable layer (top cap) and above it is permeable, it is vital to know for sure whether the observation of this study was due to close placement of constant temperature boundary to the reservoir or not.

Finally, a new type of problem initialization procedure, where methane migration from the bottom of initially 100% water saturated reservoir is imitated, would ensue in a temperature gradient fully complying with geothermal gradient and may provide some insight on how the mechanism of hydrate reservoirs should be. For the case of hydrate reservoirs formed from in-situ gas, hydrate reservoir boundary temperatures may be imposed on a conventional gas

reservoir with high water saturation. Or gas sources may be assigned to the grids of a water saturated reservoir for a certain period of time permitting hydrate formation from this in-situ gas. Unfortunately, these types of initializations would probably not allow obtaining the desired saturation distribution and a dissociation front at the desired depth. Assignment of boundary temperatures complying with geothermal gradient would as well delay the decomposition occurring at the top of hydrate zone since upper boundary would be cooler then.

## REFERENCES

1. Sloan, E.D. Jr.; *Clathrate Hydrates of Natural Gases*, Marcel Dekker, NY, 641 pp. 1990.
2. Holder, G.D., John, V.T. and Yen, S.; Geological Implications of Gas Production from in-situ Gas Hydrates, 1980; SPE/DOE 8929.
3. Sloan E.D. Jr. "Gas Hydrates: Review of Physical/Chemical Properties" *Energy and Fuels* 12 (1998) p. 191-196.
4. Makogon, Y.F.; *Hydrates of Hydrocarbons*, Pennwell Books, 482 pp. 1997.
5. W. K. Sawyer, C. M. Boyer, J. H. Frantz Jr. and A. B. Yost II; Comparative Assessment of Natural Gas Hydrate Production Models; 2000; SPE 62513.
6. Moridis, G.J. and Collet T.S.; Gas Production from Class 1 Hydrate Accumulations, 2003; LBNL-52827.
7. Rose, W.; Unconventional Ideas about Unconventional Gas; 1982; SPE/DOE 10836.
8. Ji, C., Ahmadi, G. and Smith, D.H.; Natural gas production from hydrate decomposition by depressurization; 2000; *Chemical Engineering Science* 56 (2001) p. 5801-5814.
9. Khaikhah, D., Pooladi-Darvish, M., Bishnoi, P.R., Collett, T.S., and Dallimore, S.R., 1999: Production potential of the Mallik field reservoir; in *Scientific results from JAPEX/JNOC/GSC Mallik 2L-38 gas hydrate research well, Mackenzie delta, northwest territories, Canada* (ed.) S.R. Dallimore, T. Uchida and T.S. Collett; geological survey of Canada, bulletin 544, p.377-390.
10. Rose, W.; Production Scheme for Deep Water Hydrate Deposits; 1982; SPE 11106.
11. Holder, G.D. and Angert, P.F.; Simulation of Gas Production from a Reservoir Containing Both Gas Hydrates and Free Natural Gas, 1982; SPE 11105.
12. McGuire, P.L.; Recovery of Gas From Hydrate Deposits Using Conventional Technology; 1982, SPE/DOE 10832.
13. Khataniar, S., Kamath, V.A., Omenihu, S.D., Patil, S.L. and Dandekar, A.Y.; Modeling and Economic Analysis of Gas Production from Hydrates by Depressurization Method, 2002; *The Canadian Journal of Chemical Engineering*, Volume 80, February 2002.

14. Swinkels, W.J.A.M. and Drenth, R.J.J.; Thermal Reservoir Simulation Model of Production from Naturally Occurring Gas Hydrate Accumulations; 1999; SPE 56550.
15. Burshears, M., O'Brien, T.J. and Malone R.D.; A Multi-Phase, Multi-Dimensional, Variable Composition Simulation of Gas Production from a Conventional Gas Reservoir in Contact with hydrates; 1986; SPE 15246.
16. J-C Iseux, Gas Hydrates: Occurrence, Production and Economics; 1991; SPE 21682
17. Debendra K. D. and Srivastava, V.; Calculation of Gas Hydrate Dissociation with Finite-Element Model; 1993; Journal of Energy Engineering, Vol.119 No.3 December 1993.
18. Durgut, I., and Parlaktuna, M.; A numerical method for the gas production process in gas hydrate reservoirs; 2<sup>nd</sup> International Conference on Natural Gas Hydrates, Toulouse, France June 2-6 1996.
19. Ji, C., Ahmadi, G., Zhang, W. and Smith, D.H; Natural Gas Production from Hydrate Dissociation: A Comparison of Axisymmetric Models, 4th International Conference on Gas Hydrate, Yokohama, Japan, May 19-23, 2002.
20. Goel, N., Wiggins, M. and Shah, S.; Analytical modeling of gas recovery from in situ hydrates dissociation, 2001; Journal of Petroleum Science and Engineering 29 (2001) 115 – 127.
21. Moridis, G.J., Apps, J., Pruess, K., and Myer, L.; EOSHYDR: A TOUGH2 Module for CH<sub>4</sub> – Hydrate Release and Flow in the Subsurface, 1998; LBNL-42386.
22. Moridis, G.J; Numerical Studies of Gas Production from Methane Hydrates, 2002; SPE 75691.
23. Moridis, G.J. Kowalsky, M.B. and Pruess, K: TOUGH-Fx/HYDRATE v1.0 User's Manual: A Code for the Simulation of System Behavior in Hydrate Bearing Geologic Media, 2005, LBNL.
24. Pruess, K., Oldenburg, C. and Moridis, G.J.; TOUGH2 User's Guide, Version 2.0, 1999
25. Ertekin, T., Abou-Kassem, J.H. and King, G.R.; *Basic Applied Reservoir Simulation*, 2001.

## APPENDICES A

### HYDRATE FORMATION CONDITIONS

Hydrates form under a specific temperature corresponding to system pressure. Using the experimental and computed data, Pressure - Temperature phase diagrams for pure hydrocarbon gases are plotted. These plots indeed mark the hydrate formation conditions.

#### A.1 Phase Diagrams for Hydrates of Pure Hydrocarbons

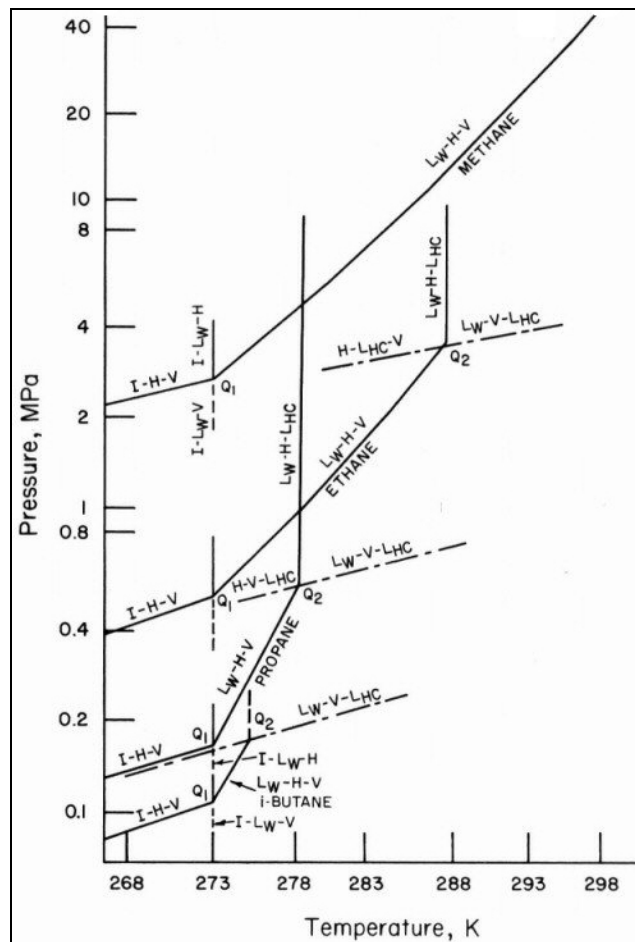


Figure A. 1: P - T diagram for hydrates of pure hydrocarbons (Sloan [1])

In Figure A. 1; I, H, LW, LHC, V indicates ice, hydrate, liquid water, liquid hydrocarbon and vapor (vapor of water and gaseous hydrocarbon) respectively.

In addition to triple points, quadruple points ( $Q_1$ ,  $Q_2$ ) exist in Pressure-Temperature plots of hydrates. At  $Q_1$  ice, water, hydrate and vapor (I -  $L_W$  - H - V) and at  $Q_2$  water, hydrate, vapor and liquid hydrocarbon ( $L_W$  - H - V -  $L_{HC}$ ) coexist. These quadruple points are unique for every hydrocarbon gas, thus present a distinguishing property.

The composition of hydrate forming gas and the ingredients found in aqueous solution of water (such as salt or alcohol) affect the hydrate formation temperature and pressure.

## A.2 Phase Diagrams for Hydrates of Gas Mixtures

Phase diagrams for systems of gas mixtures and water can be obtained by superposition of hydrate formation conditions plot on the phase diagram of gas mixture.

In Figure A. 2, curve  $AQ_1KCD$  is the hydrate equilibrium line where curve  $ECFKL$  is the phase envelope for gas mixture. The vertical line passing through  $Q_1$  marks the ice formation temperature. The quadruple point  $Q_2$  of pure components, where  $L_W$  - H - V -  $L_{HC}$  coexists, corresponds to the curve  $CK$  in the plot for gas mixtures. The line for  $L_W$  - V -  $L_{HC}$  in the pure gases transforms into phase envelope incase of mixtures.

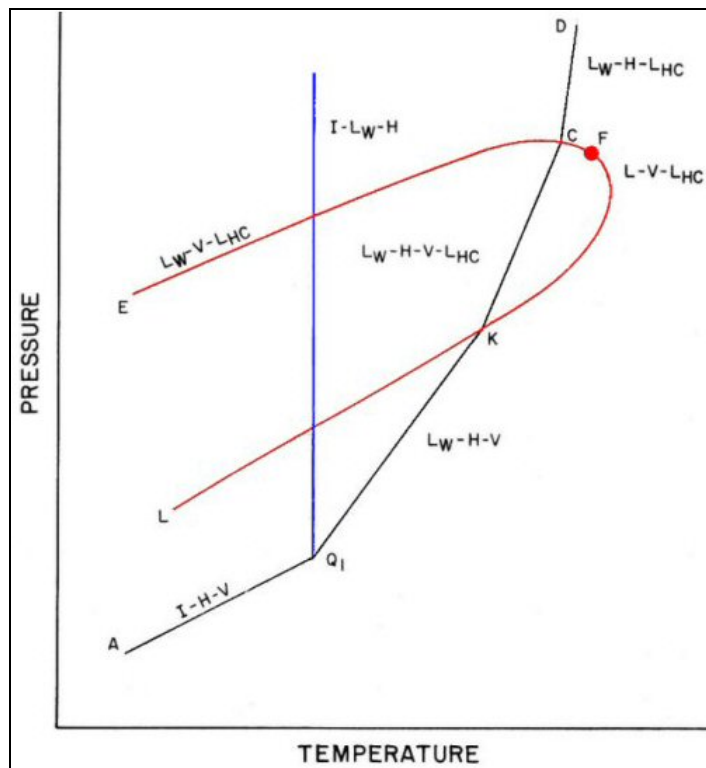


Figure A. 2: P - T diagram for hydrates of hydrocarbon mixtures (Sloan [1])

### A.3 The Hysteresis of Hydrate Formation

Magokon [4] has proved that during dissociation hydrates do not completely dissolve but leave partial structures that will form hydrate more easily when formation conditions prevail again. For instance assume that hydrate is formed initially at temperature  $T_1$  and pressure  $P_1$  from gas and water phases without any prior hydrate structure and dissolved back. Then due to hydrate structures that had not dissociated, hydrate will form at some temperature  $T_2$  greater than previous temperature of  $T_1$  again at the same pressure  $P_1$ .(Figure A. 3)

This phenomenon is similar to capillary pressure hysteresis in reservoir engineering. Nevertheless, the residual crystal network completely decays above 315 K.

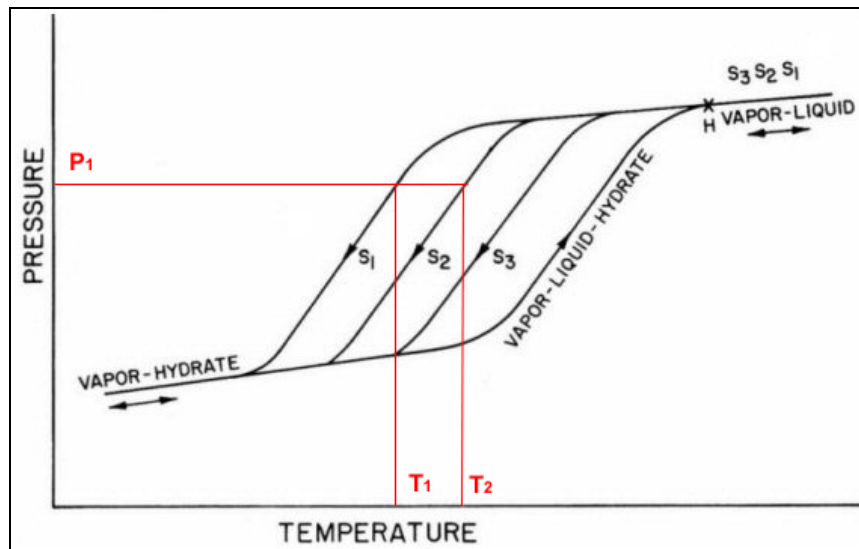


Figure A. 3: Hydrate formation hysteresis (modified from Sloan [1])

In Figure A. 3  $S_1$ ,  $S_2$ ,  $S_3$  lines are the phase diagrams of successive hydrate formation. Apparently hydrate forms at a higher temperature second time ( $S_2$ ), even higher temperature third time ( $S_3$ ) of hydration.

### A.4 Effect of Inhibitors on Hydrate Formation

The ingredients found in aqueous solution of water (such as salt or alcohol) affect the hydrate formation conditions. Alcohols, salts and similar components which are significantly soluble in water, usually inhibit hydrate formation by decreasing formation temperature (or increasing formation pressure) for a certain system pressure (or temperature) as they would

do for ice. This is mainly because water molecules initially prefer to be attached these substances due to higher molecular attraction (Figure A. 4).

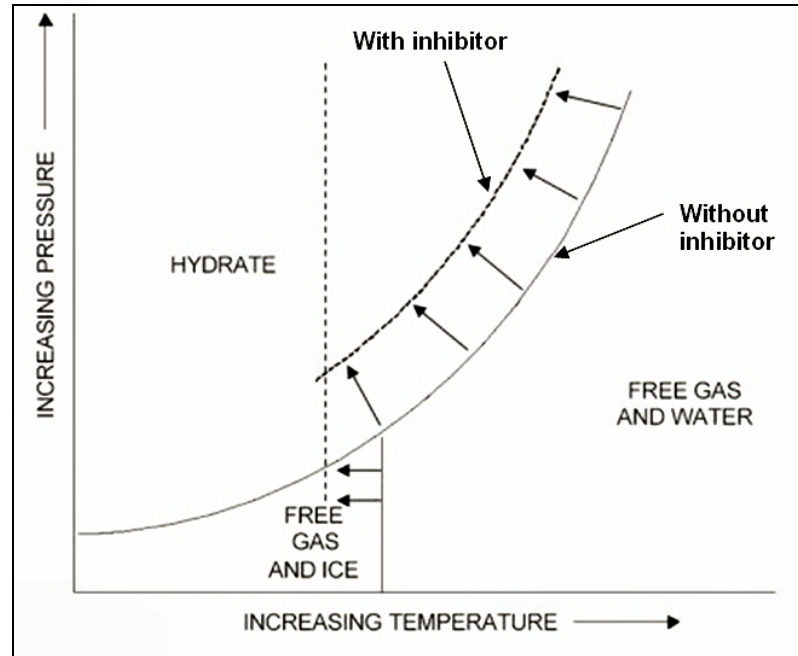


**Figure A. 4: Effect of inhibitors on hydrate formation (modified from Sawyer [5])**

Among many possible inhibitors, methanol is the most popular due to its cost and effectiveness. The depreciation it causes on the temperature of hydrate formation can be modeled by Equation (A-1), which is a result of experimental work of Nielsen and Bucklin (Sloan [1]).

$$\Delta T = -129.6 * \ln(1 - X_{MeOH}) \quad (\text{A-1})$$

Where;

T is temperature in Fahrenheit

$X_{MeOH}$  is weight percent of methanol in the liquid

Owing to polar nature of the solutes, salts have a higher effect of inhibition on formation of hydrates which can be calculated by the equation (A-2).

$$T_s = \left[ \frac{1}{T_w} - \frac{N_H * \Delta H^f}{\Delta H^0} \left( \frac{1}{273.15} - \frac{1}{T_{fs}} \right) \right]^{-1} \quad (\text{A-2})$$

Where;

$T_s$  is the hydrate formation temperature in the presence of salt (Kelvin)

$T_w$  is the water temperature (K)

$N_H$  is the hydration number

$\Delta H^f$  is the heat of fusion (melting) of ice (J/kg)

$\Delta H^o$  is the heat of dissociation of hydrate (J/kg)

$T_{fs}$  freezing point of the salt solution (K)

## APPENDICES B

### DETERMINATION OF HYDRATE FORMATION CONDITIONS

The two of the most common methods available for the determination of formation conditions of natural gas hydrates are:

- The distribution coefficient ( $K_i$  value) method by Wilcox, Carson and Katz (Sloan [1])
- Gas gravity method by Katz (Sloan [1])

#### B.1 Distribution Coefficient ( $K_i$ value) Method

Carson and Katz have noticed that their experimentally found hydrate composition changed at different temperatures and pressures (here the pressure has to be equal to the corresponding equilibrium pressure or vice a versa). This suggested some sort of solid solution concept where hydrate and forming gas coexisted (with no free water or indeed ignoring the presence of free water and its presence in gas phase as vapor). Hence it was possible to consider the mol fraction of quest component in the solid phase of mixture. It is important to note that what is meant by hydrate composition here is the relative amounts of distinct hydrocarbon species found in a hydrate mass containing a single mole of gas mixture (Wilcox, Carson, Katz, 1941).

Vapor-solid distribution coefficient ( $K_{vsi}$ ) is defined for each component:

$$K_{vsi} = y_i / x_{si} \quad (\text{B-3})$$

Where;

$y_i$  is mol fraction of component  $i$  in water free vapor (perhaps means compute disregarding the present water vapor)

$x_{si}$  is mol fraction of component  $i$  in solid

$K_{vsi}$  values can be presented as function of temperature and pressure:

$$\ln K_{vsi} = A + B * T + C * \Pi + D * T^{-1} + E * \Pi^{-1} + F * \Pi * T + G * T^2 + H * \Pi^2 + I * \Pi * T^{-1} + J * \ln(\Pi * T^{-1}) + K * (\Pi^{-2}) + L * T * \Pi^{-1} + M * T^2 * \Pi^{-1} + N * \Pi * T^{-2} + O * T * \Pi^{-3} + P * T^3 + Q * \Pi^3 * T^{-2} + R * T^4 \quad (\text{B-4})$$

Where;

$\Pi$  is pressure in psia

T is temperature in °F

The values of coefficients (parameters) are different for each component. Some of the values are presented in Table B. 1.

**Table B. 1: Parameters of  $K_{vsi}$  equation (Sloan [1])**

PARAMETERS	COMPONENTS			
	CH <sub>4</sub>	C <sub>2</sub> H <sub>6</sub>	C <sub>3</sub> H <sub>8</sub>	CO <sub>2</sub>
A	1.63636	6.41934	-7.8499	9.0242
B	0.0	0.0	0.0	0.0
C	0.0	0.0	0.0	0.0
D	31.6621	-290.283	47.056	-207.033
E	-49.3534	2629.10	0.0	0.0
F	-5.31E-6	0.0	-1.17E-6	4.66E-5
G	0.0	0.0	7.145E-4	-6.992E-3
H	0.0	-9.0E-8	0.0	-2.89E-6
I	0.128525	0.129759	0.0	6.223E-3
J	-0.78338	-1.19703	0.12348	0.0
K	0.0	-8.46E4	1.669E4	0.0
L	0.0	-71.0352	0.0	0.0
M	0.0	0.596404	0.23319	0.27098
N	-5.3569	-4.7437	0.0	0.0
O	0.0	7.82E4	-4.48E4	0.0
P	-2.3E-7	0.0	5.5E-6	8.82E-5
Q	-2.0E-8	0.0	0.0	2.55E-6
R	0.0	0.0	0.0	0.0
CORRELATION COEFFICIENT	0.999	0.998	0.998	0.996

Then using the  $K_{vsi}$  equation, initial hydrate formation conditions can be computed in a manner to what we are familiar in vapor-liquid equilibrium line (phase envelope) computations.

At the triple point of a certain gas composition; mol fraction of each component in gas phase is divided by the  $K_i$  value for that component and when the individual results are summed up they must be equal to one.

$$\sum_{i=1}^n \frac{y_i}{K_{vsi}} = 1.0 \quad (\text{B-5})$$

For a given temperature (or pressure) the pressure (or temperature) is changed and following it the  $K_i$  values change and above sum computed. This process is repeated until the sum is equal to 1.

This method assumes that both the hydrate and gas phases are ideal solutions where  $K_{vsi}$  of a given component is not dependent on any other component present.

## **B.2 Gas Gravity Method (Katz)**

In essence this method is somewhat derived utilizing the  $K_i$  value method. Employing the limited amount of experimental data in correlation with  $K_i$  value method calculations some charts are obtained. Using the generated plots, one can easily determine the hydrate forming pressure (or temperature) at a certain temperature (or pressure) for known gas gravity. Although the method is less accurate compared to the  $K_i$  value method where it is derived from, it is apparently much more practical for the field.

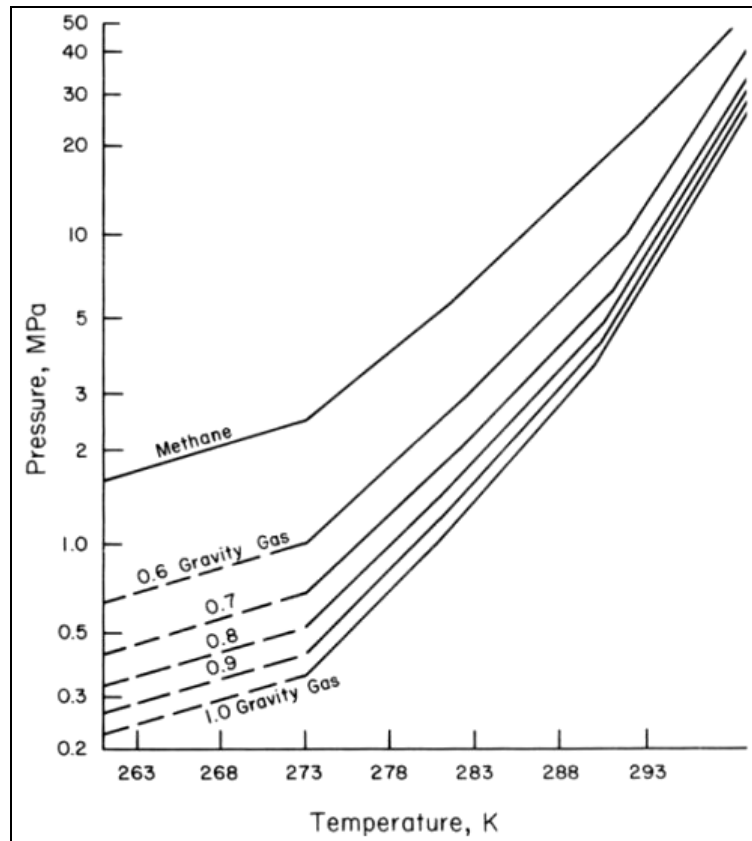


Figure B. 1: Hydrate formation conditions from gas gravity (Sloan [1])

### B.3 Pressure - Temperature Phase Diagram for Methane Hydrate

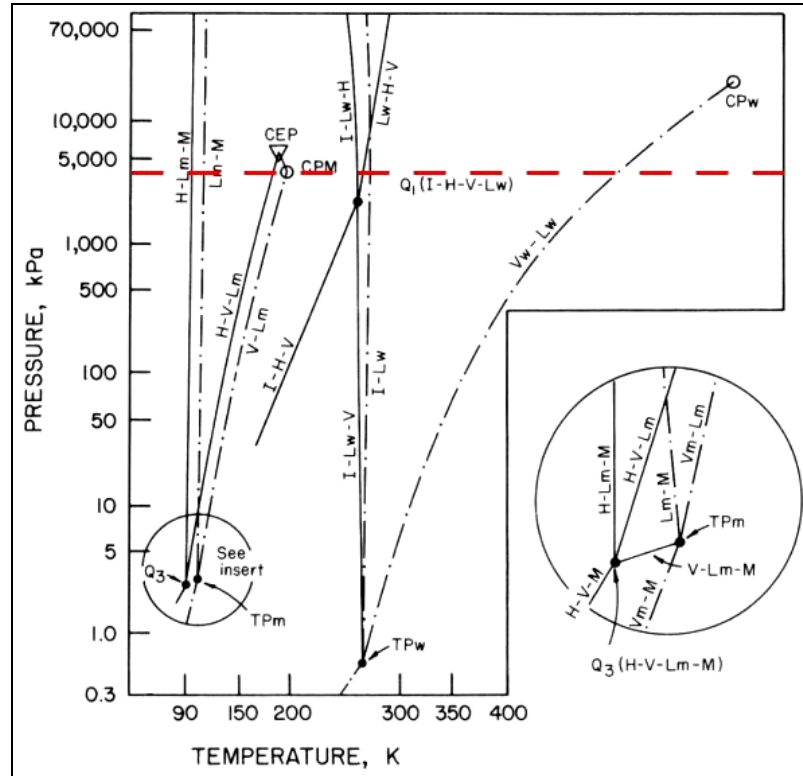


Figure B. 2: P-T diagram for methane hydrate (modified from Sloan [1])

In the Figure B. 2:

M is solid methane

$L_m$  is liquid methane

CP's are critical points

TP's are triple points

The case can be expressed more clear when one considers the phase diagrams of pure methane. In the first figure of Pressure-Temperature plot, solid lines represent three phase equilibrium for methane hydrate system. And broken (dash-dot) lines are for the two phase equilibrium of components (methane and water) individually. The dashed line drawn near 5000 MPa is to indicate constant pressure. At this constant pressure one would obtain a Temperature-Composition diagram as shown in Figure B. 3.

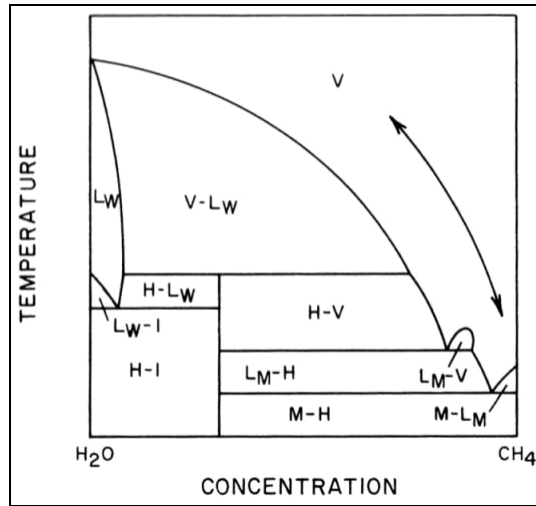


**Figure B. 3: Temperature-Concentration diagram for pure methane (Sloan [1])**

The figure shows the presence of phases at a specific pressure with varying temperature and component concentration. In the plot, concentration of methane on molar basis increases from 0 % at left to 100 % at right.

#### **B.4 Determination of Hydrate Number $N_H$**

When he studied experiments of the era, Villard concluded that hydrates can be expressed by the general formula:



Where M represents a single molecule of the gas and the general hydrate number is 6. This direct determination of hydration number is also known as Villard's Rule.

#### **Indirect Determination by de Forcrand's Clapeyron Method:**

This method is still widely used and besides being perhaps the most useful one, it is accurate in a wider range of pressure and temperature compared to other available methods.

Method requires the calculation of individual enthalpies of hydrate formation from both water and ice. Then the difference of these enthalpies may be divided by the enthalpy of fusion of water (heat of melting) yielding the moles of water consumed during hydration.



$$\Delta H_3 = \Delta H_1 - \Delta H_2 \quad (\text{B-10})$$

$$N_H = \frac{\Delta H_3}{\Delta H_f} \quad (\text{B-11})$$

Where;

$\Delta H_f$  is the enthalpy of fusion of water which is well known.

## B.5 Hydrate Composition

What meant by hydrate composition is the relative amounts of hydrocarbon components in hydrate phase or in other words the gas composition in hydrate phase. It is quite difficult to predict the composition of hydrates since it varies with temperature, pressure and composition of the involved gas mixture. Nevertheless, the K value method (see Appendices B.1), which also enables us to predict formation pressure and temperature for hydrates of gas mixtures, indeed makes it possible to determine hydrate composition.

Magokon [4] has concluded that methane content in the hydrate increases with hydrate formation at higher temperatures and pressures. The amount of heavy components in hydrates decrease, when temperature and pressure are increased (Methane content increase).

## B.6 System Composition

The ratio of host molecules to guest molecules as well may vary with temperature and pressure, even for hydrates of pure gases such as methane. This is a matter of occupancy of cages and note that the frequently used hydration number of 6.00 is an average value.

At a specific pressure, depending on the temperature obviously, the phases present in the system change according to the amount of hydrocarbon molecules and water molecules present in the whole system. For instance, at a temperature below equilibrium conditions, if ratio of water molecules to hydrocarbon molecules is less than average hydration number than hydrate will co-exist with hydrocarbon gas because of the excess gas in the system.

## APPENDICES C

### MESSOYAKHA FIELD

Messoyakha field in Siberia permafrost (Figure C. 1) is the first hydrate deposit to be discovered and put into industrial production in 1967. The hydrate estimated to enclose one third of the whole gas in the reservoir where this was a “free gas and water below hydrate” type reservoir. Total gas reserve is over  $37 \times 10^9 \text{ m}^3$  where  $15 \times 10^9 \text{ m}^3$  is free gas and therefore  $22 \times 10^9 \text{ m}^3$  of gas resides in hydrate initially. The field has been produced initially by depressurization method. Later inhibitor injection and combination of both methods followed.

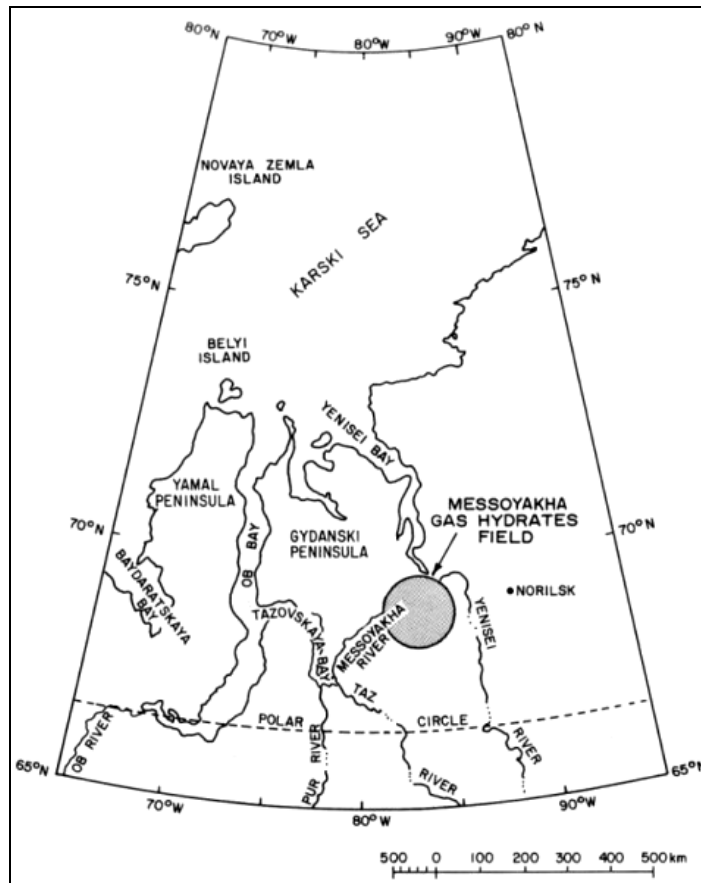


Figure C. 1: Location of Messoyakha Field (Sloan [1])

Reservoir properties of Messoyakha Field and gas composition (water free) are shown in Table C. 1 and Table C. 2 respectively. Figure C. 2 presents cross-section of the reservoir.

**Table C. 1: Reservoir properties of Messoyakha Field**

AREA OF PAY ZONE	12.5 KM * 19 KM
THICKNESS OF PAY ZONE	84 M
POROSITY	16 – 38% (25% AVERAGE)
RESIDUAL WATER SATURATION	29 – 50% (40% AVERAGE)
HYDRATE SATURATION	40% (AT THE TOP) – 20% (ABOVE GAS ZONE)
INITIAL RESERVOIR PRESSURE	7.8 MPA
RESERVOIR TEMPERATURE RANGE	281 – 285 K
WATER SALINITY	< 1.5 WEIGHT %

**Table C. 2: Gas composition of Messoyakha Field**

METHANE CH <sub>4</sub>	98.6 %
ETHANE C <sub>2</sub> H <sub>6</sub>	0.1 %
PROPANE C <sub>3</sub> H <sub>8</sub>	0.1 %
CARBON DIOXIDE CO <sub>2</sub>	0.5 %
NITROGEN N <sub>2</sub>	0.7 %

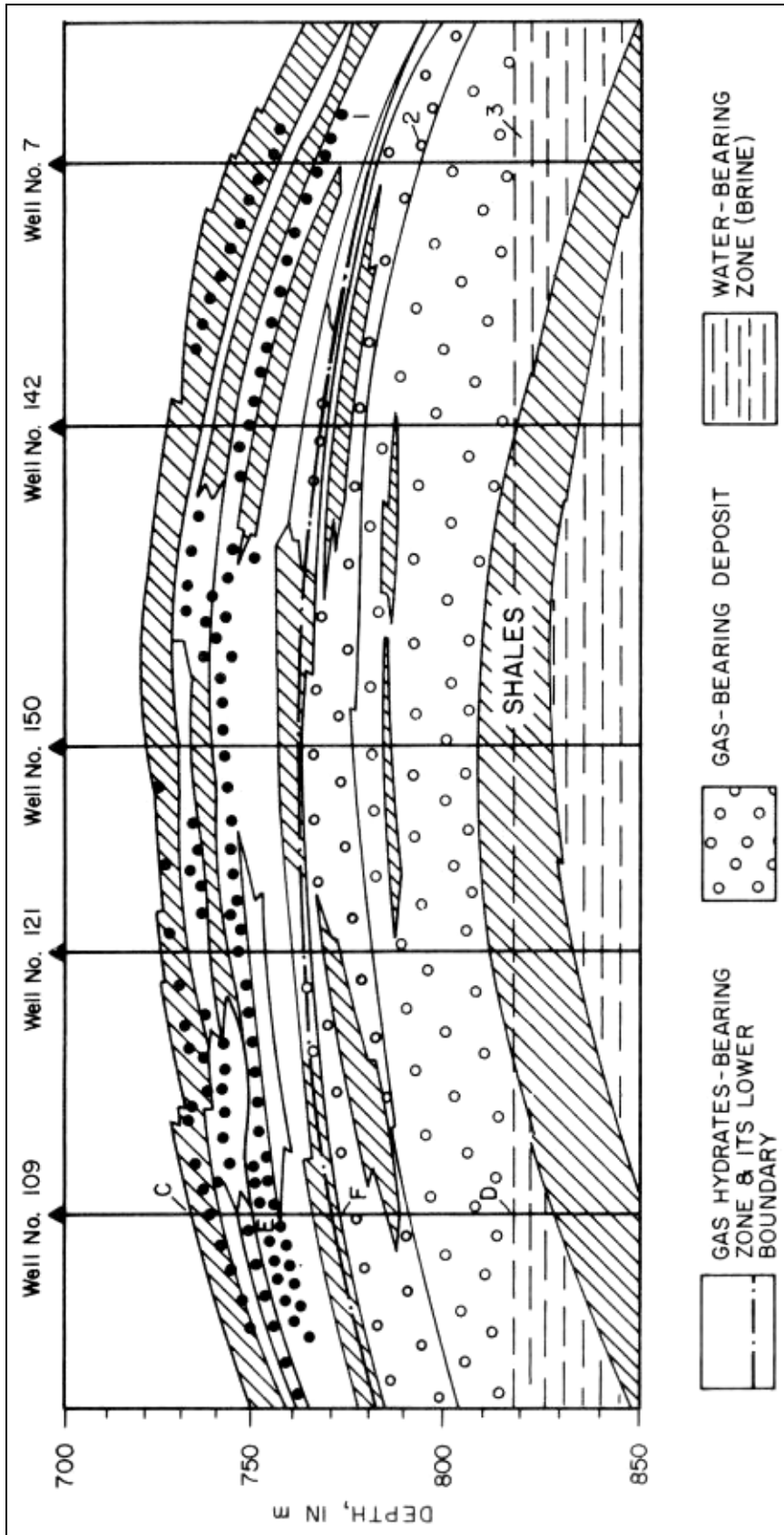
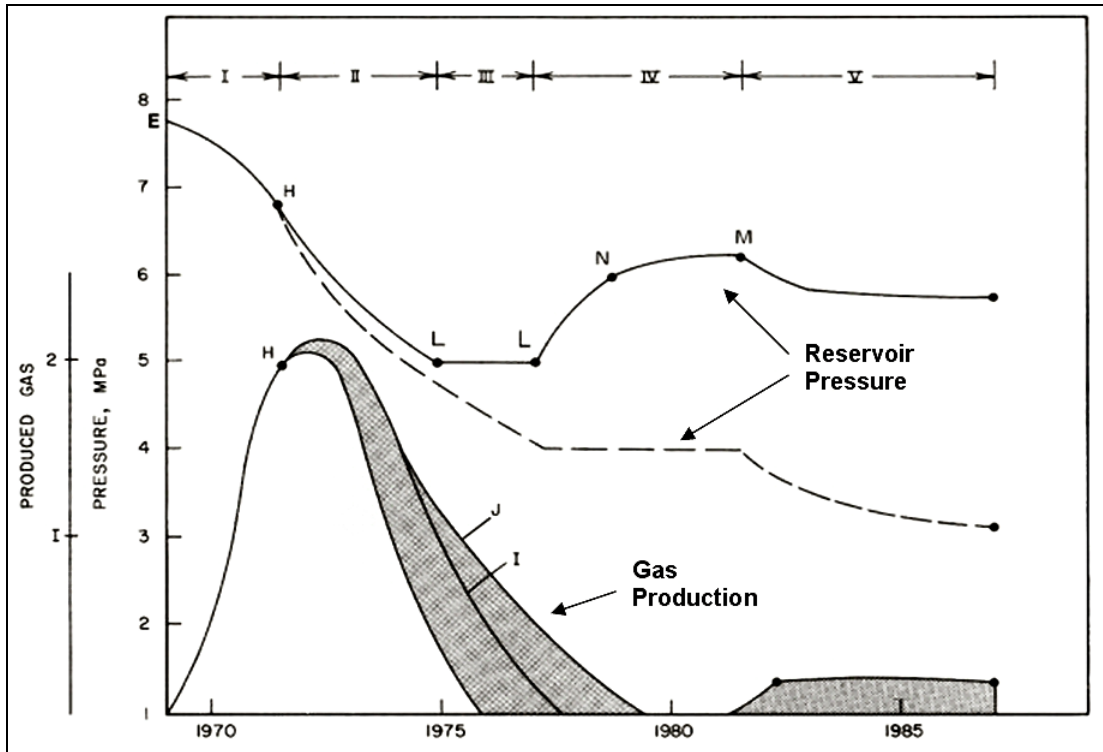


Figure C. 2: Cross-sectional view of Messoyakha Field (Sloan [1])



**Figure C. 3: Production history of Messoyakha Field (modified from Sloan [1])**

Figure C. 3 includes plots of gas production (below curves) versus time and reservoir pressure (above curves) versus time. At the top of the plot there are time periods indicated by roman numbers. The dashed reservoir pressure curve shows the case if there had not been hydrate. And the shaded produced gas sections indicate contribution of hydrate gas.

The path of temperature pressure changes in the reservoir are also shown on phase diagrams as in the Figure C. 4 and Figure C. 5.

Where:

Line AB is the hydrate equilibrium line

Point E is the average initial P-T point in the reservoir

Point C is the P-T point at the top of the pay zone

Point D is the P-T point at the gas-water contact

Point F is the P-T point at the gas-gas hydrate contact

The location of points C, D, E, and F are also marked in the Figure C. 2 along the line representing borehole of well 109.

Points H, L, M, and N indicate the pressures at different times during production of reservoir.

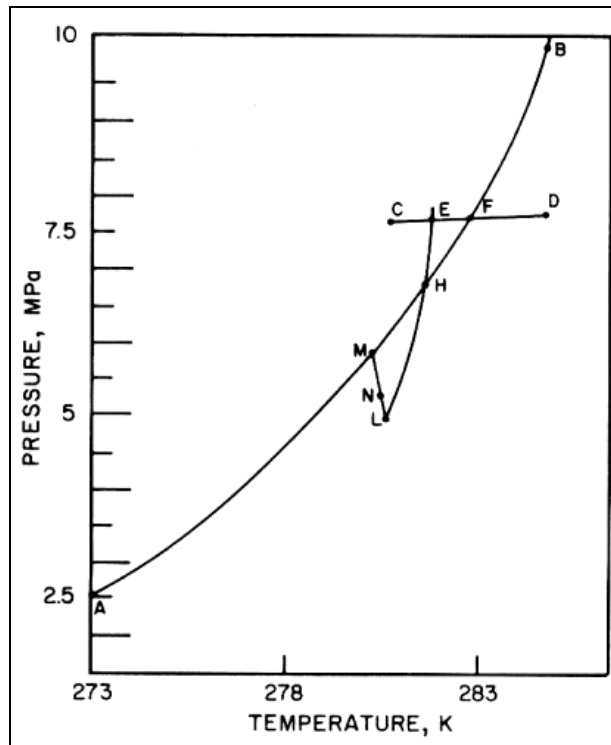


Figure C. 4: Reservoir pressure change for Messoyakha Field (Sloan [1])

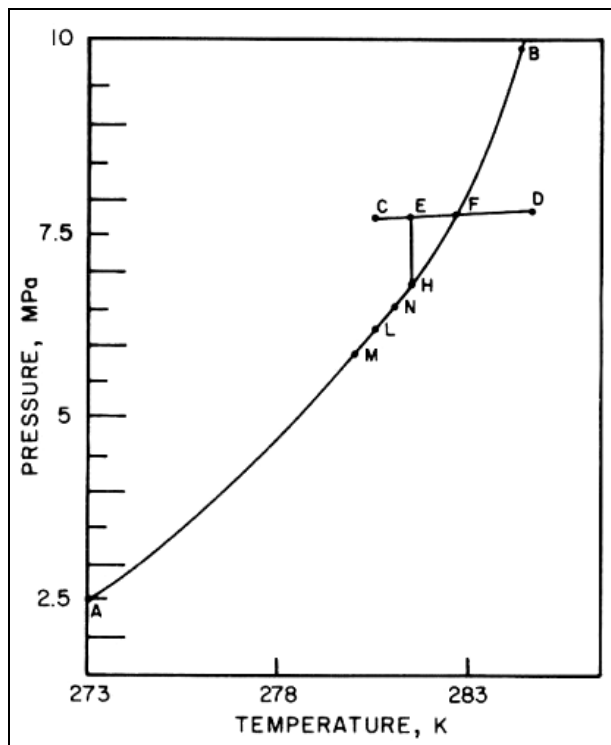


Figure C. 5: Dissociating front pressure change for Messoyakha Field (Sloan [1])

Figure C. 4 shows the average reservoir conditions, while Figure C. 5 is for the conditions at hydrate-gas interface. While the letters (E, H, L, M, N) in the previous three figures correspond to same time value in each plot, pressure values are only same in the Figure C. 3 And Figure C. 4 because they both represent average reservoir data. And apparently pressure values of Figure C. 5 differ from these since it is for the conditions at dissociating front.

**Period I:**

The average pressure in the reservoir decreases from an initial of point E to point H as free gas is produced during 5 years.

**Period II:**

After point H (the equilibrium point for hydrate) is reached, decomposition of hydrate and contribution of liberated gas begins. The shaded produced gas sections in Figure C. 3 indicate contribution of hydrate gas after point H. Similarly, the reservoir pressure is higher than anticipated due to this contribution of liberated hydrate gas. This period lasted for about 4 years.

As the production continues after point H is reached; average pressure in the reservoir is below equilibrium value while at the gas-gas hydrate surface (dissociation front) it is always equal to equilibrium value unless all the hydrate is decomposed. The P-T graph for dissociation front is given in Figure C. 5. In this figure, P-T points of the two previous plots correspond to different values since this graph is for the dissociation front while others are for average reservoir conditions away from hydrate interface.

**Period III:**

During this period of 3 years, average reservoir pressure was almost constant due to released hydrate gas. Obviously the released gas was able to fully replenish the produced amount in this period and hence the pressure remained the same.

This replenishment also requires not all the released gas to be produced. The curve I separating the shaded region into 2 sectors in Figure C. 3 is the actual total produced gas. However, if all the released gas was produced then total gas production would have followed curve J. so some amount of the liberated hydrate gas remained in the reservoir keeping average pressure constant during 3<sup>rd</sup> period.

**Period IV:**

After sometime, in order to produce from other high pressure reservoirs in the region, reservoir was shut-in (approximately 4 years). Nevertheless the decomposition of the

hydrates continued until the average pressure in the reservoir rose to equilibrium value (M) at a new lower temperature. When given enough time it is supposed that reservoir temperature and pressure will attain their initial values as hydrates decompose and surrounding strata supply heat.

**Period V:**

Production is re-initiated at the new reservoir pressure at point M and continued for about 8 years more.